

A071886

MASSACHUSETTS INSTITUTE OF TECHNOLOGY
LINCOLN LABORATORY

TECHNOLOGY ASSESSMENT FOR FUTURE MILSATCOM SYSTEMS:
THE EHF BANDS

D. J. FREDIANI

Group 61

PROJECT REPORT DCA-5

12 APRIL 1979

Approved for public release; distribution unlimited.

LEXINGTON

MASSACHUSETTS

**Best
Available
Copy**

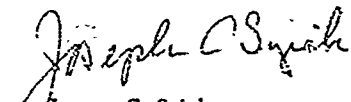
The work reported in this document was performed at Lincoln Laboratory, a center for research operated by Massachusetts Institute of Technology, for the Military Satellite Communications Systems Office of the Defense Communications Agency under Air Force Contract F19628-78-C-0002.

This report may be reproduced to satisfy needs of U.S. Government agencies.

The views and conclusions contained in this document are those of the contractor and should not be interpreted as necessarily representing the official policies, either expressed or implied, of the United States Government.

This technical report has been reviewed and is approved for publication.

FOR THE COMMANDER


Joseph C. Syiek
Acting Chief, ESP Lincoln Laboratory Project Office

ABSTRACT

Severe crowding of the radio frequency spectrum and of the geostationary orbital arc, coupled with DoD requirements for increased bandwidth, motivate a transition of future MILSATCOM systems to operating frequencies between 20 and 50 GHz (EHF). The identification of potential users, the frequency selection process and the transitional architecture are the focus of DCA/MSO studies. This report, prepared in support of the DCA/MSO Frequency Selection Working Group, assesses the technology necessary to support MILSATCOM evolution to EHF.

The technology assessment delineates the present, near term (3-5 years) and far term (6-10 years) availabilities of the major MILSATCOM subsystems. The major subsystems and systemic requirements are derived from strawman systems defined by the DCA/MSO Frequency Selection Working Group. The specific subsystems assessed include low-noise receivers, RF power amplifiers and antennas for the space and ground segments. The antenna gain limitations at EHF imposed by antenna surface accuracy and tracking accuracy are also addressed. As rain attenuation at EHF impacts system design and technology requirements, a global rain attenuation model is presented and the related issues of system availability, duration and impact of rain outages, and site diversity are assessed. Finally, recommendations are presented for technology development efforts and further studies necessary to support future EHF MILSATCOM deployment.

Accession For	
NTIS GRA&I	<input checked="checked" type="checkbox"/>
LDC TAB	<input type="checkbox"/>
Unannounced	<input type="checkbox"/>
Justification	
By _____	
Distribution/	
Availability Codes	
Dist	Availand/or special

TABLE OF CONTENTS

	<u>Page</u>
Abstract	iii
List of Illustrations	vi
List of Tables	x
 I. INTRODUCTION	 1
1.1 Background	1
1.2 EHF Frequency Bands	2
1.3 Technology Assessment Methodology	4
1.4 "Strawman" EHF MILSATCOM	4
1.5 Overview	8
 II. LOW-NOISE RECEIVERS	 10
2.1 Background	10
2.2 Mixer/IF Amplifiers	12
2.3 Parametric Amplifiers	14
2.4 FET Amplifiers	17
2.5 Summary	19
 III. RF POWER AMPLIFIERS	 22
3.1 Background	22
3.2 Traveling-Wave Tube Amplifiers	24
3.3 Solid-State Power Amplifiers	37
3.4 Summary	45
 IV. ANTENNA GAIN LIMITATIONS	 48
4.1 Background	48
4.2 Antenna Surface Accuracy	50
4.3 Antenna Tracking Accuracy	58
4.4 Radomes	73
4.5 Technological Limits	81
4.6 Summary	84

TABLE OF CONTENTS (Cont'd)

	<u>Page</u>
V. ANTENNAS	86
5.1 Background	86
5.2 Ground Segment	86
5.3 Space Segment	92
5.4 Summary	115
VI. PROPAGATION EFFECTS	117
6.1 Background	117
6.2 Attenuation Due to Atmospheric Absorption, Clouds, Fog, Snow and Sleet	117
6.3 Rain Attenuation Estimation Models	124
6.4 Proposed Rain Attenuation Model	137
6.5 Global Rain Attenuation Estimates	156
6.6 Availability Considerations	157
6.7 Summary	175
VII. TECHNOLOGY DEVELOPMENT/STUDY RECOMMENDATIONS.	180
7.1 Overview	180
7.2 Low-Noise Receivers	182
7.3 TWT Power Amplifiers	183
7.4 Solid-State Power Amplifiers	186
7.5 Antenna Surface Accuracy	188
7.6 Antenna Tracking Accuracy	189
7.7 Radomes	189
7.8 Ground-Segment Antennas	190
7.9 Space-Segment Antennas	191
7.10 Rain Attenuation Factors	194
Acknowledgements	196
References	197
Appendix A Estimates of Rain Attenuation	201

LIST OF ILLUSTRATIONS

	<u>Page</u>
Fig. 1.1 Technology assessment methodology for future military communications satellite systems.	5
Fig. 2.1 Clear-sky thermal noise characteristics of the atmosphere versus frequency for various elevation angles (Bismark, N. D., mean February conditions) (From Ref. 1.)	11
Fig. 2.2 Noise figure of mixer/IF amplifiers.	13
Fig. 2.3 Noise figure of parametric amplifiers.	16
Fig. 2.4 Noise figure of FET amplifiers.	18
Fig. 3.1 RF power-output projections: ground-segment TWTAs.	28
Fig. 3.2 RF power-output projections: space-segment TWTAs.	36
Fig. 3.3 RF power-output projections: IMPATT diodes.	40
Fig. 3.4 RF power-output projections: GaAs FETs.	42
Fig. 4.1 Effect of reflector surface accuracy on antenna radiation pattern.	51
Fig. 4.2 Loss in antenna gain versus antenna surface accuracy in wavelengths.	53
Fig. 4.3 Loss in antenna gain versus antenna surface accuracy with frequency as a parameter.	54
Fig. 4.4 Antenna gain limitations due to antenna surface accuracy.	57
Fig. 4.5 Antenna tracking loss.	61
Fig. 4.6 Loss in antenna gain versus antenna tracking accuracy in half-power beamwidths.	62
Fig. 4.7 Loss in antenna gain versus antenna tracking accuracy-diameter product with frequency as a parameter.	63
Fig. 4.8 Antenna gain limitations due to antenna tracking accuracy.	69
Fig. 4.9 Required downlink tracking accuracy versus uplink-to-downlink frequency ratio (F_U/F_D).	74

LIST OF ILLUSTRATIONS (Cont'd)

	<u>Page</u>
Fig. 4.10 Typical electromagnetic performance characteristics of a metal space frame radome (nominal diameter 68 ft.).	77
Fig. 4.11 Typical transmission loss of shipboard radomes (nominal diameter 6.5 ft.).	79
Fig. 4.12 Antenna gain limitations due to gravitational distortion.	83
Fig. 5.1 Radiation pattern of 12-inch reflector antenna with 8-inch absorber tunnel at 9.375 GHz (H-plane).	89
Fig. 5.2 Radiation pattern of 12-in. reflector antenna with 8-inch absorber tunnel at 9.735 GHz (E-plane).	90
Fig. 5.3 Adaptive sidelobe cancellation.	91
Fig. 5.4 Electrical and mechanical characteristics of EHF phased arrays.	93
Fig. 5.5 Required satellite transmitter power and ground terminal antenna diameter versus satellite antenna beamwidth.	96
Fig. 5.6 Hexagonal time-hopped-beam geometry.	99
Fig. 5.7 Minimum gain for hexagonal time-hopped-beam antenna versus number of elements ($\theta_m = 9^\circ$).	102
Fig. 5.8 Calculated radiation patterns of 37-beam waveguide lens showing minimum gain ($\theta_m = 9^\circ$).	103
Fig. 5.9 Calculated radiation patterns of 37-element phased array showing minimum gain ($\theta_m = 9^\circ$).	104
Fig. 5.10 Calculated gain and mechanical characteristics of 43-GHz, 37-beam phased array ($\theta_m = 9^\circ$).	105
Fig. 5.11 Power consumption of phase-shifters in a time-hopped-beam array versus switching rate.	106
Fig. 5.12 Loss in satellite antenna gain to a user as a function of the angular separation ($\Delta\theta_1$) of a single jammer in nulling antenna peak-to-first-null width (T).	109

LIST OF ILLUSTRATIONS (Cont'd)

	<u>Page</u>
Fig. 5.13 Loss in satellite antenna gain to a user as a function of the jammer separation in miles with nulling antenna aperture as a parameter (90° elevation angle).	110
Fig. 5.14 Loss in satellite antenna gain to a user as a function of the jammer separation in miles with nulling antenna aperture as a parameter (20° elevation angle).	111
Fig. 6.1 Theoretical one-way zenith attenuation from specified height to top of the atmosphere for a moderately humid atmosphere (7.5 g/m ³ at the surface).	118
Fig. 6.2 Theoretical one-way zenith attenuation through the atmosphere for various relative humidities (M = 43% at 20°C).	119
Fig. 6.3 Attenuation by water clouds or fog at various temperatures as a function of frequency (From Ref. 39).	122
Fig. 6.4 Coefficients of specific attenuation as a function of frequency.	128
Fig. 6.5 Height of the melting layer (0°C isocherm) for various CCIR rain climate regions.	130
Fig. 6.6 Canonic model of Earth-satellite path.	131
Fig. 6.7 Effective path length versus elevation angle.	132
Fig. 6.8 CCIR rain rate climate regions (From Ref. 45).	134
Fig. 6.9 Percentage of an average year for which rainfall rate is exceeded for the five CCIR rain climates (From Ref. 45).	135
Fig. 6.10 Predicted slant path rain attenuation at 20 GHz for 90° elevation angle.	136
Fig. 6.11 Global rain rate climate regions.	138
Fig. 6.12 Rain rate climate regions, United States.	139
Fig. 6.13 Rain rate climate regions, Europe.	140
Fig. 6.14 Rain rate climate regions, ocean areas.	141

LIST OF ILLUSTRATIONS (Cont'd)

	<u>Page</u>
Fig. 6.15 Rain rate distributions.	142
Fig. 6.16 Effective path average factor versus rain rate for a 10 Km path.	145
Fig. 6.17 Effective path average factor model for different path lengths.	146
Fig. 6.18 Multiplier in path average model, $\gamma(D)$.	147
Fig. 6.19 Exponent in path average model, $\delta(D)$.	148
Fig. 6.20 Latitude dependence of zonally averaged 0°C isotherm height.	150
Fig. 6.21 Multiplier in specific attenuation model, $\alpha(F)$.	151
Fig. 6.22 Exponent in specific attenuation model, $\beta(F)$.	152
Fig. 6.23 Attenuation statistics for an Earth-space path at 15.3 GHz.	154
Fig. 6.24 Required path versus terminal availability with system availability as a parameter.	163
Fig. 6.25 Automatic satellite message transfer time (From Ref. 51).	171
Fig. 6.26 Fade duration histograms at 19 and 37 GHz (From Ref. 52).	173
Fig. 6.27 Fade duration histogram at 30 GHz (From Ref. 53).	174
Fig. 6.28 Fade duration histogram at 18 GHz (From Ref. 54).	174

LIST OF TABLES

<u>Table</u>		<u>Page</u>
1.1	Current United States Government Frequency Allocations for EHF Satellite Service.	3
1.2	Strawman EHF Terminal Characteristics.	7
2.1	Low-Noise Receiver Availability.	20
3.1	TWTA Survey: Ground Segment.	26
3.2	RF Power Amplifier Availability: Ground Segment.	31
3.3	TWTA Survey: Space Segment.	33
3.4	RF Power Amplifier Availability: Space Segment.	47
4.1	Current Antenna Surface Accuracies ($D \geq 4$ ft.).	52
4.2	Current Antenna Surface Accuracies ($D \leq 8$ ft.).	56
4.3	Loss in Antenna Gain Due to Antenna Surface Accuracy ($D = 40$ ft.).	59
4.4	Current Antenna Tracking Accuracies.	68
4.5	Antenna Gain and Diameter Limitations Due to Antenna Tracking Accuracy.	71
4.6	Antenna Tracking Accuracy Requirements.	72
4.7	Environmental Specifications of Metal Space Frame Radome (Nominal Diameter 68 ft.).	75
4.8	Typical Electromagnetic Performance Characteristics of a Metal Space Frame Radome (Nominal Diameter 68 ft.).	78
4.9	Transmission Loss of Dual-Band Airborne Radome (AN/ASC-28).	80
4.10	Antenna Gain Limitations Due to Gravitational Distortion.	82
5.1	Comparison of Time-Hopped-Beam Phased Array and Lens Antenna.	98

LIST OF TABLES (Cont'd)

<u>Table</u>		<u>Page</u>
5.2	Optimum Time-Hopped-Beam Antenna Parameters ($\theta_m = 9^\circ$).	100
5.3	Potential Resolution of a 100λ Adaptive-Nulling Antenna.	112
6.1	Atmospheric Attenuation Due to Oxygen and Water Vapor Absorption.	121
6.2	Zenith Attenuation for Various Climatological Conditions.	125
6.3	Rain Rate Distribution Values (mm/h).	143
6.4	Satellite Observations of Rain Attenuation.	155
6.5	Estimates of Atmospheric Plus Rain Attenuation.	158
6.6	Required Path Availability Versus Terminal Availability.	164
6.7	Required Path Margins Due to Atmospheric and Rain Attenuation (20° Elevation Angle).	165
6.8	Required Path Availability Versus Terminal Availability for Dual Diversity System.	167
6.9	Average Outages Versus Path Availability.	172

1. INTRODUCTION

1.1 Background

Current U. S. MILSATCOM systems operate in the UHF (240-400 MHz) and 8/7 GHz bands, and share these bands both with other satellite services and extensive terrestrial systems. The MILSATCOM terminal inventory includes (in addition to fixed earth terminals) aeronautical, maritime and mobile earth terminals. The UHF band is allocated for Fixed and Mobile service (terrestrial), and Mobile-Satellite service in this band is recognized only by a footnote to the Allocation Tables. The proliferation of UHF networks throughout the world is extensive and mutual interference between MILSATCOMs and terrestrial services is a serious problem in this band. The 8/7 GHz band is allocated for Fixed-Satellite service and is also shared with terrestrial systems. Mobile-Satellite service in the 8/7 GHz band is not in conformance with the International Radio Regulations and the operation of mobile-satellite terminals in this band must be on a noninterfering basis with the allocated users. Thus, MILSATCOM operation in the UHF and 8/7 GHz bands requires intensive frequency management on a global basis and is increasingly more difficult to coordinate. In addition, due to the increasing numbers of satellite systems vying for geostationary orbit locations in these bands, crowding of the orbital arc is increasing and desirable geostationary-orbit positions are becoming more difficult to obtain.

Coincident with this crowding of the radio frequency (RF) spectrum and of the geostationary orbital arc, is a growing requirement within the DoD for increased bandwidth. Projected capacity requirements show the need for greater bandwidth to accommodate higher data rates for data relay and increased numbers of satellite circuits for mobile users. Another significant bandwidth requirement stems from the longstanding, unsatisfied need for anti-jam (AJ) protection for MILSATCOM users, particularly for small mobile terminals. The AJ limitations of small terminals in the UHF band has long been recognized as well as the need to move to higher frequencies. Although the particular AJ modulation techniques to be implemented (pseudonoise or frequency hopping) are current

issues the need for wide, contiguous bandwidths for spread-spectrum modulation is fundamental.

In view of these problems, uncertainties and unsatisfied needs, the evolution of MILSATCOM systems to higher frequency bands is evident and is the focus of current DCA/MSO studies. In particular, the DCA/MSO EHF Working Group on Frequency Selection for future MILSATCOM system architecture explored the potential benefits of the EHF frequency band as an adjunct to the UHF and 8/7 GHz bands. The specific objectives of the Working Group were:

1. Identify factors which make operation at EHF attractive (i.e., capacity, AJ and LPI (low probability of intercept)).
2. Identify potential users of the EHF bands based on their current and projected unsatisfied needs.
3. Match candidate EHF bands to potential users.
4. Assess EHF technology for both the ground and space segments.

This report, prepared in support of the DCA/MSO Frequency Selection Working Group, addresses the EHF technology issues.

1.2 EHF Frequency Bands

The selection of higher frequency bands for MILSATCOM use is based on International and U. S. Government frequency allocations, available bandwidth, competing services, propagation effects, state of the technology and the unique communication needs of the DoD community. Table 1.1 lists the potential EHF bands for MILSATCOM use based on current U. S. frequency allocations for Government use. Also included in Table 1.1 are the current U. S. proposals for GWARC-79 regarding these frequency bands. The mapping of potential user communities into these EHF bands, based on their capacity, AJ and LPI requirements, is the task of the DCA/MSO Working Group. The assessment of the propagation effects, as they impact this frequency selection process and future system design, is included in this technology report.

TABLE 1.1
CURRENT UNITED STATES GOVERNMENT FREQUENCY ALLOCATIONS FOR
EHF SATELLITE SERVICE

Frequency Band (GHz)	Service Allocation	GWARC 79 Proposal
20.2 - 21.2 ⁽¹⁾	Fixed-Satellite (Space-to-Earth)	Add Mobile-Satellite service as a primary service.
30.0 - 31.0 ⁽¹⁾	Fixed-Satellite (Earth-to-Space)	Add Mobile-Satellite service as a primary service.
40.0 - 41.0 ⁽²⁾	Fixed-Satellite (Space-to-Earth)	Add Terrestrial service.
43.0 - 48.0 ⁽³⁾	Aeronautical and Maritime Mobile-Satellite (no designation)	Allocate 43.0-45.0 GHz for Earth-to-Space. Add Mobile- Satellite service.
50.0 - 51.0 ⁽²⁾	Fixed-Satellite (Earth-to-Space)	Add Terrestrial service.

- (1) Exclusive Government service allocation.
- (2) Shared with non-Government Fixed-Satellite and Mobile service.
- (3) Shared with Government Aeronautical and Maritime Mobile, Aeronautical and Maritime Radionavigation, and Aeronautical and Maritime Radionavigation-Satellite services; all services in this band shared with non-Government users.

1.3 Technology Assessment Methodology

Technology assessment is one of the tasks conducted by Lincoln Laboratory in support of the DCA/MSO. The technology assessment task is directed toward defining the technology needed to support the deployment of future MILSATCOM systems. The technology assessment methodology (Fig. 1.1) first draws on existing MILSATCOM architectures and studies to develop "strawman" versions of these systems. The strawman systems are defined by frequency band leading to UHF, X-band, EHF, etc., strawman MILSATCOMs and corresponding technology assessments. From the operations requirements of the strawman system, the performance characteristics of the major subsystems are defined. In parallel with the characterization of the MILSATCOM system, a relevant technology base is established from a survey of operational systems, the current state-of-the-art, on-going research and development, and estimates and projections of future technology developments. Next, the strawman subsystem requirements are assessed vis-a-vis the technology data base to determine areas of deficiency. Finally, specific areas warranting research and development effort and for further study are delineated as an input to the DCA/MSO technology development recommendations.

During the past year the technology assessment effort has been directed toward the EHF (20-50 GHz) bands in support of the DCA/MSO Frequency Selection Working Group. The initial effort was focused on the 30/20 GHz bands and was published previously⁽²⁶⁾. This report, covering the EHF bands, is an expansion of the previous report, both in the depth and breadth of the areas being assessed. In particular, the emphasis in this effort has been directed toward defining the frequency dependence and frequency boundaries of the various competing technologies, and examining the technological limits.

1.4 "Strawman" EHF MILSATCOM

The DCA/MSO Frequency Selection Working Group, with the support of the Military Services and Departments, has completed its tasks of exploring the potential user communities for transition to EHF, and of matching the potential users to specific EHF bands as dictated by their unique mission requirements.

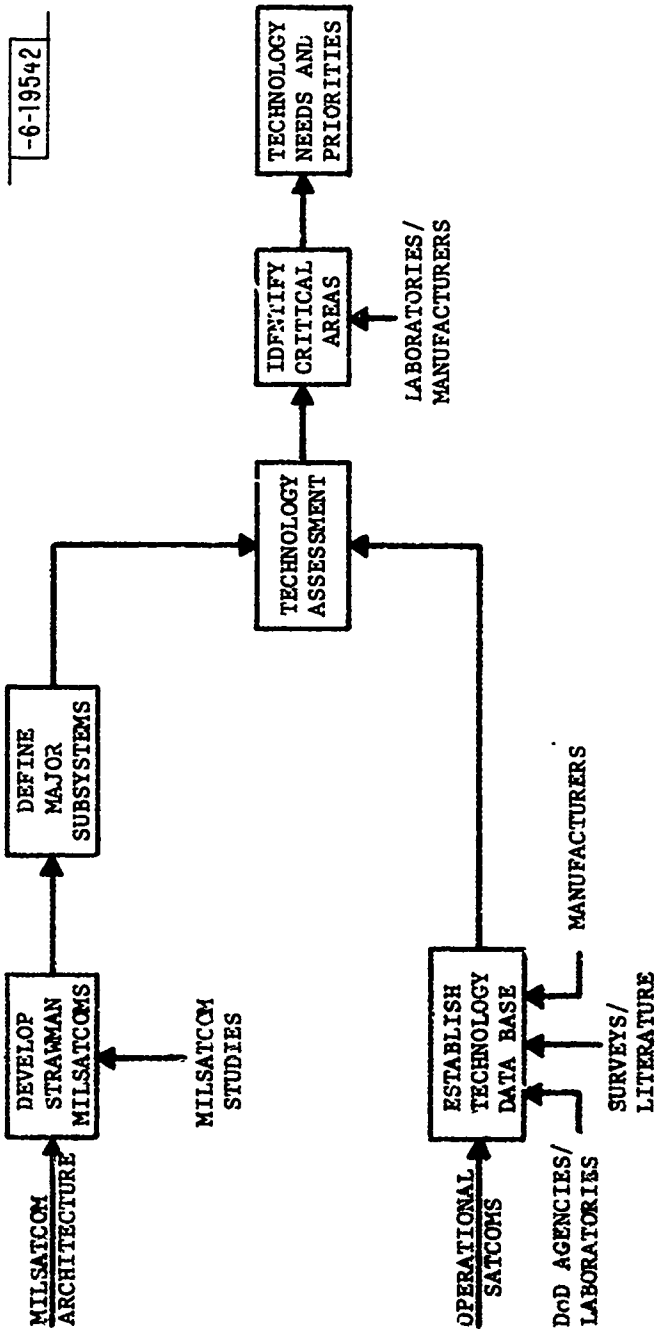


Fig. 1.1. Technology assessment methodology for future military communications satellite systems.

Current DCA/MSO studies, combining the findings of the Frequency Selection and Modulation Working Groups, are addressing the EHF evolutionary architecture and will address such systemic considerations as the tradeoff between terminal and spacecraft complexity. The scope of the technology assessment is quite broad and should provide an adequate technology data base to assess the critical areas of technology necessary to support future system designs.

The primary reason for considering EHF is the increased available RF spectrum. Operation at EHF, with its wider available bandwidth, affords the capabilities for improved AJ and LPI performance, increased numbers of satellite channels, and higher data rates than can be realized at UHF and 8/7 GHz. Analyses of the frequency dependence of AJ and LPI performance, and rain attenuation were conducted by the DCA/MSO Frequency Selection Working Group. These findings, coupled with the potential users' mission-unique priorities (i.e., capacity, availability, AJ and LPI) led to the mapping of the user communities into candidate EHF bands which are delineated in the Working Group Report. As part of the Working Group's AJ, LPI and propagation analyses, strawman satellite and terminal characteristics were defined. It must be noted that these are preliminary, baseline characteristics which were adequate for the tasks of the Working Group (i.e., system design and optimization were not among the chartered tasks of the Working Group). Table 1.2 summarizes these strawman EHF terminal characteristics. Note that the terminal antenna sizes and transmitter power levels are typically less than those currently in use at UHF and 8/7 GHz. Note also that the satellite antennas provide simple area coverage beams. The tenuity of the terminal characteristics may be easily demonstrated by considering, for example, that the use of TDMA with time-hopped beams and average-power-limited tubes might easily allow a factor-of-four reduction in satellite antenna beamwidth. This reduction in satellite antenna beamwidth could permit for FLTOPS or small multichannel GMF a reduction either in antenna diameter from 4 ft. to 1 ft. (allowing simple step tracking) or in transmit power from 500 W to 30 W (allowing solid-state transmitters). Future system studies will address the specific design tradeoffs between

TABLE 1.2
STRAWMAN EHF TERMINAL CHARACTERISTICS

User	Ground Segment			Space Segment		
	Antenne Diameter (Ft)	Transmitter Power (W)	Noise Temperature (°K)	Antenna Beamwidth (Deg)	Transmitter Power (W)	Noise Temperature (°K)
Small Aircraft	0.75	100	500	9.0	8	1150
Large Aircraft	1.5	500	500	4.5	8	1150
FLTOPS	4	500	500	9.0	8	1150
GMF	1.5	100	500	4.5	8	1150
	4	500	500	4.5	8	1150
	8	500	500	4.5	8	1150
Wideband Relay	40	1000	300	4.5	8	1150

satellite and ground terminal complexity; this assessment attempts to include the technology which would encompass such future designs.

1.5 Overview

There are several fundamental factors regarding EHF technology which are relevant to this report

1. Within the EHF band there are specific frequency limits on desired technology, e.g., low-noise and power FETs.
2. There are areas which are not technology limited, but have technology boundaries whereby achieving a desired performance level requires a more costly and complex technology, e.g., step tracking versus monopulse tracking.
3. Operation at EHF will entail larger separations between uplink and downlink frequency bands (an exception being 44/40 GHz) than at 8/7 GHz, and will impact the antenna feed design, tracking accuracy requirements and radomes.

The impact of these considerations on final frequency selection and system design/cost analyses is beyond the scope of this report; however, these factors are emphasized throughout this report.

The technology assessment is divided into three time periods which are indicators of

Present -- the capability of current commercial technology to support EHF MILSATCOMS.

Near Term (1984) -- the current R&D efforts at EHF and/or extrapolations of demonstrated technology at other frequency bands.

Far Term (1988) -- projected improvements in technology contingent upon funded research programs.

Section II addresses the availability and viability of parametric amplifiers, low-noise FETs and mixers as EHF low-noise receivers. Section III

assesses RF power amplifiers for the ground and space segments. In particular, the limits on air-cooled versus liquid-cooled and PPM versus solenoid-focused TWTAs for the ground segment, and solid-state versus TWT amplifiers for the space segment. The antenna gain limitations imposed by antenna surface accuracy and antenna tracking accuracy are addressed in Section IV. This section also discusses the requirements for antenna tracking and radomes in relation to the frequency separation of the EHF bands. Section V addresses antennas, specifically, multiple-beam, time-hopped-beam and adaptive-nulling antennas for the satellite, and low-sidelobe antennas for the ground terminals. In Section VI, a global rain attenuation estimation model is presented and recommended for use in determining rain attenuation margin requirements. The related issues of system availability, duration and impact of rain outages, and site diversity are discussed to place the role of rain attenuation at EHF in proper perspective. Finally, Section VII presents a summary of recommended technology development efforts and areas for further study.

II. LOW-NOISE RECEIVERS

2.1 Background

In each segment of a SATCOM system (particularly the space-to-earth link), maximizing G/T (ratio of antenna gain to system noise temperature) is desired to achieve the required signal-to-noise ratio with reasonable demands on the transmitter power and antenna size of the transmitting terminal. Providing the required G/T is a tradeoff between increased antenna gain and reduced noise temperature of the receiver. Increasing the antenna gain (size) of the ground terminals incurs the increased costs due to maintaining the required antenna surface accuracy and tracking accuracy*, radome requirements, and the antenna integration for airborne and shipboard terminals. The antenna gain for the space segment is typically restricted by requirements on the coverage area. The burden of achieving the required G/T then falls on the low-noise receiver for both the satellite and ground terminals. This section assesses the performance of currently available and projected low-noise amplifier for the space and ground segments, in particular: currently available broadband mixer/IF amplifiers and potential improvements with image-enhancement techniques or cryogenic cooling; cryogenically-and thermoelectrically-cooled, and uncooled paramps; and rapidly emerging low-noise FET technology.

In considering desired performance levels for low-noise receivers at EHF, the receiver's impact on system noise temperature must be considered relative to other noise contributions. For the satellite, the antenna is looking at the earth background which is at a temperature of $\approx 290^\circ\text{K}$. Consequently, the antenna noise temperature is a significant determinant in the system noise temperature and limits the effectiveness of low-noise receivers in substantially reducing the system temperature. For ground terminals operating at EHF, the clear-sky noise contribution due to atmospheric emission (see Fig. 2.1)⁽¹⁾ may range from 20°K (90° elevation angle at 20 GHz) to 200°K (10° elevation angle at 40 GHz). The value of sky noise increases significantly during rain

*Current antenna fabrication and tracking technology also impose limits on the maximum achievable antenna gain and are discussed in Section IV.

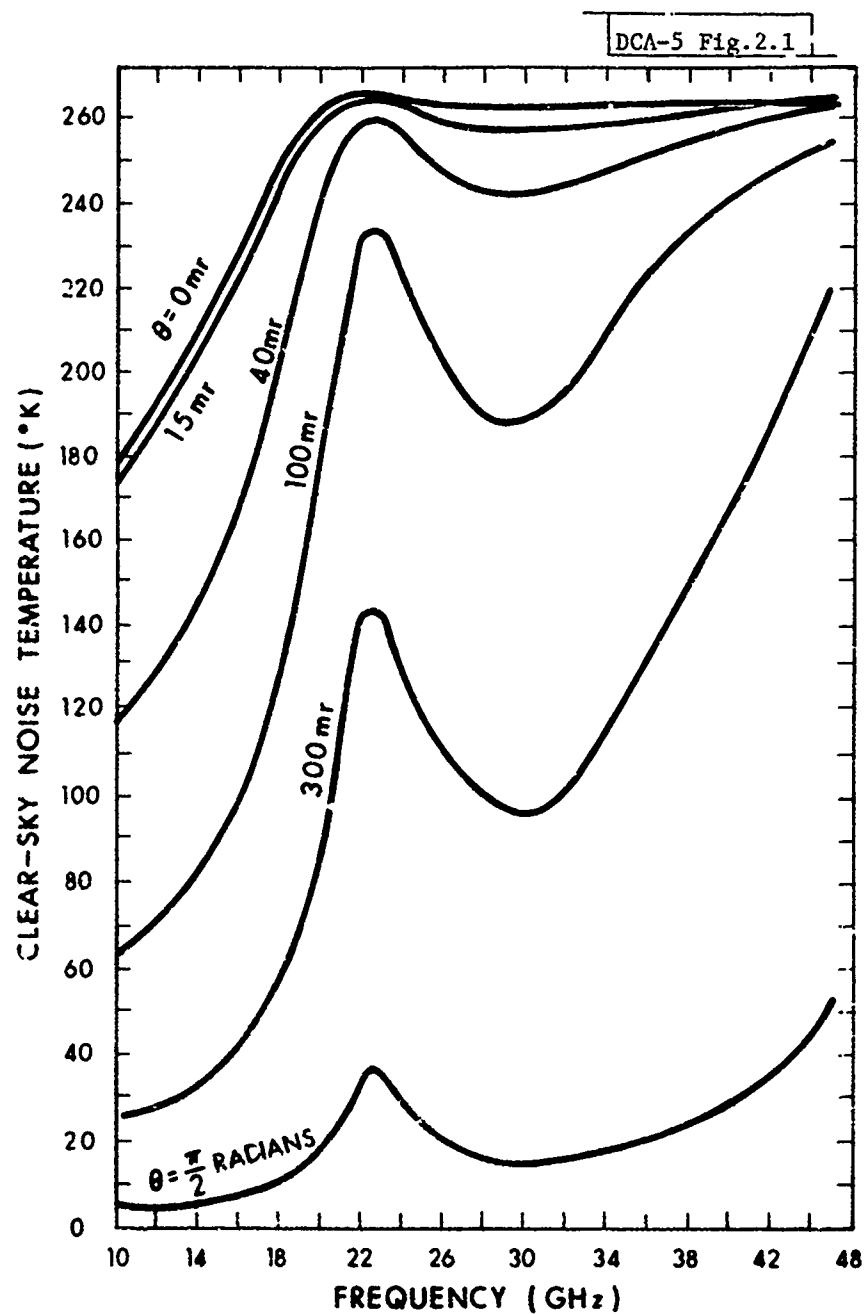


Fig. 2.1. Clear-sky thermal noise characteristics of the atmosphere versus frequency for various elevation angles (Bismark, N. D., mean February conditions), (from Ref. 1.)

and approaches a maximum temperature, $T_M \approx 275^\circ\text{K}$ (e.g., for 10 dB rain attenuation along the path, the sky temperature is $\approx 250^\circ\text{K}$). Consequently, for EHF ground terminals, receivers with noise temperatures of the order of 100°K (cryogenically-cooled paramps) would not significantly improve system performance and are not generally recommended for development. An exception would be the 20 GHz downlink for the wideband data relay, if high elevation angles were afforded to reduce the noise contribution due to atmospheric emission and site diversity were employed to mitigate the increased noise contribution due to rain attenuation.

2.2 Mixer/IF Amplifiers

The simplest and most conventional receiver front end in the millimeter-wave region is the mixer/IF (intermediate frequency) transistor-amplifier. The single-sideband (SSB) noise figure (NF) of this basic front end may be expressed as

$$NF = L_c (F_{IF} + T - 1) \quad (2.1)$$

where L_c = conversion loss of mixer

F_{IF} = noise figure of IF amplifier

T = noise ratio of mixer diode

The noise-temperature ratio of the mixer diode is a function of the IF frequency and for IF frequencies > 1 MHz, $T \approx 1$. Hence, for the applications of interest, the noise figure of a mixer/IF amplifier is essentially the product of the mixer conversion loss and IF amplifier noise figure. IF amplifier noise figures of about 2 dB have been obtained for frequencies up to 4 GHz using Ga As MESFETS with $1\mu\text{m}$ gate lengths. Advances in Schottky-barrier diode technology, particularly in Ga As, have made available mixer diodes with high-cutoff frequencies (800 GHz at 0-V bias) and low junction capacitance (0.1 pF), with mixer conversion losses ≤ 5 dB at EHF. Consequently, mixer/IF amplifiers with noise figures of ≈ 8 dB at EHF are now possible; the expected noise figures are presented in Fig. 2.2.

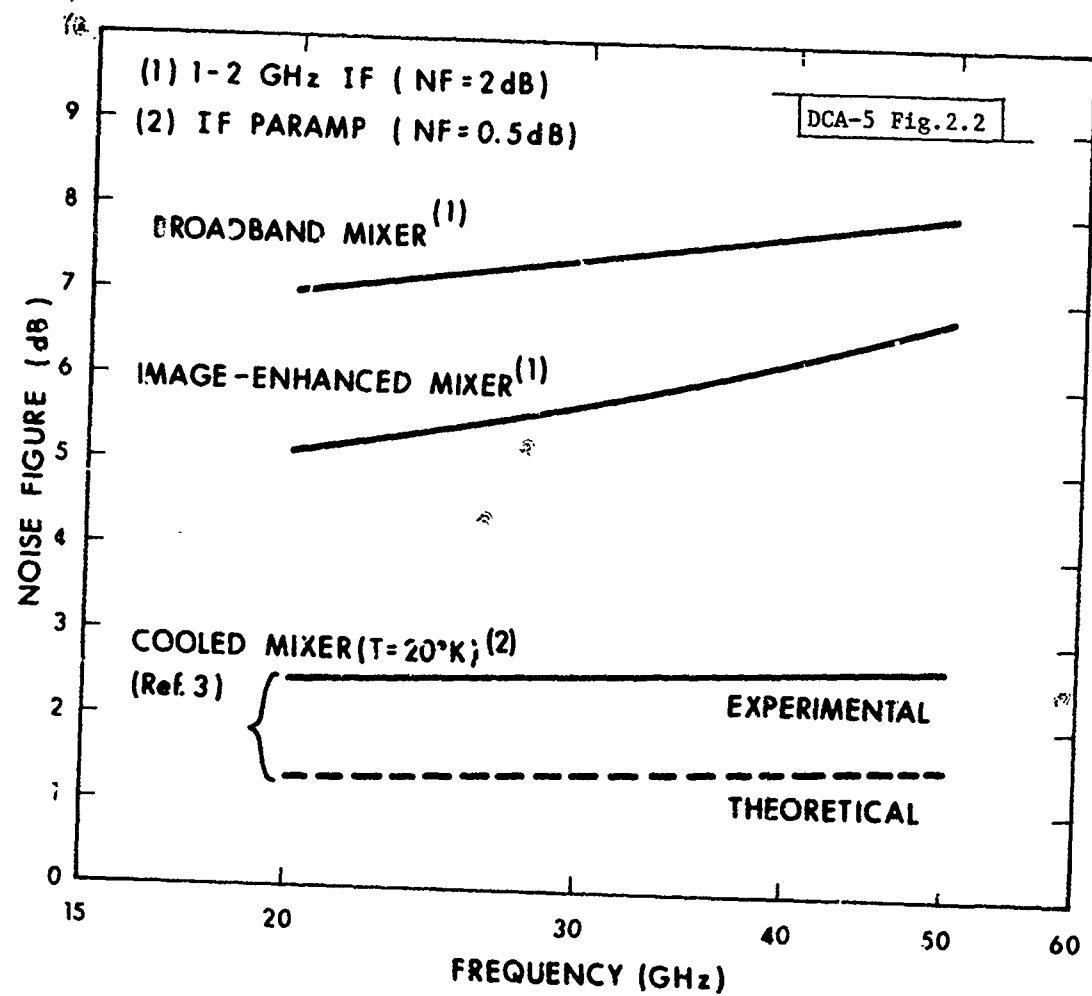


Fig. 2.2. Noise figure of mixer/IF amplifiers.

It has long been known that proper reactive termination of the image frequency (and higher-order product frequencies) of a mixer causes energy converted to the image frequency to be reflected back into the mixer and reconverted to IF. This technique offers the potential reduction of the mixer conversion loss and noise figure of SSB downconverters of ≈ 2 dB (i.e., ≈ 6 dB at EHF). The practical realization of the potential of image-enhanced (IE) mixers has been brought about by the advent of high-quality Ga As Schottky diodes. The implementation of IE mixers requires locating the reactive image termination in close proximity to the diodes to minimize dispersion. Depending upon the bandwidth requirement, the use of waveguide circuits may not be possible and integrated circuit technology may be required. Reported⁽²⁾ results of an IE mixer/IF amplifier operating at 35 GHz using laminate-mode waveguide technology demonstrate a SSB noise figure of 5.8 dB (3.1 dB conversion loss, 2 dB NF of 1.2 GHz IF amplifier, and 0.7 dB filter loss). Fig. 2.2 presents the theoretical⁽²⁾ performance of IE mixer/IF amplifier front ends and includes the loss due to the waveguide filter which provides the image rejection and termination.

It has been shown⁽³⁾ that cryogenically cooling ($\approx 20^\circ\text{K}$) a Schottky-barrier mixer gives a considerable reduction in mixer noise. Experimental results for broadband mixers indicate that in conjunction with a cooled paramp IF amplifier, SSB receiver noise figures of 2-3 dB are presently obtainable at EHF; the predicted performance of these receivers is presented in Fig. 2.2.

2.3 Parametric Amplifiers

Ground terminals of satellite communications systems typically employ parametric amplifiers (paramps) whose effective noise temperature is primarily dictated by the cutoff frequency of the varactor diode, the pump frequency and the operating temperature of the varactor diode. The effective noise temperature (T_e) of a nondegenerate paramp (SSB) can be expressed as

$$T_e = \frac{\frac{f_1}{f_2} + \frac{f_1 f_2}{M^2}}{1 - \frac{f_1 f_2}{M^2}} T_D \quad (2.2)$$

where f_1 = signal frequency

f_2 = idler frequency = $f_p - f_1$

f_p = pump frequency

M = varactor figure of merit = $(C_1/C_0)f_c$

C_1/C_0 = varactor nonlinearity ratio

f_c = varactor cutoff frequency

T_D = varactor junction temperature

Assuming that the varactor diode cutoff frequency and the pump frequency are fixed at the current limit of commercial technology (typically 700 GHz and 50 GHz, respectively), the achievable noise temperature is then determined by the operating temperature of the paramp. Paramps may be generically categorized by operating temperature (T_{Op}) as:

- a. cryogenically cooled, $T_{Op} \approx 20^\circ\text{K}$
- b. thermoelectrically (TE) cooled, $T_{Op} \approx -40^\circ\text{C}$
- c. uncooled or TE stabilized, $T_{Op} \approx \text{ambient} + 10^\circ\text{C} \approx 40^\circ\text{C}$

Cryogenically-cooled paramps could achieve noise temperatures of $\approx 75^\circ\text{K}$ ^(2,4) (NF ≈ 1 dB) at EHF (Fig. 2.3) and would require development. However, cryogenic cooling systems require a great deal of maintenance and, as previously discussed, the low noise temperatures achieved may not be warranted at EHF (a possible exception being the 20 GHz downlink for wideband data relay).

Based on a survey of manufacturers, thermoelectrically-cooled paramps could provide noise temperatures of 170 to 440°K (NF = 2-4 dB) at EHF (Fig 2.3) and are recommended for large fixed terminals. These paramps would represent

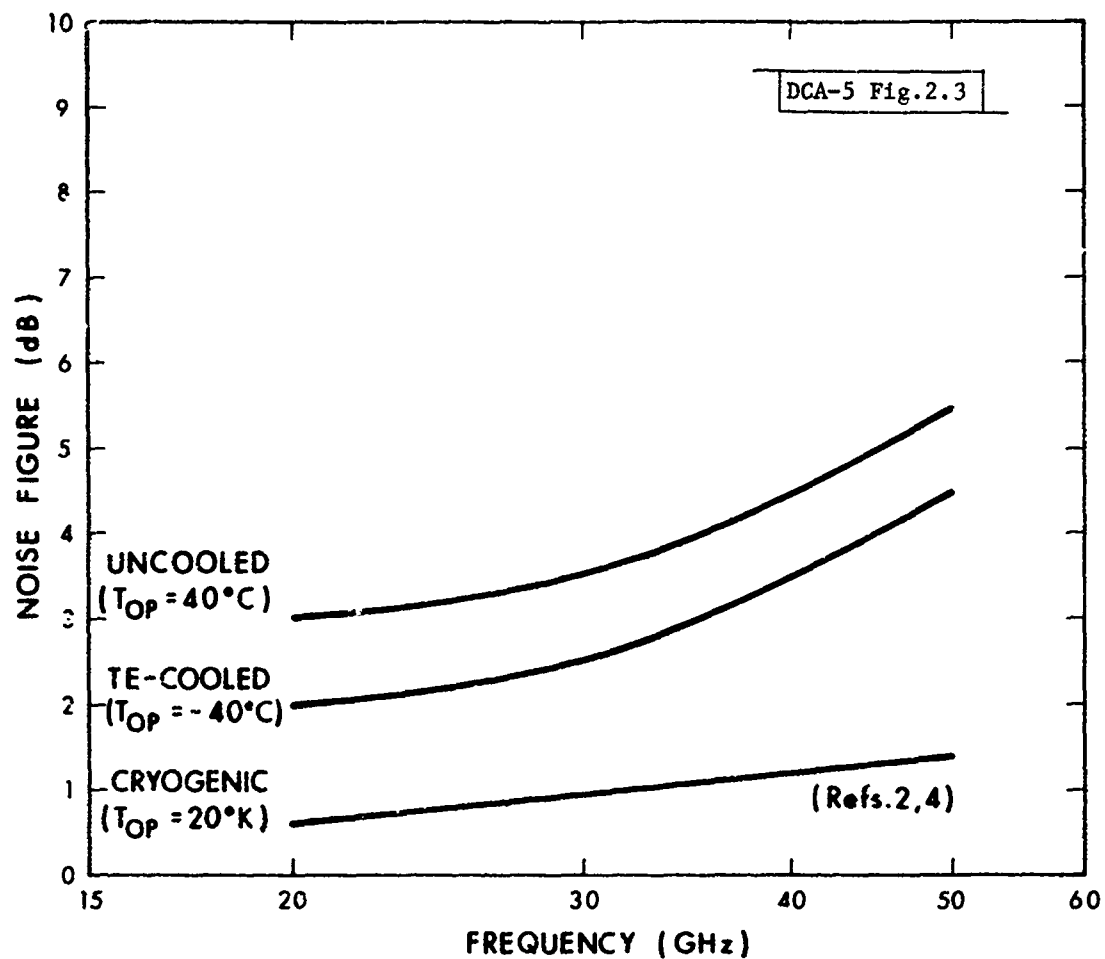


Fig. 2.3. Noise figure of parametric amplifiers.

a reasonable compromise between low-noise performance and maintenance, and are recommended for development.

Uncooled (TE-stabilized) paramps have already been developed or are under development at EHF. Typical examples include: 20 GHz paramp ($T_{OP} = 60^{\circ}\text{C}$) with 300°K noise temperature (3 dB NF) developed for SATCOMA by COMTECH Labs; 37 GHz paraconverter (paramp/mixer/IF amplifier) with 440° K (4 dB NF) developed for NOSC by LNR. Uncooled paramps are appropriate for mobile terminals for near term implementation and require little or no development effort; the expected performance (1 GHz bandwidth) is presented in Fig. 2.3. Far term improvements in paramp performance (0.5-1 dB) are predicted* based on potential improvements in varactor quality ($f_c \approx 1400$ GHz) and solid-state pump sources ($f = 100$ GHz). However, for far-term development efforts in low-noise receivers, the field-effect transistor (FET) amplifier is recommended and is discussed in the following section.

2.4 FET Amplifiers

The FET amplifier characteristics of gain, low-noise figure, stability and wide bandwidth, coupled with reliability and relatively low cost, make it an attractive candidate for low-noise front ends for SATCOM systems. Recent FET developments have extended the high frequency limit making the FET amplifier a viable candidate for EHF MILSATCOM operation and affords a technology opportunity to achieve highly reliable, low cost receivers for both the space and ground segments. Demonstrated performance of low-noise FETs includes: 2.5 dB NF device with 7 dB associated gain at 18 GHz⁽⁵⁾; 6 dB** NF amplifier with 6 dB gain at 30 GHz⁽⁶⁾. Other manufacturers (Plessey and Hughes) have produced devices having 3.0 to 3.5 dB noise figures at 18 GHz⁽⁷⁾. Current availability of FET amplifiers (0.5 μm gate length) is presented in Fig. 2.4; also included is the anticipated performance with near-term development efforts. Note in the latter case, achievement of a 5 dB NF at 30 GHz would provide a 2 dB improvement in satellite receiver noise figure over mixer/IF amplifiers. Development

*LNR, private communication

**Hughes Research Laboratories under AFAL sponsorship. Current efforts include development of 35 GHz amplifier with 8 dB NF.

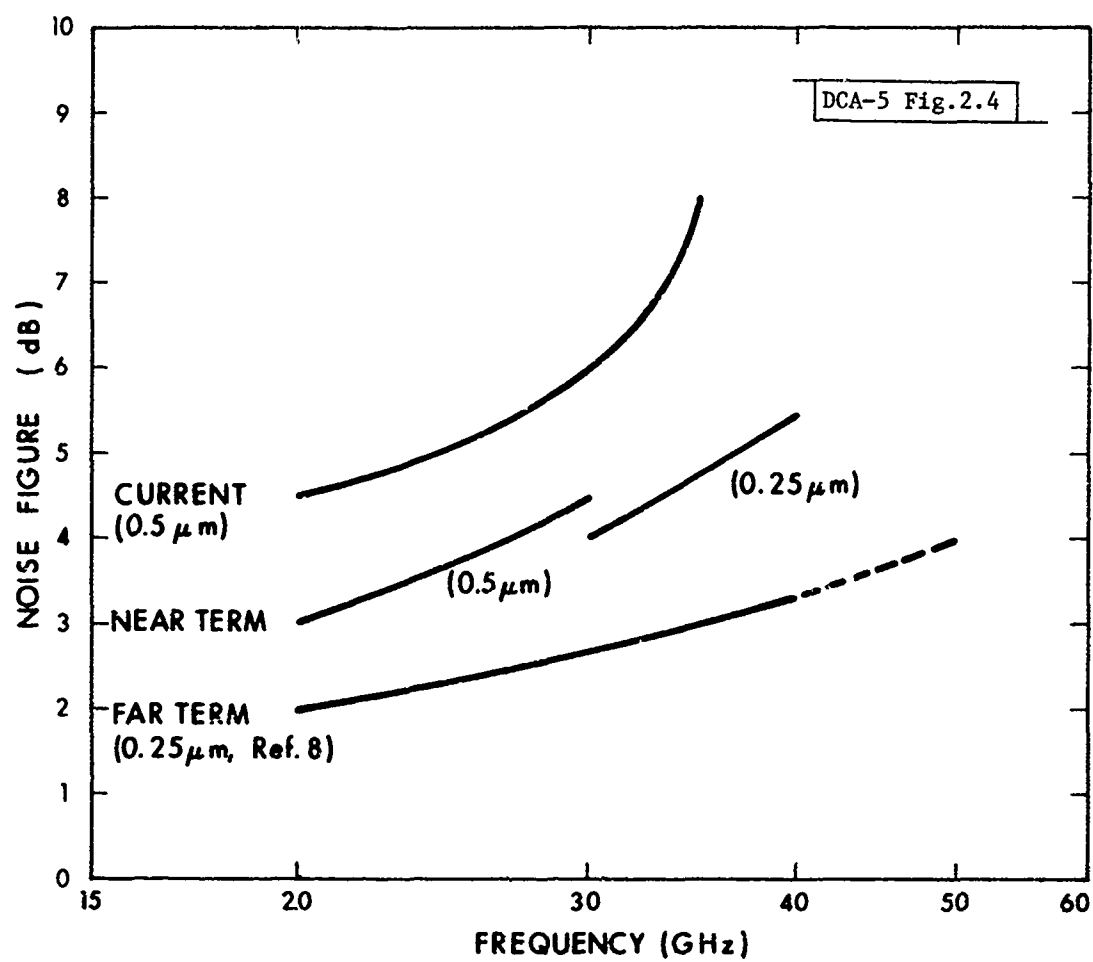


Fig. 2.4. Noise figure of FET amplifiers.

of low-noise FETs for use at frequencies ≥ 40 GHz requires development of gate lengths $< 0.5 \mu\text{m}$. Efforts are underway in this area e.g., Plessey has reported the fabrication of $0.2 \mu\text{m}$ devices with predicted NF of 4.5 dB at 40 GHz and Hughes (ERADCOM supported) has on-going development of Ga As FETs with gates $\leq 0.25 \mu\text{m}$.

For the far term, theoretical results predict⁽⁸⁾ noise figures of 2 dB at 20 GHz, 2.5 dB at 30 GHz, 3.5 dB at 40 GHz for $0.25\text{-}\mu\text{m}$ gate Ga As MESFETs (Fig. 2.4). (These results are based on the analytical optimization of material and geometric parameters and do not address the fabrication and implementation problems.) The realization of such devices would negate the need for cooled paramps for the fixed terminals. As regards the fixed terminals, a 1.2 dB noise figure at 20 GHz could be achieved⁽⁵⁾ with a FET amplifier cooled to 77°K.

2.5 Summary

Current, near-term and far term availabilities of viable low-noise receiver technology are summarized in Table 2.1 (cryogenically-cooled devices are omitted). Requirements for low-noise receivers can be adequately satisfied with currently available devices, i.e., mixer/IF amplifiers for the satellite, and TE-stabilized ($T_{\text{OP}} = 40^\circ\text{C}$) and TE-cooled ($T_{\text{OP}} = -40^\circ\text{C}$) paramps for the mobile and fixed terminals, respectively. However, rapidly emerging low-noise FET technology affords the opportunity for improved receiver performance for the satellite, and for reduced cost and maintenance for all ground terminals. It would appear reasonable to employ mixer/IF amplifiers and paramps for EHF system demonstrations, while FETs would be implemented in an operational system. On-going DoD Ga As FET developments at EHF (e.g., AFAL) should be expanded and are required, as little commercial development effort is occurring in this frequency range. The first priority should be development of devices and amplifiers for the specific frequencies of interest, i.e., 20 (3 dB NF) and 30 (5 dB NF) GHz in the near term and 40 and 44 GHz in the far term. (If FET developments at frequencies ≥ 40 GHz prove not to be commercially viable, IE mixers may provide a reasonable performance/cost compromise.)

TABLE 2.1

LOW-NOISE RECEIVER AVAILABILITY

RECEIVER TYPE	NOISE FIGURE (dB)						
	PRESENT		NEAR TERM			FAR TERM	
SPACE SEGMENT	30 GHz	44 GHz	30 GHz	44 GHz	30 GHz	44 GHz	44 GHz
Mixer/IF Amp ⁽¹⁾							
Broadband	7.5 dB	8 dB	-	-	-	-	-
Image-Enhanced	5.5 dB	6 dB	-	-	-	-	-
Low-Noise FET	-	-	5 dB	-	2.5 dB	4 dB	-
GROUND SEGMENT	20 GHz	40 GHz	20 GHz	40 GHz	20 GHz	40 GHz	40 GHz
Fixed Terminal							
Cooled PARAM ⁽²⁾	2 dB	3.5 dB	1.5 dB	2.5 dB	-	-	-
Low-Noise FET	-	-	-	-	2 dB	3.5 dB	-
Mobile Terminal							
Uncooled PARAM ⁽³⁾	3 dB	4.5 dB	2 dB	3.5 dB	-	-	-
Low-Noise FET	-	-	3 dB	-	2 dB	3.5 dB	-

(1) 1-2 GHz IF

(2) -40°C (TE)

(3) 40°C

Should future system studies show that extremely low-noise figures are desired for large fixed terminals, a tradeoff study between cryogenically-cooled FETs, IE mixer/IF amplifiers and paramps should be conducted.

III. RF POWER AMPLIFIERS

3.1 Background

A. Capacity Limitations

As is typical of COMSATS operating in other frequency bands, MILSATCOMs operating at 8/7 GHz are typically bandwidth limited, and the most optimistic predictions for future allocations in that band would only maintain the status quo. At EHF the situation is significantly different in that MILSATCOM capacity may be initially downlink power limited. Whereas the bandwidth limitation at 8/7 GHz is beyond the control of system architects, the power limitation at EHF can be removed by development efforts. Long-term, coordinated development programs for RF power amplifiers are then required to accommodate future system growth (both in the data rates for wideband data relay and in the numbers of satellite circuits for mobile users).

B. Space Segment

Supporting the required downlink capacity in a SATCOM system is a trade-off between terminal G/T and satellite EIRP (Effective Isotropically-Radiated Power). As discussed in Section II, there are practical limits at EHF on achievable system noise temperature (due to atmospheric emission and rain attenuation noise contributions) and antenna gain (primarily due to the complexity of the required tracking capability as discussed in Section IV). It is then desirable to maximize the satellite EIRP which is dependent on its antenna gain and RF transmitter power. A limit is typically imposed on the satellite antenna gain by the coverage area requirement of the specific user community. In the far term, operational EHF MILSATCOMs may remove this restriction by employing time-hopped narrow-beam antennas in a satellite-switched time division multiple access (SS-TDMA) mode. However, in the near term, the burden of supporting the required downlink capacities falls on the satellite RF amplifier. The available RF power is dependent on the gain, efficiency, weight and reliability of the amplifier employed. These performance characteristics are determined by such factors as: The generic device (i.e.,

solid-state or thermionic); the specific device technology (e.g., IMPATT diodes versus FETs or helix versus coupled-cavity TWTAs); the number of devices employed (single-envelope or distributed amplifier) and the method of combining them. There are numerous potential tradeoffs between these technologies and they represent long-term technology opportunities at EHF. As the development of RF power amplifiers represents the most significant hardware development at EHF, these technology options should be pursued in depth; recommendations are made for specific areas to be addressed.

C. Ground Segment

In typical SATCOM systems, a larger carrier power-to-noise density ratio (C/N_0) is achievable for the uplink than for the downlink, due primarily to the higher available transmitter power of the ground terminals. Consequently, SATCOM systems are designed to have larger uplink margins in order to insure that the downlink is indeed the limiting factor in determining system C/N_0 . Operation at EHF may require even larger uplink margins to mitigate the attenuation due to rain* and thereby afford the required uplink C/N_0 .

For fixed terminals carrying high data rate traffic to a node, it is probably more cost effective to increase their uplink availability by increasing their uplink margin. This is a viable alternative to employing site diversity on the uplink with its concomitant problems of data buffering, switchover and interruptions (the viability of site diversity is addressed in detail in Section VII). Assuming the uplink satellite antenna gain to be dictated by the coverage area required, the increase in uplink margin must be provided by an increase in the ground terminal's EIRP. For large fixed terminals, the antenna gain is limited by the antenna surface and antenna tracking accuracies. It is then judicious to maximize the available RF power, within practical economic and technological limits, to provide the required uplink margins.

For mobile terminals, the use of site diversity is irrelevant and uplink

* Rain attenuation margins and other EHF propagation considerations are addressed in Section VII.

margin alone* may have to provide the required availability. Antenna size is obviously constrained for airborne and shipboard terminals. In addition, although antenna tracking accuracy does not impose a limit on antenna gain for mobile terminals, the cost and complexity of the required technology is a constraint. Maximizing RF power output, within the limits imposed by the terminal on the weight, power consumption and cooling method of the amplifier, is certainly indicated.

3.2 Traveling-Wave Tube Amplifiers

Traveling-wave tube amplifiers (TWTAs) have been used in the ground and space segments of SATCOM systems since the advent of satellite communications. There have been extensive improvements both in TWT technology and theoretical analysis. For lower frequency or lower power applications, solid-state devices may replace TWTAs. However, for high power requirements at EHF, TWTAs will continue their role both in the ground and space segments. This section addresses the current availability, near and long term projections, and technological limits of TWTAs.

A. Ground Segment

For the ground terminals, coupled-cavity TWTAs are capable of providing the necessary power and bandwidth required at EHF and are reasonable extensions of current technology. However, the need for improved efficiency, reduced cost and increased power in the long term will require continuing development efforts.

1. Current Availability

A survey of domestic manufacturers of TWTAs at EHF shows the following tubes developed by Hughes: a 200-watt, air-cooled TWI (Model 914H developed for SATCOMA) operating from 30 to 31 GHz with 36 dB gain and 25% efficiency⁽⁹⁾ (A complete transmitter incorporating this tube is being integrated into the 30/20 GHz terminal being developed by SATCOMA.); a 100-watt, air-cooled TWT

* For a given availability, the system tolerance to short delays in communications may significantly reduce the margin requirements (Section VII). However, the margin requirements will still exceed those of "clear weather" operation.

(Model 913H developed for NOSC) operating from 36 to 38 GHz with 45 dB gain and 25% efficiency (This TWT was developed as a back-up for LES-8/9 communications experiments.); a 250-watt, liquid-cooled TWT (Model 915H developed for NOSC) operating over a 2 GHz band at 44 GHz with 50 dB gain and 25% efficiency. It should be noted that other domestic TWT manufacturers do not have comparable tubes available above 18 GHz. TWTAs providing power levels of 300 to 800 W at 30 GHz have been developed by Nippon Electric Company⁽¹⁰⁾ (NEC) for the ground segment of the Communication Satellite experiment (CS). Other notable TWT developments are due to Siemens and include: a 1000-watt, liquid-cooled TWT (Model RW 3010)⁽¹¹⁾ operating from 36 to 38 GHz with 41 dB gain and 25% efficiency (transmitters incorporating this tube have been used in airborne (AFAL AN/ASC-22) and submarine (NOSC) communications experiments with LES-8/9); a 500-watt, liquid-cooled TWT (Model V-784)⁽¹²⁾ operating over a 2 GHz band at 44 GHz with 43 dB gain and 25% efficiency (This tube has been incorporated in an airborne terminal (AFAL AN/ASC-28) and will be flight tested later this year); a 1200-watt, liquid-cooled TWT operating over a 2 GHz band at 30 GHz with 43 dB gain and 25% efficiency is under development (German Space Administration) and should be available in mid-1979. These tube developments demonstrate an adequate technology base to support EHF power amplifier requirements, in particular for the mobile users. For the large fixed terminals, development of higher power tubes may be indicated as an alternative to site diversity for providing required availability on the uplink. The development of TWTs with output power > 1 Kw will require the use of solenoid focusing (the tubes previously described employed periodic-permanent magnet (PPM) focusing). A solenoid-focused tube has been developed⁽¹³⁾ which provides 5-Kw power output from 14.0 to 14.5 GHz (Hughes Model 870H) and a tube is under development (Hughes Model 813H) with 1000-watt power output over a 1 GHz band at 55 GHz with 25 dB gain. The results of this survey of current TWT capabilities are summarized in Table 3.1. Note that the tubes are categorized by focusing technique, PPM or solenoid, and cooling method, forced-air (FAC) or liquid (L).

TABLE 3.1
TWTA SURVEY: GROUND SEGMENT

FREQ (GHz)	MFG/ MODEL	POWER (W)	EFF (%)	GAIN (dB)	BW (GHz)	COOLING	COMMENTS*
30	Hughes 914H	200	25	36	1.0	FAC	Developed for SATCOMA
37.4	Hughes 913H	100	25	45	2.0	FAC	Developed for NOSC
30	Siemens --	1200	25	43	2.0	L	Under Development Available Mid '79
37.4	Siemens RW-301C	1000	25	41	1.5	L	AFAL/NOSC LES 8/9 Experiments
44	Hughes 915H	250	25	50	2.0	L	Developed for NOSC
44	Siemens V-784	500	25	43	2.0	L	Developed for AFAL AN/ASC-28
55	Hughes 813H	1000	--	25	1.0	L	Under Development Solenoid
55	Hughes 819H	5000	--	20	1.0	L	Lab Demonstration Solenoid

*All tubes are PPM focused unless otherwise indicated.

2. Projected Availability

The projected limits on TWTA output power are dependent upon the technology of the constituent tube parameters, e.g., cavity, cathode, and thermal designs. The relationship between power output and frequency is also dependent upon these specific design parameters. The results of a survey of TWTA power limitations based on current technology are presented in Fig. 3.1. Although there is some variability in these estimates they are believed to be representative; the power output is assumed to be related to frequency (F) as F^{-2} . Also included in Fig. 3.1 is the estimated performance of advanced TWTA's based on current laboratory demonstrations of 5 Kw at 55 GHz and 1 Kw at 94 GHz (Hughes Malibu Laboratory). Note that these tubes are experimental and do not represent current technology. As a large-scale development effort would be required to bring this technology to production readiness, this capability will probably not be available until the 1990's.

3. Pulsed Tubes

The use of satellite-switched time division multiple access (SS-TDMA) employing time-hopped beams has potential application in future EHF systems. The narrow time-hopped beams offer obvious advantages over an area-coverage beam in reducing the size, complexity and cost of the ground terminals, and in improving the anti-jam (AJ) protection. In a TDMA system it is generally assumed that: the ground terminals operate in a burst mode through a single dedicated wideband transponder; and each terminal utilizes the entire available bandwidth for the minimum time required to satisfy its throughput capacity. Two advantages are attributed to a TDMA system compared with an FDMA system: 1) if the user's peak transmit power is proportional to the burst rate, higher system capacity can be achieved for the same bandwidth (assuming the TDMA synchronization, time guard bands, etc. are optimized); 2) by utilizing a narrow time-hopped beam on the satellite, additional AJ protection is afforded via the beam discrimination. The realization of these advantages is predicated on the user's capability to maximize his energy per bit both against noise and jammer signals. A typical TDMA user in an N-user system

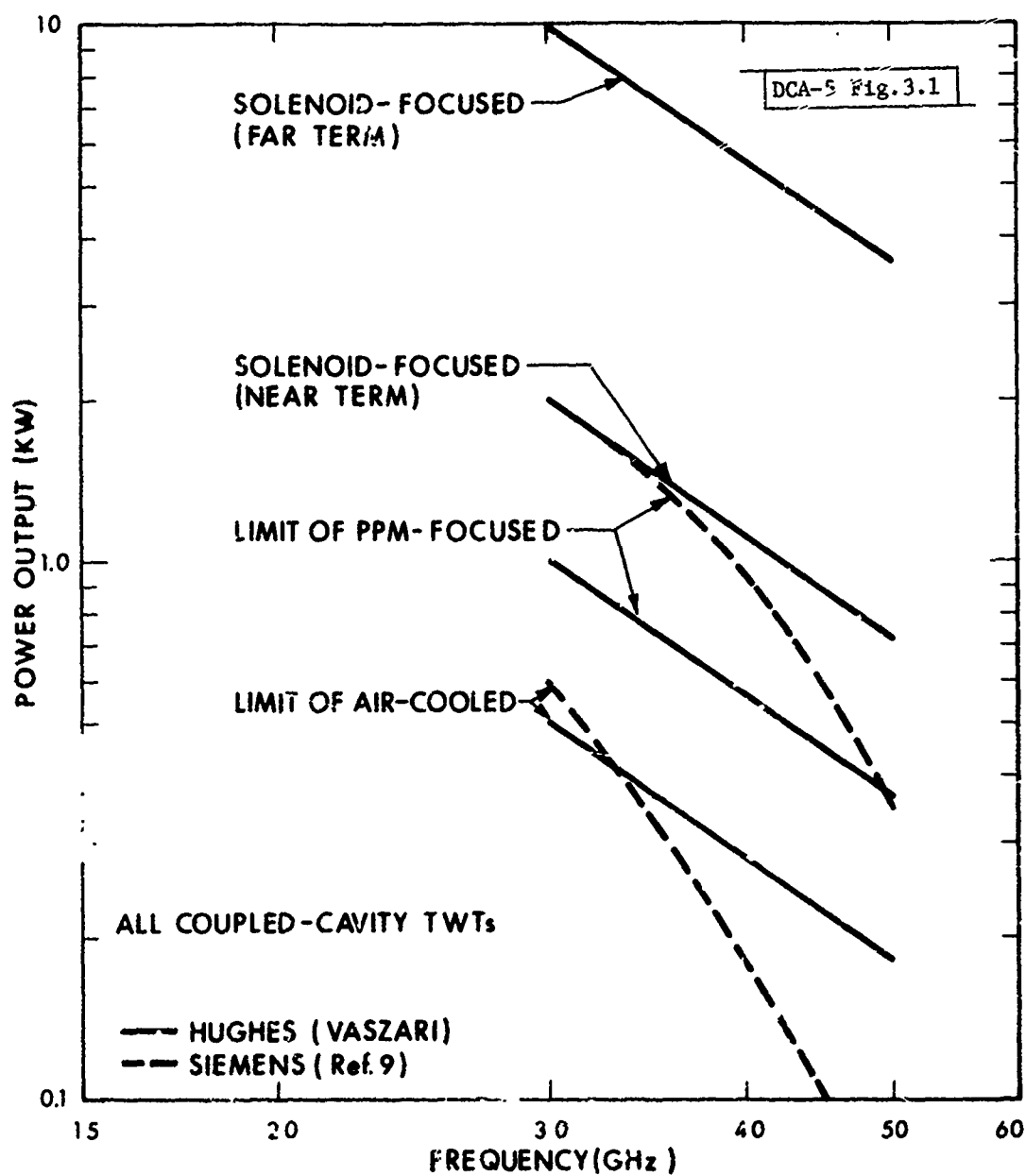


Fig. 3.1. RF power-output projections: ground-segment TWTAs.

would communicate at the same average data rate, R_d , as an FDMA user, but the TDMA transmissions would occur in bursts at a rate equal to NR_d . However, with current peak-power-limited transmitters, TDMA users would have only $1/N$ times the energy per bit and $1/N$ times the jamming resistance of FDMA users. Consequently, without the development of average-power-limited transmitters, the potential advantages of TDMA cannot be realized. Current communications amplifiers (TWTAs) are typically broadband, CW devices and are peak-power-limited, i.e., the output power of the tube is limited by breakdown considerations rather than thermal dissipation. Consequently, operation at a lower duty cycle does not afford a proportionate increase in peak output power. Conversely, tubes developed for radar applications (e.g., klystrons) are noted for their peak output power at a very low duty cycle but lack the necessary bandwidth to utilize the full transponder capabilities for the wide bandwidths afforded at EHF. The development of EHF average-power-limited transmitters having the required communications characteristics (bandwidth, linearity, etc.) must be undertaken to support the future implementation of TDMA.

4. Gyrotron

The electron-cyclotron maser or gyrotron is currently in the early stages of development^(14, 15) and offers the potential capability for producing extraordinarily large power output at EHF frequencies (e.g., 200 kW CW at 28 GHz has already been achieved). It is included here for possible far-term applications for large fixed terminals either for providing larger uplink margin or for potential use in TDMA applications. The present application of the gyrotron is for plasma generation and future use in communications systems will require solving the problems of coupling, propagating and radiating power levels which exceed the RF-breakdown of standard waveguide components. However, considering the gyrotron's potential, its future use in microwave applications (e.g., radar systems) is inevitable, and it remains to determine if the gyrotron characteristics (efficiency, gain, bandwidth, etc.) are amenable to communications usage. It is recommended that future applicability of the gyrotron to EHF communications be studied.

5. Summary

The current, and projected near-term and far-term availabilities of RF power amplifiers are presented in Table 3.2. The projected capabilities for liquid-cooled, PPM-focused TWTAs appear adequate to support the strawman mobile terminals; the development of specific tube capabilities at the required frequencies remains to be undertaken. For air-cooled TWTAs, the projected power capability is $\approx 1/2$ that for liquid cooling, and further studies of specific terminal requirements and restrictions are indicated. For the large fixed terminals, potential power outputs are available which range from a few kW (PPM-focused TWTAs) to tens of kW (gyrotron). However, the cost and development efforts associated with the various technologies required must be assessed vis a vis alternative approaches to providing large uplink margins and/or to implementing TDMA. Future system studies should address these trade-offs.

The evolution of MILSATCOM systems over the next decade affords the opportunity to develop improved RF transmitters for the ground segment. While initial demonstrations of EHF MILSATCOM capabilities may be supported by current commercial technology, the long-term technology development efforts to support operational deployment should address improved performance, extended life and reduced costs. Among the specific areas warranting development effort are:

1. Incorporate latest design technology (e.g., cavity, cathode, collector, etc.) including European developments to increase power and efficiency.
2. Extend tube lifetime (1000's of hours) with improved thermal designs, encapsulation developments, etc.
3. Reduce costs by developing new circuit designs to simplify manufacturing processes.

TABLE 3.2

RF POWER AMPLIFIER AVAILABILITY: GROUND SEGMENT

AMPLIFIER* TYPE	POWER OUTPUT (WATTS)											
	PRESENT			NEAR TERM					FAR TERM			
	30 GHz	44 GHz	50 GHz	30 GHz	44 GHz	50 GHz	30 GHz	44 GHz	50 GHz	30 GHz	44 GHz	50 GHz
Air-Cooled TWTA** (Vehicular)	200	-	-	(1) 500	250	200						
Liquid-Cooled** TWTA (Mobile)	-	250/ 500	-	(2) 1000	500	400						
Solenoid-Focused TWTA (Fixed)	-	-	-	2000	1000	800	10K	5K	4K			
Gyrotron***	-	-	-	-	-	-	100K	50K	40K			

*All tubes are coupled-cavity devices.

**PPM focused.

***Potentially an average-power-limited transmitter.

(1) Limit of current air-cooled technology.

(2) Limit of current PPM-focused technology.

B. Space Segment

TWTAs have played a dominant role in space communications and, for high power requirements at EHF, will continue to maintain a significant role. To maintain this role at EHF, critical design improvements must be pursued to provide long life (7 to 10 years), higher efficiencies and higher power.

1. Current Availability

A 4-watt helix TWT (Hughes Model 1294H developed for the CS) operating over a 1 GHz bandwidth in the 17.75 to 21.15 GHz band with a gain of 50 dB and efficiency of 17% is the most notable example of an on-orbit TWT at EHF. Examples of TWT developmental models at EHF include: 5 W at 35 GHz⁽¹⁶⁾ (Hughes) and 10 W at 35-40 GHz⁽¹⁷⁾ (Watkins-Johnson Model 3638). European efforts are currently directed at achieving 10 watts at 20 GHz and are under development by Thomson-CSF and AEG Telefunken. The current availability of space TWTAs is summarized in Table 3.3. Note that the 4-watt tube is the highest power TWT flown in space (CS) at EHF. This tube has not been space qualified to Military specification nor has a tube been built at the specific frequency band of interest. Considering the criticality of space TWTs and the long-term space-qualification and life testing requirements, development efforts in this area should be underway.

It is generally agreed that the practical upper-frequency limit of helix tubes is above 40 GHz and that helix TWTAs will be available for satellite transmitters at EHF. However, for the long term, as system requirements grow, the need for higher output power (e.g., ≥ 100 watts) may arise and may only be satisfied by the coupled-cavity tube. The coupled-cavity TWT offers higher output power at EHF (factor of 3-5 greater than helix TWT), adequate bandwidth for communications applications and efficiencies of 40-50%. An example is the 200-watt tube operating at 12 GHz with an efficiency of 40% which was flown on the Communications Technology Satellite⁽¹⁸⁾ (CTS). A 450-watt tube operating at 12 GHz has been developed both by Siemens and AEG Telefunken. Design studies⁽¹⁹⁾ have been conducted (Hughes) of 100 to 200-watt TWTs operating at

TABLE 3.3

TWTA SURVEY: SPACE SEGMENT

FREQ (GHz)	MFG/ MODEL	POWER (W)	EFF (%)	GAIN (dB)	FW (GHz)	TYPE	COMMENTS
20	Hughes 1294H	4	17	50	1	Helix	Flown on JCS
36	Hughes -	5	22	40	1	Helix	Development Model
35-40	WJ 1257	10	24	28	5	Helix	Development Model
20	Thomson CSF	10	33	50	1.5	Helix	Under Development (1982)
20	AEG Telefunken	11	35	50	1	Helix	Under Development
42	Hughes 944H	100	42	44	0.5	Coupled- Cavity	Under Development for NASA
42	Hughes 943H	200	42	47	2	Coupled- Cavity	Under Study

42 and 85 GHz. Hughes is currently developing (Model 944H) for NASA a 100-watt TWT operating at 42 GHz with 47 dB gain and 42% efficiency. These coupled-cavity tube developments are summarized in Table 3.3. It must be noted that the coupled-cavity TWT is heavier, larger and more costly than its helix counterpart. In addition, experience with coupled-cavity tubes in space is rare. Consequently, coupled-cavity TWTs will only be achievable in the long term and only with substantial development effort and demonstration of tube reliability in a space environment.

2. Projected Availability

As was discussed in relation to TWTA power limitations for the ground segment, the power limits are dependent on the specific technology employed in each of the tube components. For space applications it is necessary to back off the output power from what would be achieved for terrestrial applications because of reliability considerations. The consideration of reliability for space particularly impacts the maximum cathode loading and operating voltages, and the mechanical and thermal design. These parameters also affect the dependence of tube output power on operating frequency. In addition for helix TWTs at EHF, the frequency dependence is affected by the minimum practical beam diameter. A survey of helix TWT manufacturers shows near term projections as: 40 watts at 20 GHz and 10 watts at 40 GHz (Hughes); 30 watts at 20 GHz (design study by Thomson-CSF); 20 watts at 20 GHz and 10 watts at 40 GHz (Watkins-Johnson). Hughes has completed a feasibility study of developing a 50-watt helix TWT capability over the 20 to 40 GHz frequency range and plans to start an internal R&D program this year. This program will incorporate the latest technology (e.g., dispenser cathodes, depressed collectors, etc.) and most significantly will use diamond helix support rods (developed under RADC funding). These diamond support rods provide a substantial increase in the thermal capacity of the TWT circuit and hence in the maximum power output. Based on these efforts, long-term projections are for 75 watts at 20 GHz and 50 watts at 40 GHz. A recent article⁽²⁰⁾ predicts a maximum output power for helix TWTs, based on European technology in terrestrial tubes, of 80 watts at

20 GHz and 12 watts at 40 GHz, and a frequency dependence, $F^{-8/3}$, under the assumption of constant operating voltage. Under the assumption of a required 7-year life, design constraints were imposed, e.g., cathode loading $\leq 1 \text{ A/cm}^2$ and beam voltage $\leq 6 \text{ kV}$, predicted power levels were 30 watts at 20 GHz and 9 watts at 40 GHz. The survey results are summarized in Fig. 3.2. Note the large bounds in the estimated power output. Although these bounds are dependent upon the specific technology assumed, they also reflect considerations of tube reliability. It is imperative that EHF space tube developments commence, in particular, extended life tests, to assure the availability of reliable tubes for future MILSATCOM deployment.

3. TWT Technology Developments

The technology assessment of EHF TWTAs has addressed the current and projected power output with only general references to the need for improvements in efficiency and reliability. However, the further development of TWT technology must be considered as important a task as developing specific tube capabilities based on currently available technology. Basic developments and improvements in TWT technology provide broad support to all MILSATCOM systems as well as to other DoD programs. SAMSO has funded programs in this area with efforts directed toward increasing output power, efficiency and reliability. The goal in the SAMSO TWT reliability program is to double (30% to 60%) the confidence level of a TWT pair (active & spare) for a 10-year on-orbit life. Specific areas being addressed in this regard include improved production and encapsulation processes, failure analysis and reliability assurance, and improved and extended life tests. This TWT improvement program should be provided expanded support and long-term continuity. Recommended areas of TWT technology development to be addressed include:

1. Multi-stage depressed collectors for increased TWT efficiency.
2. Dispenser-type cathodes for increased current-density loading.
3. Materials for the helix, helix support and internal attenuator to reduce loss and operating voltages and increase thermal capacity.

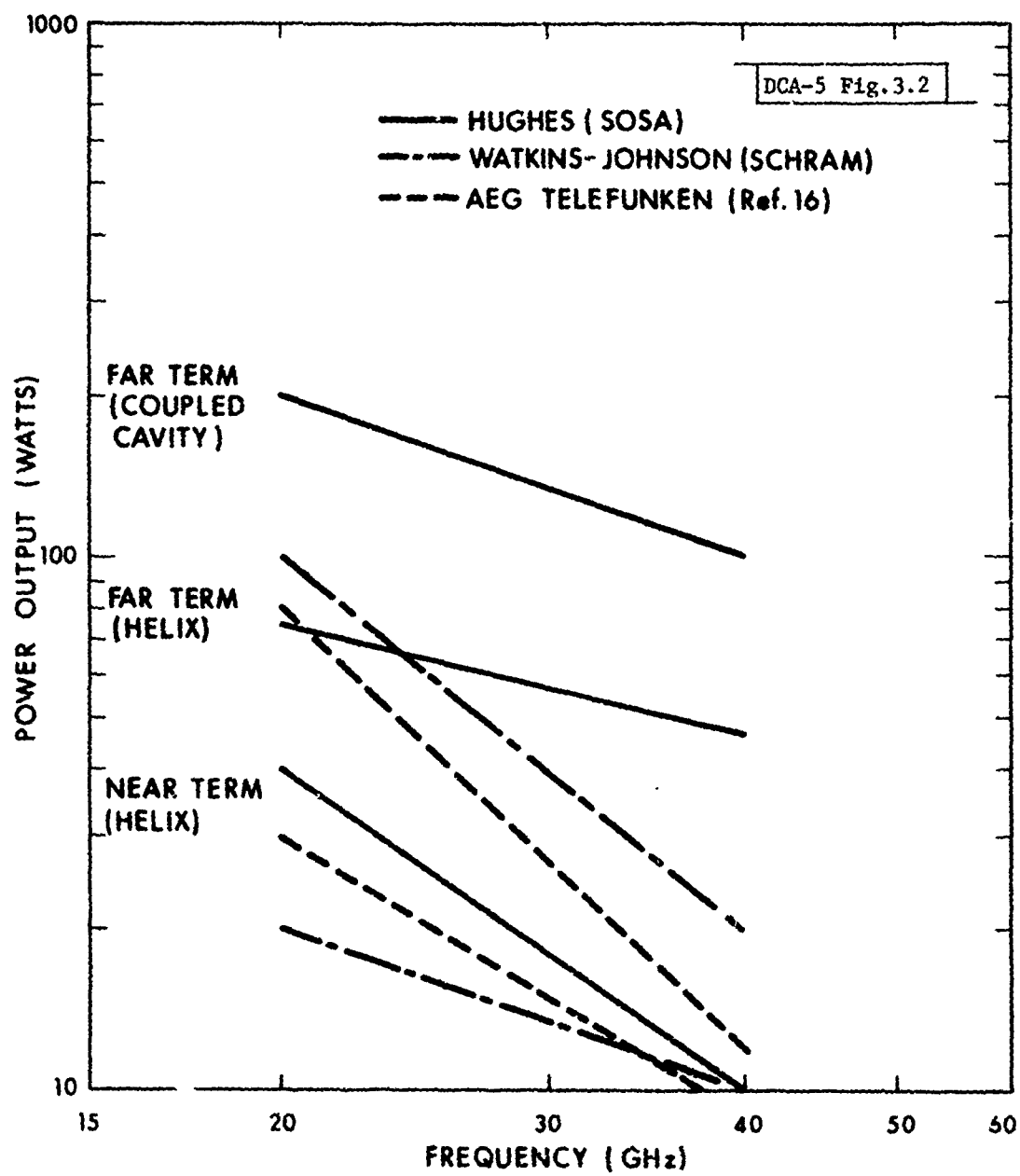


Fig. 3.2. RF power-output projections: space-segment TWTAs.

4. Velocity tapering of the helix both for higher interaction efficiency (pitch reduction) and lower AM/PM conversion (pitch increase), i.e., double-taper helix.
5. Improvements in production, testing and reliability assurance.
6. Improvements in life testing

Develop accelerated and space-simulated life tests.

Begin life-testing phase early in development program.

Develop high-voltage power supply reliability and life tests.

3.3 Solid-State Power Amplifiers

Historically, solid-state devices have long been projected as one-for-one replacements for thermionic devices. In space applications, this has been essentially true with the exception of the TWTA's role as a power amplifier. Recent developments in solid-state power devices (particularly FETs) indicate that they may fill this role at frequencies below 8 GHz and have the potential for assuming this role at EHF. It is unlikely that solid-state amplifiers will surpass TWTA's in output power or efficiency. However, solid-state devices offer the potential for orders-of-magnitude improvements in reliability and reductions in size, weight and voltage requirements. This section addresses the current and future availability of solid-state power devices. The choice between solid-state and TWT amplifiers can only be resolved through parallel, competitive development efforts. It should be noted that advances in antenna technology (e.g., time-hopped-beam phased array) may considerably reduce the requirements for high power in a single envelope and create a unique role for solid-state devices.

A. IMPATT Diodes

IMPATT diodes exhibit negative resistance at microwave frequencies and therefore can be used as RF amplifiers. Their useful upper-frequency limit

may be of the order of several hundred gigahertz rendering them a candidate device for EHF amplifier applications. IMPATT diodes offer the highest potential added power of any solid-state device at EHF but have two inherent difficulties. The potential high reliability attributed to solid-state devices has only recently been approached for IMPATT diodes. The basic reason for the difficulty in achieving high reliability is that efficient charge carrier multiplication requires high current density across the junction, raising the junction temperature, i.e., maximum power output and efficiency are achieved just below diode burnout. Recent improvements in thermal design have somewhat mitigated this difficulty. The second difficulty with IMPATT diodes, being negative resistance devices, is that there is no isolation between input and output. Consequently, circulators are required between amplifier stages increasing the weight and loss. Achieving broadband, stable amplifier performance then requires careful amplifier design. In addition, as IMPATT diode amplifiers are highly nonlinear, their application is restricted to angle-modulated, single-carrier systems. However, the trend toward TDMA provides an ideal application for the saturated operation of IMPATT diode amplifiers. This section assesses the current and projected power-added capability of IMPATT diodes; questions regarding stability, reliability and failure modes of IMPATT amplifiers must be addressed in future development efforts.

1. Current Availability

IMPATT diode technology is rapidly advancing at EHF under SAMSO/AFAL sponsorship. The most notable results to date are the laboratory demonstrations of ≈ 1.2 watts at 40 GHz with 17% efficiency (Raytheon). These are mid-contract results of a two-year program with a goal of 2 watts (1.9 watts was achieved at 36 GHz). The diodes are Ga As double-drift (essentially a series-connected pair of single-drift diodes with improved efficiency and high power capability) Read-profile devices. The added power achieved is approximately the same as the best silicon IMPATTs and the efficiency is higher than the best silicon double-drift (DD) devices. It should be noted that the added power capability would have to be degraded $\approx 25\%$ for high-reliability operation; reliability tests are now in progress. It is generally agreed that

within the EHF band, added power capability may be scaled as F^{-2} (Fig. 3.3). Based on the 40 GHz results, IMPATTs could provide 4 watts with an efficiency approaching 20% at 20 GHz. AFAL is planning Ga As Read diode development at 20 GHz with goals of added power >5 watts and efficiency >20%; this development effort should commence immediately.

2. Projected Availability

Long-term projections of potential IMPATT capability predict a factor of 2 to 4 increase in output power over devices currently under development (Fig. 3.3). The realization of such devices is obviously contingent upon research funding; commercial interest in EHF devices is currently negligible and may not change in the foreseeable future. The particular areas of interest for development, for near-term as well as far-term improvements, include improvements in:

1. thermal designs, e.g., diamond heat sinks.
2. profiles for increased efficiency.
3. impedance matching, e.g., integrated matching circuits.
4. higher-yield, lower-cost manufacturing technology.
5. reliability and life testing.

B. Ga As FETs

Gallium arsenide field-effect transistors (Ga As FETs) have recently developed to the point where they are a candidate replacement for TWTs as satellite power amplifiers at 8 GHz. Their application at 20 GHz can be realized in the near term and they offer the potential for application at 40 GHz in the long term. The interest in developing FETs over IMPATTs stems from the following advantages:

1. linear amplification
2. higher efficiency

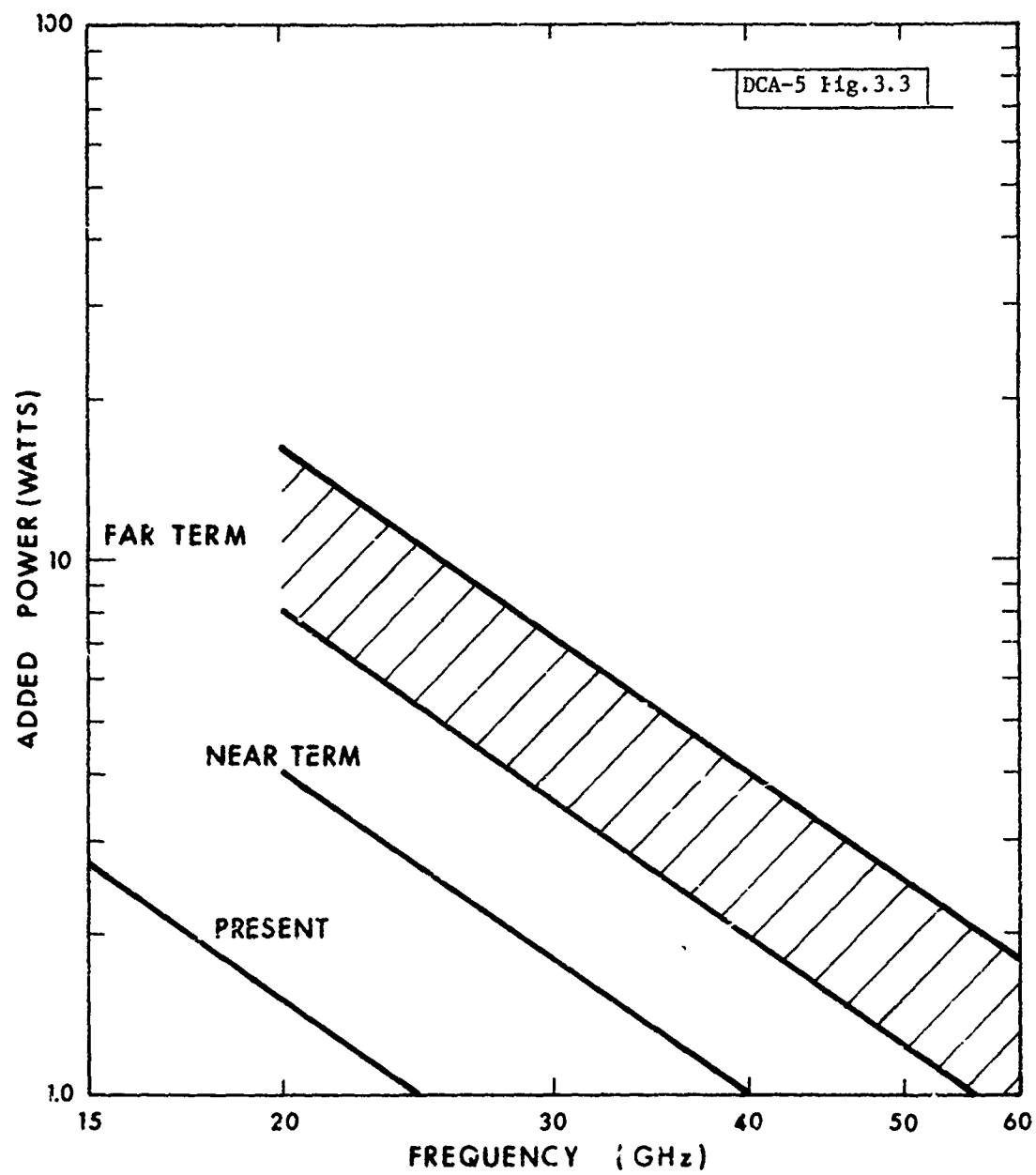


Fig. 3.3. RF power-output projections: IMPATT diodes.

3. wider bandwidth
4. lower noise figure
5. ease of combining

However, the availability of IMPATTs with useful added power capability across the EHF band is a certainty and, in this band, IMPATTs will provide typically a factor-of-four higher power than available FETs. The choice of the particular solid-state device will depend upon the operating frequency, required amplifier characteristics (primarily the need for power or linearity) and developments in the respective technologies.

1. Current Availability

At the present time, power FETs have not been designed for operation at EHF (Fig. 3.4). However, their performance at lower frequencies is impressive. At 4 GHz, 15 watts⁽⁷⁾ has been achieved for a single device by Bell Laboratories (3 dB gain) and Fujitsu (5 dB gain). At 8 GHz, 5 watts has been achieved with 5 dB gain and 35% efficiency (Texas Instruments for AFAL and NRL). A notable example of current high power/high frequency capability (Texas Instruments) is the achievement of 1.1 watts at 16 GHz with 4 dB gain and 30% efficiency. This device provides 0.85 watt, 4 dB gain and 24% efficiency at 18 GHz and could provide 0.5 watt at 20 GHz (this device is not optimized for these higher frequencies). Current FET devices are designed with high enough cutoff frequencies so that the power-per-unit gate width falls off slowly with frequency up to 16 GHz (e.g., from 1.2 W/mm at 4 GHz to 0.9 W/mm at 16 GHz). Above 16 GHz, device output power will decrease as F^{-2} . The inherent problems are in the device fabrication and implementation at these higher frequencies, i.e., uniform illumination of the device without phase errors, parasitic effects and circuit matching to the device.

2. Projected Availability

Based on current power FET performance at 16 GHz, the realization of 20-GHz devices is assured. Under SAMSO/AFAL sponsorship, the development of a 20 GHz

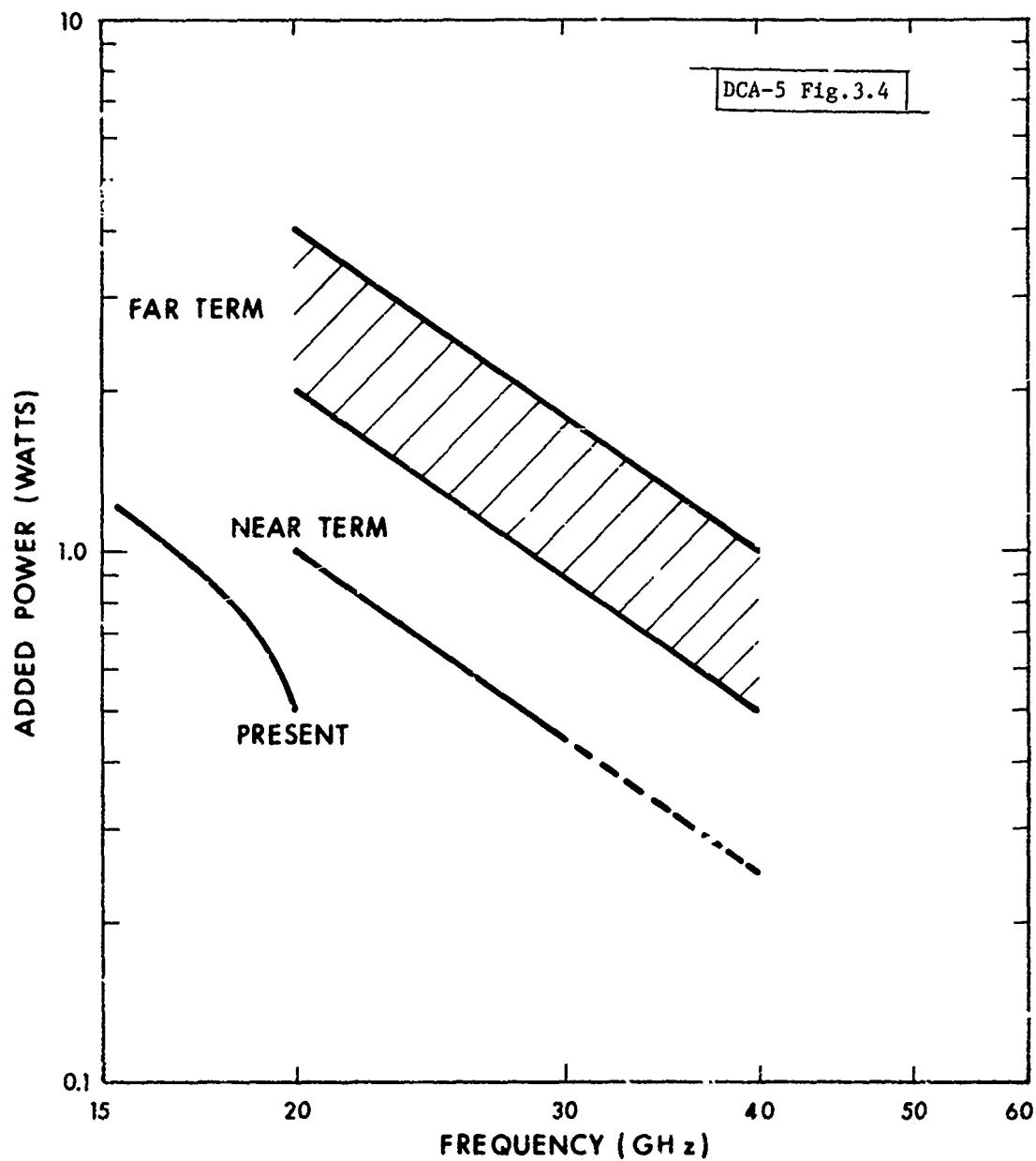


Fig. 3.4. RF power-output projections: GaAs FETs.

FET has begun (Texas Instruments) with goals of 1 watt added power and 25% efficiency. Simple extrapolation would predict a useful power level of 0.25 watt at 40 GHz (Fig. 3.4). However, the fabrication and implementation technology is not currently available to realize such devices. As no FET development effort is now directed at this frequency band, R&D support will be required to provide far-term availability of 40 GHz power FETs. In the far-term, further improvements in the performance of Ga As power FETs are anticipated, particularly at EHF. These improvements will require innovative device designs to yield lower thermal resistance, reductions in parasitic reactances, more uniform drain-current distribution under the gate, and improved impedance matching of large gate-width devices. In the far term, increases in added power of a factor of 2 to 4 (2- to 4-watt devices) are projected (Fig. 3.4) at 20 GHz. At 40 GHz, gate lengths much shorter than $1\text{ }\mu\text{m}$ will be required to achieve sufficient gain. Short gate lengths have been avoided in power FETs due to lower drain-gate breakdown voltage. Further developments in device physics and device parameter tradeoffs will be required to achieve potential power capabilities at 40 GHz (e.g., 1/2 to 1 watt).

C. Power Combiner Technology

The power limitations of individual solid-state devices can be considerably extended by power-combining techniques. Possible power-combining techniques include internal package combining, external circuit combining, and spatial or antenna combining.

In-package combining, e.g., paralleling elementary devices within one package, should be pursued within the limits imposed by manufacturing technology and parasitic reactances on reliability and bandwidth. Currently there is little or no effort directed toward power combining FETs at the chip level and this area warrants investigation. For IMPATTs, the potential improvement may be considerably less as it is difficult to achieve proper load sharing between multiple negative-resistance devices.

As discussed previously, spatial or antenna combining (i.e., individual amplifiers on each feed or array element) offers a unique role for solid-state

devices. The anticipated device power requirements are of the order of a watt at EHF and appropriate devices should be available with continuing development efforts (in the near term, FETs or IMPATTs at 20 GHz and IMPATTs at 40 GHz). The area requiring additional development is the study and evaluation of power-combining antenna performance, in particular, the degradation in antenna performance due to phase and amplitude differences among the individual amplifiers and due to individual amplifier failures. Testing of an 8 GHz power combining antenna (32-element array feed for a 12-ft. Cassegrain antenna developed by JPL for NASA) is currently in progress under SAMSO/AFAL sponsorship. Future antenna development programs should address the power combining performance of the specific antenna designs (phased array or multiple-beam antenna) and solid-state devices intended for EHF SATCOM use.

External circuit combining affords the opportunity for achieving medium power (tens of watts) solid-state amplifiers. The primary disadvantages of circuit power combiners are the increased weight and circuit losses. However, the potential advantages of distributed thermal loads, reduced operating voltages, higher reliability and graceful degradation* make the solid-state amplifier a viable alternative to the TWT. Circuit combiners may be generally classified as resonant and nonresonant. Among nonresonant combiners, the simplest to implement is an N-level binary network of cascaded 3-dB hybrids combining 2^N devices. This approach provides good heat sinking and graceful amplifier degradation. However, the weight and cumulative losses of the hybrids limit the practical number of combining levels (e.g., $N=4$). An alternative nonresonant combiner is the single, N-way power divider/combiner. While more difficult to design, the single multiport combiner has considerable advantage in size and weight over the binary combiner and maintains the graceful degradation characteristics of the latter. In resonant combiners, power combining of individual devices takes place in a single cavity via coupling of the electromagnetic fields. Resonant combiners are more compact and lightweight than binary combiners and may be applied to two-terminal devices. However, the cavity size limits the practical number of devices to be combined

* Ideally, failure of one or more devices in the combiner results in a proportionate loss in output power, not in complete amplifier failure.

(particularly at EHF) and the degradation characteristics with device failure are not well understood. Due to the inherent characteristics of IMPATT diodes, power combining techniques are limited to binary networks and resonant cavities. The size, weight and loss penalties associated with binary dividers has been discussed; development efforts in IMPATT amplifiers have consequently been directed toward cavity combiners. Previously reported results include a 5-watt, 37-GHz IMPATT amplifier (TRW/AFAL)⁽²¹⁾ utilizing a cylindrical-cavity resonator. Current efforts include a 41 GHz amplifier with goals of 10 watts output power, 10 to 15% efficiency and 7-year life (TRW/AFAL). This program will investigate the performance characteristics of rectangular as well as cylindrical cavity combiners and will emphasize reliability and failure-mode analyses. A similar effort is planned at 60 GHz using Si DD IMPATTs (Hughes) with a goal of 5 watts using a rectangular-cavity combiner. For FETs, non-resonant combining techniques may be applied and have been demonstrated at X-band. Recent developments include combining 12 FETs in a radial combiner⁽²²⁾ with a combining efficiency of 90% over a 30% bandwidth at 8.5 GHz, and combining 6 FETs in a planar network⁽²³⁾ with a combining efficiency of 80% over a 40% bandwidth at 10 GHz. Future projections⁽²⁴⁾ predict a 40-way radial combiner providing 100 watts over the 8-12 GHz band. Development of power combiner networks for FETs is a current SAMSO/AFAL program (Raytheon). The initial phase will study combiner technology applicable to combining up to 20 devices at frequencies up to 20 GHz. It is assumed that the on-going FET developments at 20 GHz will be time-phased with this effort. Future developments must address the viability of FET combiner techniques at 40 GHz.

3.4 Summary

1. Ground Segment

For the ground segment, an adequate TWTa technology base exists to support projected CW high power amplifier requirements (Table 4.2). An exception may be for terminals restricted to air cooling with a concomitant restriction on output power. Otherwise, liquid-cooled TWTAs offer adequate power capability to support mobile terminals. For large fixed terminals, the potentially available

power ranges over orders-of-magnitude (1-100 kw): however, the cost and development efforts associated with the various technologies must be assessed. Detailed system studies must be conducted to delineate the required tube capabilities and the development of specific TWTAs undertaken. In these TWTA developments, incorporation of the latest technology and cost-reduction processes must be emphasized. As regards the future implementation of TDMA and time-hopped-beam satellite antennas, the development of average-power-limited TWTAs is required to achieve the potential advantages.

2. Space Segment

The potential availability of both solid-state and TWT power amplifiers at EHF affords the opportunity to employ the optimum device for the specific application. This competition between solid-state and TWT devices is not only on a one-for-one replacement basis. While there are medium power requirements (10 to 20 watts) where this is true, there are also unique applications for each. Requirements for higher power (100 watts) in a single envelope (e.g., wideband data relay users) will best be served by TWTAs. Requirements for individual power amplifiers (1 watt) on each feed or array element (e.g., time-hopped beams for mobile users) would best be served by solid-state devices. Consequently, parallel development efforts are recommended in both areas. The potential RF amplifier availabilities for these technologies are summarized in Table 3.4. As regards TWTAs, development of a 20-watt TWTA operating at 20 GHz should be undertaken immediately to insure the achievement of high reliability. The capability of helix TWTAs at 40 GHz should be studied and appropriate developments undertaken. Development efforts (SAMSO/AFAL) directed at IMPATT and FET devices and related combiner technology should be expanded and provided long-term continuity. Reliability testing must be emphasized in device development efforts to insure that increases in their power capability are not made at the expense of their potential high reliability. Developments in combiner technology must also emphasize failure mode analysis and testing, as well as communications performance testing (e.g., AM/PM conversion, BER, etc.).

TABLE 3.4
RF POWER AMPLIFIER AVAILABILITY: SPACE SEGMENT

AMPLIFIER TYPE	POWER OUTPUT (WATTS)						
	PRESENT		NEAR TERM		FAR TERM		
	20 GHz	40 GHz	20 GHz	40 GHz	20 GHz	40 GHz	
<u>SOLID-STATE</u>							
IMPATT							
One Device	1	-	4	1	12	3	
Multiple Devices ⁽¹⁾	4	-	40	10			
FET							
One Device	-	-	1	0.2	3	0.5	
Multiple Devices ⁽²⁾	-	-	10	2			
<u>TWTA</u>							
Helix	4	-	20/40	10/20	40/80	20/40	
Coupled-Cavity ⁽³⁾	-	-	-	-	200	100	

- (1) 12-diode resonant-cavity combiner.
(2) 12-transistor radial or planar combiner.
(3) Coupled-cavity TWTA's could be developed in the near term if needed.

IV. ANTENNA GAIN LIMITATIONS

4.1 Background

Gain is perhaps the key performance parameter of single, pencil-beam antennas. The desirability of maximizing the antenna gain to increase EIRP, G/T and AJ performance is obvious. This section addresses the gain limitations on paraboloidal reflector antennas operating at EHF as imposed by current antenna technology.

The gain of an aperture antenna is commonly expressed as

$$G = \eta_T \left(\frac{4\pi A}{\lambda^2} \right)$$

where G = antenna gain (numeric)

η_T = overall antenna efficiency

A = aperture area

λ = free-space wavelength

The parenthetical expression in Eq. 4.1 represents the maximum theoretical gain. The antenna efficiency, η_T , represents the percentage of the aperture area that is effectively used and is the product of the various efficiency factors which reduce the antenna gain. For a circular aperture, it follows that

$$G = \eta_T \left(\frac{\pi D}{\lambda} \right)^2 \quad (4.2)$$

where D is the diameter of the aperture. For the paraboloidal reflector antennas to be discussed, the total efficiency can be expressed* as

$$\eta_T = \eta_I \eta_S \eta_B \eta_X \eta_D \eta_{RS} \quad (4.3)$$

where η_I = aperture illumination efficiency

* Other aperture efficiency factors are often included; these represent the dominant ones.

- η_S = (1 - spillover loss)
- η_B = (1 - aperture blockage loss)
- η_X = (1 - cross-polarization loss)
- η_D = reflector dissipative and/or leakage efficiencies
- η_{RS} = reflector surface accuracy efficiency

The overall antenna efficiency is typically in the range $.55 \leq \eta_T \leq .75$, where the lower value is representative of standard commercial reflector antennas and the upper value represents high efficiency, shaped reflector systems.

The efficiency factors delineated above are primarily dependent on the reflector geometry and feed horn design and, hence, are not dependent on the operating frequency. An exception is the reflector surface accuracy which is fixed by current manufacturing technology and consequently, imposes an upper limit on the maximum useable frequency and corresponding maximum antenna gain. In an analogous manner, antenna tracking accuracy* which is fixed by current technology, the operating environment and platform dynamics imposes an upper limit on the maximum operating frequency and antenna gain. It is antenna surface accuracy and antenna tracking accuracy which are the dominant, frequency-dependent antenna gain factors and which limit the achievable gain for antennas operating at EHF frequencies.

The following sections contain:

1. a review of the loss relationships between antenna gain and surface and tracking accuracy.
2. the current state-of-the-art in these areas and the concomitant gain limitations.
3. a brief assessment of the current technology in radomes.

* Antenna tracking accuracy is not commonly included in the antenna efficiency budget as it does not represent a loss in antenna gain in the rigorous sense; i.e., the antenna gain is unchanged, only the realized gain is reduced in an operational situation.

4. estimates of the technological limits on antenna gain imposed on large, ground-based jammers.
5. recommendation for further studies or improvements in the technology

4.2 Antenna Surface Accuracy

A. Loss Relationships

Antennas with gain greater than about 40 dB are almost always reflector surfaces illuminated by a feed. This is because of either economic considerations or technical limitations. The surface accuracy of a reflector antenna limits the maximum achievable gain; i.e., the achievable gain is maximum, G_m , in the sense that for a given surface tolerance and antenna diameter, increasing the operating frequency increases the antenna gain until it equals G_m . Further increasing the operating frequency will actually decrease the antenna gain. This section first reviews the relationship between surface accuracy and antenna gain. Next empirical relationships between surface accuracy and antenna diameter are presented based on current technology. Finally, the corresponding antenna gain and diameter limitations imposed by the technology are discussed.

The gain of a parabolic reflector antenna, taking into account the loss due to antenna surface accuracy, may be expressed as⁽²⁵⁾

$$G = \eta \left(\frac{\pi D}{\lambda} \right)^2 e^{-\left(\frac{4\pi\epsilon}{\lambda} \right)^2} \quad (4.4)$$

where η is the antenna efficiency when $\epsilon=0$ and ϵ is the rms reflector surface accuracy. The effect of surface errors on the radiation pattern⁽²⁵⁾ is shown in Fig. 4.1 for a circular aperture with tapered distribution^{*}. Shown are the expected power diffraction and scatter patterns for mean-square phase errors of 0.2 and 1.0 corresponding to tolerance gain losses of 0.9 and 4.3 dB, respectively. The complete radiation pattern is the power sum of the diffraction and scatter patterns. Note that the diffraction pattern is reduced by the exponential tolerance factor and that the energy lost appears in the scattered pattern.

^{*}Aperture field distribution of the form $(1-v^2)$, where v is the normalized aperture radius.

78-6-19572

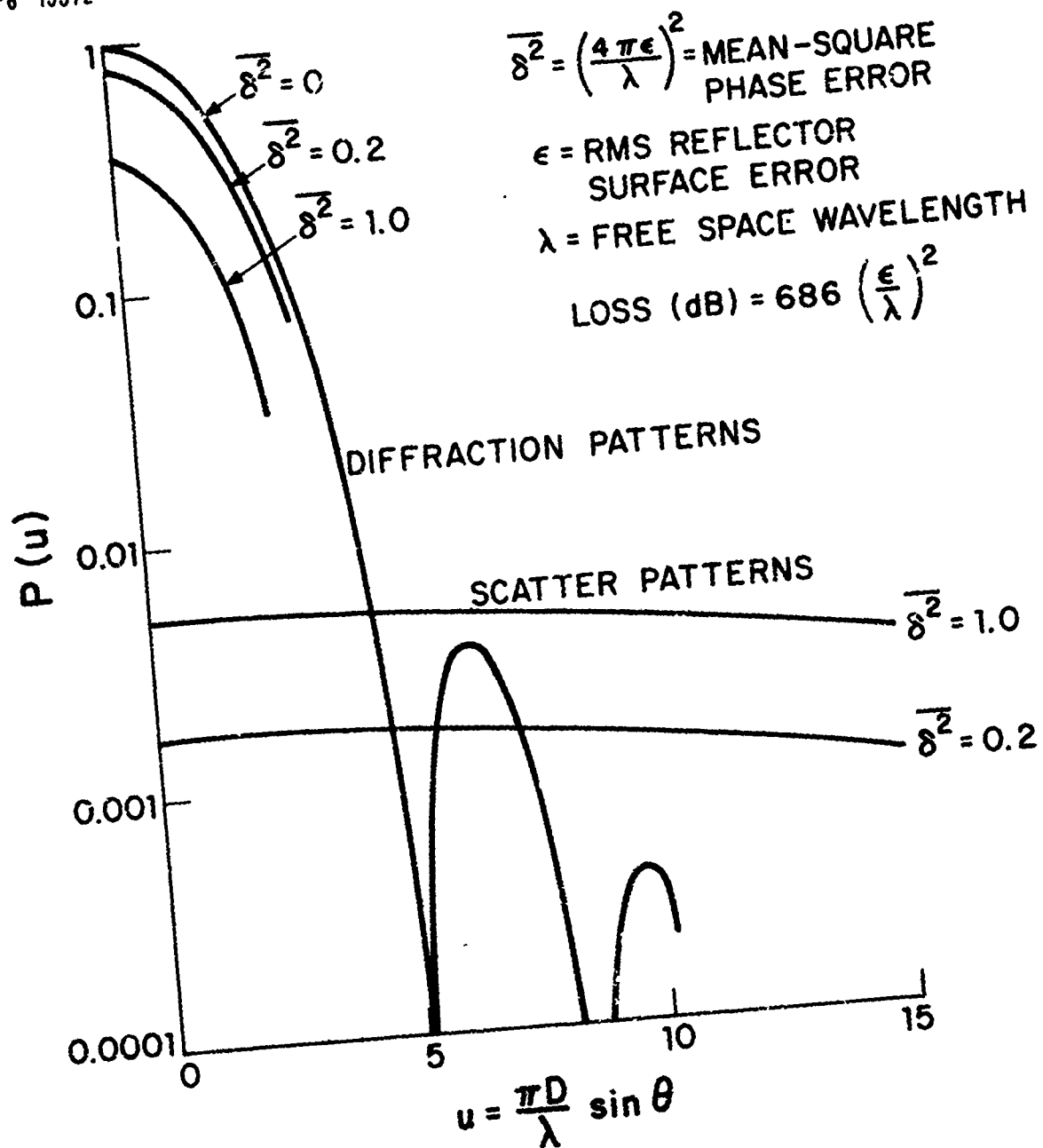


Fig. 4.1. Effect of reflector surface accuracy on antenna radiation pattern.

The exponential loss factor of Eq. 4.4 may be expressed as the loss in gain

$$\Delta G = -686 \left(\frac{\epsilon}{\lambda} \right)^2 \quad (\text{dB}) \quad (4.5)$$

Eq. 4.5 is plotted in Fig. 4.2. A typical goal for antenna surface accuracy is $\lambda/32$ corresponding to a loss of 0.7 dB; a typical upper limit is $\lambda/16$ corresponding to a loss of 2.7 dB. Gain loss versus surface accuracy is presented in Fig. 4.3 with the frequencies of interest as a parameter. Note that at 8 GHz and $\Delta G < 1$ dB, ϵ must be $< .050$ in. and is representative of current commercial production of paraboloid reflectors with $D \approx 80$ ft. or less. Note that at EHF, ϵ must be $< .015$ in. for $\Delta G < 1$ dB.

B. Current Technology

Antennas having diameters ≤ 4 ft. are one-piece reflectors and the currently achievable surface accuracies for antennas of this size are presented in Table 4.1.

Table 4.1
CURRENT ANTENNA SURFACE ACCURACIES ($D \leq 4$ Ft.)

<u>Surface Accuracy (in.)</u>	<u>Manufacturing Technique</u>
.025	Standard stamping or spinning
.012	Precision spinning or molding
.005	Machined casting or molding

In accordance with the results of the previous section, the desired surface accuracy is achievable; the most cost-effective manufacturing process remains to be determined.

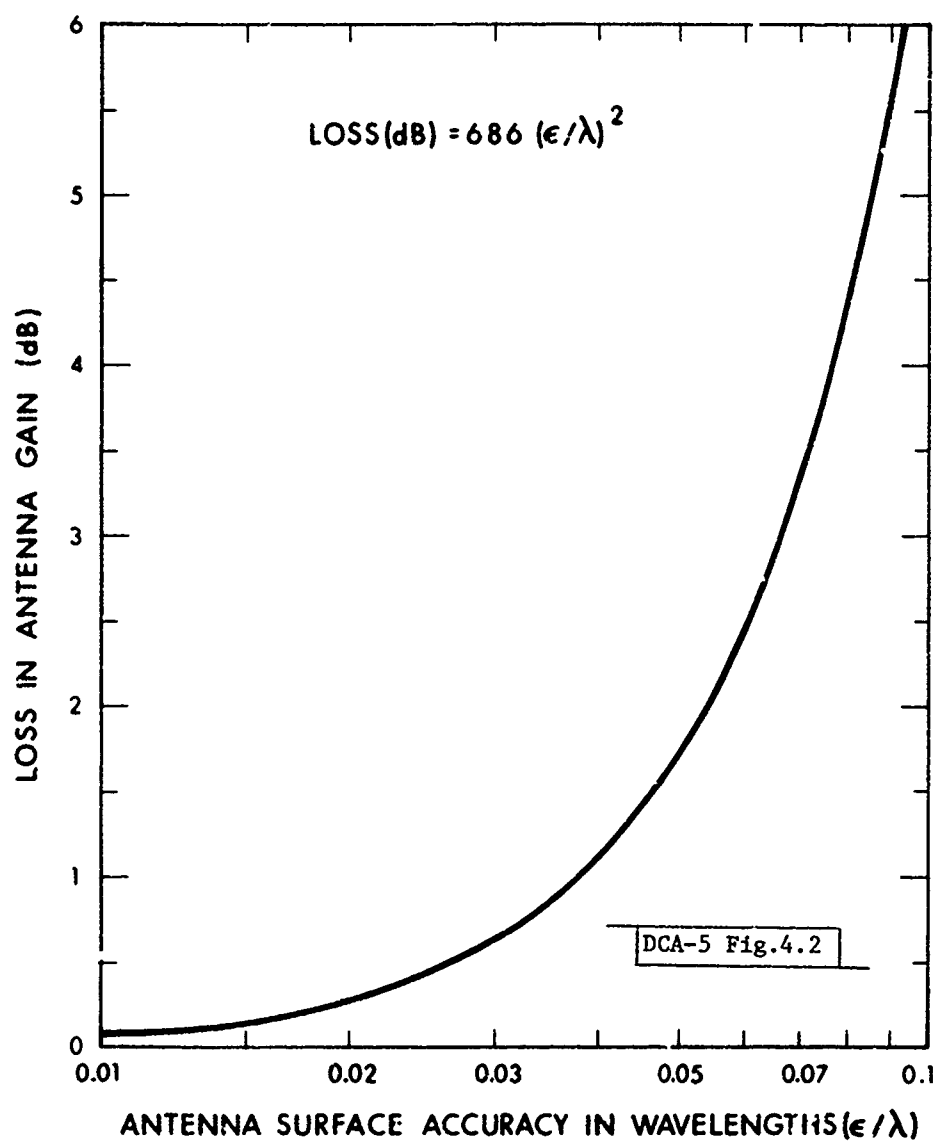


Fig. 4.2. Loss in antenna gain versus antenna surface accuracy in wavelengths.

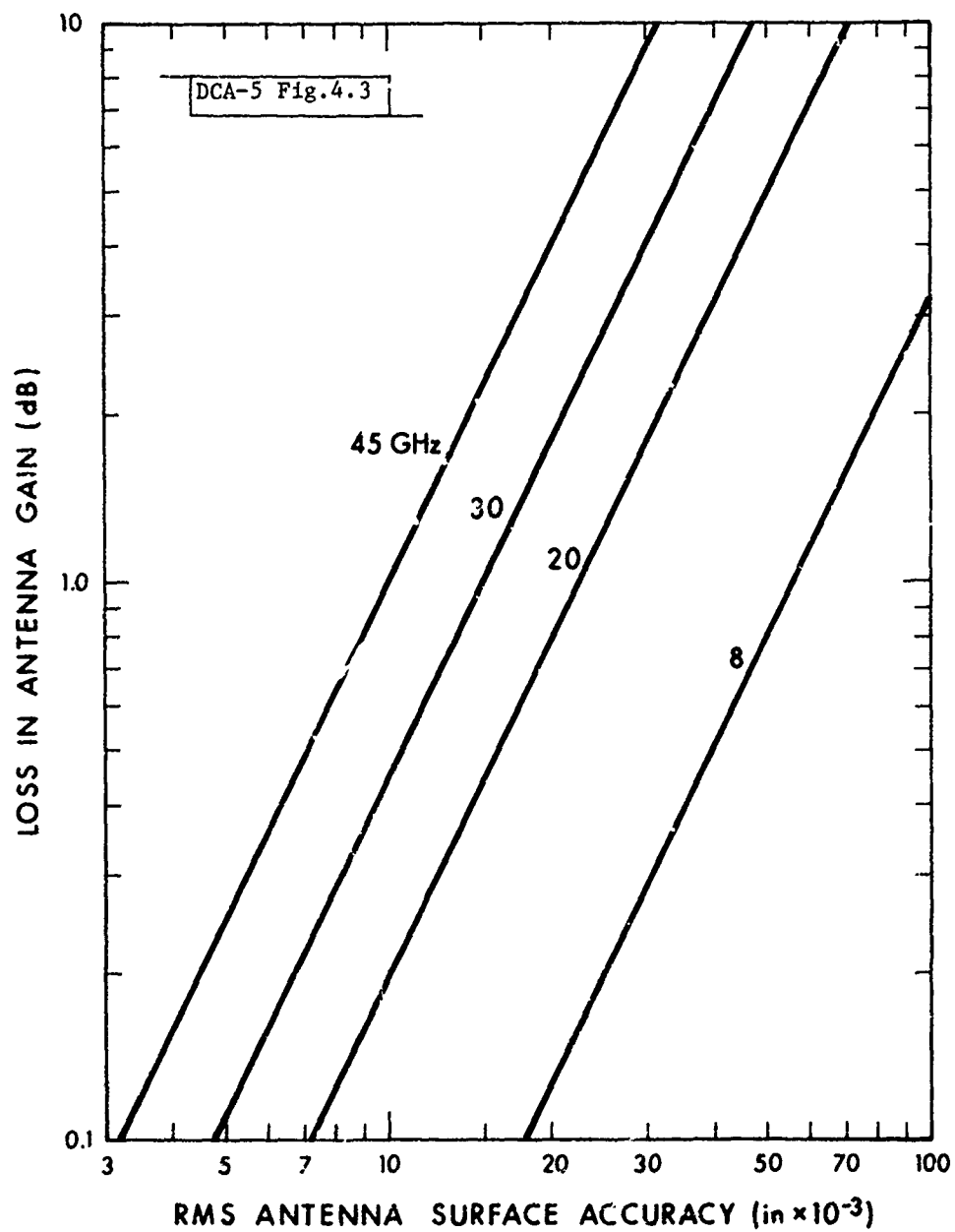


Fig. 4.3. Loss in antenna gain versus antenna surface accuracy with frequency as a parameter.

Antennas having diameter ≥ 8 ft. are typically fabricated from panels and the factors contributing to the operational antenna surface accuracy include:

1. Manufacturing factors

- Panel fabrication
- Backup structure fabrication
- Antenna assembly

2. Environmental factors

- Wind loads
- Thermal gradients
- Gravity

The achievable antenna surface accuracy is of course dependent on the manufacturing process but, for a given process, is related to the antenna diameter. Empirical relationships of the form $\epsilon/D = \text{constant (K)}$ were derived from a limited data base and are presented in Table 4.2 with comments on the relative availability of the corresponding technology. Substituting the relationship between antenna diameter and surface accuracy into Eq. 4.4, yields for the antenna gain

$$G = 10 \log (\eta) + 20 \log \left(\frac{\pi D}{\lambda} \right) - 686 K^2 \left(\frac{D}{\lambda} \right)^2 \quad (\text{dB}) \quad (4.6)$$

Eq. 4.6 is plotted in Fig. 4.4 with the empirical values of K as a parameter for an assumed antenna "efficiency" (η) of 55%. The limiting effect of the antenna surface tolerance on antenna gain is evident. Note that the maximum achievable gain results in a gain loss, $\Delta G = 4.34$ dB ($\epsilon/\lambda = .08$). This loss in gain is unacceptable as it represents an inefficient use of antenna aperture (a gain loss < 1 dB is usually tolerable).

Table 4.2
CURRENT ANTENNA SURFACE ACCURACIES ($D \geq 8$ FT.)

Antenna Diameter (Ft.)	Surface Accuracy (ϵ/D)	Comments
$8 \leq D \leq 20$	2×10^{-4}	Standard Commercial Availability* Limit of Commercial Technology Machined Cast or Molded Panels
	10^{-4}	
	5×10^{-5}	
$30 \leq D \leq 80$	10^{-4}	Standard Commercial Availability* Limit of Commercial Technology
	5×10^{-5}	
	2.5×10^{-5} 10^{-5}	
		Commercially Unavailable Radome-Enclosed Radio-Telescope Technology

*For example, low-cost formed-aluminum panels.

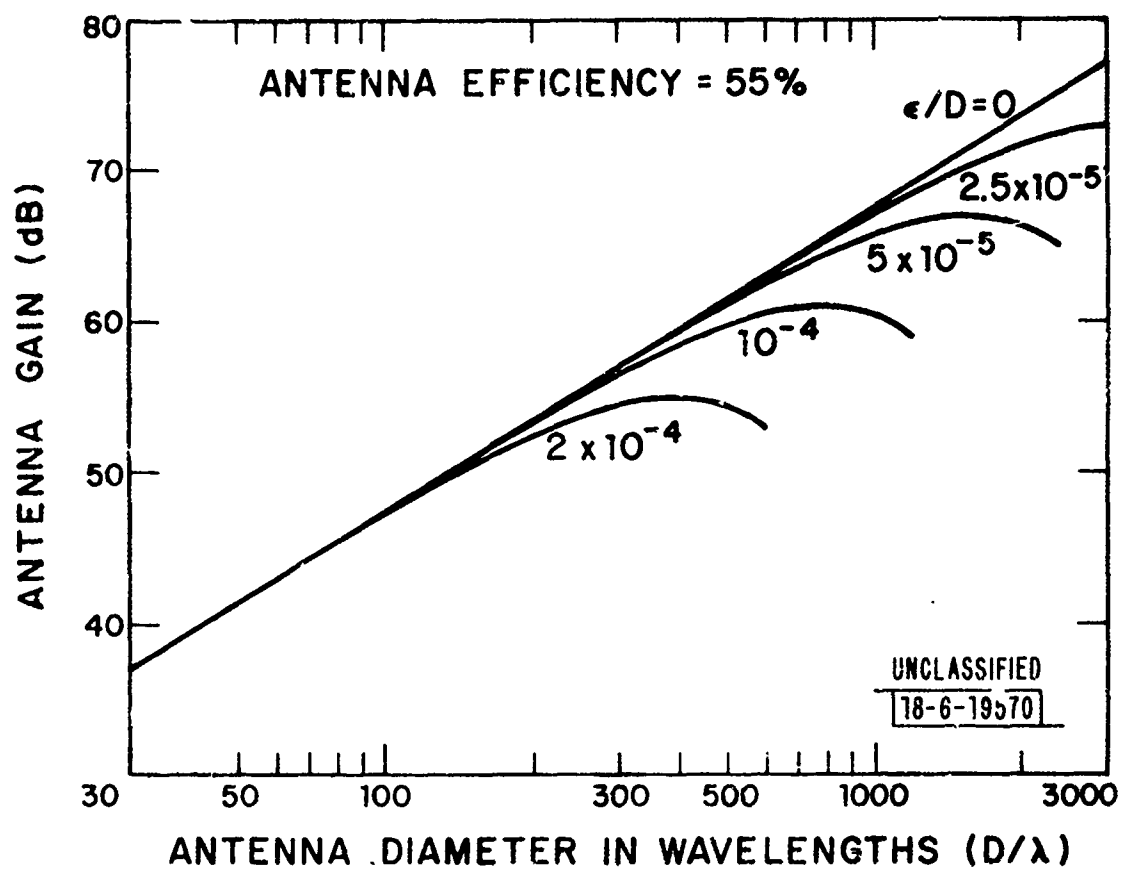


Fig. 4.4. Antenna gain limitations due to antenna surface accuracy.

C. Summary

For the present discussion, 40-ft. diameter antennas are the largest being considered for EHF operation. Table 4.3 presents the gain loss for a 40-ft. antenna based on the available technology. Note that adequate surface accuracy cannot be achieved even at the limit of current commercial technology (i.e., based on potential improvements in the manufacturing and assembly techniques employed for 8/7 GHz antennas). More than adequate surface accuracy is achieved for radio telescopes but this technology is not currently applied to SATCOM terminals. The required surface accuracy falls within these bounds and new technology requires development. Further improvements in commercial technology will require new structural and thermal designs. As the wind and thermal loads are major contributors to the surface accuracy of exposed antennas, the use of radomes may offer a viable alternative.

In summary, for small mobile terminals, the required antenna surface accuracy (.012 in.) can be realized with refinements in current manufacturing techniques; the most cost-effective process remains to be determined. For large fixed terminals ($D \approx 40$ ft.) improvements in current fabrication techniques will not provide adequate antenna surface accuracy. A study must be undertaken to assess the cost and performance tradeoff between the development of new fabrication techniques and the use of radomes.

4.3 Antenna Tracking Accuracy

A. Loss Relationships

Antenna tracking accuracy, the accuracy with which the peak of an antenna's beam can be directed toward a source or receiver, limits the maximum realizable gain. The achievable gain is maximum, G_M , in the sense that for a given antenna pointing accuracy and operating frequency, increasing the antenna diameter increases the antenna gain until it equals G_M . Further increasing the antenna diameter will actually decrease the realized gain in an operational situation. This section reviews the relationship between antenna tracking loss and antenna tracking accuracy and beamwidth, surveys current tracking accura-

TABLE 4.3
LOSS IN ANTENNA GAIN DUE TO ANTENNA SURFACE ACCURACY (D = 40 FT.)

RMS Surface Accuracy (in.)	Loss (dB)			Comments
	20 GHz	44 GHz	50 GHz	
0.048	10.2	22	28	Standard Commercial Technology
0.024	2.6	5.5	7.1	Limit of Commercial Technology
0.012	0.6	1.4	1.8	Required Surface Accuracy
0.006	0.2	0.3	0.4	Radio-Telescope Technology

cies for the various platforms and assesses the concomitant antenna gain limitations.

The gain of a parabolic reflector antenna, taking into account the loss due to antenna tracking accuracy, may be expressed as⁽²⁶⁾

$$G = \eta \left(\frac{\pi D}{\lambda} \right)^2 e^{-2.77 \left(\frac{\Delta\theta}{\theta_3} \right)^2} \quad (4.7)$$

where $\Delta\theta$ = antenna tracking accuracy

θ_3 = antenna half-power beamwidth

The exponential loss factor of Eq. 4.7 may be expressed as the loss in gain

$$\Delta G = 12 \left(\frac{\Delta\theta}{\theta_3} \right)^2 \quad (\text{dB}) \quad (4.8)$$

The above parameters are pictorially presented in Fig. 4.5. Eq. 4.8 is plotted in Fig. 4.6. A reasonable limit for antenna tracking loss under required operating conditions is 1.5 dB, corresponding to a tracking accuracy of approximately one-third the half-power beamwidth ($\Delta\theta/\theta_3 \approx 1/3$). The half-power beamwidth of a paraboloidal reflector may be approximated as

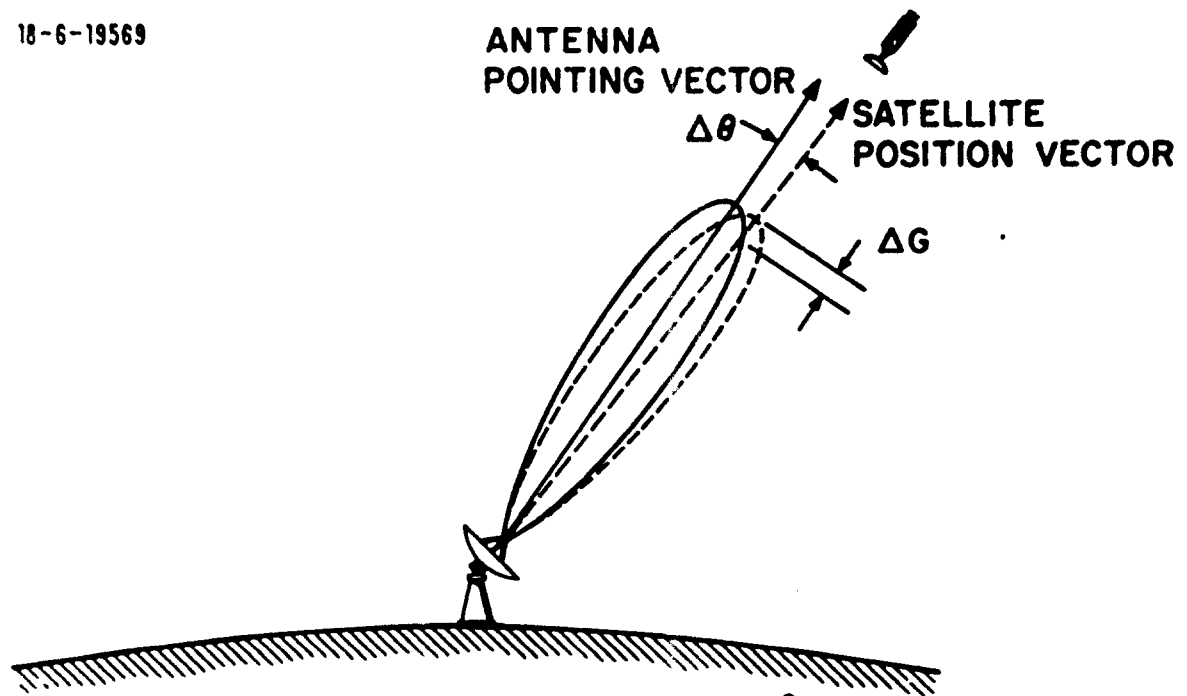
$$\theta_3 = \frac{70\lambda}{D} \quad (4.9)$$

Substituting Eq. 4.9 into Eq. 4.8, yields for the antenna tracking loss

$$\Delta G = 1.76 \times 10^{-5} [\Delta\theta \cdot D \cdot F]^2 \quad (\text{dB}) \quad (4.10)$$

where F is the operating frequency. Note that for a fixed antenna diameter and tracking accuracy, the antenna tracking loss increases as F^2 . Of more relevance, if it is desired to use the same diameter antennas at EHF as at 8/7 GHz (e.g., for AJ, LPI or margin improvements), the tracking accuracy must improve in proportion to the increase in operating frequency to maintain a specified tracking loss. Eq. 4.10 is plotted in Fig. 4.7 with the frequencies

18-6-19569



$$\Delta G = \text{ANTENNA TRACKING LOSS} = 12 \left(\frac{\Delta\theta}{\theta_3} \right)^2 \text{ (dB)}$$

$\Delta\theta$ = ANTENNA TRACKING ACCURACY

θ_3 = ANTENNA HALF-POWER BEAMWIDTH

Fig. 4.5. Antenna tracking loss.

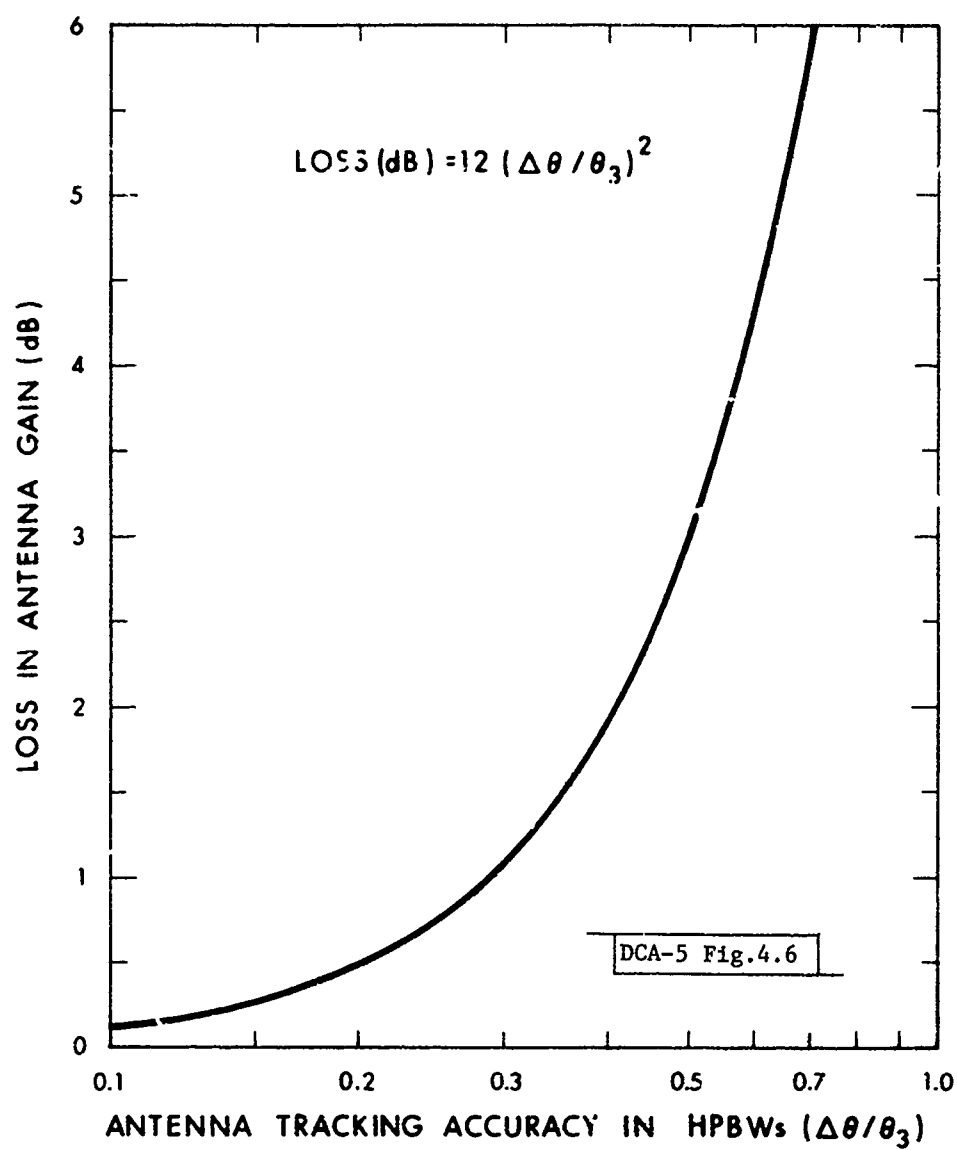


Fig. 4.6. Loss in antenna gain versus antenna tracking accuracy in half-power beamwidths.

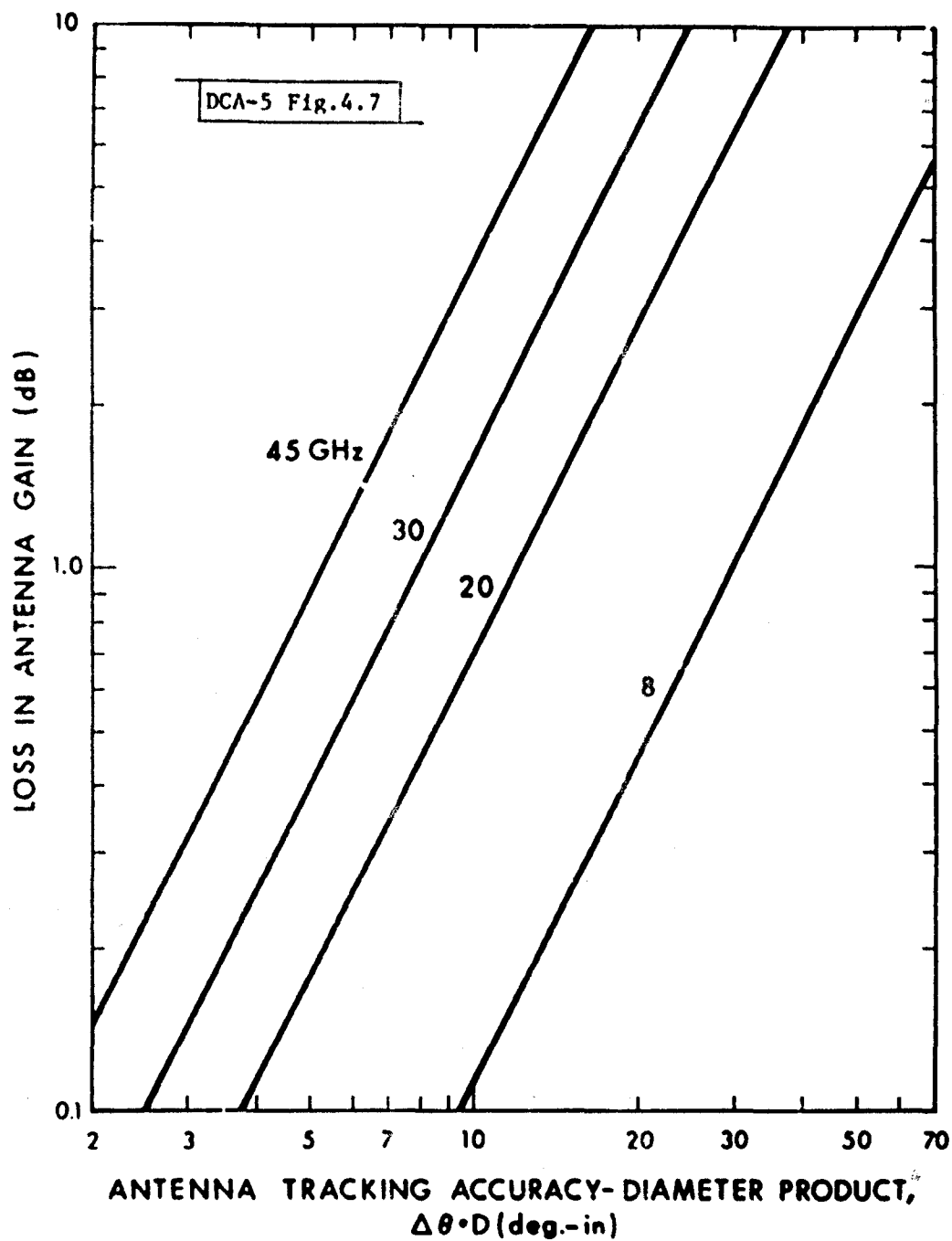


Fig. 4.7. Loss in antenna gain versus antenna tracking accuracy-diameter product with frequency as a parameter.

of interest as a parameter; the functional relationships discussed are evident.

B. Current Technology

The factors contributing to the overall antenna tracking accuracy include

1. Fundamental factors

- Antenna beamwidth
- Antenna servo systems

2. Operational factors

- Platform Dynamics
- Environment
 - Windloads
 - Thermal gradients

Neglecting platform dynamics and environmental effects (primarily wind loads), antenna tracking accuracy is limited to either a few hundredths of the antenna half-power beamwidth by the angular sensitivity of the tracking feed or few thousandths of a degree by the angular resolution of the positioning subsystem; in these cases, the antenna tracking capability would be considered to be beamwidth limited or servo limited, respectively. However, for mobile terminals and for exposed fixed terminals, the platform dynamics and wind loads are the limiting factors on tracking accuracy. The antenna tracking accuracies presented for typical MILSATCOM terminals reflect these operational limitations.

Current antenna tracking capabilities were assessed from terminal specifications, manufacturers' analyses and estimates, and discussions with appropriate DoD agencies. Tracking accuracy data based on operational experience was not obtained and should be collected to compare in situ performance with specifications and estimates. Note that in some cases, the tracking capabilities reported do not represent technological limits but rather represent adequate tracking accuracies for the antenna beamwidth involved (typically 8/7 GHz terminals). In these cases, incorporation of an EHF tracking

subsystem would improve the antenna accuracy to the limit imposed by the platform dynamics, environment or antenna servo system.

1. Satellites

The typical pointing* accuracy of spin and three-axis stabilized satellites is 0.2° , e.g., DSCS-II** and DSCS-III⁽²⁷⁾. The tracking loss relationship given in Eq. 4.8 is more applicable to ground terminals, as the tracking error is associated with the peak of the antenna's beam. For the satellite, when regional coverage is required, the tracking error must be considered at the beam angle associated with the edge of that region. For a specified relative gain level, $P(\phi)$, at the edge of a coverage region defined by the beam angle, ϕ , the tracking loss is

$$\Delta G = 12 \left[\frac{\phi + \Delta\theta}{\theta_3} \right]^2 - P(\phi) \quad (\text{dB}) \quad (4.11)$$

As an example, the previously discussed criterion of $\Delta\theta/\theta_3 = .35$ corresponds to a tracking loss of 1.5 dB when the tracking error is associated with the peak of the beam; when associated with the 3 dB contour of the beam, the tracking loss is 5.7 dB (i.e., minimum relative gain = -8.7 dB). The assessment of the required satellite tracking accuracy is then dependent on the specified relative gain at the edge of the coverage area and the acceptable additional loss due to tracking accuracy. As operation at EHF will afford the opportunity for narrower beamwidth antennas (particularly MBAs and time-hopped beams), the requirements for satellite pointing accuracy will become more stringent and may require significant improvements in open-loop satellite pointing. For such antennas, a viable alternative is closed-loop tracking of the user terminal. Closed-loop tracking can provide accuracies ≤ 0.1 of the half-power beamwidth and has been demonstrated ($.05^\circ$ tracking accuracy) by the LES-8/9 36/38 GHz reflector antenna. Multiple beam antennas (MBAs) and adaptive nulling antennas would have the basic controls required (i.e., beam-forming networks and weighting networks, respectively) to perform closed-loop tracking.

*Open-loop as well as closed-loop tracking is considered for completeness.

** TRW Briefing to the DCA/MSO.

2. Airborne Terminals

Antenna pointing accuracy of 0.5° has been demonstrated by AFAL in airborne communications experiments with LES-8/9. This pointing accuracy would be adequate for antennas up to 1 ft. in diameter operating at 45 GHz. However, maintaining reliable communications would be dependent on the accuracy of the aircraft's inertial navigation system and the satellite ephemeris data. It will be assumed that antenna pointing capability will continue to be used for initial satellite acquisition and that closed-loop antenna tracking will then be used. As regards the latter, antenna tracking accuracy of 0.1° has been demonstrated with the AFAL SATCOM terminal (AN/ASC-22)⁽²⁸⁾ operating at 36/38 GHz (LES-8/9) with a 3-ft. antenna utilizing a nutating subreflector*.

3. Shipboard Terminals

Antenna pointing accuracy of 0.5° has also been demonstrated by NOSC for shipboard terminals (LES-8/9, 36/38 GHz experiments); the limitations and utility of antenna pointing were previously discussed. A tracking accuracy of 0.2° has been specified for the WSC-6 terminal (mast-mounted, 4-ft., 8/7 GHz antenna with radome) and has been demonstrated on roll/pitch fixtures. It should be noted that the tracking accuracy of the WSC-6 terminal is dictated by the use of step-tracking technique (i.e., scanning of the entire reflector) and is not a fundamental limitation. It is estimated that a tracking accuracy of 0.1° could be achieved, but may require the addition of a tracking subsystem (e.g., nutating subreflector) with a concomitant increase in cost and weight. A tracking accuracy of 0.1° is specified for the WSC-2(V)⁽²⁹⁾ terminal (8-ft., 8/7 GHz antenna) which utilizes a monopulse tracking feed.

4. Transportable Ground Terminals

Antenna tracking accuracies for transportable terminals in the DSCS inventory range from 0.03° for a 38-ft. antenna (AN/MSC-61)⁽³⁰⁾ to 0.2° for an 8-ft. antenna (AN/TSC-86)⁽³¹⁾. These tracking accuracies are based on limiting the tracking loss at 8/7 GHz to 1 to 2 dB under operational conditions and the tracking specifications are typically stated in terms of the maximum tracking

* In a Cassegrain antenna system, the subreflector is offset or tilted slightly from the focal axis and rotated to provide a conical scanning of the antenna beam.

loss versus wind loads. For tactical, ground-mobile terminals (e.g., AN/TSC-86), tracking accuracies of 0.1° and 0.2° are achieved for 20-ft. (LT-2) and 8-ft. (LT-1) terminals, respectively. These tracking accuracies will be assumed for the assessment of ground-mobile terminals. It should be noted that the tracking technique employed for mobile terminals is dependent on the antenna beamwidth in the following manner: for antenna beamwidth $> 0.5^\circ$, a step-tracking system is typically used; while for antenna beamwidths $< 0.5^\circ$, some form of monopulse tracking is used with a concomitant increase in cost and complexity.

5. Fixed Ground Terminals

A tracking accuracy of 0.02° is specified for large fixed terminals, e.g., 60-ft. DSCS terminal (AN/FSC-78)⁽³²⁾, operating without a radome for steady winds up to 45 mph and for gusts up to 60 mph. The wind speed is the major limiting factor in the tracking accuracy of large, fixed terminals (e.g., for steady winds of 30 mph and gusts to 45 mph, the tracking accuracy is $\approx 0.01^\circ$). Consequently, if improved tracking accuracy is required, radomes can afford up to a ten-fold improvement in tracking accuracy, within the limits imposed by the antenna beamwidth and servo system.

The results of this survey of current antenna tracking accuracies are presented in Table 4.4. The antenna gain, corrected for antenna tracking loss, may be expressed as

$$G = 10 \log (\eta) + 20 \log \left(\frac{\pi D}{\lambda} \right) - 2.45 \times 10^{-3} \left[\Delta \theta \left(\frac{D}{\lambda} \right) \right]^2 \quad (\text{dB}) \quad (4.12)$$

Eq. 4.12 is plotted in Fig. 4.8 with the current antenna tracking accuracies as a parameter for an assumed antenna efficiency (η) of 55%. Note the limiting effect of the antenna tracking accuracy on the achievable antenna gain. The maximum achievable gain is realized when the gain loss, $\Delta G = 4.34$ dB, as is the case for the gain limitation imposed by antenna surface accuracy, this loss in gain represents an unacceptably inefficient use of antenna aperture. Since tracking losses are typically limited to 1 to 2 dB under operating conditions, a maximum tracking loss of 1.5 dB is chosen as the criterion for assessing

Table 4.4
CURRENT ANTENNA TRACKING ACCURACIES

Terminal Type	Tracking Accuracy (deg)	Tracking Method	Comments
Airborne and Shipboard	0.5	Open-Loop	Demonstrated by AFAL and NOSC with LES-8/9 (36/38 GHz)
Satellite	0.2	Open-Loop	Typical of Spin or Three-Axis Stabilization (e.g., DSCS-II or DSCS-III)
	0.05	Sequential Scan	Demonstrated by LES-8/9 (18-inch, 36/38 GHz Antenna)
Shipboard	0.2	Step Track	Specified for WSC-6 (4-foot, 8/7 GHz Terminal)
	0.1	Monopulse	Specified for WSC-2 (V) (8-foot, 8/7 GHz Terminal)
Airborne	0.1	Conical Scan	Demonstrated by AFAL ASC-22 (3-foot, 36/38 GHz Terminal)
Transportable Ground	0.2	Step Track ($\Theta_3 > 0.5^\circ$)	Specified for TSC-86 (LT-2) (8-foot, 8/7 GHz Terminal)
	0.1	Monopulse ($\Theta_3 < 0.5^\circ$)	Specified for TSC-86 (LT-2) (20-foot, 8/7 GHz Terminal)
Fixed Ground	0.02	Monopulse	Specified for FSC-78 (60-foot, 8/7 GHz Terminal) for wind gusts < 60 mph

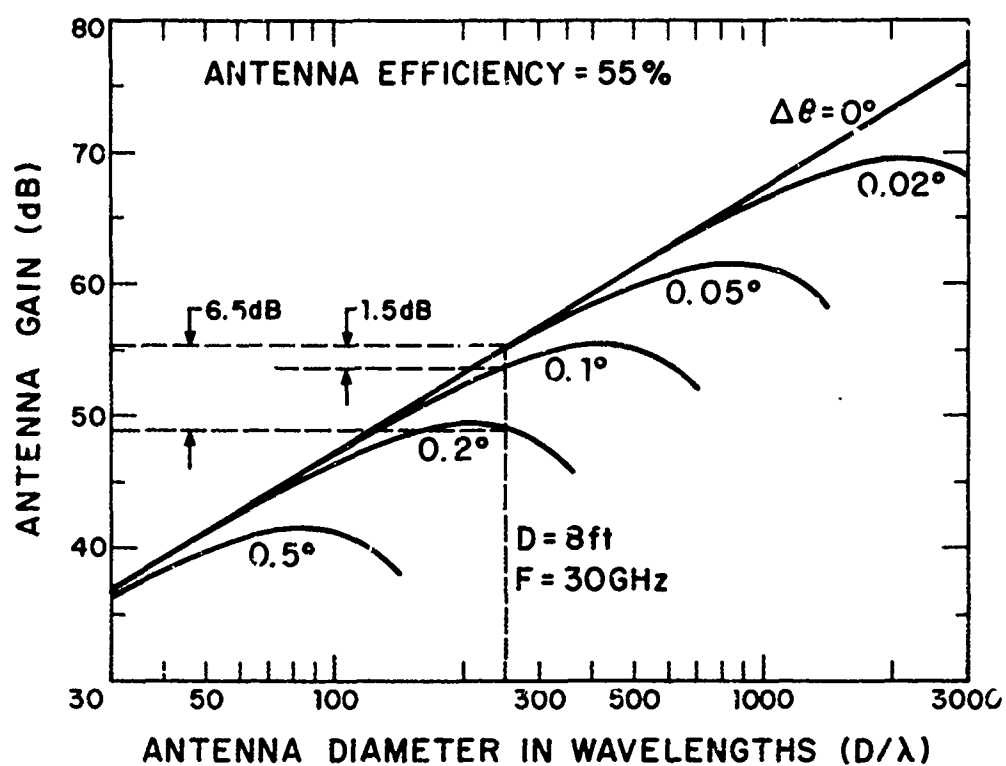


Fig. 4.8. Antenna gain limitations due to antenna tracking accuracy.

the gain limitations.

C. Summary

Table 4.5 presents the antenna gain limits and corresponding diameter limits for current tracking accuracies with frequency as a parameter. Note that for antenna diameters ≥ 40 ft., the tracking accuracy required is at the limit of current technology. In this case, improvements in tracking accuracy may be necessary and, as wind loads are a dominant factor, the potential use of radomes must be addressed. Note that for airborne terminals, the demonstrated tracking accuracy of 0.1° will accommodate larger antennas than would be considered. For the mobile community, current technology will permit operation of the proposed antennas at EHF. However, not evident in Table 4.5 is the technology required to provide the indicated performance. Table 4.6 presents tracking accuracy requirements for a given antenna diameter with the frequencies of interest as a parameter. In this table the boundaries between the various technologies are indicated (these boundaries are coarse but representative). It is beyond the scope of this report to assess the cost and complexity of the various tracking systems but these factors should be included in system studies as potential limits on terminal antenna size and gain.

A final point regarding antenna tracking accuracy addresses the ratio of uplink (F_U) to downlink (F_D) frequency. The previous discussions have addressed the tracking accuracy requirement for a given antenna diameter or tracking loss on an individual frequency basis, regardless of the actual link direction. This is valid for 8/7 GHz operation where the ratio $F_U/F_D \approx 1$ and, consequently, the tracking losses at the uplink and downlink frequencies are essentially the same. Operation at EHF, however, will entail larger ratios of F_U/F_D (an exception being the use of 44/40 GHz). Considering that for a given tracking loss, ΔG , at the downlink frequency, the tracking loss at the uplink frequency is $(F_U/F_D)^2 \cdot \Delta G$, it is apparent that the specified downlink tracking loss must be much lower at EHF than is currently required at 8/7 GHz. For example, operation at 45/20 GHz will require a specified maximum tracking loss at 20 GHz under operational conditions of 0.3 dB to limit the tracking loss at 45 GHz to 1.5 dB.

Table 4.5
ANTENNA GAIN AND DIAMETER LIMITATIONS
DUE TO ANTENNA TRACKING ACCURACY

Tracking Accuracy (deg)	Gain* Limit (dB)	Antenna Diameter Limit (Ft.)				
		20 GHz	30 GHz	37 GHz	44 GHz	50 GHz
0.5	39.7	2.4	1.6	1.3	1.1	1.0
0.2	47.7	6.1	4.1	3.3	2.8	2.4
0.1	53.7	12.2	8.1	6.6	5.5	4.9
0.05	59.7	24.3	16.2	13.2	11.1	9.7
0.02	67.7	60.8	40.6	32.9	27.6	24.3

*Based on 1.5 dB tracking loss; 55% efficiency assumed.

TABLE 4.6
ANTENNA TRACKING ACCURACY REQUIREMENTS

ANTENNA DIAMETER (ft)	REQUIRED TRACKING ACCURACY (deg)*				
	20 GHz	30 GHz	37 GHz	44 GHz	50 GHz
	STEP TRACKING				
1	1.2	0.8	0.7	0.6	0.5
2	0.6	0.4	0.35	0.3	0.25
4	0.3	0.2	0.17	0.14	0.12
8	0.15	0.1	0.08	0.07	0.06
16	0.07	MORE COMPLEX TRACKING 0.05	0.04	0.035	0.03
40	0.03		0.016	0.014	0.012
			BEYOND CURRENT CAPABILITIES		

*BASED ON 1.5 dB TRACKING LOSS

Consequently, the tracking accuracy requirement for the downlink frequency will be more stringent in terms of antenna beamwidth ($\Delta\theta/\theta_3$). In the above example for 45/20 GHz, the required tracking accuracy at 20 GHz in half-power beamwidths is $\Delta\theta/\theta_3 < 0.16$. Fig. 4.9 presents tracking accuracy versus F_U/F_D with tracking loss as a parameter. Also indicated in the figure are approximate boundaries for various tracking technologies. These boundaries are broad as the achievable tracking accuracy is obviously dependent on factors other than the tracking technique (e.g., tracking bandwidth, S/N, operating environment, etc.). However, the consequence is that the ratio of F_U/F_D will dictate the required tracking technology and corresponding cost and complexity.

The foregoing analysis assumes the uplink and downlink beams are coaxial. Antenna designs are possible in which the uplink and downlink beam controls are independent (e.g., prime-focus downlink feed and Cassegrain uplink feed with a dichroic subreflector). Detailed system studies must address the cost/performance tradeoffs among the various antenna feed techniques.

4.4 Radomes

The need for radomes for large, fixed terminals to mitigate the effect of wind loads on antenna surface and tracking accuracy has been indicated. Radomes will also be required for airborne and shipboard terminals and are included here for completeness. This assessment of radomes is rather limited and further studies will be required.

A. Fixed Ground Terminals

Metal space frame radomes have been developed by Electronics Space Systems Corporation (ESSCO) for use up to 200 GHz. The ESSCO radome is a faceted, truncated sphere composed of individual triangular panels bolted together to form the structure. Each of the individual triangular panels is composed of a thin plastic laminate membrane supported by an aluminum extrusion frame. The electromagnetic performance of the radome relies on the spatial distribution of the framework as well as membrane characteristics. The environmental specifications of this type of radome are presented in Table 4.7. Typical

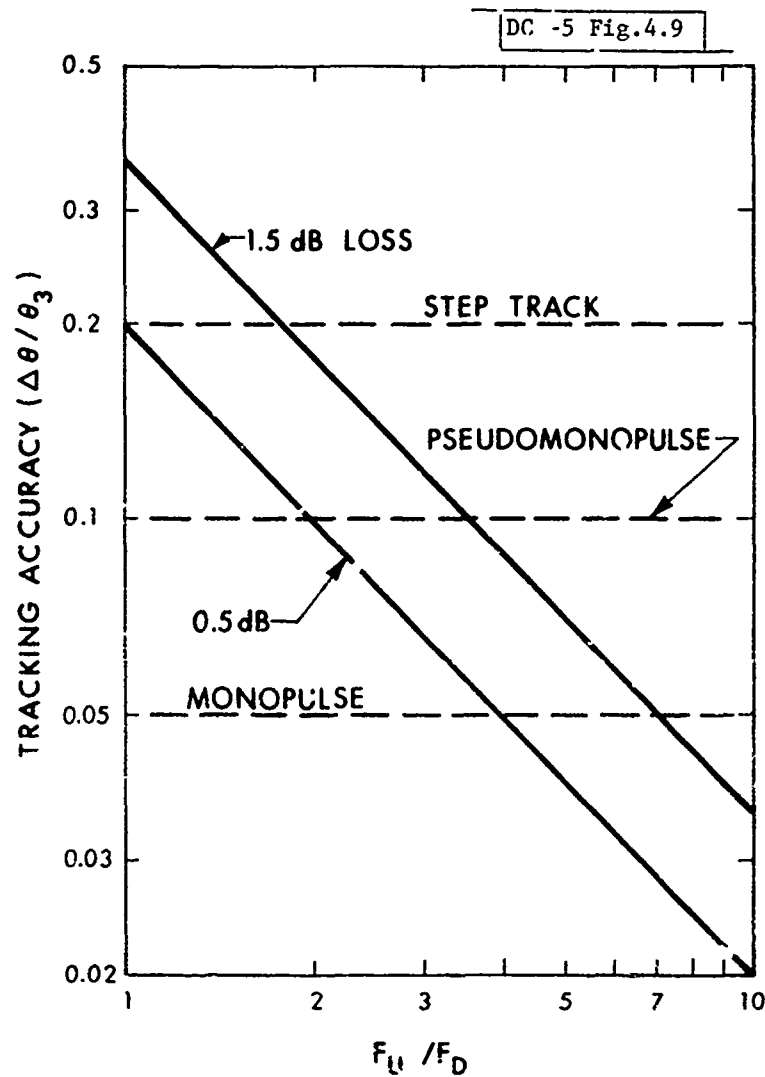


Fig. 4.9. Required downlink tracking accuracy versus uplink-to-downlink frequency ratio (F_U/F_D).

Table 4.7
ENVIRONMENTAL SPECIFICATIONS OF METAL SPACE
FRAME RADOME (NOMINAL DIAMETER 68 FT.)

Operating wind load	150 mph
Operating temperature range	-65°F to 140°F
Relative humidity	0 to 100%
Ice or snow loads	70 psf
Salt atmosphere	MIL-STD-810
Sand and dust	MIL-STD-210
Solar radiation rejection	≥ 90%

electromagnetic performance characteristics of a 68-ft. diameter radome are presented graphically in Fig. 4.10. These characteristics are summarized in Table 4.8 for the frequencies of interest. Note in the table that the bore-sight shift and noise temperature contributions are negligible. An assessment of the impact of the transmission loss through the radome will require consideration of the surface accuracy and tracking losses with the radome and comparison with the losses incurred for exposed antennas. As the transmission loss associated with the membrane is a function of its thickness for a given material and frequency of interest, the membrane thickness can be chosen to minimize the loss at the desired operating frequency. In particular, the EHF band lies near a maximum in the transmission loss characteristics of the radome discussed (Fig. 4.10). The transmission loss can be reduced by reducing the membrane thickness. However, this results in an increase in the number of panels and the cost of the radome - there is an obvious tradeoff between radome performance and cost.

A final consideration regarding radome transmission loss is the effect of rain, specifically laminar water flow on the radome during rain. Radomes are manufactured with integrally bonded films to inhibit the formation of water film and appropriate materials for in situ coatings have been developed. However, the performance and maintenance requirements regarding rain effects, must be addressed in radome studies.

B. Shipboard Terminals

Radomes for shipboard (or ground) terminals are available for use at frequencies up to at least 40 GHz from ESSCO. These radomes are truncated spheres molded in one piece. Two types are available: a glass-fabric-reinforce solid laminate (L) or a lightweight sandwich construction (S) with glass-fabric-laminate skins over a honeycomb core. The outside of the radome is finished with a high-quality enamel. Both models are designed to survive 150 mph wind loads and models are available designed for resistance to nuclear blast. Typical transmission loss performance of several 6.5-ft. diameter radomes is presented in Fig. 4.11. Note at the design frequency the transmission

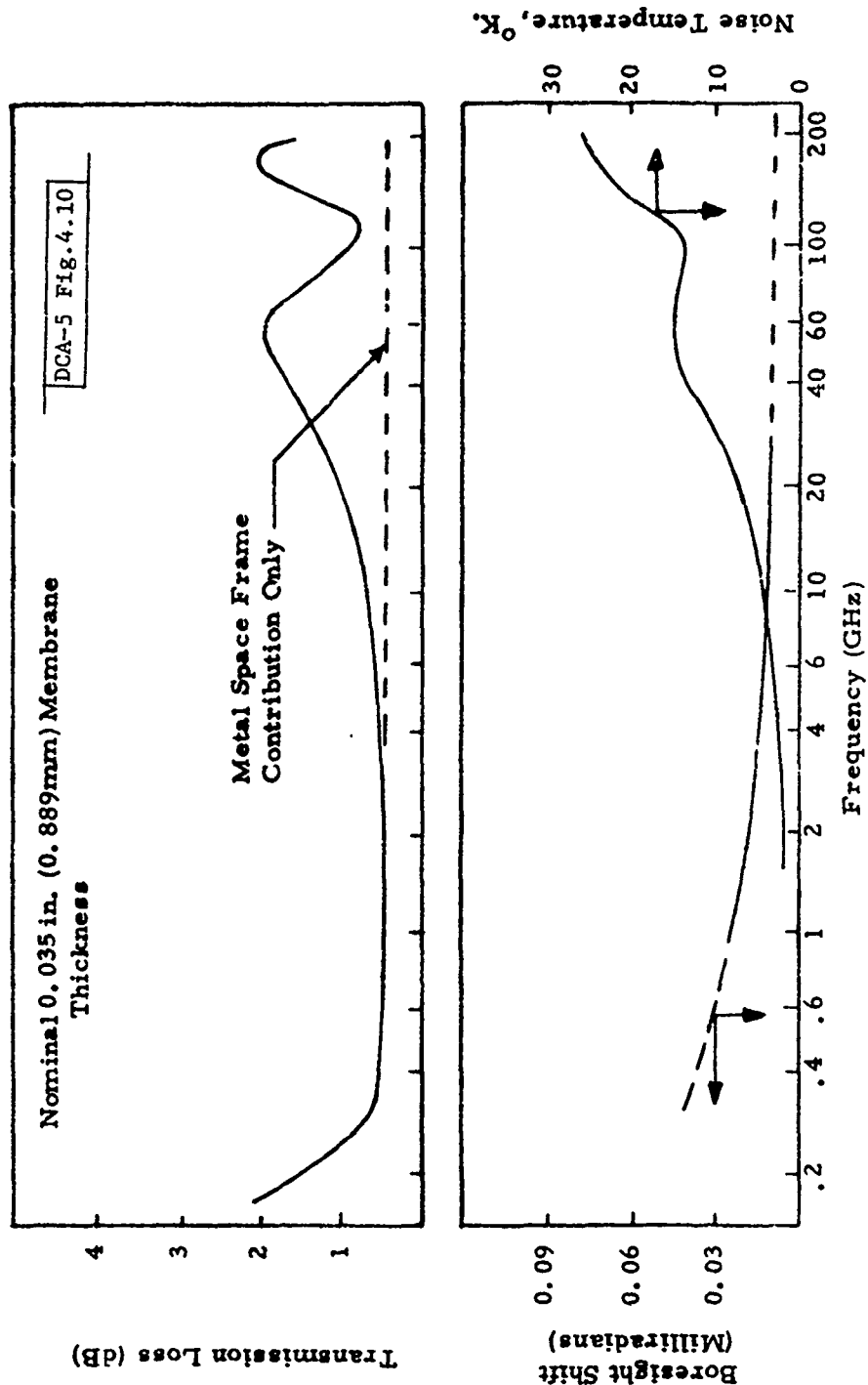


Fig. 4.10. Typical electromagnetic performance characteristics of a metal space frame radome (nominal diameter 58 ft.).

Table 4.8
TYPICAL ELECTROMAGNETIC PERFORMANCE CHARACTERISTICS
OF A METAL SPACE FRAME RADOME* (68 FT. DIAMETER)

Frequency (GHz)	Transmission Loss (dB)	Boresight Shift (deg.)	Noise Temperature (°K)
7	0.6	7×10^{-4}	3
20	1.0	5×10^{-4}	7
30	1.3	5×10^{-4}	10
45	1.8	5×10^{-4}	14
50	1.9	5×10^{-4}	15

*Nominal membrane thickness 0.035 in.

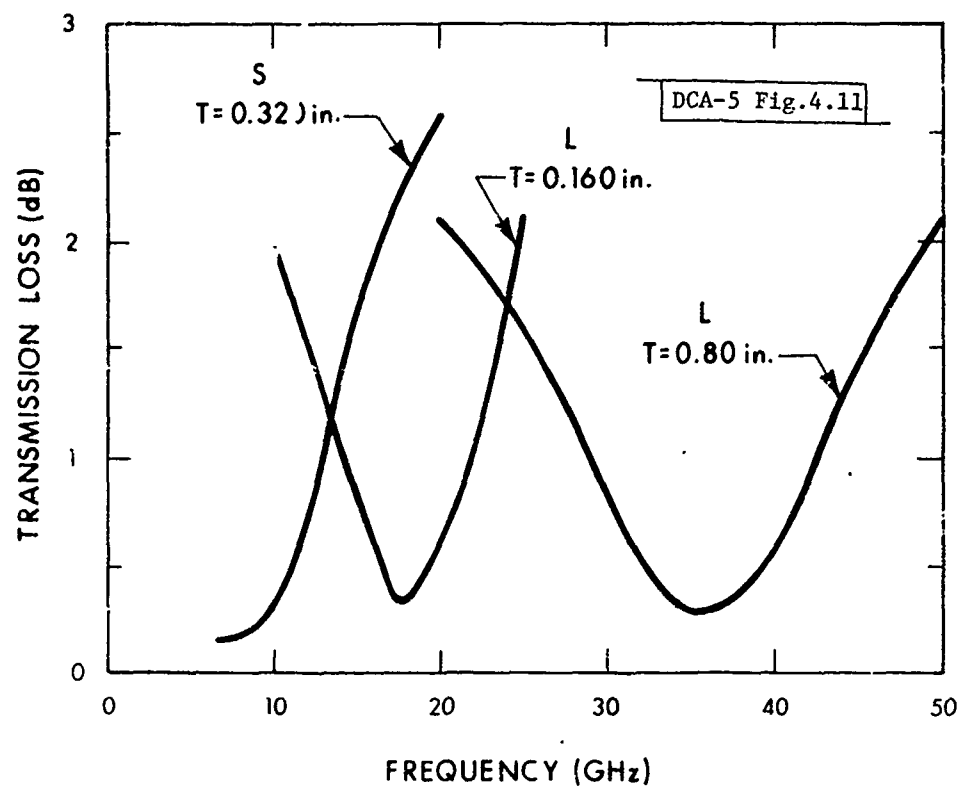


Fig. 4.11. Typical transmission loss of shipboard radomes (nominal diameter 6.5 ft.).

loss is < 0.5 dB (> 90% transmission) even at 35 GHz. Note also that for the solid laminates the 1 dB bandwidth is not wide enough to accommodate even 30/20 GHz. As pointed out previously, operation at EHF entails more widely separated uplink and downlink frequencies than previous MILSATCOM bands. As regards radomes for shipboard terminals at EHF, either larger transmission losses must be tolerated if a solid laminate radome is used, or a sandwich construction must be employed to afford dual-tuned performance. A study is indicated.

C. Airborne Terminals

Radomes have been built and flight tested for airborne terminals which operate at 8/7 GHz and 36/38 GHz (AN/ASC-28). This dual-band radome houses a 3-ft. antenna and has dimensions of approximately 20 ft. x 4 ft. x 4 ft. Typical transmission loss values measured after environmental testing are presented in Table 4.9.

Table 4.9
TRANSMISSION LOSS OF DUAL-BAND
AIRBORNE RADOME (AN/ASC-28)

Transmission Loss (dB)			
Average ⁽¹⁾		Maximum ⁽²⁾	
8/7 GHz	36/38 GHz	8/7 GHz	36/38 GHz
0.5	1.5	1.0	3.0

(1) Averaged over 0° to 80° antenna elevation angle and over the frequency band.

(2) Actual maximum value within the specified elevation angle and frequency range.

This radome demonstrates the feasibility of designs capable of operating over the largest conceivable band separation encompassing EHF. Present EHF plans require new radome designs for the specific frequencies, antenna diameters and operational requirements.

4.5 Technological Limits

This section briefly addresses the technological limits on antenna gain, not as regards MILSATCOM terminals, but for large land-based jammers.

A. Antenna Tracking Accuracy

The gain limit imposed by antenna tracking accuracy may be obtained by differentiation of Eq. 4.12, yielding (for an assumed antenna efficiency of 55%) for the maximum gain

$$G_{MAX}^T = 35.5 - 20 \log (\Delta\theta) \quad (\text{dB}) \quad (4.13)$$

Under the assumptions that the wind and thermal loads are mitigated by a radome and temperature control, and there is no limit on attainable antenna beamwidth, the tracking accuracy would be limited by the antenna servo system. Under these conditions, antenna tracking accuracies of $\approx 0.001^\circ$ have been achieved⁽³³⁾ and the corresponding gain limit would be $G_{MAX} \approx 95$ dB. As will be discussed next, the gain is limited in practice to much lower values. This calculation merely shows that antenna tracking (servo) accuracy is not the fundamental limit on antenna gain.

B. Antenna Surface Accuracy

Examining the technological gain limit imposed by antenna surface accuracy, Eq. 4.6 is differentiated to obtain (for an assumed antenna efficiency of 55%)

$$G_{MAX}^S = -19 - 20 \log \left(\frac{\epsilon}{D} \right) \quad (\text{dB}) \quad (4.14)$$

However, assuming that wind and thermal loads are mitigated and assuming no surface inaccuracies due to fabrication (i.e., panel and assembly accuracy are cost dependent), the antenna surface accuracy would ultimately be limited by gravity. Analysis⁽³⁴⁾ of conventional (aluminum or steel construction) radio telescope structures shows that the gravitational limit on antenna surface accuracy is related to the antenna diameter as

$$\epsilon = 4.5 \times 10^{-7} D^2 \quad (\text{m}) \quad (4.15)$$

Substitution of Eq. 4.15 into the gain expression, yields for the maximum antenna gain

$$G_{\text{MAX}}^S = 61 + 10 \log [F(\text{GHz})] \quad (\text{dB}) \quad (4.16)$$

Note in Eq. 4.16 that the gain limit is directly proportional to frequency. Eq. 4.16 is plotted in Fig. 4.12. Table 4.10 presents the gain limits for the uplink frequencies of interest.

Table 4.10
ANTENNA GAIN LIMIT DUE TO GRAVITATIONAL DISTORTION

f (GHz)	G _{MAX} (dB)*	D _{MAX} (Ft.)	ε (in.)
30	76	115	.022
45	78	95	.015

*Assuming 55% efficiency. No radome or other losses included.

Note that the gain values do not include the losses due to the required radome, the residual surface inaccuracies of panel fabrication and antenna assembly, and antenna tracking accuracy. It may be concluded that a maximum

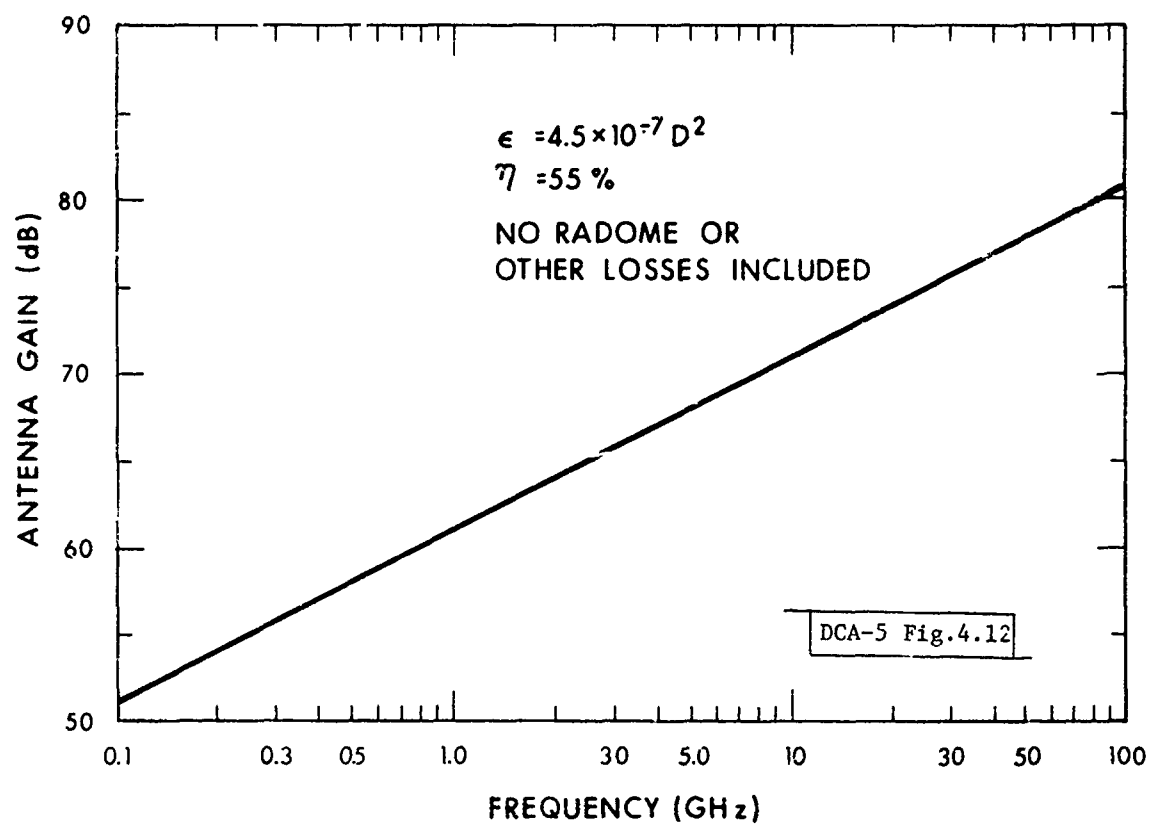


Fig. 4.12. Antenna gain limitations due to gravitational distortion.

achievable antenna gain of ≈ 75 dB is representative of the technological limit for ground-based jammers operating at EHF.

4.6 Summary

With the exception of large fixed terminals, the current technology in antenna surface accuracy and tracking accuracy will not restrict the deployment of the antenna sizes proposed for EHF. However, the relevant issue is the cost and complexity of the required technology and must be considered in determining the limiting antenna sizes. These factors are beyond the scope of this report. Future studies should address this issue in the design tradeoff between satellite complexity and terminal size. The following is a summary of the findings of this section and may be useful in such studies.

A. Antenna Surface Accuracy

1. For $D \leq 4$ ft., requirements satisfied with refinements in current manufacturing processes; the most cost-effective process remains to be determined.
2. For $8 \text{ ft.} \leq D \leq 20 \text{ ft.}$, requirements satisfied at 1 of current commercial technology, i.e., machined cast or molded panels.
3. For $D \geq 40$ ft., requirements not currently satisfied by commercial technology; tradeoff between new fabrication techniques and radomes.

B. Antenna Tracking Accuracy

1. Satellite: open-loop pointing accuracy (0.2°) is adequate for near term; for beamwidths $< 1^\circ$, closed-loop tracking may be required and has been demonstrated.
2. Airborne Terminals: demonstrated tracking accuracy (0.1°) will accommodate larger antennas than being considered.
3. Shipboard and Transportable Ground Terminals: available technology will accommodate planned antenna sizes; cost and complexity of required technology (e.g., step tracking vs monopulse) should be assessed as a determination.

4. Fixed Ground Terminals: required tracking accuracy at the limit of current technology - use of radomes indicated.

5. Dual-Band Terminals ($F_U \gg F_D$): require stringent tracking accuracy or complex feeds - cost versus performance tradeoff.

C. Radomes

1. Fixed Ground Terminals: radome design study required including cost/performance tradeoffs between existing and new radomes, and rain effects.

2. Shipboard Terminals: new designs are required to accommodate widely separated frequency bands; cost/performance tradeoff between solid laminate (single-tuned) and sandwich (double-tuned) construction.

3. Airborne Terminals: dual-band radome design has been demonstrated; design, fabrication and testing of radomes for the specific frequencies, antenna diameters and operational conditions are required.

D. Technological Gain Limit

Technological limit on antenna gain at EHF (due to gravitational distortion) is ≈ 75 dB.

V. ANTENNAS

5.1 Background

Advances in satellite antenna technology have upgraded the function of antennas from their simple role of providing a single area-coverage beam. Current antenna capabilities can provide variable-beam and multiple-beam coverage. The potential use of narrow time-hopped beams in a TDMA system affords the opportunity for significantly reducing ground terminal size and cost and/or increasing capacity. In addition, the implementation of adaptive nulling antennas offers orders of magnitude improvement in AJ protection and the potential for reducing terminal size and complexity. While this advanced antenna technology is not frequency dependent per se, the realization of high resolution antenna beams or nulls (e.g., of the order of 1°) is practically impossible at UHF (e.g., 230-ft. aperture), difficult at X-band (9-ft. aperture), and readily achievable at EHF (1.5-ft. aperture at 44 GHz). MILSATCOM operation at EHF then affords the opportunity to implement this advanced antenna technology to full advantage and future studies should address its integration into the EHF system architecture. This section assesses the current state of this technology.

For the ground segment, antenna requirements will be satisfied by parabolic reflector antennas; the need for improved fabrication and tracking techniques was discussed in Section IV. This section briefly assesses the impact of the bandwidth requirements and insertion loss at EHF on antenna subsystem design, and the potential use of low-sidelobe antennas.

5.2 Ground Segment

A. Antenna Bandwidth and Loss Considerations

As discussed in Section IV with regard to antenna tracking and radome requirements, operation at EHF will entail much larger ratios of uplink to downlink frequency than operation at 8/7 GHz. This frequency separation impacts the antenna feed and microwave component designs. For operation at 20/20 GHz, the band separation is equivalent to the 6/4 GHz bands and terminal antenna designs can benefit from the extensive development effort expended in the

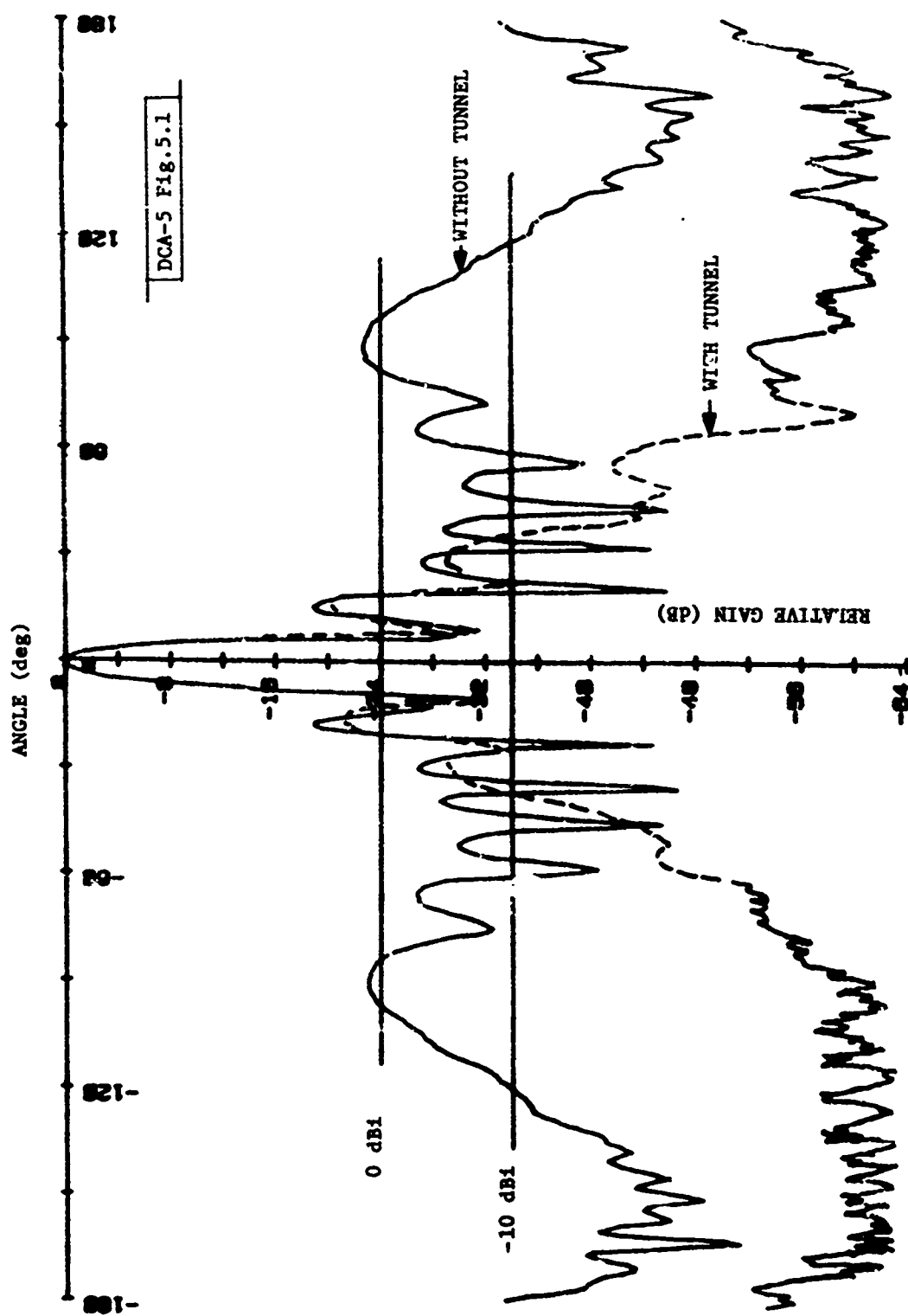
commercial bands, e.g., 6/4 GHz high-efficiency feed designs, circular polarizers, duplexers, etc. However, this technology cannot be simply scaled due to the tolerance requirements at FHF and some development effort will be required in fabrication techniques. For larger frequency separations, new feed and component designs will be required. Another consideration for operation at EHF is the higher waveguide insertion loss. To minimize these losses, the use of higher-order mode waveguide is recommended. NOSC has developed and built oversize circular waveguide (0.5-in. ID) operating in the TE_{01} mode for use in the 40 to 45 GHz band with insertion loss of ≈ 5 dB/100 ft. (compared to ≈ 25 dB/100 ft. theoretical loss for silver-plated, standard rectangular waveguide) and also have developed flexible waveguide, bends, rotary joints, mode suppressors, pressure barriers and transitions. These components for the 44 GHz band should be brought to production availability and similar hardware should be developed for the 30/20 GHz band. An alternative approach for the large fixed terminals is the use of beam-waveguide techniques (multiple reflecting mirrors) to eliminate the waveguide and rotary joints.

B. Low-Sidelobe Antennas

One of the prime motives for the evolution of MILSATCOMs to EHF is the available bandwidth for spread spectrum modulation AJ protection. The specific frequency band selected at EHF is also driven by the user's LPI requirements. The DCA/MSO Frequency Selection Working Group addressed the AJ and LPI threats in detail. One of the constituent parameter of both AJ and LPI analyses is the sidelobe level of the ground terminal antenna. Specifically, the LPI detection range and tolerable AJ threat levels for both downlink and uplink jamming (assuming a frequency-follower or repeat-back jamming threat against a frequency-hopping, spread-spectrum system) are directly proportional to the terminal antenna sidelobe levels. Consequently, reductions in antenna sidelobe levels should be investigated and should be implemented within the constraints of reasonable cost and minimum impact on the terminal operation and performance. It is beyond the scope of this report to conduct such a tradeoff analysis; areas warranting further study are recommended.

In performing AJ or LPI analyses it is typically assumed that the antenna sidelobes well away from the main beam of a standard parabolic reflector antenna have an average level of ≈ -10 dBi (dB relative to an isotropic radiator) with corresponding peak levels of ≈ -7 dBi. Reductions in these sidelobe levels may be achieved by passive or active techniques. Among the passive techniques, the simplest approach is special antenna feed and feed-support designs, but the inherent blockage due to the feed (or subreflector) and feed supports limits the achievable reduction in sidelobes. However, refinements in analytic methods coupled with development efforts have led to improved designs. Advantage should be taken of this technology in the specification of sidelobe levels for EHF ground terminal antennas. The more complex passive techniques for sidelobe reduction include offset-fed reflectors (to eliminate blockage effects) and absorber tunnels. Offset-fed reflectors coupled with appropriate feed designs offer potential reductions in wide-angle sidelobes of 10 to 20 dB. However, this performance improvement must be weighed against the cost and operational constraints involved. Absorber tunnels (cylindrical shroud lined with absorbing material with the antenna at one end) may be used with standard focal-fed parabolas and also offer 10 to 20 dB reductions in wide-angle sidelobe levels (Figs. 5.1 and 5.2) with negligible loss in antenna gain. However, the "optimum" tunnel length is $\approx 2/3$ the antenna diameter and, consequently, the achievable performance must be weighed against the cost, and environmental and maintenance considerations.

Active sidelobe reduction for downlink jamming can be achieved by adaptive sidelobe cancellation techniques (Fig. 5.3) and can provide 30 dB additional suppression of downlink jammer signals. Extensive work has been done on adaptive nulling circuits both for sidelobe cancellation for radar applications and antenna nulling for satellites. Considering the potential improvement in AJ protection, adaptive sidelobe cancellation at EHF should be investigated. As the required circuit technology (analog or digital) is extant, emphasis should be placed on the number of cancellation loops, design and implementation of the auxiliary antenna, and performance evaluation.



DCA-5 Fig. 5.1

Fig. 5.1. Radiation pattern of 12-in. reflector antenna with 8-inch absorber tunnel at 9.735 GHz (H-plane).

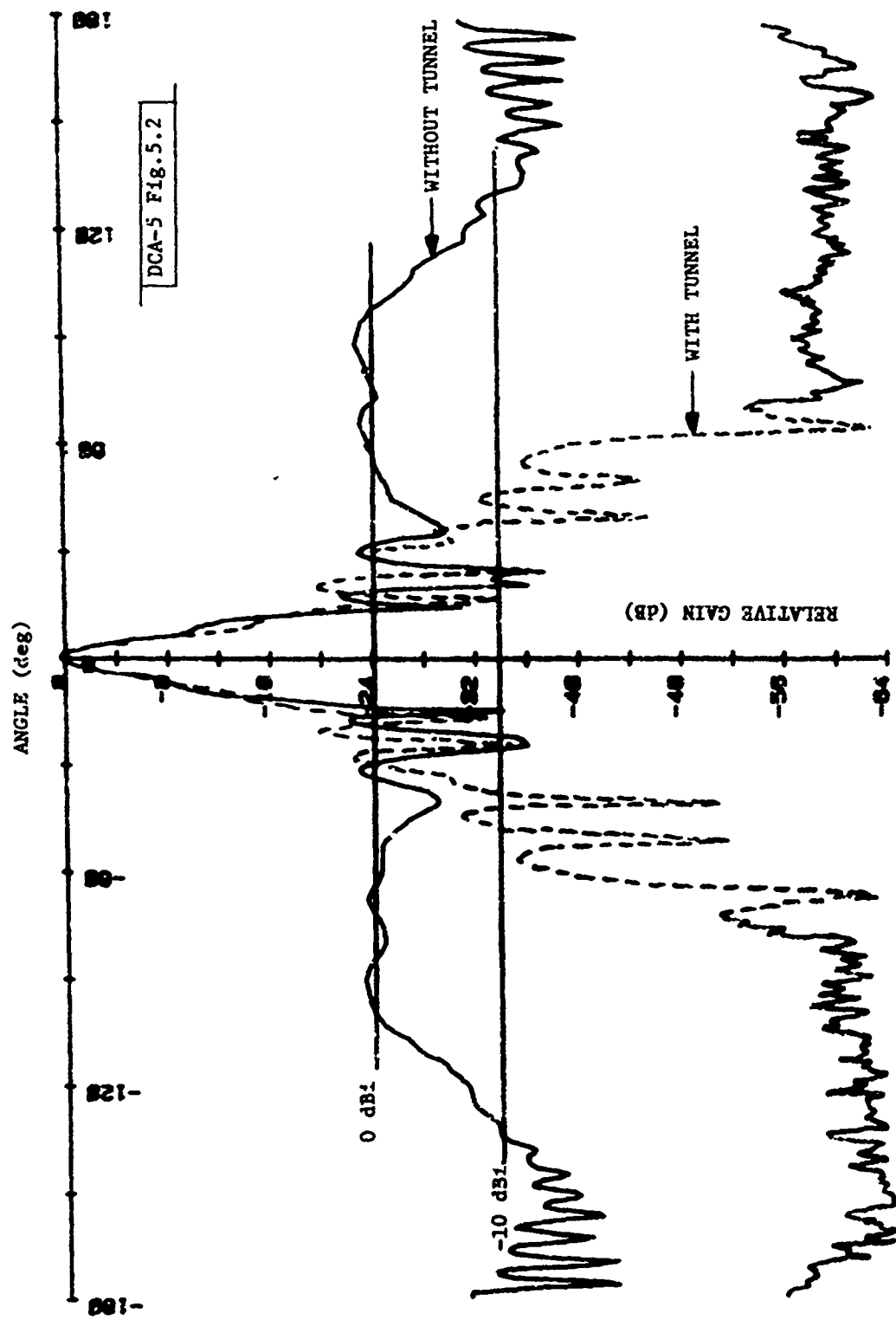


Fig. 5.2. Radiation pattern of 12-in. reflector antenna with 8-inch absorber tunnel at 9.735 GHz (E-plane).

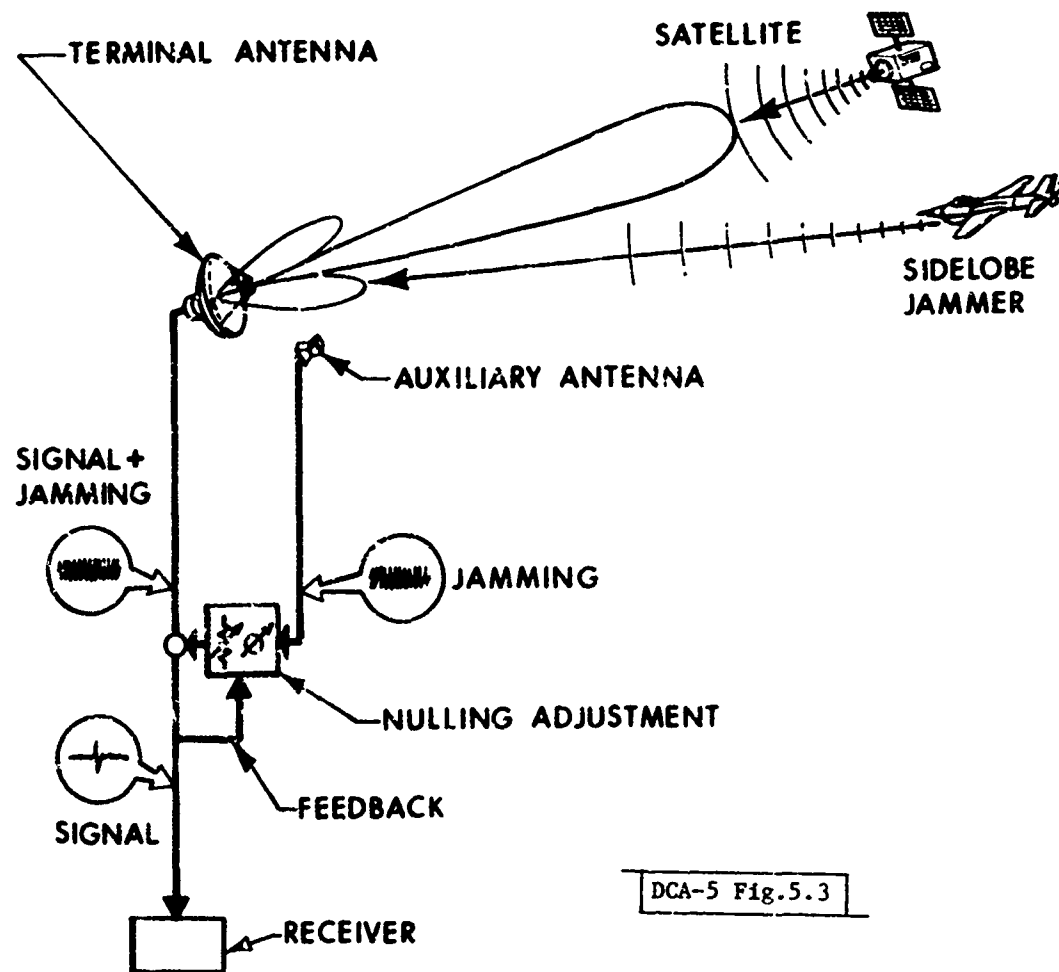


Fig. 5.3. Adaptive sidelobe cancellation.

5.3 Space Segment

The generic types of antennas typically employed on satellites include horns, parabolic-reflector antennas, shaped-beam reflector antennas, arrays and multiple-beam antennas (MBAs). Examples of these antennas in EHF satellites include the dual-reflector antennas employed in the 36/38 GHz LES-8/9 communications experiments and the horn-reflector antenna providing shaped beams used in the 30/20 GHz Japanese Communications Satellite (CS). These examples demonstrate that the requisite antenna fabrication techniques exist (e.g., 0.002-in. rms surface tolerance for the LES-8/9 reflectors) to implement current antenna technology. This section addresses the potential use of phased array antennas for the near term and time-hopped beam and adaptive-nulling antennas for the far term.

A. Phased Arrays

To provide a single beam for spot or area coverage, the use of phased arrays should be considered as an alternative to mechanically steerable reflector antennas. As the maximum scan angle is only 9° , the array elements can be earth-coverage horns, and light-weight fabrication techniques are available. Fig. 5.4 presents the estimated electrical and mechanical characteristics of such arrays at EHF. For downlink applications where a single high power amplifier is used or for uplink applications (where it is assumed a single low-noise receiver is used), the tradeoffs between the phased array and reflector antenna are:

1. weight, volume and packaging constraints of the respective antenna systems.
2. reliability of electronic (phase shifters) versus mechanical (gimbals and rotary joints) beam steering.
3. relative gain of the respective antenna systems for a given beam-width, i.e., losses in the corporate feed network and phase shifters versus flexible waveguide and rotary joints.

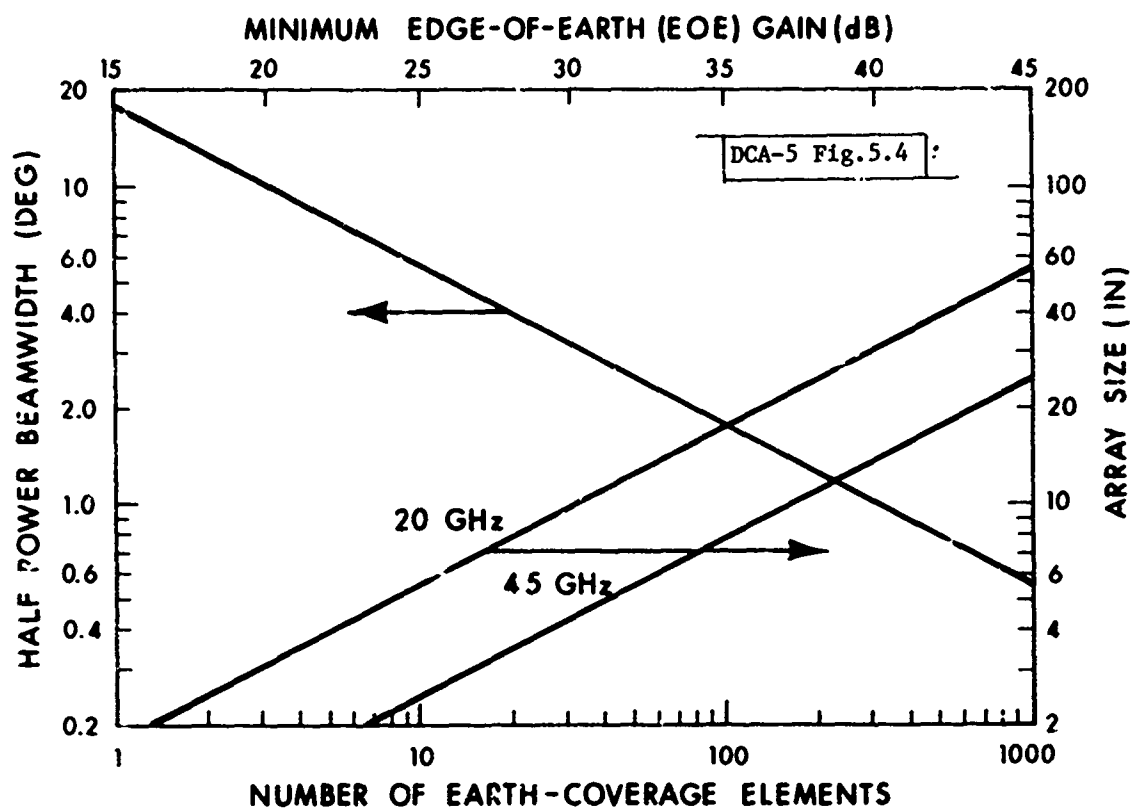


Fig. 5.4. Electrical and mechanical characteristics of EHF phased arrays.

The choice between phased arrays and reflector antennas for single-beam applications requires an in-depth comparison of the above parameters and should be addressed as specific antenna requirements are defined.

The application for which the phased array has unique advantage over the reflector antenna is the combining of a number of power amplifiers (power combining may be required either to increase EIRP or to utilize solid-state devices). To combine the power output of N amplifiers at a single point to feed a reflector requires $N-1$ binary power combiners and incurs a concomitant insertion loss. The array requires N phase shifters to steer the beam but their insertion loss may be mitigated by locating the amplifiers at the input of each antenna element. The array then offers the potential for reduced losses and/or increased numbers of combined devices. For either antenna configuration, using hybrid combiner circuits affords the advantage of graceful degradation with source failure; i.e., the output power is $(M/N)^2$ times the input power, where M is the number of devices operating and N is the total number of devices. For the phased array, the failure of a device also incurs the loss of an array element. The antenna gain is then reduced by M/N but is negligible for a reasonable number of elements (e.g., failure of 1 device in a 16-element array reduces the array gain by ≈ 0.3 dB). The application of phased arrays for spatial power combining should then be addressed as an adjunct to solid-state device development as discussed in Section III. The areas to be addressed should include the effects of device degradation and failure on antenna performance. In addition to its role as a power combining technique, phased arrays may offer potential advantages for time-hopped-beam applications and is discussed next.

B. Time-Hopped-Beam Antennas

The use of a narrow time-hopped beam has been previously referred to as a method of reducing satellite transmitter power requirements, increasing capacity and/or path margins, reducing the size of ground terminals, and providing AJ protection via beam discrimination. The potential reduction in satellite transmitter power or ground terminal antenna diameter as a function of satellite

antenna beamwidth is presented in Fig. 5.5. The required development of average-power-limited transmitters to support TDMA operation was addressed in Section III; this section addresses the required antenna technology and areas for development.

There exist two generic types of antennas capable of providing a single, time-hopped beam: an electronically-focused antenna (phased array) and an optically-focused antenna (array of feeds in the focal plane of a lens or reflector). Since the reflector antenna either incurs aperture blockage or must utilize offset feeds, a lens will be considered for the optically-focused case. To obtain the same minimum gain within the field-of-view (FOV) over which the beam is hopped, the phased array and feed array of the lens require approximately the same number of elements. For an N-element phased array, all array elements are excited at constant amplitude by individual variable 360° phase shifters from an N-way power divider. For the N-element feed of a lens, each feed element is excited individually by an N-way switch. As the N-way power divider of the phased array and N-way switch of the lens feed array would typically both be fabricated from binary power dividers (i.e., $N=2^n$), the difference in beam control is phase shifters versus switches, respectively. For the phased array, the insertion loss is due to only 1 phase shifter (parallel connection); for the lens feed the insertion loss for 2^n elements is due to n switches in series and may be considerable. The reliability of phase shifters versus switches must also be determined. Higher reliability is required for the switch as a failure results in the loss of one or more beams; whereas for the phased array, failure of a phase shifter results in a loss in gain of $1/N$ and minor degradation in the radiation pattern (i.e., increase in sidelobe levels). The prime power requirements and number of state changes will be greater for the phase shifters, as, in general, all N phase shifters must change state for each beam position versus a maximum of n state changes for the switches (prime power requirements for rapid-switching applications are discussed later in more detail). Either antenna type may be used with a single power amplifier. However, only the phased array is amenable to spatial power

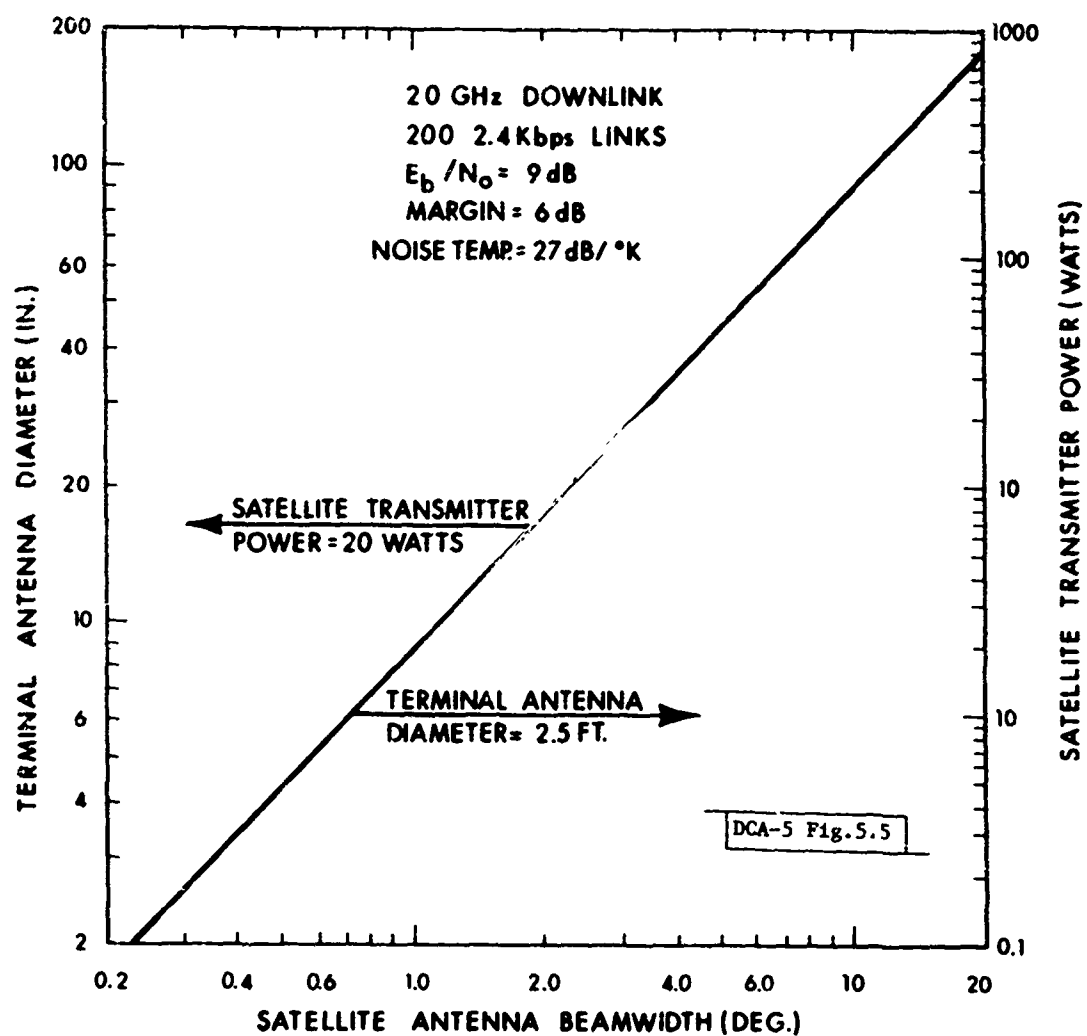


Fig. 5.5. Required satellite transmitter power and ground terminal antenna diameter versus satellite antenna beamwidth.

combining of N devices and, as described in the previous section, the loss due to the phase shifter may be mitigated by locating the amplifier at the input to the array element. The phased array has the additional advantage of being physically smaller for a given beamwidth: the aperture diameter of the phased array is $\approx 30\%$ less than the lens because the aperture efficiency is higher; the depth of the phased array may also be less than a lens antenna. The primary advantage of the lens antenna is its relative ease of fabrication. Specifically, the corporate feed network of the phased array must maintain equi-phase path lengths to each array element (no phase coherence is required among the feed elements of the lens), and the fabrication complexity, size and weight increase rapidly with the number of elements. Broadband-waveguide or dielectric lens would also offer wider bandwidth than the phased array. The relative merits of the phased array versus lens antenna are summarized in Table 5.1. The choice leans toward the phased array. As the final selection will depend upon the type of power amplifier used, the number of elements required, the technology of the beam-control devices, and reliability and bandwidth considerations, further studies are required. The following section assesses the theoretical performance and estimated size of a time-hopped-beam antenna.

To provide an optimum beam which is uniformly hopped within a circular coverage angle, Θ_M , the beam geometry is a hexagonal array as shown in Fig. 5.6 for a 37-beam antenna. The relation between the number of beams in the hexagonal array (N) and the number of beams on the center row (N_C) are related by

$$N = (3N_C^2 + 1)/4 \quad (5.1)$$

For the sake of comparison, the number of elements in the phased array and in the feed array of a lens are assumed equal to the number of beams. The parameter to be optimized is the minimum directive gain over the required coverage angle, G_{MIN} , which occurs at the center of the triangular-lattice subarrays of beams. For the phased array, it is assumed that the element geometry is identical to the geometry of the beam array. The array element is a circular aperture of diameter, d , equal to the element spacing and is excited by the TE_{11}

TABLE 5.1

COMPARISON OF TIME-HOPPED-BEAM PHASED ARRAY AND LENS ANTENNAS*

ANTENNA PARAMETER	PHASED ARRAY	LENS
Beam Control		
Method	N phase shifters	N-way switch
Insertion Loss	1 phase shifter	n switches for 2^n elements
Failure Mode	Loss in gain ($1/N$) and increase in sidelobe levels	Loss of 1 or more beams
Prime Power	Maximum of N state changes	Maximum of n state changes
Power Amplifier Type	Single HPA or spatial power combining	Single HPA only
Implementation	Equipphase divider network required - complexity increases rapidly with N	No phase coherence required - simpler fabrication
Size	Aperture area $\approx 50\%$ smaller; Depth and weight increase rapidly with N	---
Bandwidth	Minimum gain dependent upon bandwidth	Greater bandwidth with broadband-waveguide or dielectric lens

*Assuming N-element phased array and lens with N-element feed both excited by 2^n binary power divider network.

DCA-5 Fig.5.6

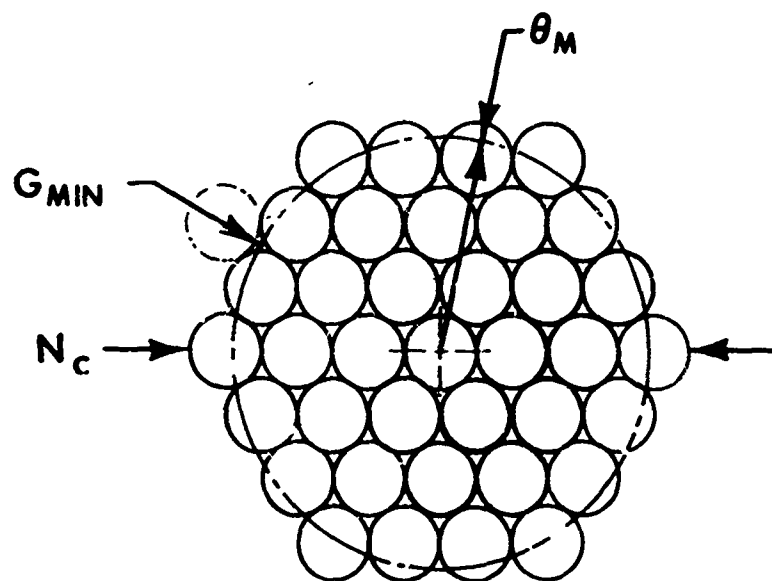


Fig. 5.6. Hexagonal time-hopped-beam geometry.

mode (efficiency = 83.5%). For the lens antenna, it assumed a feed array which is an image of the beam array is located in the focal plane of a lens. The diameter, d , of the circular aperture elements is equal to their spacing. The calculated directive gain includes the loss resulting from spillover and non-uniform amplitude distribution of the lens aperture. The results of this optimization* are summarized in Table 5.2 for earth coverage from synchronous altitude ($\theta_M = 9^\circ$).

TABLE 5.2
OPTIMUM TIME-HOPPED-BEAM ANTENNA PARAMETERS ($\theta_M = 9^\circ$)

PARAMETER	PHASED ARRAY	LENS
Antenna Diameter (D/λ)	$2.49 N_c (1 - 0.15 N_c \Delta F/F)$	$3.64 N_c$
Element Diameter (d/λ)	$2.68 (1 - 0.15 N_c \Delta F/F)$	$1.32 f/D$
G_{MIN}	$22.9 N (1 - 0.25 N_c \Delta F/F)$	$26.8 N$
ΔG (dB)	2.6	6.0
Beam Spacing/HPBW	0.81	1.10

where $\Delta F/F$ = fractional bandwidth

f/D = Focal length-to-diameter ratio

ΔG = gain variation within a beam coverage area

Note that for nearly equal minimum gain, G_{MIN} , over the required coverage angle, θ_M , the aperture diameter of the phased array is $\approx 30\%$ smaller. Note also that the variation in gain, ΔG , within an individual beam coverage angle is significantly smaller for the phased array. The larger variation in gain of the lens antenna indicates a larger gain slope and, therefore, the lens antenna requires better beam pointing accuracy. Based on these factors alone, the phased array appears to be the preferred choice. The theoretical minimum

*A. R. Dion, Internal Memorandum.

gain for an earth-coverage antenna ($\theta_M = 9^\circ$) is presented in Fig. 5.7 as a function of the number of beams in the hexagonal beam array. Calculated antenna patterns containing the minimum gain condition for $\theta_M = 9^\circ$ and $N=37$ are presented in Figs. 5.8 and 5.9 for the lens and phased array antennas, respectively. Estimated physical parameters and realizable gain for a 37-beam, 32-element* phased array at 44 GHz are presented in Fig. 5.10. The final choice between phased array and lens antennas can only be based on the realized performance and difficulty of implementation, and can only be resolved through actual development efforts.

A final factor regarding time-hopped-beam antennas is the prime power consumption of the state-changing devices employed. Diode phase shifters have a constant switching power requirement regardless of switching rate but have relatively high (4-5 dB at 20 GHz) insertion loss. Ferrite phase shifters offer lower insertion loss (1.2 dB at 44 GHz) but prime power requirements are directly proportional to the switching rate. A comparison of ferrite and diode phase-shifter power requirements is presented in Fig. 5.11. It is evident in this figure that for fast beam hopping rates, e.g., of the order of 10,000 hops per second, ferrite phase shifters cannot be used in a phased array and the higher insertion loss of diode phase shifters must be incurred. As discussed previously, the insertion loss of the phase shifters in a phased array may be mitigated by locating a power amplifier at the input to each array element. However, the power gain needed may require multistage amplifiers, substantially increasing the number of solid-state devices employed. An alternative for fast beam hopping may be to use the lens antenna with feed array. The insertion loss of a ferrite switch is ≈ 0.3 dB at 20 GHz and for $N = 2^n$ elements, a maximum of n state changes is required. The maximum prime power requirement of the lens is then n/N less than the phased array. There may be switching sequences for either antenna type which require considerably less power (state changes) than the maximum (for the lens antenna, only one state change may be required). In summary, for fast beam-hopping applications, prime power consumption of the beam-control devices may be the dominant factor in antenna selection, and further studies are required.

*Binary power divider network employed; reduction in minimum directive gain for 32 versus 37 elements = 0.3 dB.

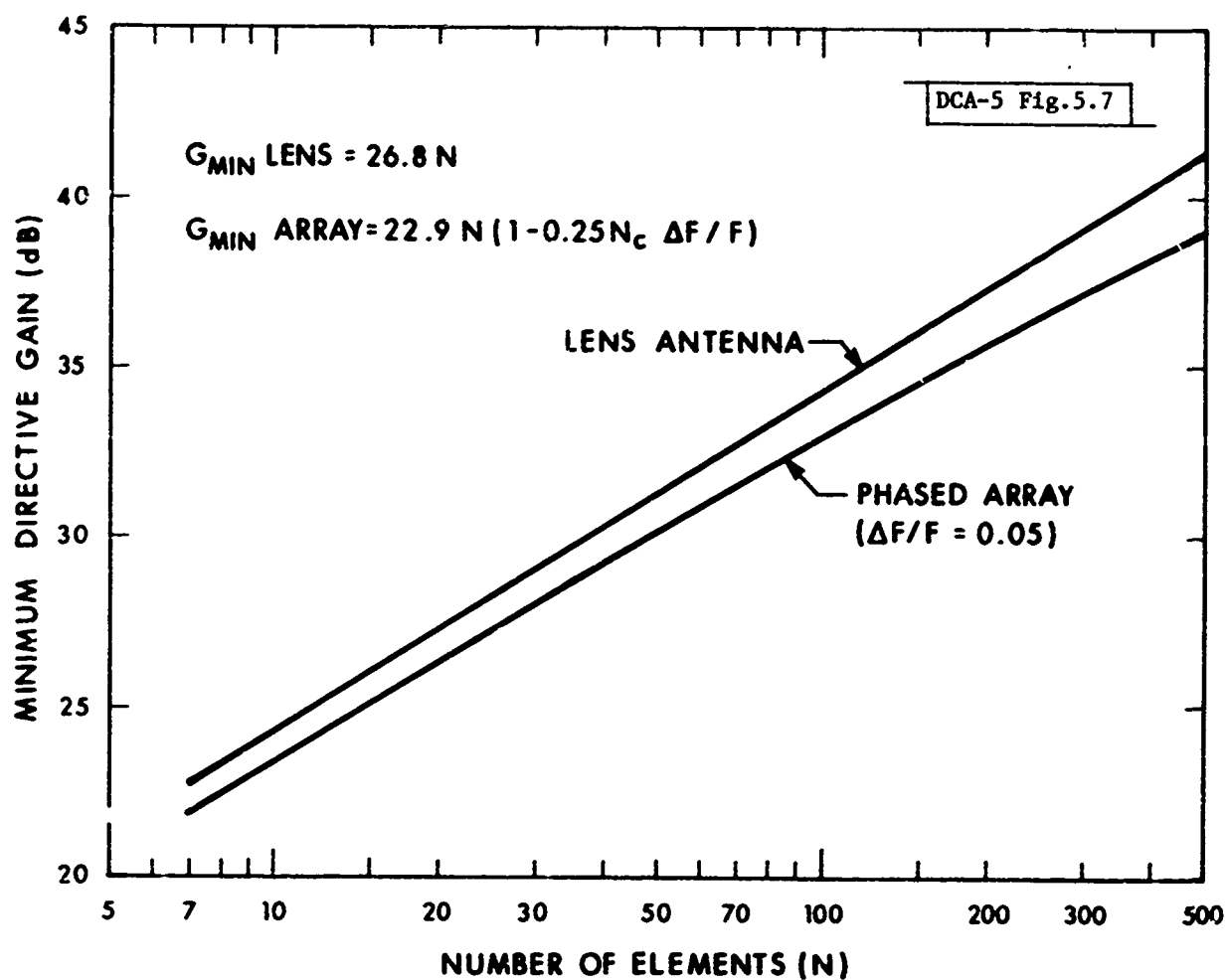


Fig. 5.7. Minimum gain for hexagonal time-hopped-beam antenna versus number of element ($\theta_m = 90^\circ$).

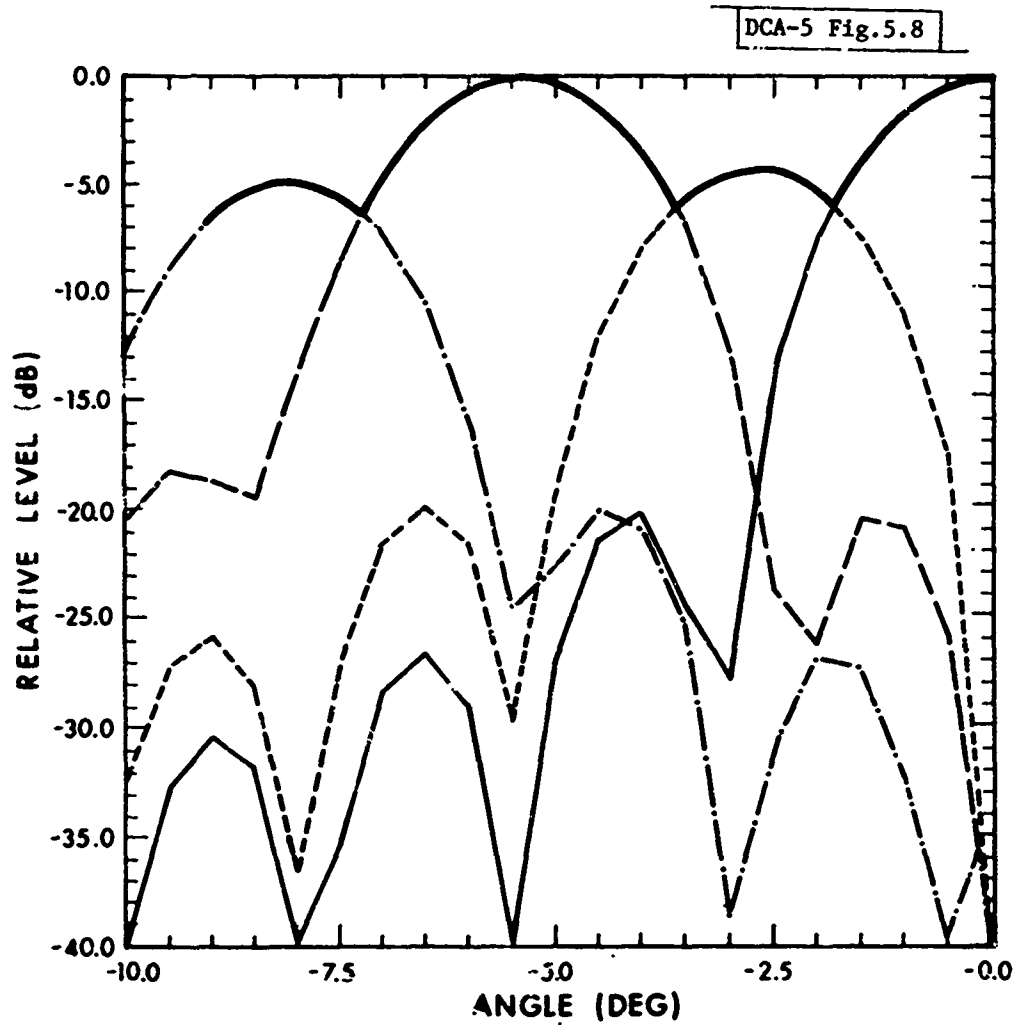


Fig. 5.9. Calculated radiation patterns of 37-beam waveguide lens showing minimum gain ($\theta_m = 90^\circ$).

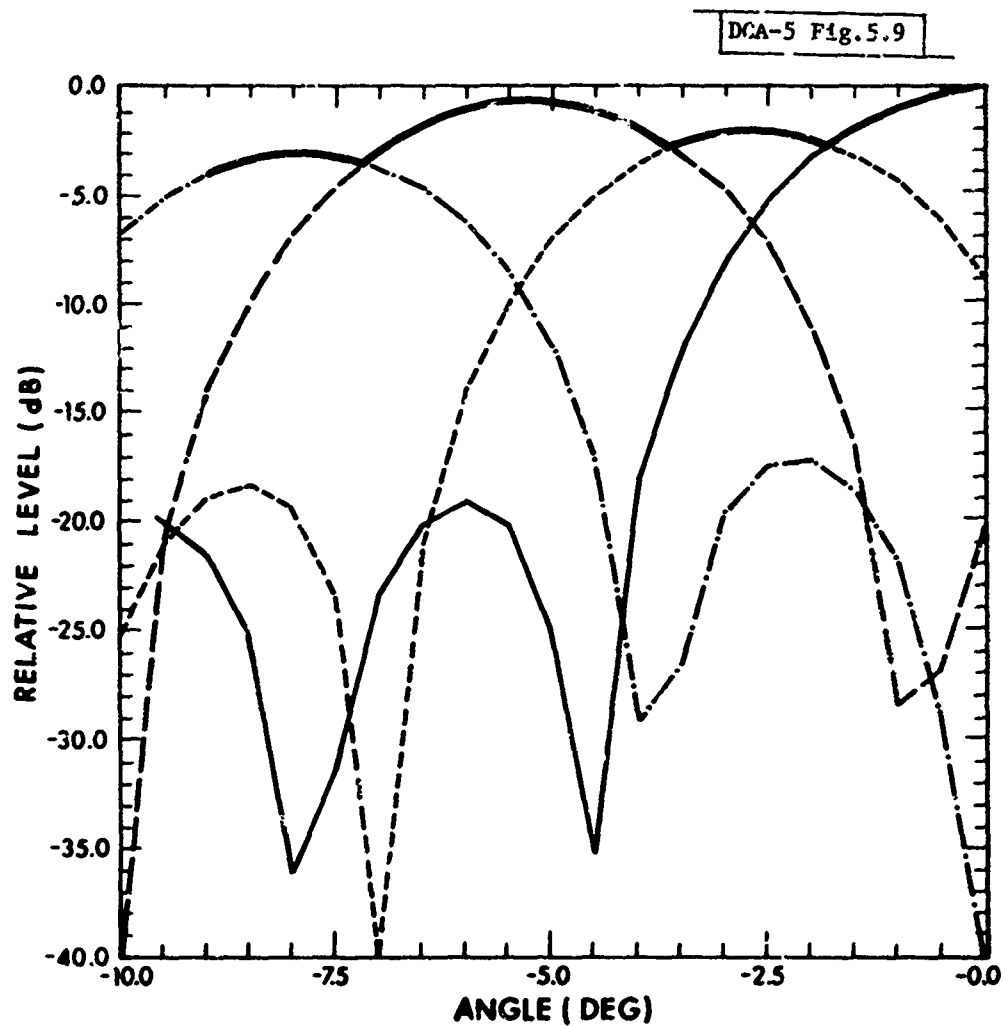
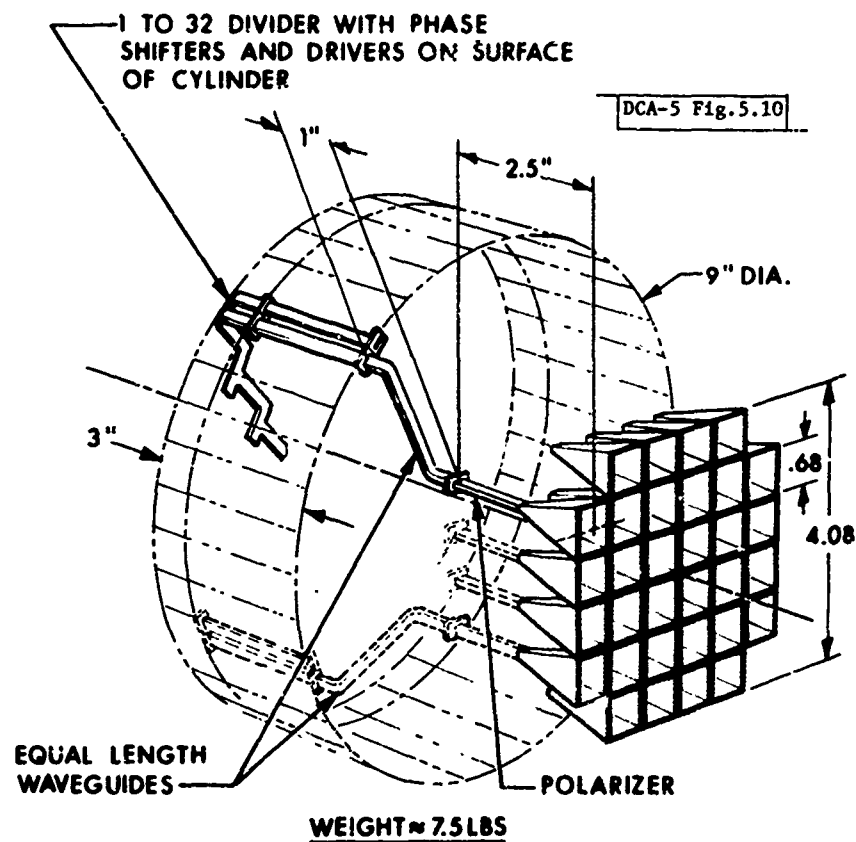


Fig. 5.9. Calculated radiation patterns of 37-element phased array showing minimum gain ($\theta_m = 9^\circ$).



RF LOSSES

FERRITE PHASE SHIFTERS	1.2 dB
WAVEGUIDE	0.4 dB
MISMATCH	0.2 dB
POLARIZATION	0.2 dB
QUANTIZATION	0.1 dB
<u>RF LOSSES</u>	<u>2.1 dB</u>
81% ELEMENT EFFICIENCY	0.9 dB
THEORETICAL GAIN	28.6 dB
<u>CALCULATED LOSSES</u>	<u>3.0 dB</u>
MINIMUM GAIN	25.6 dB

Fig. 5.10. Calculated gain and mechanical characteristics of 43-GHz, 37-beam phased array ($\theta_m = 90^\circ$).

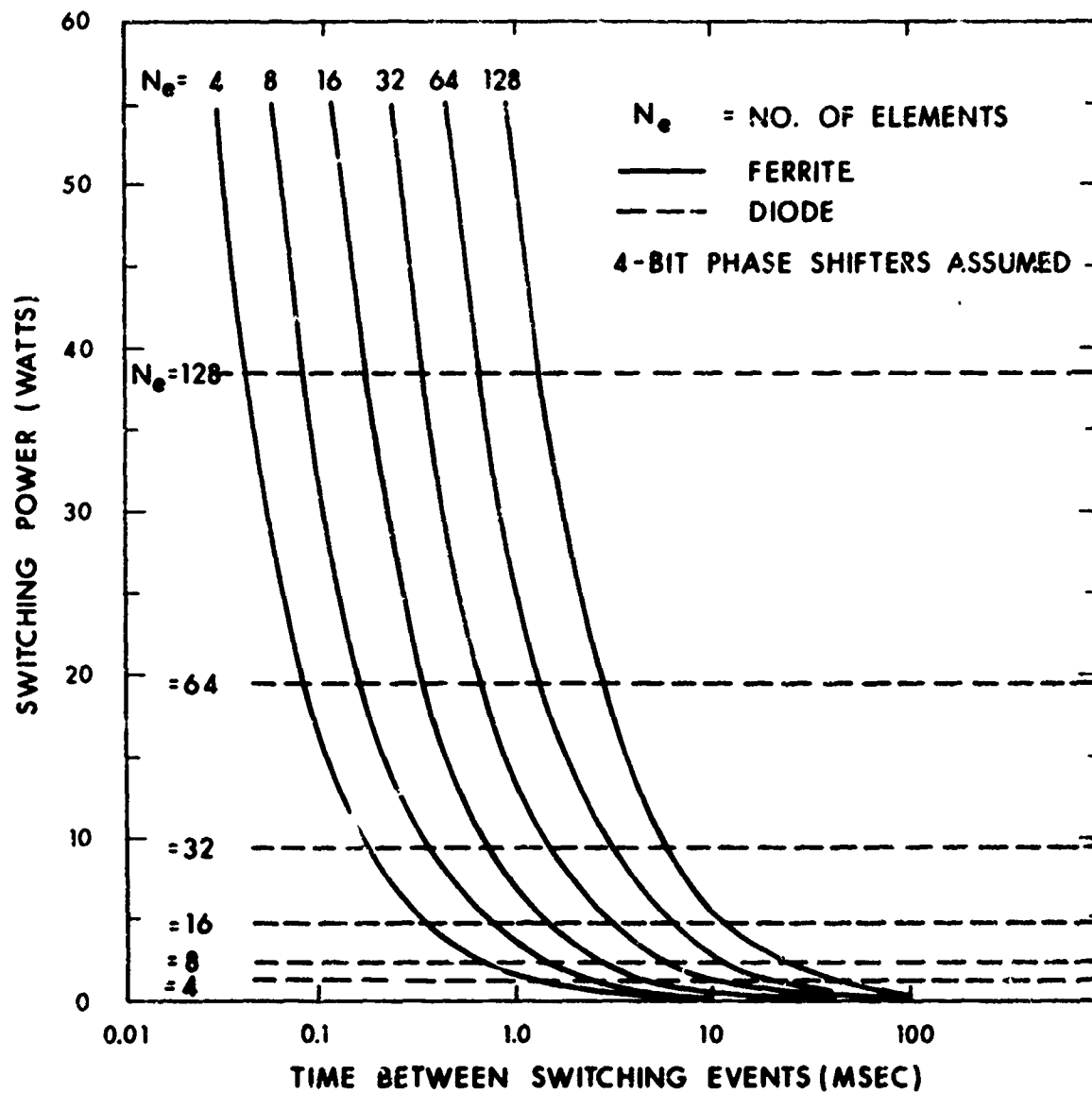


Fig. 5.11. Power consumption of phase-shifters in a time-hopped-beam array versus switching rate.

C. Multiple-Beam Antennas

The capabilities of multiple-beam antennas (MBAs) are numerous, e.g., beam steering, beam shaping, sidelobe control and adaptive nulling. Considering their potential for increasing system capacity, operational flexibility and increasing AJ protection, it is probable that MBAs will be utilized in EHF MILSATCOMs. The choice of the generic MBA is among the reflector, phased array and lens. The reflector MBA, while providing high gain, wide bandwidth and light weight, is only well suited for applications requiring a small number of beams or compatibility with offset feeds. The phased array, while providing the greatest flexibility, imposes null bandwidth limitations and the greatest weight, loss and complexity penalty. The lens, while providing comparable performance to either of the other MBA types, has had a bandwidth limitation (dispersion of the waveguide lens) or a weight penalty (dielectric lens) associated with it. However, a technique for broadbanding (i.e., $\approx 25\%$ bandwidth) the waveguide lens has recently been developed⁽³⁵⁾. In addition, the smaller aperture required at EHF (e.g., ≈ 8 -in. diameter lens for 61-beam MBA at 44 GHz) may remove the weight restriction of a dielectric lens. The lens seems a viable choice for MBA applications at EHF: the tradeoff between a broadband-waveguide and a dielectric lens remains to be determined. Utilization of the MBA capabilities at the EHF bands requires a broadband beam-forming network (BFN) having the requisite performance characteristics. A recommended BFN configuration would employ variable power dividers (VPDs) based on the DSCS-III technology, and requires development.

D. Adaptive-Nulling Antennas

Adaptive-nulling antennas afford the opportunity for 30 dB or more suppression of jammer signals. They offer the potential for reducing terminals cost and complexity against current jamming threats or mitigating future increased jamming threats. The use of adaptive nulling antennas at EHF allows the practical realization of high resolution nulls capable of providing AJ protection in tactical scenarios. This section briefly addresses the theoretical performance and implementation issues associated with adaptive nulling.

The primary performance characteristics of adaptive-nulling antennas are:

1. Degrees of freedom
2. Resolution
3. Jammer suppression
4. Nulling bandwidth

The degrees of freedom are approximately equal to the number of weighted beams and are dictated by the potential number of jammers, jammer locations and desired jammer suppression. As these are primarily system design considerations, the degrees of freedom required are not addressed herein. The primary factors affecting resolution are:

1. Antenna aperture size
2. Bandwidth

Fig. 5.12 presents the theoretical loss in satellite antenna gain to the user for 40 dB suppression of a single jammer as a function of their angular separation ($\Delta\theta_1$) normalized to the nulling antenna peak-to-first-null width (T). Note the difference in the loss in gain to the user depending upon whether the nulling antenna is operating in an earth-coverage or spot-beam mode. In particular, for the spot-beam mode, the nulling of a jammer whose angular separation is only 1/3 the nulling antenna beamwidth causes only a 5 dB reduction in user signal and a net reduction in jammer signal of 35 dB. The need for high resolution antennas, e.g., time-hopped-beam, in conjunction with adaptive nulling is evident. Figs. 5.13 and 5.14 present similar theoretical results when the jammer separation is expressed in miles on the Earth surface with nulling-antenna aperture as a parameter, for elevation angles of 90° and 20°, respectively. Table 5.3 summarizes the results for 100 λ adaptive antenna (note that a 100 λ aperture at 30 and 44 GHz is of the order of 3 ft. and 2 ft., respectively).

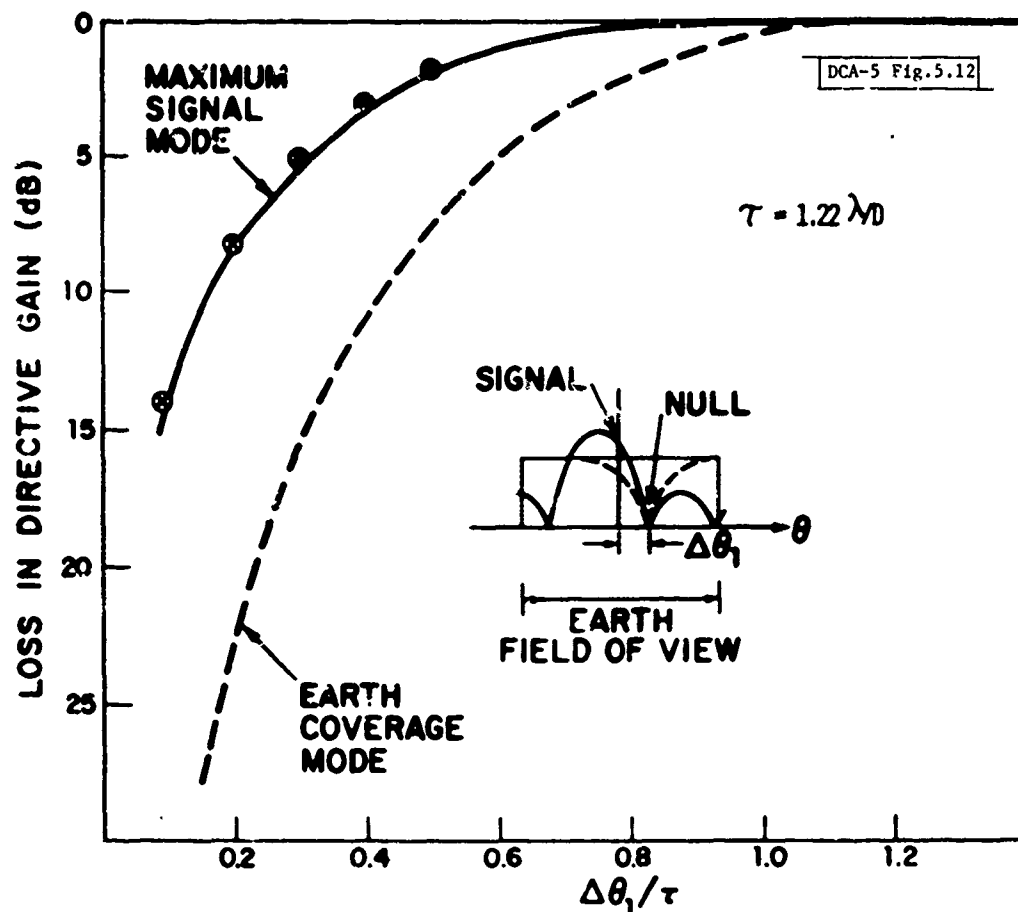


Fig. 5.12. Loss in satellite antenna gain to a user as a function of the angular separation ($\Delta\theta_1$) of a single jammer in nulling antenna peak-to-first-null width (T).

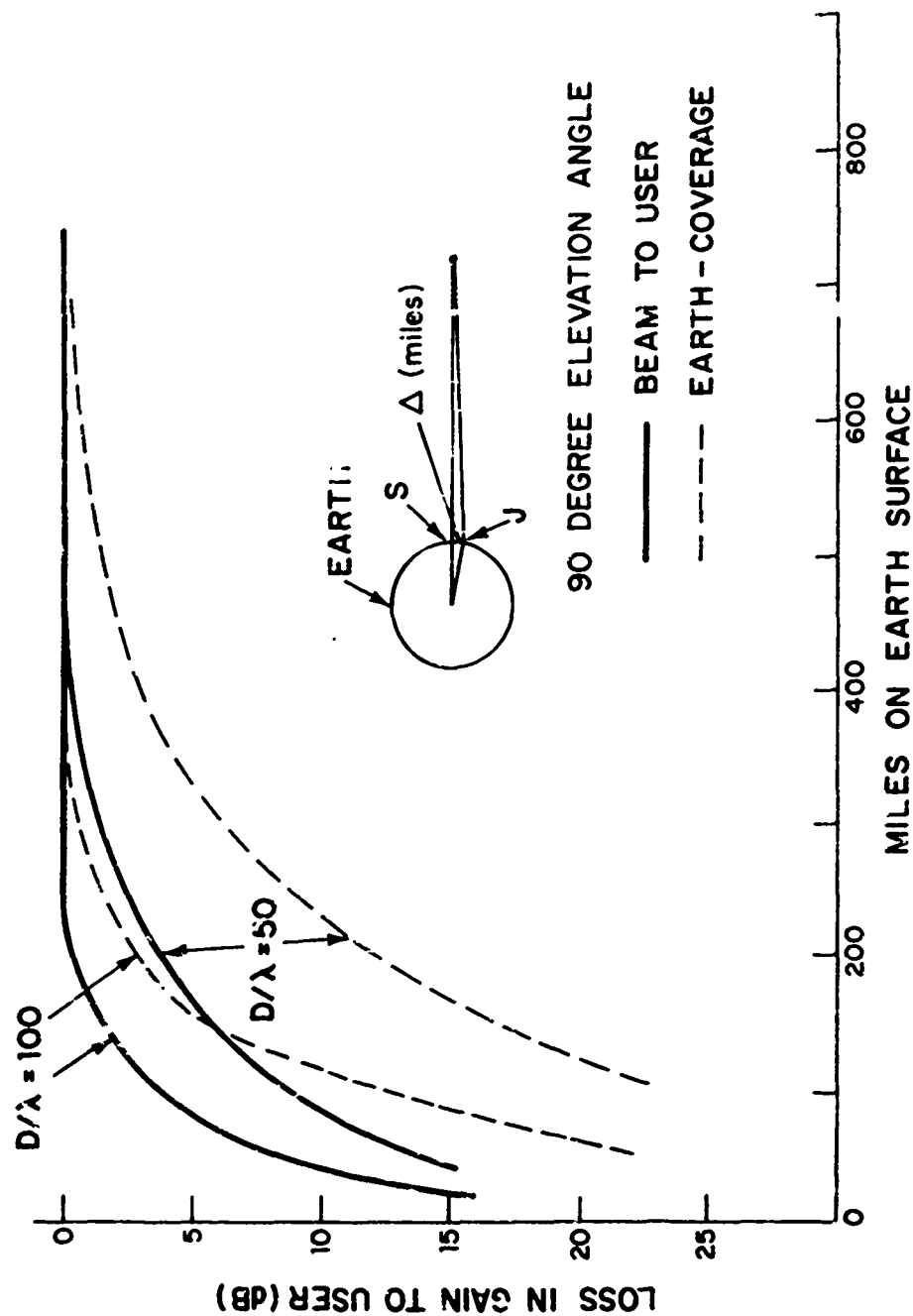


Fig. 5.13. Loss in satellite antenna gain to a user as a function of the jammer separation in miles with nulling antenna aperture as a parameter (90° elevation angle).

18-6-19645

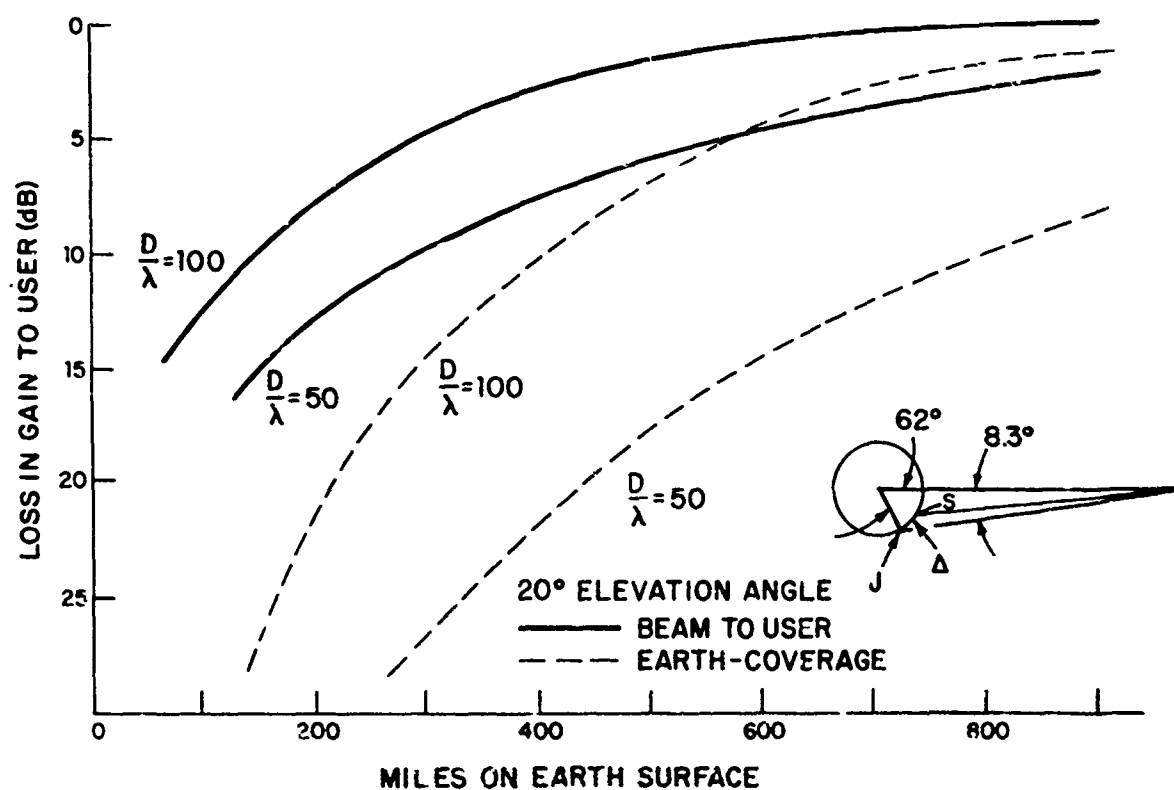


Fig. 5.14. Loss in satellite antenna gain to a user as a function of the jammer separation in miles with nulling antenna aperture as a parameter (20° elevation angle).

TABLE 5.3
POTENTIAL RESOLUTION OF A 100λ
ADAPTIVE NULLING ANTENNA*

PARAMETER	ELEVATION ANGLE (deg.)			
	90		20	
SPOT SIZE (MILES)	280		930	
USER-JAMMER SEPARATION (MILES)	120	50	380	150
USER LOSS IN GAIN (dB)	3	10	3	10

*40 dB cancellation

The methodology for practically assessing adaptive-nulling performance is more complex than the previous examples. The performance assessment must include:

1. Number, location, EIRP and data rate of the users.
2. Number, location and EIRP of the jammers.
3. Tolerable $E_b/(N_0 + J_0)$.
4. Percent of FOV over which required $E_b/(N_0 + J_0)$ is achieved.
5. Operating bandwidth.

Such an assessment is beyond the scope of this report and must be addressed in other studies. This report addresses the technology required for the implementation of adaptive-nulling antennas at EHF which take full advantage of the wide available bandwidth and high potential resolution.

The implementation issues to be addressed at EHF are in regard to achieving broadband nulling channels (i.e., compatible with the spread spectrum bandwidths) and the implementation of high resolution antennas. The broadband nulling circuits* may be implemented either at EHF or at an intermediate (IF) frequency. For direct weighting and combining at EHF rather than at IF, the output ports of the MBA or phased array are weighted and combined in a variable power divider (VPD) as in the DSCS-III system. The combined signal is then mixed to an IF frequency, probably at X-band, by a direct conversion mixer. The advantage of EHF nulling circuits is that the entire 1 or 2 GHz frequency-hopping bandwidth is nulled, thereby avoiding the digital complexity of implementing hop-by-hop adaption. An additional advantage of nulling the entire band is that the nulling circuitry is essentially transparent to the user's signals, thus avoiding system interactions due to timing or transients. It also allows the use of a single receiver rather than having a separate receiver in each channel. The major potential disadvantages are the weight, insertion loss and required matching of the components in the VPD, and the dimensional tolerance problems of maintaining equal RF path lengths from each input port to

*F. W. Floyd, Internal Memorandum.

the combiner output port, both in terms of fabrication and space environment. Further investigation is required to assess these potential drawbacks. Alternatively, IF nulling circuits require separate downconverters on each channel. After amplification and band-limiting at IF, the signals are weighted and then combined in a VPD network. In order to null the entire spread bandwidth with a single weight setting, the front-end mixers must be phase and amplitude matched over the entire 1 or 2 GHz band. Mixer matching is an area of uncertainty that needs to be explored as the degree of matching achieved determines the attainable null depth.

The uncertainties associated with the implementation of high resolution antennas at EHF are primarily associated with the generic type of antenna, the number of feed elements and the coverage area requirements. The antenna choice is between the phased array and the MBA. For large aperture requirements, a filled array becomes too heavy and complex, while thinning the array results in grating lobes. For the MBA, there are also weight and complexity limitations associated with the number of beams generated. For tactical applications requiring high resolution beams only within a restricted coverage area, an appropriate size lens and modest feed array would suffice. However, to vary the coverage area would require mechanical scanning of the lens antenna. Alternatively, the use of a space-fed array would provide electronic scanning of the coverage area and additional flexibility. Detailed antenna studies and development efforts are needed.

In summary, for the realization of the full advantages of adaptive nulling antennas at EHF, it is essential to:

1. Develop broadband adaptive-nulling channels capable of operating over a 1 or 2 GHz bandwidth both at EHF and IF frequencies.
2. Study and develop techniques for implementing high resolution EHF antennas, e.g., filled or thinned arrays, space-fed arrays, lens antenna.

5.4 Summary

A. Ground Segment

For the ground segment, antenna requirements will be satisfied by parabolic reflector antennas. The impact of the bandwidth requirements and insertion loss at EHF on antenna subsystem design, and the potential use of low-sidelobe antennas warrant further investigation. Specific areas warranting further study and development include:

1. Design of high-efficiency and tracking feeds, polarizers, diplexers, etc. for the EHF bands.
2. Development of low-loss, higher-order mode waveguide components for all terminals, and beam-waveguide techniques for fixed terminals.
3. Study and development of sidelobe-reduction techniques including special antenna feed and feed-support designs, offset-fed reflectors, absorber tunnels, and adaptive sidelobe cancellation.

B. Space Segment

Advances in satellite antenna technology offer significant improvements in communication capacity and AJ protection, and potential reductions in terminal size, cost and complexity. Operation at EHF allows the practical implementation of high resolution beams or nulls, and affords the opportunity to take full advantage of advanced antenna technology. Particular antenna technology warranting further study and development includes:

1. For fixed-beam applications, tradeoff studies of the electrical and mechanical characteristics between the phased-array and reflector antenna; development and evaluation of spatial-power-combining arrays.
2. For time-hopped-beam antennas, development and evaluation of phased-array and lens antennas, space-qualified phase shifters (ferrite and diode) and ferrite switches; study of prime power tradeoffs as a function of antenna, state-changing device and beam-switching rate and algorithm.

3. For multiple-beam antennas, development of a broadband waveguide or dielectric lens, and variable power dividers required for the beam-forming network.

4. For adaptive-nulling antennas, development of adaptive-nulling circuits capable of operating over a 1 or 2 GHz bandwidth at EHF or IF; study and development of techniques for implementing high resolution EHF antennas.

VI. PROPAGATION EFFECTS

6.1 Background

Rain attenuation is one of the critical parameters affecting the frequency selection for future MILSATCOM systems operating above 8/7 GHz. Alternatively, if the selection of operating frequency is driven by unique requirements such as improved AJ or LPI performance, rain attenuation dictates the margin requirements and elevation angle restrictions and impacts the system availability and cost. Accurate estimates of rain attenuation on a global basis are indicated to support such studies; it is the purpose of this section to provide these estimates based on the current state-of-the-art in predictive models.

Attenuation due to the clear atmosphere, clouds, fog, sleet and snow are first briefly examined and shown to be subordinate to the attenuation due to rain. Next, the constituent parameters of rain attenuation models are examined vis à vis the currently proposed CCIR model⁽³⁶⁾. Using this model as representative of the state-of-the-art in predictive techniques, extensive estimates of rain attenuation are presented as a function of geographic location, availability, frequency and elevation angle. The impact of rain attenuation on system availability, site diversity and response time is then briefly discussed. Finally, recommended areas for further study are delineated.

6.2 Attenuation Due to Atmospheric Absorption, Clouds, Fog, Snow, and Sleet

A. Atmospheric Absorption

Propagation through the clear atmosphere at frequencies above 10 GHz is affected by molecular absorption due to oxygen and water vapor. The combined attenuation due to these two components is shown in Figs.⁽³⁷⁾ 6.1 and 6.2. Fig. 6.1 gives the one-way zenith attenuation values between the listed start heights and the top of the atmosphere and may be of interest for airborne terminals. The relative effects of water vapor are shown in Fig. 6.2. The contribution due to water vapor is for an assumed density of 7.5 gm/m^3 , which is typical of a moderately humid atmosphere (43 percent relative humidity at 20°C). Both the 0 percent and 100 percent dashed curves are fictitious but serve to illustrate the bounds on water vapor absorption.

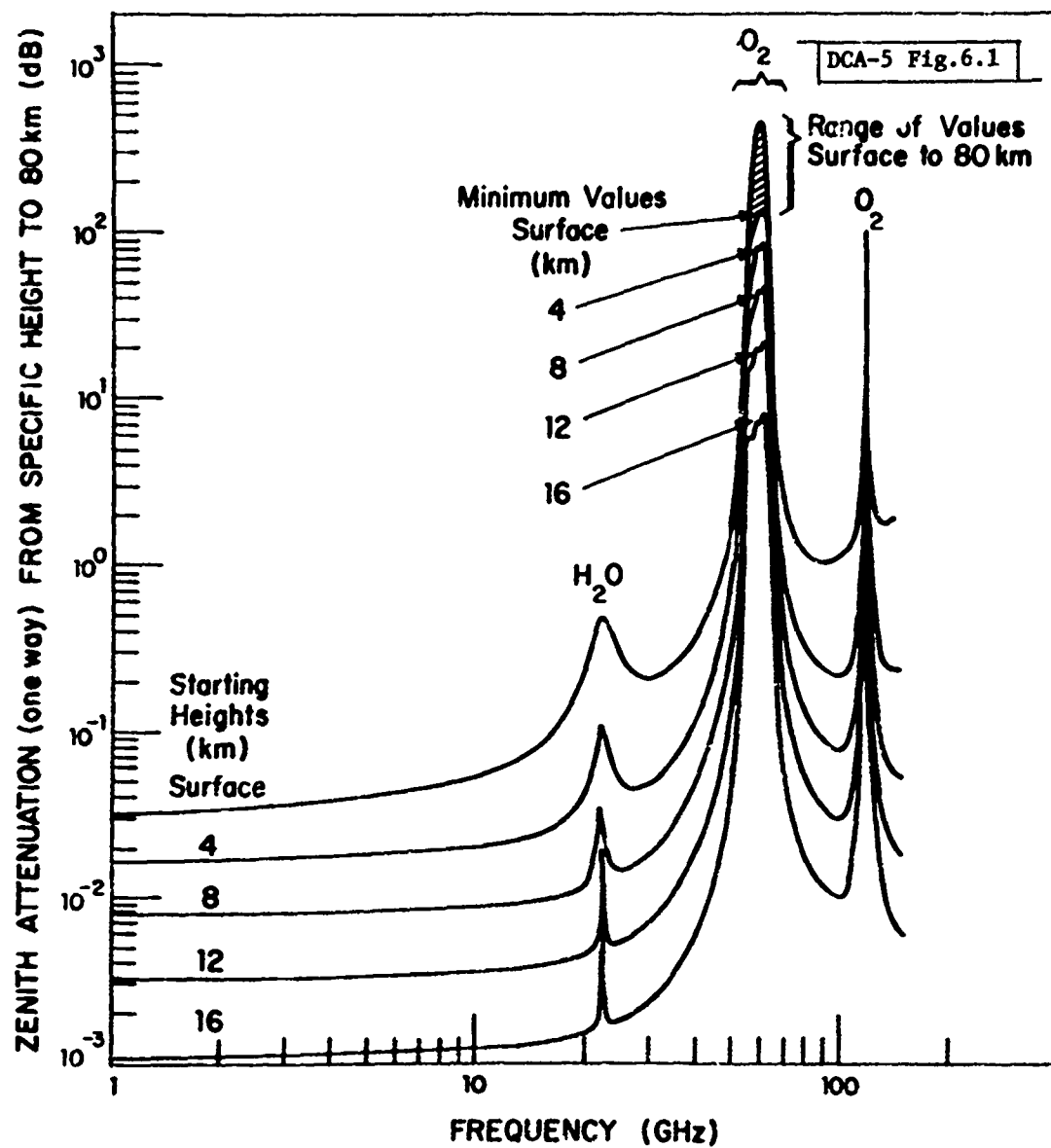


Fig. 6.1. Theoretical one-way zenith attenuation from specified height to top of the atmosphere for a moderately humid atmosphere (7.5 g/m^3 at the surface).

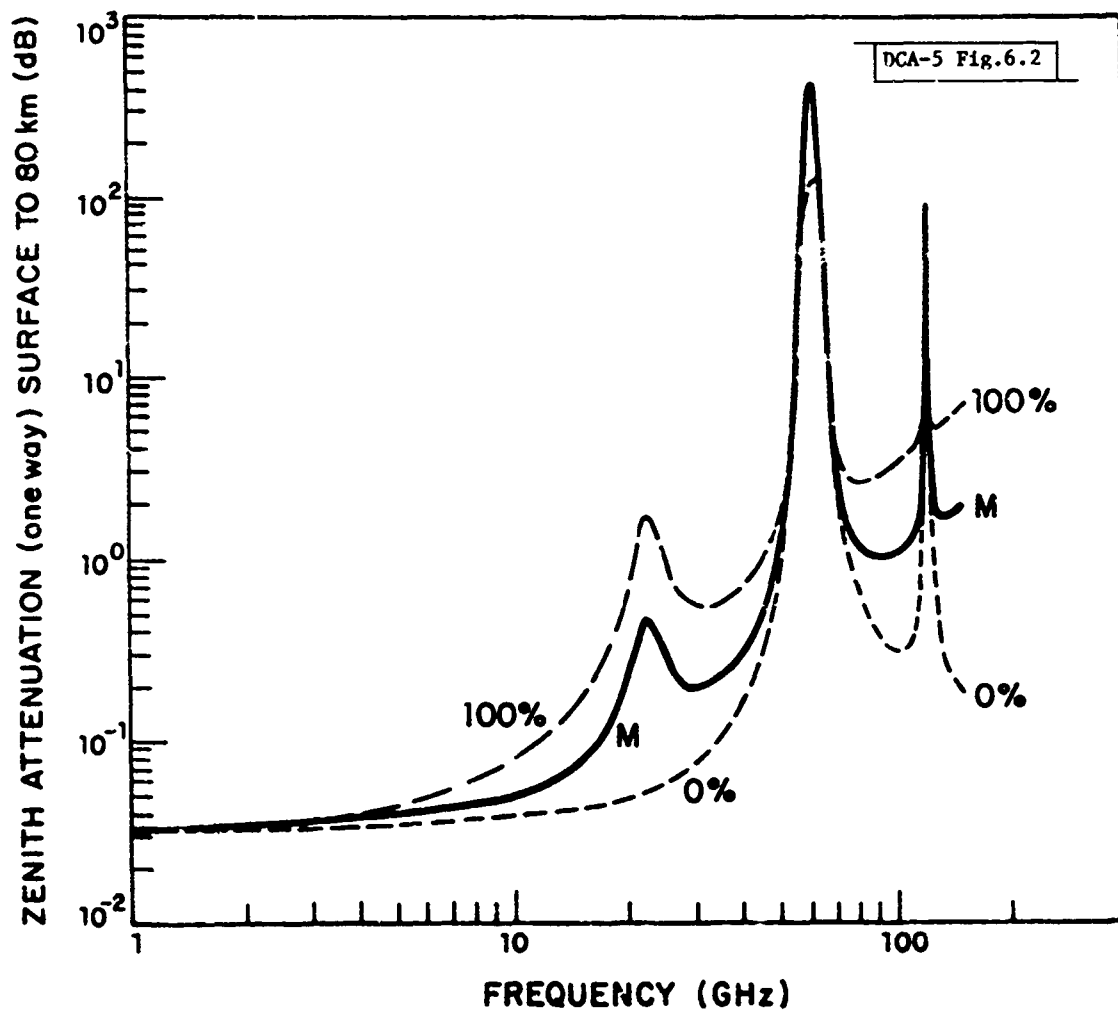


Fig. 6.2. Theoretical one-way zenith attenuation through the atmosphere for various relative humidities ($M = 43\%$ at 20°C).

Attenuation due to molecular absorption in the atmosphere is always present and must be included in the computation of total path attenuation. Assuming a flat earth, the atmospheric attenuation as a function of elevation angle is given by the zenith attenuation multiplied by the cosecant of the elevation angle. (The cosecant relationship does not hold for elevation angles less than 10° due to earth curvature and refraction effects.) Using the zenith attenuation versus frequency curve of Fig. 6.2 for a moderately humid atmosphere, atmospheric attenuation versus frequency and elevation angle are presented in Table 6.1. These attenuation values represent the minimum margins that must be provided regardless of availability requirements or use of site diversity. These "clear sky" attenuations are also added to the rain attenuation values derived later.

B. Clouds and Fog

Whereas the drop sizes of rain (between 0.5 and 5 mm in diameter) make it necessary to apply the Mie scatter theory to calculate the loss, the droplet sizes in clouds and fog (between 10 and 100 μm in diameter) permit the use of the Rayleigh approximation. Consequently, it is possible to express the attenuation due to clouds and fog in terms of the total water content per unit volume⁽³⁸⁾. Thus the absorption within such a cloud or fog can be written as:

$$A_c = K_\ell M \quad (\text{dB/Km}) \quad (6.1)$$

where A_c = the absorption coefficient

K_ℓ = attenuation coefficient in $\text{dB/Km}(\text{g/m}^3)^{-1}$

M = liquid water content in g/m^3

Values of K_ℓ are plotted in Fig. 6.3⁽³⁹⁾ for the frequency range from 7 to 50 GHz and for various temperatures. Given the liquid water content and vertical extent of clouds or fog, the zenith attenuation may be determined; for other elevation angles $\geq 10^\circ$, the cosecant relationship may be applied.

TABLE 6.1

ATMOSPHERIC ATTENUATION DUE TO OXYGEN AND WATER VAPOR

FREQ. (GHz)	ATTENUATION (dB)			
	ELEVATION ANGLE (deg)*			
	90	30	20	10
7	0.05	0.1	0.2	0.3
20	0.25	0.5	0.8	1.4
30	0.2	0.4	0.6	1.1
40	0.3	0.6	0.9	1.7
45	0.6	1.2	1.8	3.5
50	1.8	3.6	5.3	10.4

$$*A(\theta) = \text{COSECANT } (\theta) \cdot A(90^\circ), \theta \geq 10^\circ$$

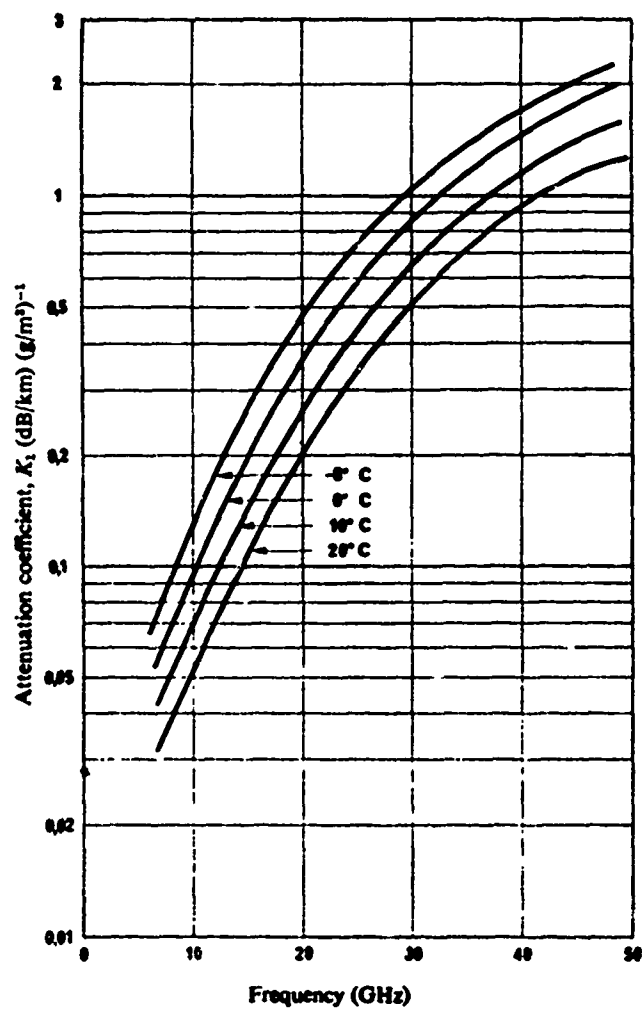


Fig. 6.3. Attenuation by water clouds or fog at various temperatures as a function of frequency (from Ref. 39).

Mist and fog were studied by Ryde and Ryde⁽³⁸⁾ and a relationship between mean water content and visibility was developed. For example, for heavy fog the visibility is 100 ft and $M = 2.3 \text{ g/m}^3$. The height of a fog layer is typically only 200 m and, consequently, attenuation due to fog is a potential problem only for terrestrial communication paths.

For the purpose of discussion, clouds will be characterized according to three types: liquid-water, fair weather and ice clouds. Liquid water clouds may have liquid-water content of 1 to 2 g/m^3 and a vertical extent of 6 Km which would extrapolate to zenith attenuation values in excess of 10 dB at frequencies above 30 GHz. However, the presence of liquid-water clouds such as nimbostratus (steady rain) and cumulonimbus (thunderstorm) implies a rain environment and are accounted for in the rain attenuation model. Fair weather cumulus clouds have a liquid water content of $\approx 0.2 \text{ gm/m}^3$ and an extent of $\approx 1 \text{ Km}$ corresponding to zenith attenuations of 0.1 to 0.5 dB from 20 to 50 GHz. If one is concerned with minimum link margins neglecting rain attenuation, the increase in path attenuation due to fair weather clouds must be added to the attenuation due to atmospheric absorption. Ice clouds, due to the difference in dielectric properties, give attenuations about two orders of magnitude smaller than water clouds of the same water content⁽³⁸⁾ and may be ignored.

C. Snow and Sleet

Attenuation by dry snow and sleet is generally negligible due to the relatively low dielectric constant of water in the solid phase. Attenuation by wet sleet and melting snow is appreciable but has not been investigated because of its relative rarity, at least at ground level. Melting snow is present in the melting layer (just below the 0°C isotherm) at the top of rain region (liquid water drops) but its contribution is small due to the relatively short path lengths through the melting region.

D. Summary

Zenith attenuation as a function of frequency for the various propagation conditions is summarized in Table 6.2. (Rain attenuation estimates are also included in Table 6.2 for the purpose of comparison.) To determine the attenuation values at other elevation angles, the cosecant relationship may be applied to the respective heights given in the footnotes (rain attenuation is excluded and will be discussed later). For considerations of the minimum margin requirements excluding rain attenuation, the clear sky and fair weather cloud attenuations must be added. As atmospheric absorption is evident all the time and the probability occurrence of clouds is not defined, only the clear sky attenuation is included later in the rain attenuation model. Finally, note that even for light rain (2 mm/h), the rain attenuation values far exceed those due to other phenomena, i.e., the rain attenuation is twice the combined attenuations due to atmospheric absorption and fair weather clouds. The remainder of this section addresses rain attenuation modelling and estimates.

6.3 Rain Attenuation Estimation Models

A. Perspective

The physics of rain scattering is well understood and the attenuation may be computed for a given geometry and distribution of raindrops. It is then generally agreed upon that, given the temperature, shape, and size distribution of raindrops along a path, the calculated attenuation would be in good agreement with experimental observations. However, the estimation of rain attenuation for satellite communication systems is dependent upon the knowledge and modelling of the statistical properties of rain.

The estimation of rain attenuation on a global basis is by necessity a statistical process. The constituent parameters of predictive models which must be based on statistical averages include:

1. rain rate versus probability of occurrence, which is a spatial and temporal average of available statistics for given geographic regions.

TABLE 6.2
ZENITH ATTENUATION FOR VARIOUS PROPAGATION CONDITIONS

FREQ (GHz)	ATTENUATION (dB)							
	CLEAR (1) SKY	CLOUDS		LIQUID (4) WATER	HEAVY (5) FOG	RAIN (6)		
		ICE (2)	FAIR (3) WEATHER			2 mm/h (3%)	10 mm/h (0.5%)	50 mm/h (0.1%)
7	0.05	.001	0.015	R A I N E N V I R O N M E N T	0.3	0.04	0.2	1
20	0.25	.01	0.1		0.2	0.7	4.0	23
30	0.2	.02	0.2		0.5	1.7	9.4	52
40	0.3	.03	0.3		0.7	2.5	12.8	66
45	0.6	.04	0.4		0.9	3.5	17.4	89
50	1.8	.05	0.5		1.1	4.3	20.4	98

(1) US standard atmosphere for July at 45° N latitude: $M=7.5 \text{ g/m}^3$ at the surface.

(2) High cirrus-type clouds: $M=0.3 \text{ g/m}^3$, $H=6 \text{ Km}$.

(3) Cumulus clouds: $M=0.2 \text{ g/m}^3$, $H=1 \text{ Km}$.

(4) Liquid water clouds included in rain model.

(5) 100-ft. visibility: $M=2.3 \text{ g/m}^3$, $H=0.2 \text{ Km}$.

(6) Rain rates exceeded (Z) of year in tropical climate: $H=4.8 \text{ Km}$.

NOTE: Attenuation due to dry snow and sleet is negligible.

2. vertical extent of the rain which has a latitude, seasonal and rain rate dependence.
3. raindrop shape and size distribution which is dependent on rain rate and temperature.
4. rain rate distribution along the propagation path.

These comments are not meant to imply that meaningful predictions of rain attenuation cannot be made, but rather that such estimates be made in the proper perspective. As will be shown in the next section, the effect of applying these statistical processes to global predictions is to incur large uncertainty bounds on the resulting estimates. To realize the most representative rain attenuation estimates it is then necessary to utilize the most accurate rain statistics and attenuation prediction model.

The literature abounds with rain attenuation models which do not show consistent agreement with widespread experimental observations. The underlying problem is the persistent disagreement between models assuming horizontally homogeneous rainfall and experimental results; the solution has been to derive empirical path correction factors based on a specific set of attenuation observations. Such empirical corrections must be used with care when applied under conditions other than those on which they are based. This section addresses each of the constituent parameters of rain attenuation models described above and, in particular, the nonhomogeneity of the rain rate.

B. Canonic Rain Attenuation Models

Attenuation due to rain is primarily dependent upon the following parameters;

1. Rain rate along the propagation path
 - raindrop size and shape
 - drop size distribution

2. Length of the path
 - vertical extent of the rain
 - terminal-to-satellite elevation angle
3. Frequency of operation

Canonic rain attenuation models relate these parameters in the following form

$$A = L [k R_0^b] \quad (\text{dB}) \quad (6.2)$$

where A = path attenuation

L = length of propagation path in Km

$k R_0^b$ = specific attenuation in dB/Km

R = point rainfall rate (mm/h) exceeded ρ percent of the time

k, b = frequency dependent coefficients based on raindrop characteristics

The estimation of specific attenuation has received considerable attention. Specific attenuation is typically computed using Mie scattering theory for water spheres assuming a Laws and Parsons dropsize distribution, and theoretical values are in good agreement with experimental observations. A comparison of theoretical and measured values of the coefficients of specific attenuation is shown in Fig. 6.4⁽²⁶⁾. (A detailed tabulation of these coefficients showing their dependence on temperature and assumed dropsize distribution is given in Ref. 40.) It is generally accepted that for a given rain rate an accurate estimate may be made of the specific attenuation from which the path attenuation may be estimated for a given path length over which that rain rate exists. The uncertainty in rain attenuation models is primarily associated with the estimation of the rain rate statistics, both the surface point rain rate distribution and the rain rate distribution along the path.

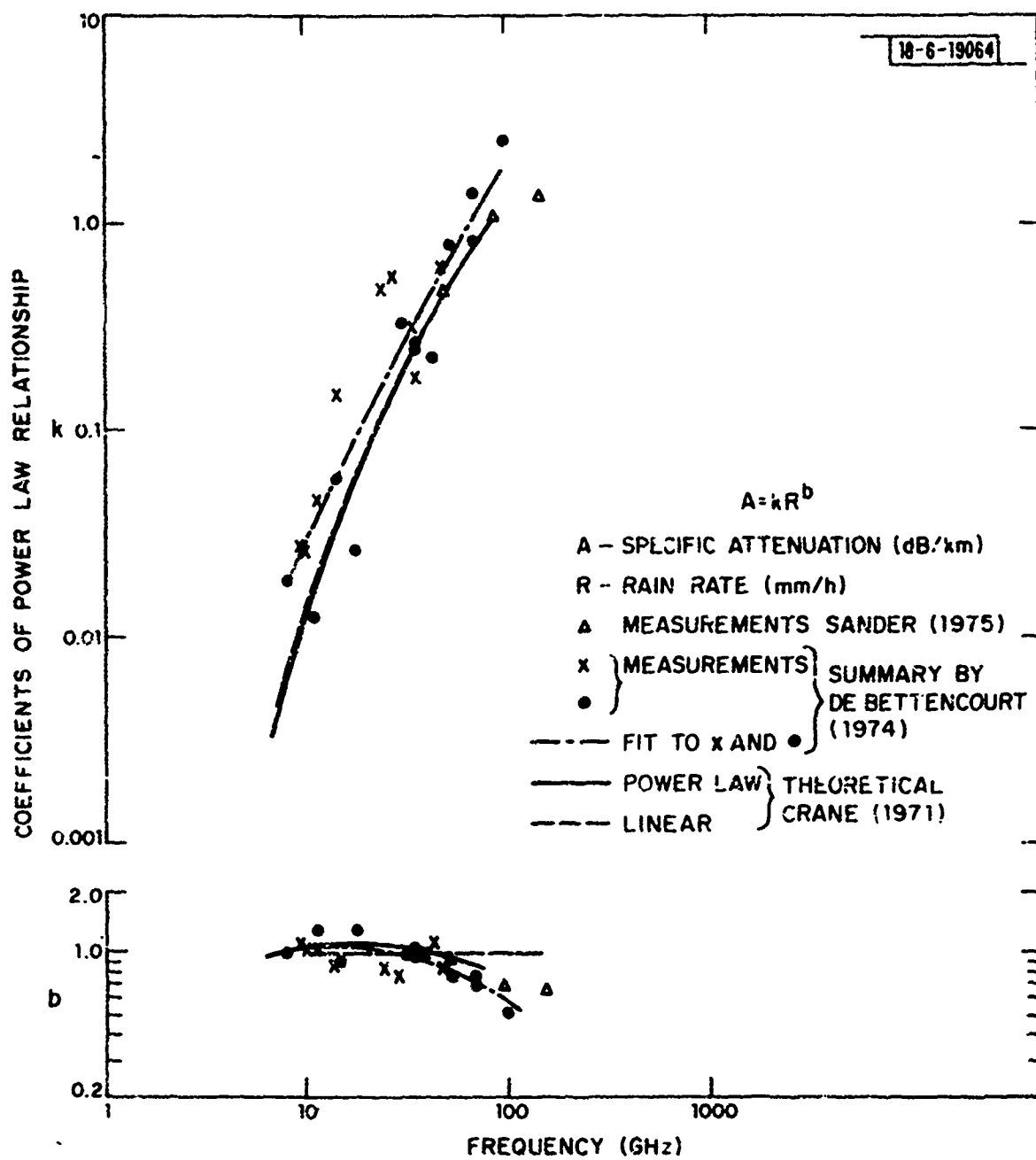


Fig. 6.4. Coefficients of specific attenuation as a function of frequency.

C. Propagation Path Length

It is generally assumed that the rain rate is uniform from the surface to the melting layer (0°C isotherm) where rapid conversion from water to ice occurs. The specific attenuation is then assumed to be constant up to the height of the melting layer (H) and zero above. There is some uncertainty associated with the height of the melting layer. Specific values are available for locations where weather radar data has been collected and typical results are given in Fig. 6.5⁽²⁶⁾. Global estimates for melting layer heights as a function of latitude and season are included in the proposed CCIR model to be addressed in the next section. To determine the propagation path, the simplest models assume a cosecant pathlength dependence, i.e., path length, $L = H \csc \theta$, for elevation angles, $\theta > 10^{\circ}$ (see for example Refs. 41 and 42). Inherent in the cosecant model is the assumption that the path average rain rate is equal to the surface point rain rate, i.e., that the rain rate is horizontally homogeneous. This canonic model of the earth-satellite path is shown in Fig. 6.6. In contrast to this model, meteorological data shows that the path average rain rate exceeded for a specified percentage of time may differ significantly from the point rain rate exceeded for the same percentage of time. This inhomogeneous rain rate distribution along the path is evident in rain attenuation observations and has led to the concept of an effective path length (see for example Refs. 43 and 44). This path length factor is typically derived from measured rain attenuation by assuming constant specific attenuation along the path and that the ratio of measured to calculated rain attenuation (A) equals the ratio of effective to physical path length, i.e., path length factor = $(A_{\text{measured}}/A_{\text{calculated}})$. Fig 6.7 shows path length factors determined from rain attenuation measurements (also included are the cosecant model and an empirical model used in previously reported⁽²⁶⁾ estimates). Note the variation in the empirically-determined path length factors for a given elevation angle, e.g., by a factor of two for elevation angles less than 60° and by a factor of three for elevation angles less than 20° ; the variation in measured path attenuation is, of course, identical. The variations in effective path length as

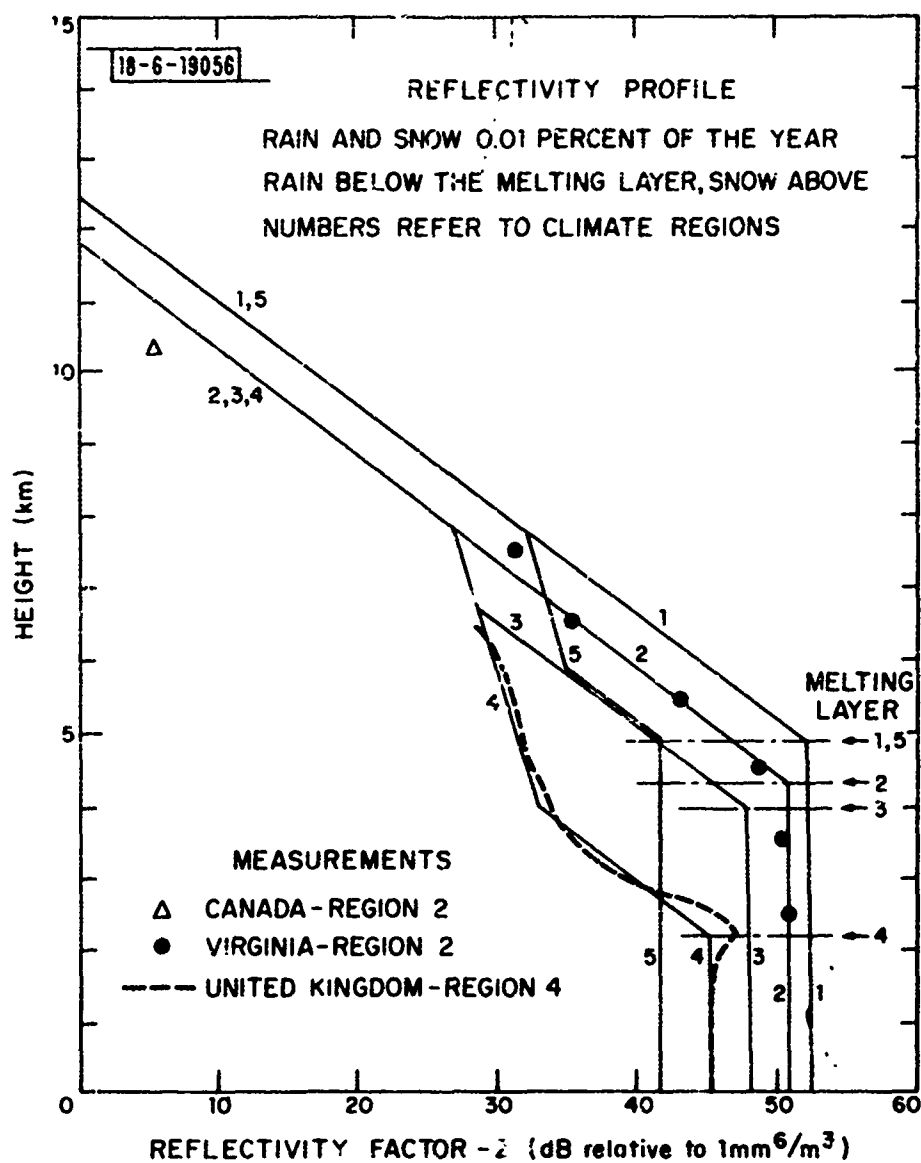
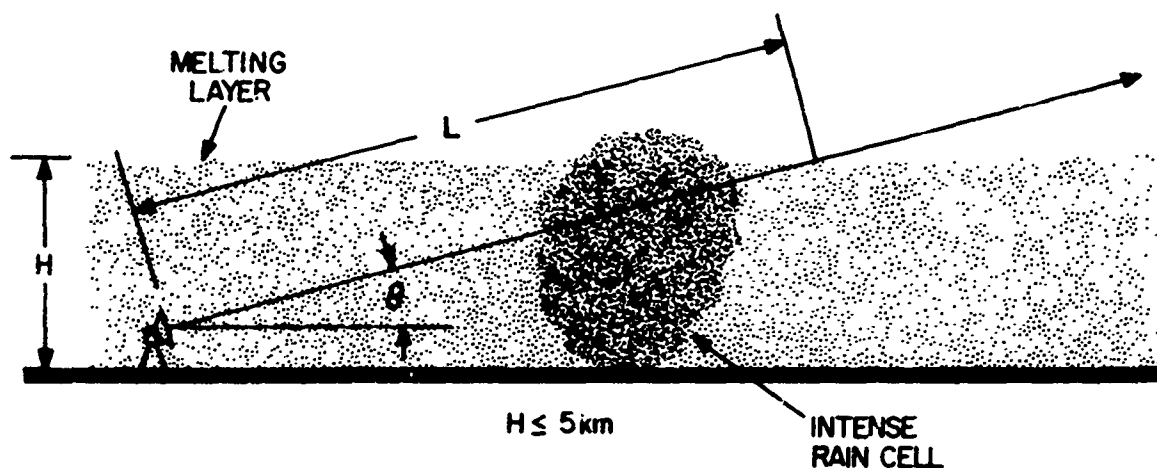


Fig. 6.5. Height of the melting layer (0°C isotherm) for various CCIR rain climate regions.

18-6-19488



GENERAL ASSUMPTION: RAIN RATE UNIFORM FROM SURFACE TO MELTING LAYER HEIGHT (0°C isotherm), H , AND VANISHES FOR HIGHER ALTITUDES

COSECANT MODEL: ASSUMES RAIN HORIZONTALLY HOMOGENEOUS $L = H \text{ COSECANT } (\theta)$, $\theta \geq 10^\circ$

EMPIRICAL MODELS: OBSERVATIONS (attenuation and weather radar) SHOW INHOMOGENEOUS RAIN DISTRIBUTION ALONG PATH LEADING TO EMPIRICAL PATH AVERAGE FACTORS

Fig. 6.6. Canonic model of Earth-satellite path.

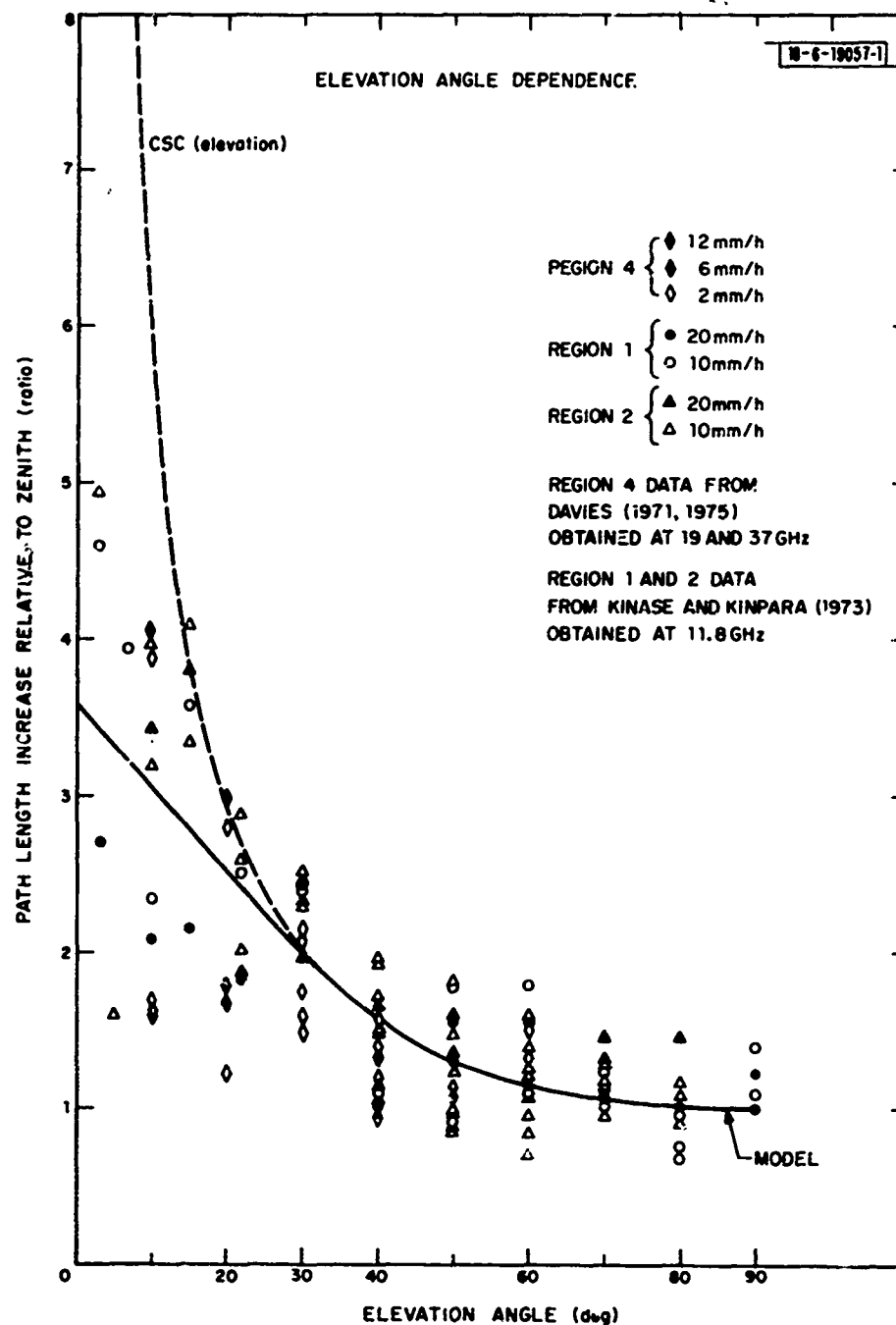


Fig. 6.7. Effective path length versus elevation angle.

as determined from measured rain attenuation are due to the limited data base (e.g., observation periods and elevation angles) and to the dependence on the specific parameters of the experiments (e.g., climate region and frequency). In the model described in Section 6.4, path length factors are determined from measurements of the rain rate distribution along a path as a function of the point rain rate and the length of the propagation path.

D. Rain Rate Statistics

Global estimates of rain attenuation, require, in addition to knowledge of the coefficients of the specific attenuation and of the effective propagation path, a global definition of rain climate regions and corresponding rain rate distributions. In 1974, the CCIR⁽⁴⁵⁾ introduced five rain climate regions (Fig. 6.8) and the surface point rain rate distribution for each climate region (Fig. 6.9). This CCIR model represented the best data available when it was developed. Since that time, the model has been revised as countries determined that the model did not accurately represent their region. In a previous report⁽²⁶⁾, rain attenuation estimates were generated using this CCIR model, the coefficients of specific attenuation in Fig. 6.4, the melting layer heights in Fig. 6.5 and the effective path length model in Fig. 6.7. Fig 6.10 shows the comparison between predicted and observed attenuation values. Note that the observed attenuation in Region 1 (heaviest rain) is a factor of 2 (Panama) and 3 (Malaysia) greater than the prediction. The discrepancies arise from the fact that the observed rain rates in these areas are factors of two and three larger than those predicted by the CCIR rain rate distributions.

E. Summary

The determination of the coefficients of specific attenuation is well understood and agreed upon. The primary discrepancies in rain attenuation estimation models arise from the rain rate statistics and the nonhomogeneity of the rain rate along the path. The shortcomings of most models include

1. Assumed homogeneous rain distribution along the path which leads to large errors at low elevation angles (e.g., factor of 3 at 20°).

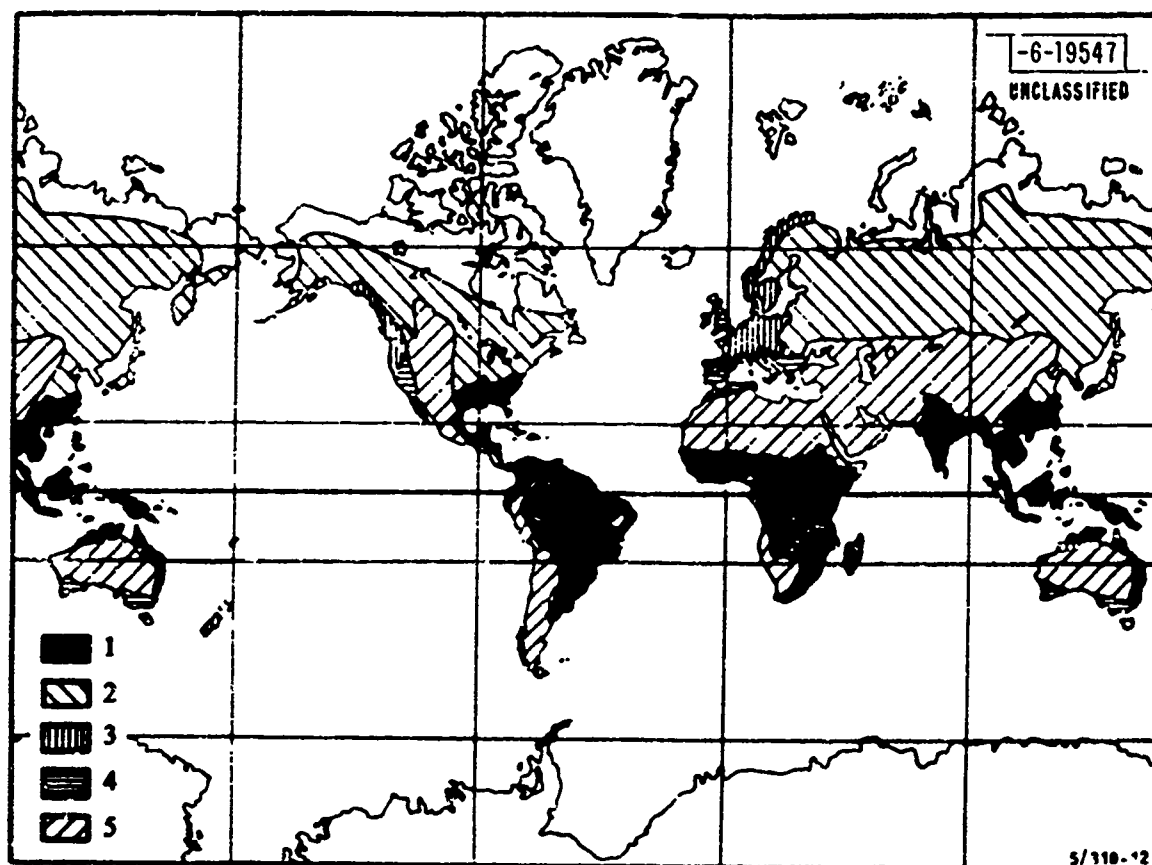


Fig. 6.8. CCIR rain rate climate regions (from Ref. 45).

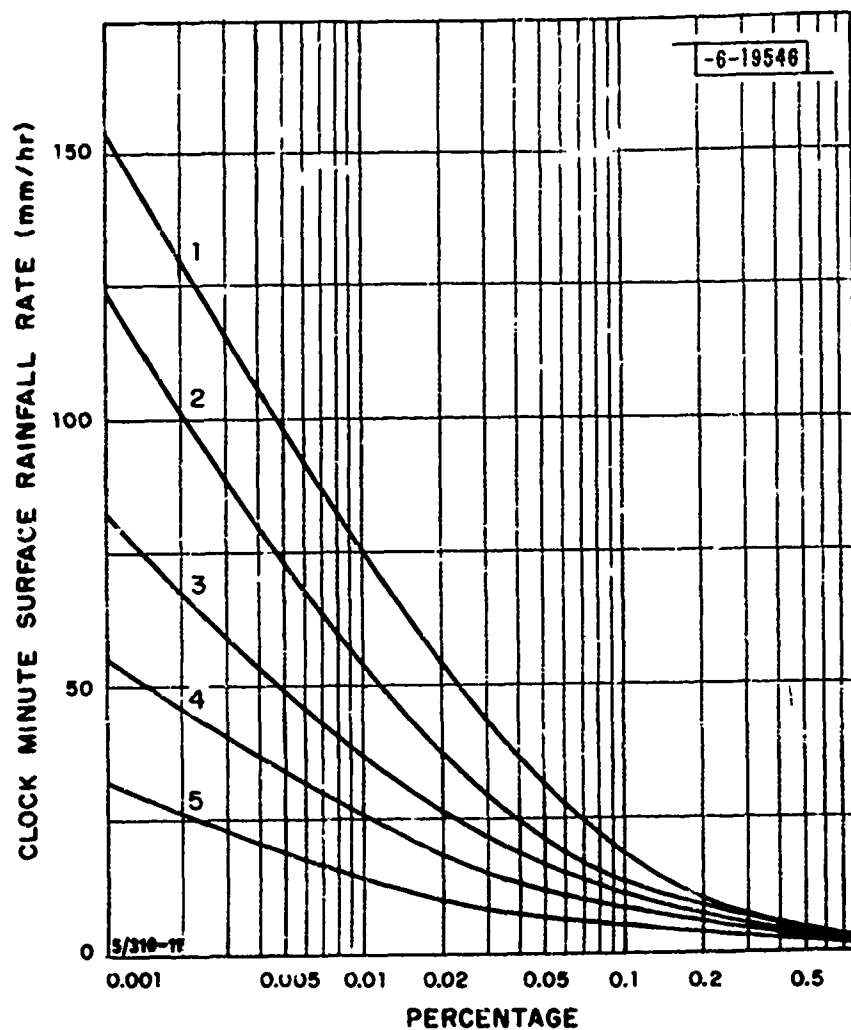


Fig. 6.9. Percentage of an average year for which rainfall rate is exceeded for the five CCIR rain climates (from Ref. 45).

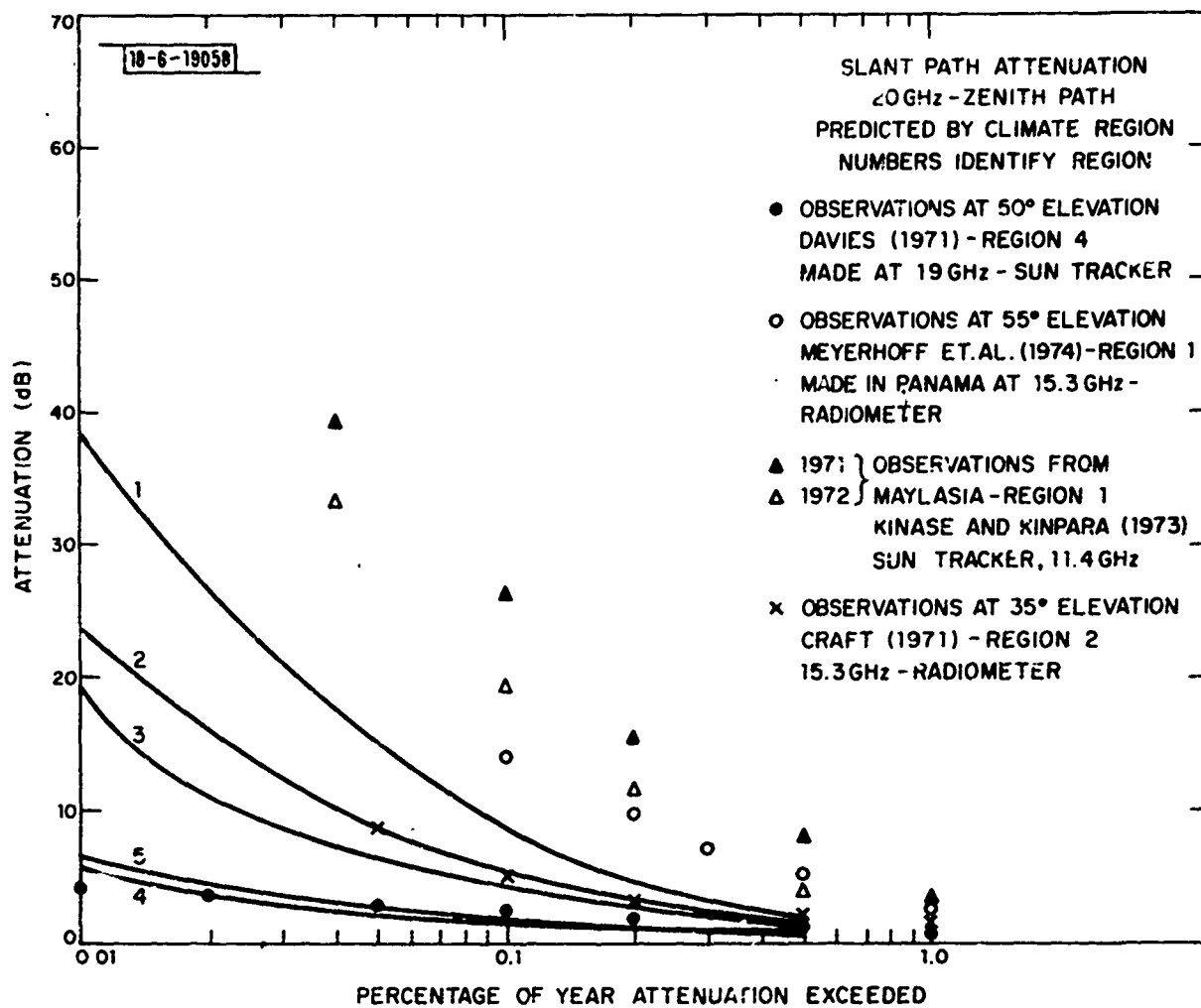


Fig. 6.10. Predicted slant path rain attenuation at 20 GHz for 90° elevation angle.

2. Effective path length factors derived from measured attenuation which are unique to the specific experiment and not applicable to global estimates.

3. CCIR rain rate distributions⁽⁴⁵⁾ which underestimate the values in the tropics by a factor of two or more.

The model described in the following section addresses these deficiencies.

6.4 Proposed Rain Attenuation Model

The rain attenuation model being proposed⁽³⁶⁾ was prepared by R. K. Crane of Environmental Research and Technology, Inc. and submitted to the CCIR as US Study Group Doc. P/105E, "Rain Attenuation Prediction", June 6, 1978. The salient parameters of this model are presented in the following sections.

A. Rain Rate Climate Model

The new rain rate climate model addresses the inadequacies of the model in CCIR Report 5631⁽⁴⁵⁾. It is consistent with the latest climatological data, i.e., annual precipitation data, number of thunderstorm days, latitude, general topography, and data on the general circulation of the atmosphere. This model incorporates the rain rate distributions for regions which include administrations who have formally amended the CCIR model (Report 5631) and the rain rate distributions presented by administrations who did not formally recommend changes to the model. In addition, the new model more accurately represents observed rain rate distributions for the tropical regions.

Fig. 6.11 presents the new global rain rate climate regions; Figs. 6.12 and 6.13 present expanded regional definitions for the United States and Europe, respectively. Fig. 6.14 presents the rain climate regions for the ocean areas. (This is not part of the model but was prepared for this report.)

The rain rate distribution functions for each climate region are presented in Fig. 6.15; selected rain rate distribution values are presented in Table 6.3. The rain climate regions were defined (within obvious constraints) so that the rain rate distributions for adjacent regions bound the possible

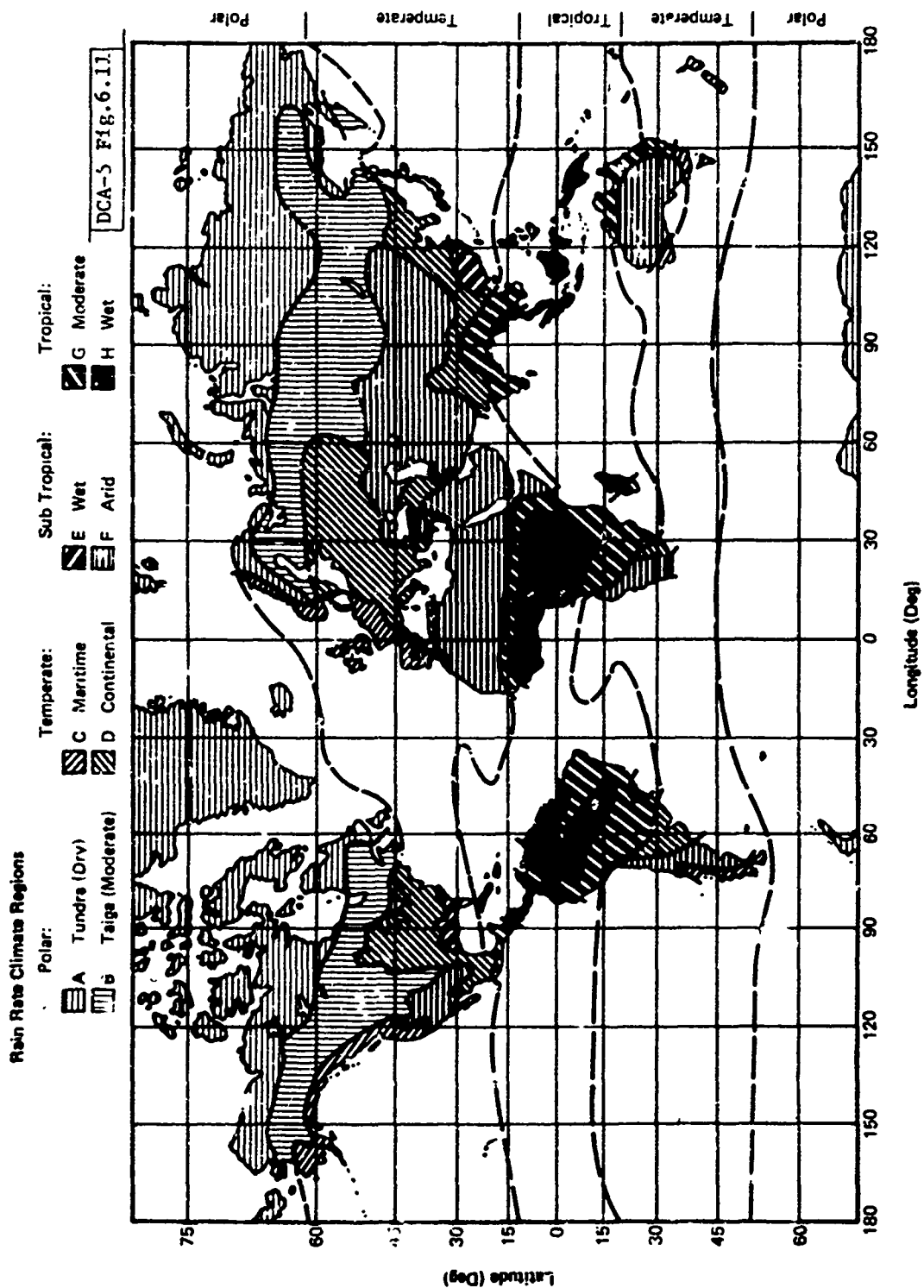
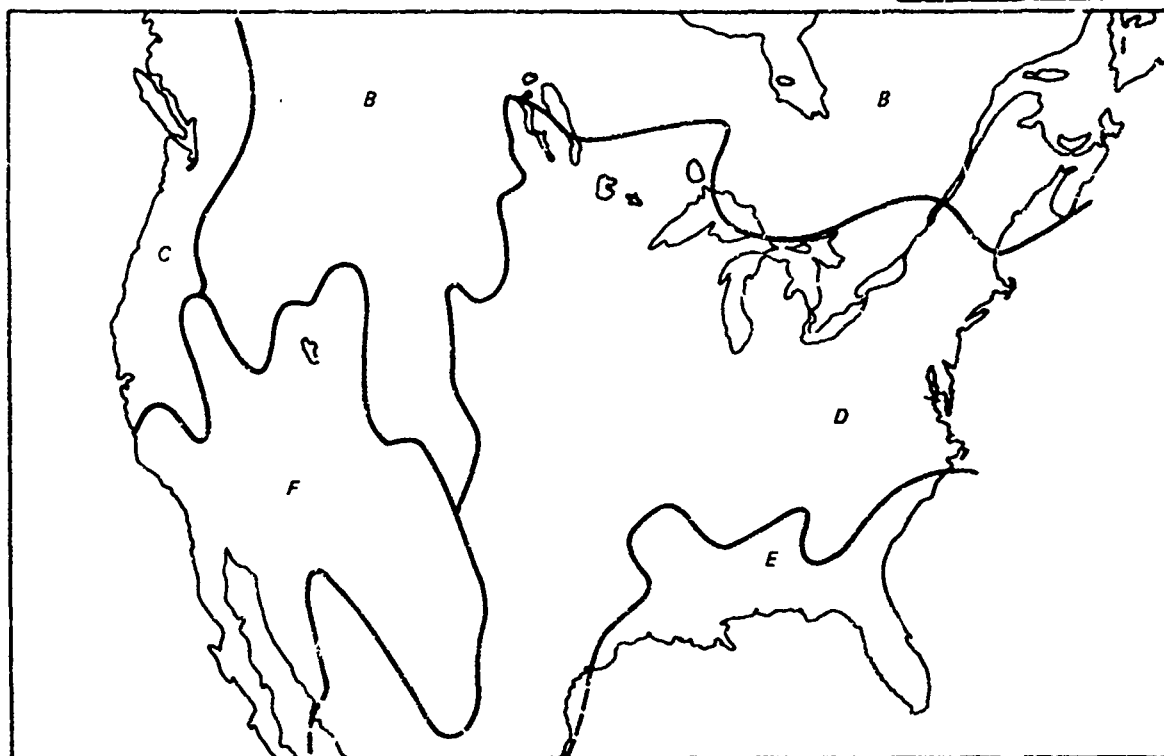
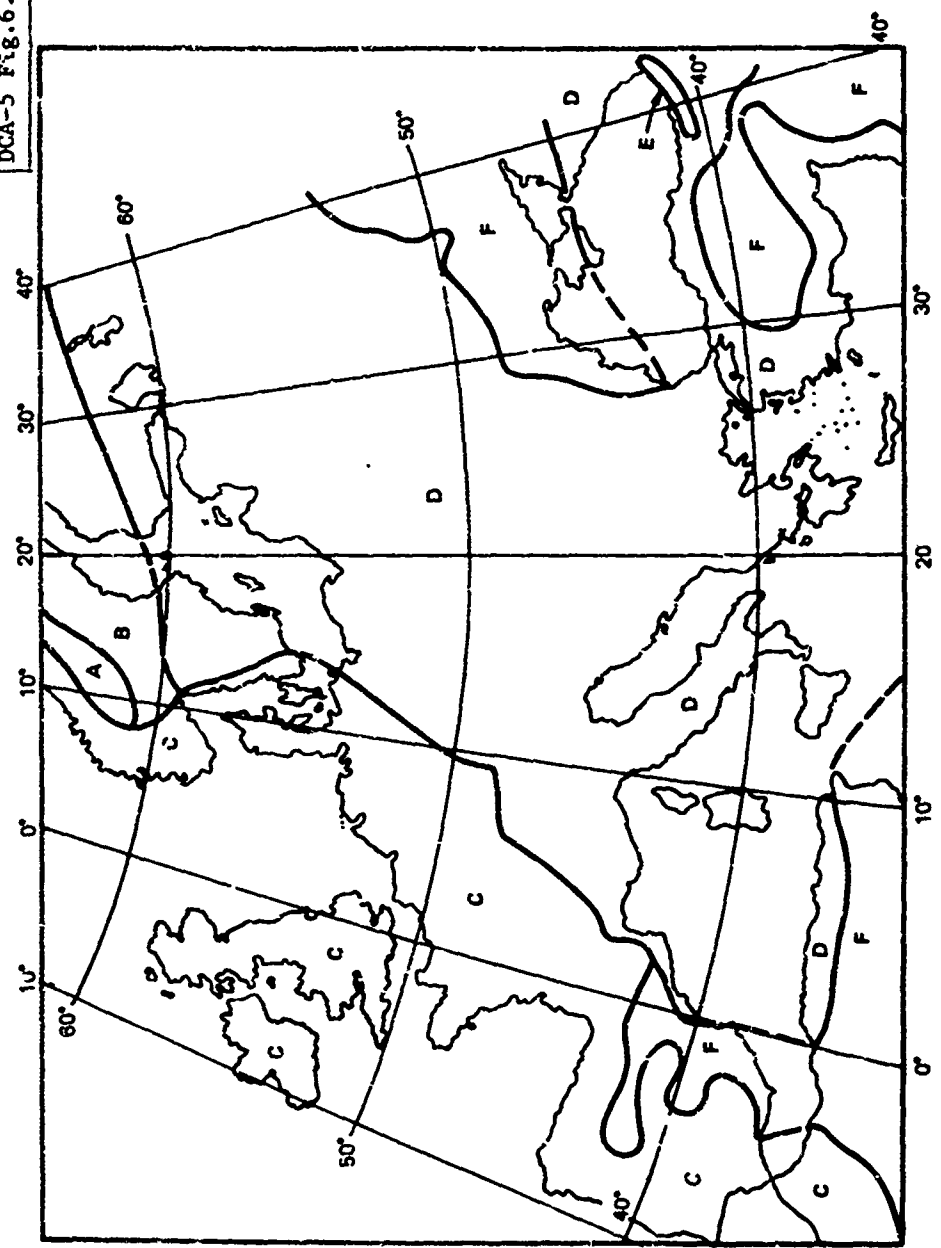


Fig. 6.11. Global rain rate climate regions.



Rain Rate Climate Regions
United States

Fig. 6.12. Rain rate climate regions, United States.



European Rain Climate Regions

Fig. 6.13. Rain rate climate regions, Europe.

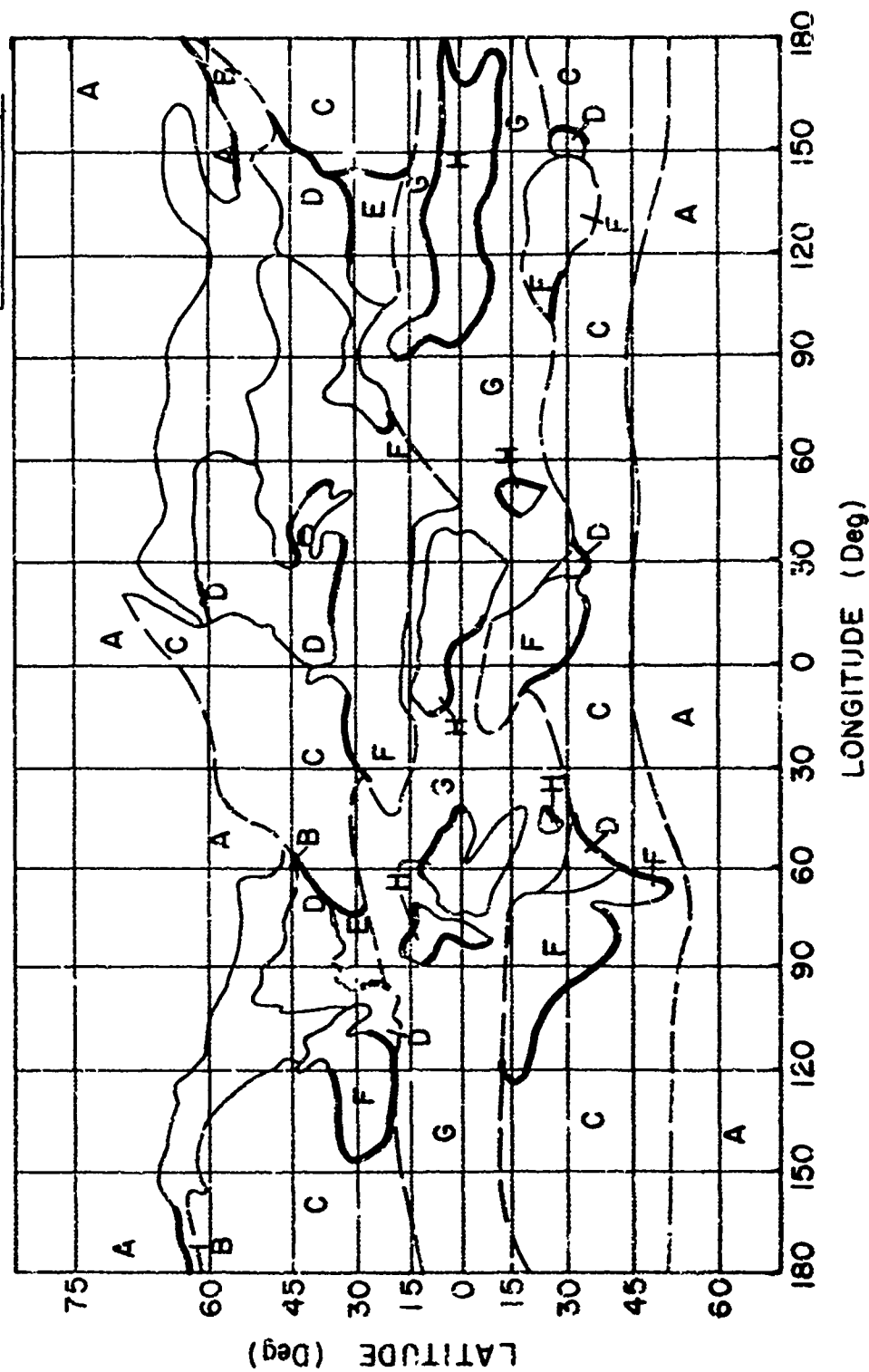


Fig. 6.14. Rain rate climate regions, ocean areas.

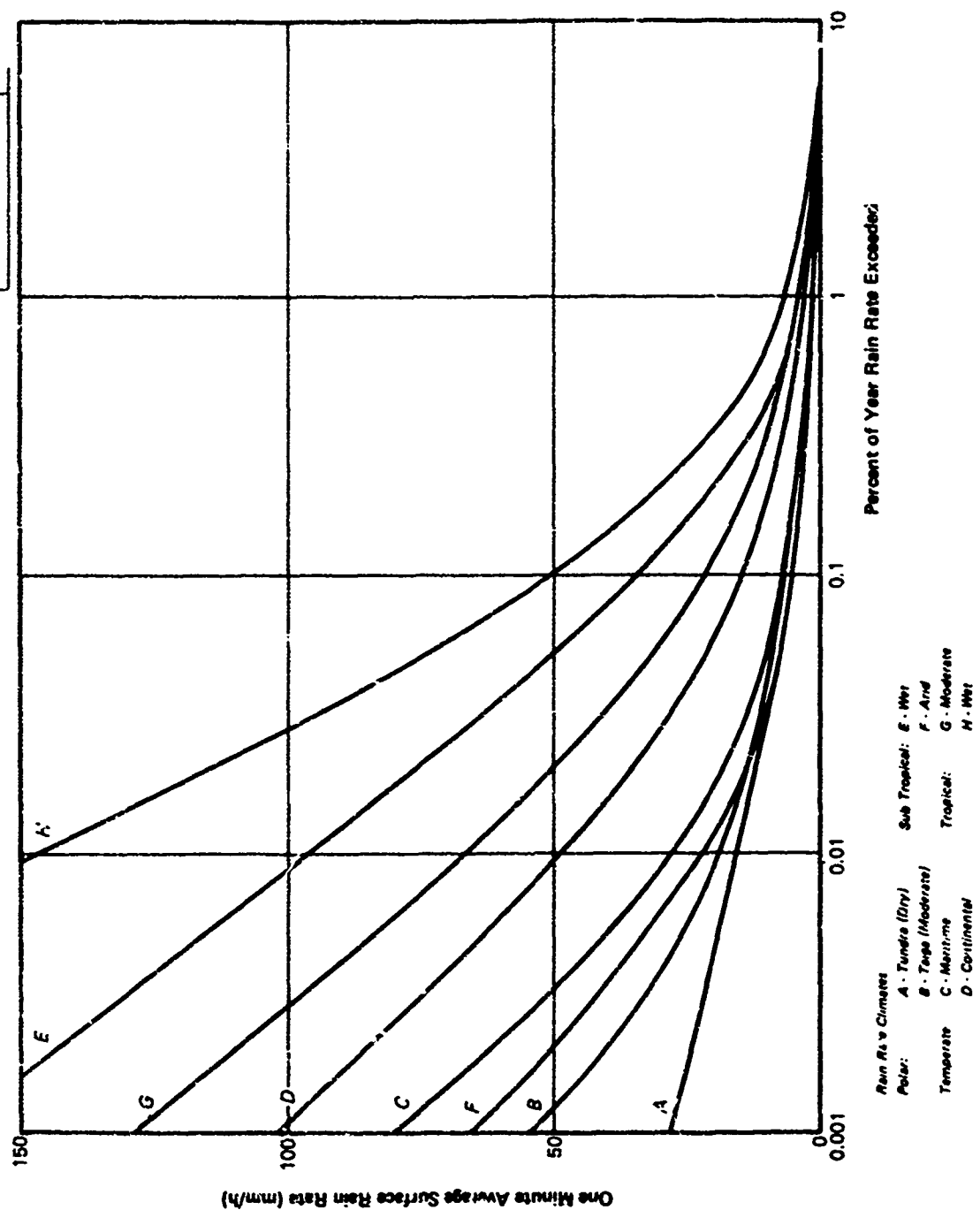


Fig. 6.15. Rain rate distributions.

TABLE 6.3
RAIN RATE DISTRIBUTION VALUES (MM/H)

PERCENT OF YEAR	RAIN RATE CLIMATE REGIONS							
	A	B	C	D	E	F	G	H
0.001	28	54	80	102	164	66	129	251
0.002	24	40	52	86	144	51	109	220
0.005	19	26	41	64	117	34	85	178
0.01	15	19	28	49	98	23	57	147
0.02	12	14	18	35	77	14	51	115
0.05	8.0	9.5	11	22	52	5.0	33	77
0.1	5.5	6.8	7.2	15	35	5.5	22	51
0.2	4.0	4.8	4.8	9.5	21	3.8	14	31
0.5	2.5	3.6	2.8	5.3	8.5	2.4	7.0	13
1.0	1.7	1.8	1.9	3.0	4.0	1.7	4.0	6.4
2.0	1.1	1.4	1.0	1.8	2.0	1.1	1.6	2.8

variation of the distribution for a region, either in time (at a point) or in space (within the region). The distributions of the adjacent regions can then be used to provide bounds on the rain attenuation estimates for a given region due to the point-to-point and year-to-year variation from the observed annual distribution functions.

B. Effective Path Length

The attenuation prediction model also includes a refinement of the techniques that have been previously employed for the estimation of the path averaged rain rate or effective path average factor. The problem lies in the fact that the path average rain rate exceeded for a specified percentage of the time may differ significantly from the surface point rain rate exceeded for the same percentage of the time. The solution applied in previous models has been to empirically derive an effective path length factor based on a set of observed attenuation values. The proposed model addresses the spatial distribution of the rain rate and uses observations from rain gauge networks to provide a basis for a point-to-path average rain rate model. Observations for a 10 Km path are shown in Fig 6.16; the dependence of the modelled effective path average factor on rain rate is evident. Fig. 6.17 shows the effective path average factor for different path lengths. From this figure it is evident that for light surface point rain rates, the rain rate along the path will include more intense rain cells whose probability of occurrence increases with increasing path length (decreasing elevation angle); for heavy surface point rain rates, the converse is true. A power law approximation was applied to the effective path average factors shown in Fig. 6.17 leading to a model of the effective path average factor which may be expressed as

$$r = \gamma(D) R_p^{-\delta(D)} \quad (6.3)$$

where R_p is the point rainfall rate (mm/h) exceeded p percent of the time, and D is the surface projection of the propagation path. The model curves for $\gamma(D)$ and $\delta(D)$ are given in Figs. 6.18 and 6.19, respectively. If D exceeds 22.5 Km,

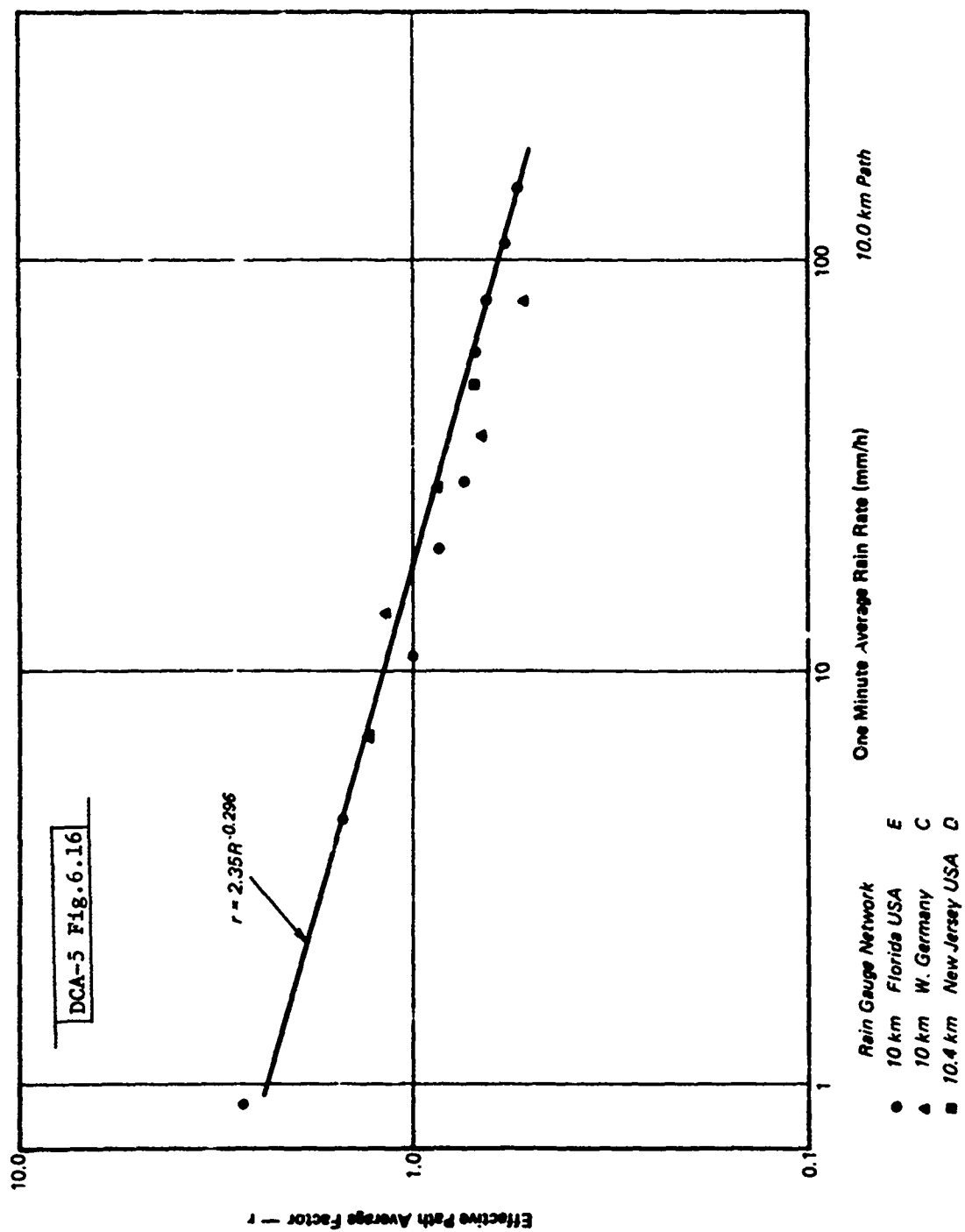


Fig. 6.16. Effective path average factor versus rain rate for a 10 km path.

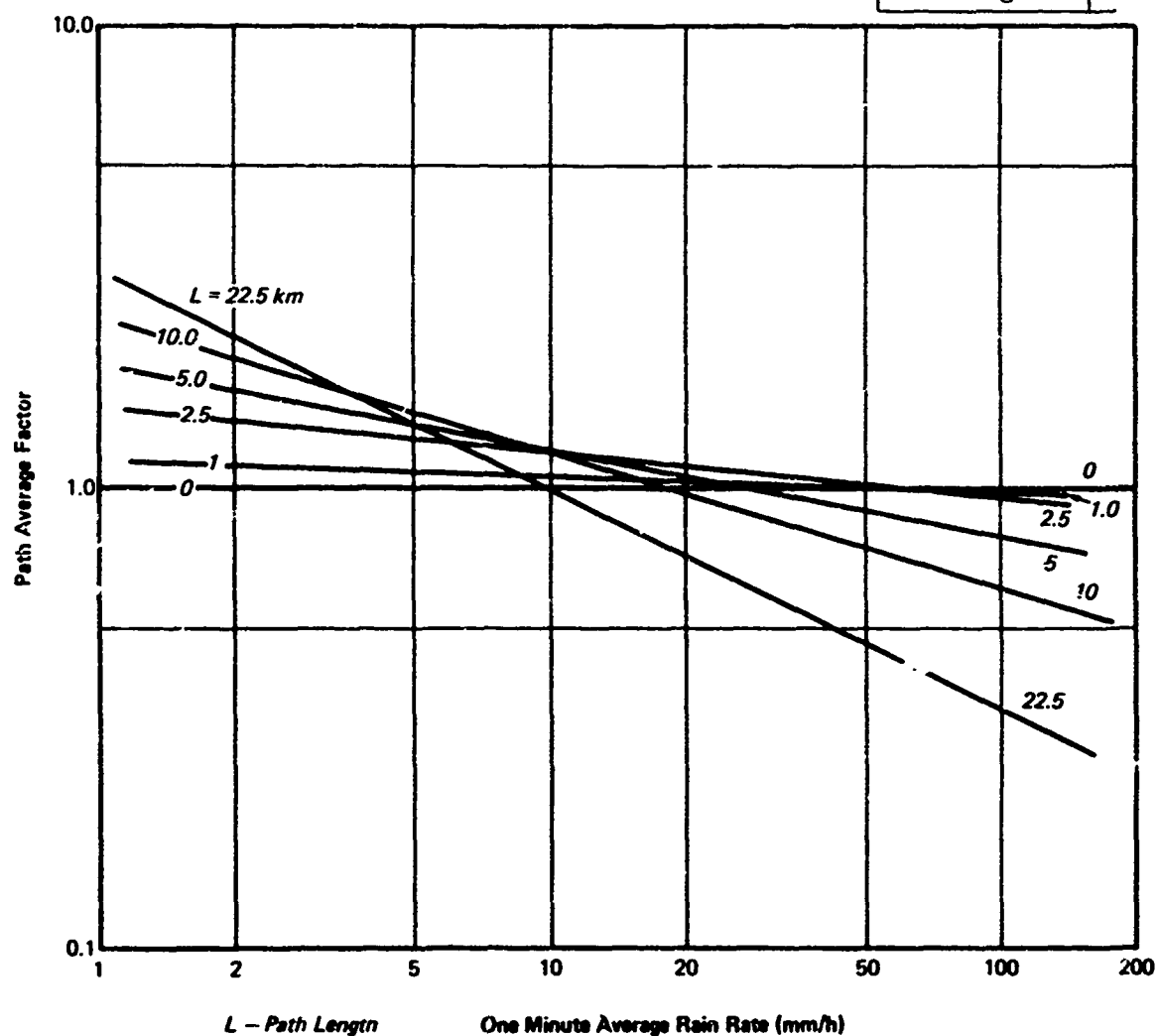


Fig. 6.17. Effective path average factor model for different path lengths.

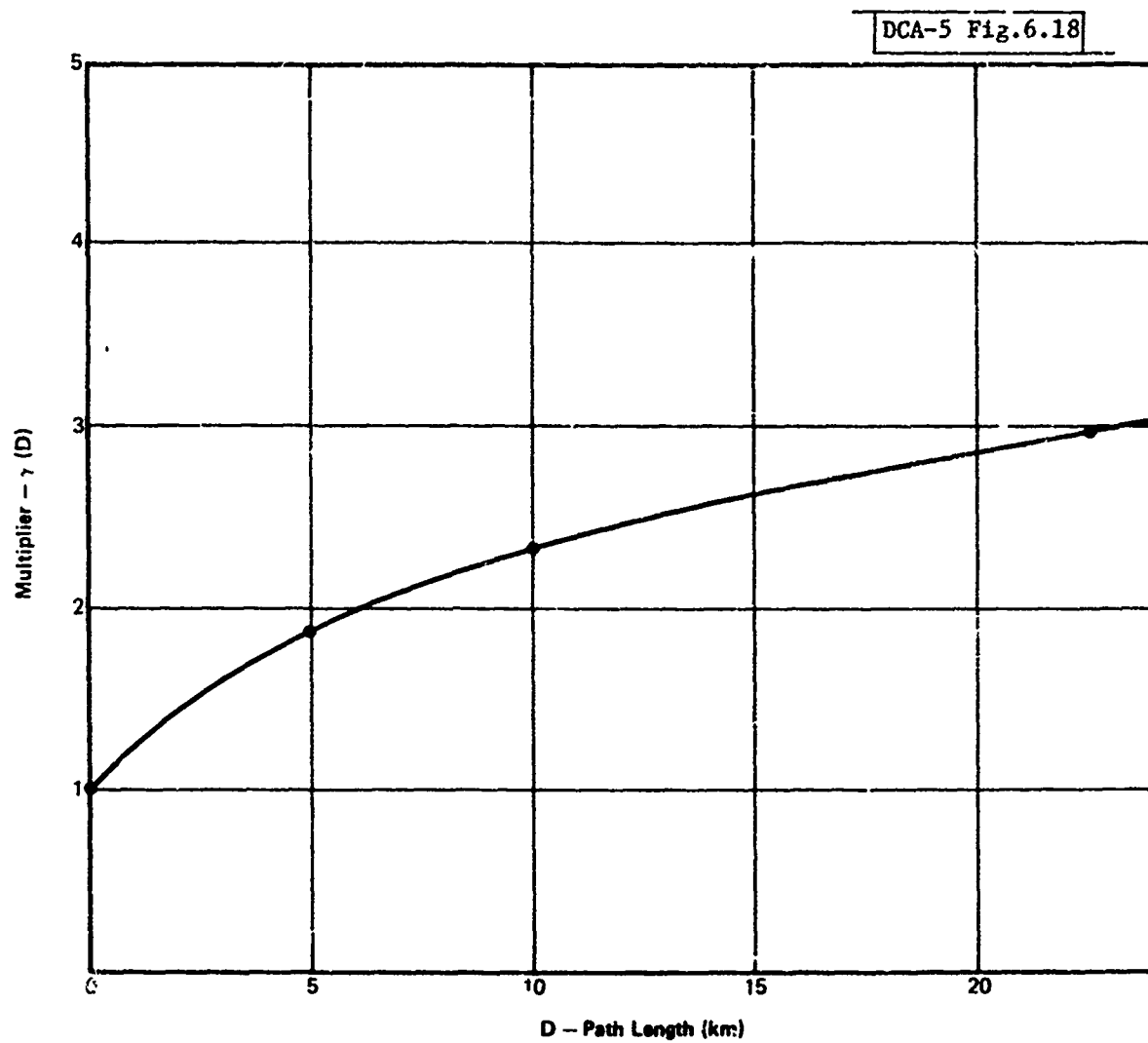


Fig. 6.18. Multiplier in path average model, $\gamma(D)$.

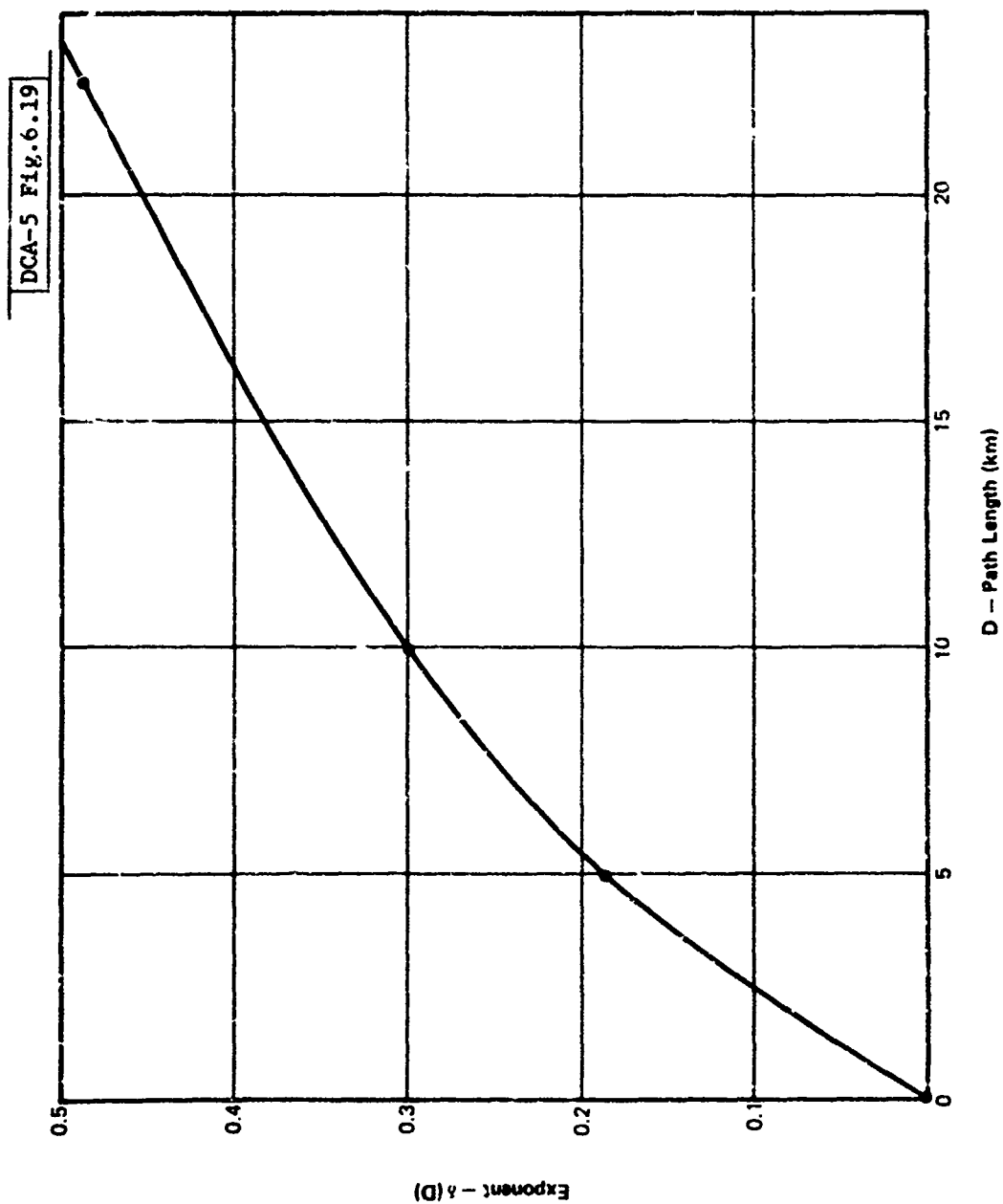


Fig. 6.19. Exponent in path average model, $\delta(D)$.

a D_0 of 22.5 Km is used for the calculation of the effective path average factor and the occurrence probabilities are multiplied by D/D_0 , i.e., it is assumed that the occurrence of rain with rates in excess of 1 mm/h are independent over distances larger than 22.5 Km.

C. Attenuation Prediction Model

The improved rain rate statistics and refined path average factor of the previous sections are now applied to the attenuation prediction model for Earthspace paths as follows:

$$A = H \csc \theta \cdot \alpha(F) \cdot \gamma(D) \cdot R_p^{[\beta(F) - \gamma(D)]} \quad (\text{dB}) \quad (6.4)$$

where H = height of the melting layer (0°C isotherm)

θ = elevation angle ($\geq 10^\circ$)

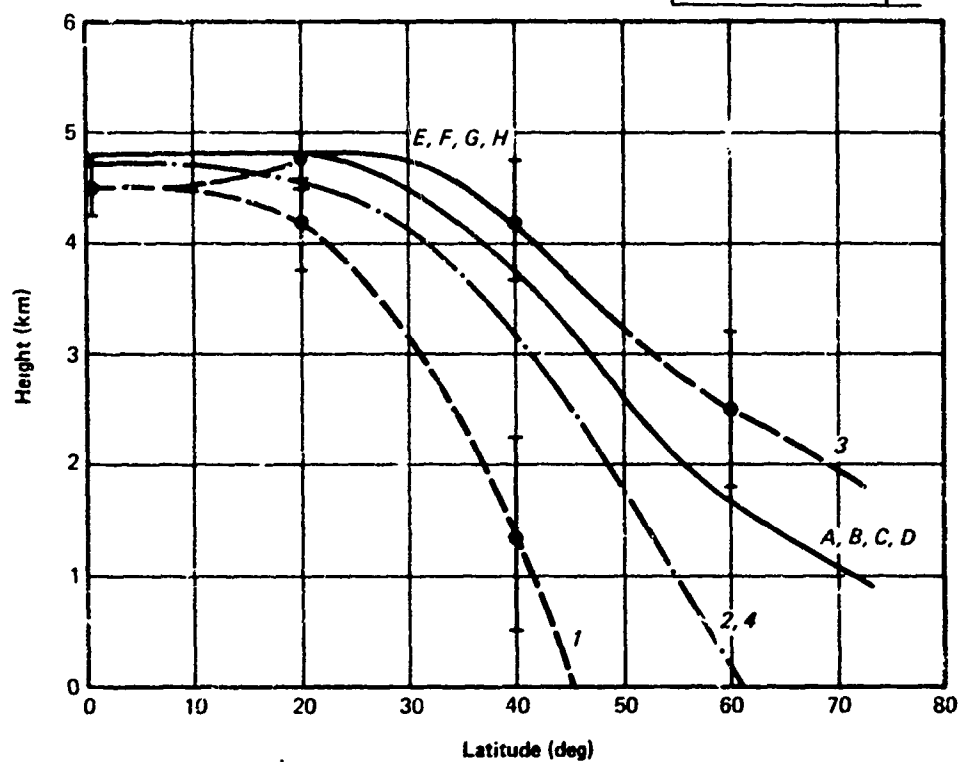
$\alpha(F)$, $\beta(F)$ = frequency dependent coefficients used to estimate specific attenuation for a given rain rate

$D = H \cot \theta$ (Km) = surface projection of the propagation path
($D \leq 22.5$ Km)

R_p = point rainfall rate (mm/h) exceeded p percent of the time

The height of the 0°C isotherm depends upon latitude and season as shown in Fig. 6.20. This figure is derived from zonally averaged temperature data and for all weather conditions. As rain does not occur uniformly during the year but has marked seasonal dependence, the 0°C isotherm height models (solid lines in Fig. 6.20) have been appropriately weighted. The height, H , to be used for the slant path attenuation estimate is obtained from Fig. 6.20 for the latitude and rain rate climate region of the Earth terminal. The coefficients of the specific attenuation $\alpha(F)$ and $\beta(F)$ are presented in Figs. 6.21 and 6.22, respectively.

The procedure for estimating the rain attenuation for a particular site or area of interest may be summarized as follows:



- Model for Rain Rate Climates A through H
- Annual
- Seasonal 1 -- Winter (Northern Hemisphere)
- 2 -- Spring
- 3 -- Summer
- 4 -- Fall

Fig. 6.20. Latitude dependence of zonally averaged 0°C isotherm height.

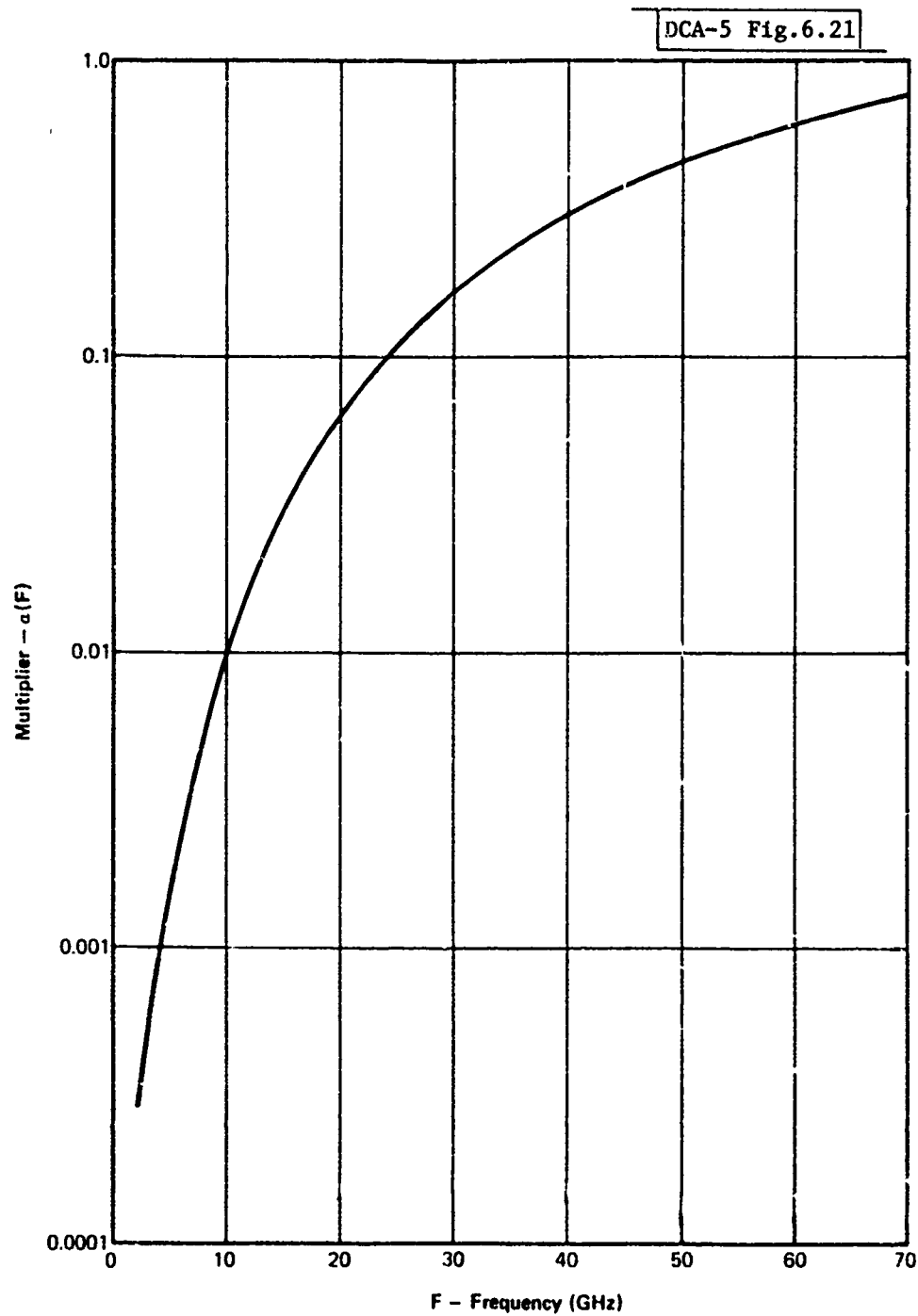


Fig. 6.21. Multiplier in specific attenuation model, $\alpha(F)$.

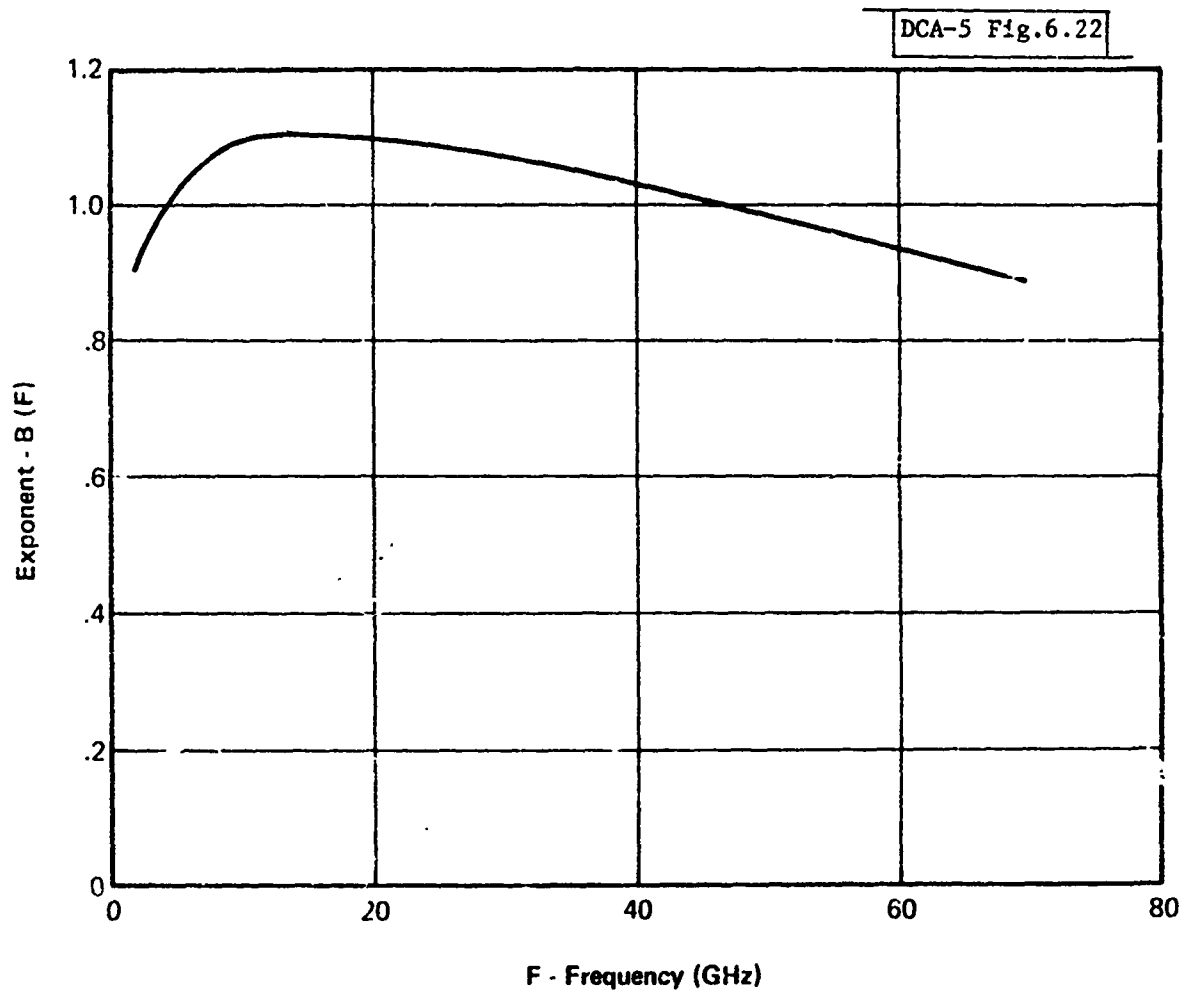


Fig. 6.22. Exponent in specific attenuation model, $\beta(F)$.

1. Select rain rate climate region from Figs. 6.11, 6.12, 6.13 or 6.14.
2. Estimation of path length
 - Estimate height of the melting layer, H , for the rain climate region and latitude from Fig. 6.20.
 - Compute the projection of the propagation path onto the surface, D , for the elevation angle(s), of interest and melting height by

$$D = H \cot \theta, \text{ for } \theta \geq 10^\circ \text{ and } D \leq 22.5 \text{ Km.}$$
3. Estimate the coefficients of the path average factor, $\gamma(D)$ and $\delta(D)$ from Figs. 6.18 and 6.19.
4. Estimate the coefficients of specific attenuation, $\alpha(F)$ and $\beta(F)$, from Figs. 6.21 and 6.22 for the frequency of interest.
5. Obtain the point rainfall rate values versus exceedence probability, R_p , for the rain climate region from Fig. 6.15 or Table 6.3.
6. Evaluate Eq. 6.4.

D. Comparison With Experiment

Fig. 6.23 presents a comparison between 3 years of satellite observations (ATS-5) and the model predictions. Note the year-to-year variation in the annual attenuation distribution curves and note that these observations are contained within the bounds of the model estimates (obtained from the rainfall rate statistics of the adjacent regions). Table 6.4 provides a comparison between the reported attenuation values for a number of satellite observations and the model estimates. It should be noted that the satellite observations are represented by a small number of samples which will lead to large variations in the observations about the true value. This limited data base is an inherent problem in the verification of rain attenuation models and the shortcoming in the development of such models from observations of rain attenuation.

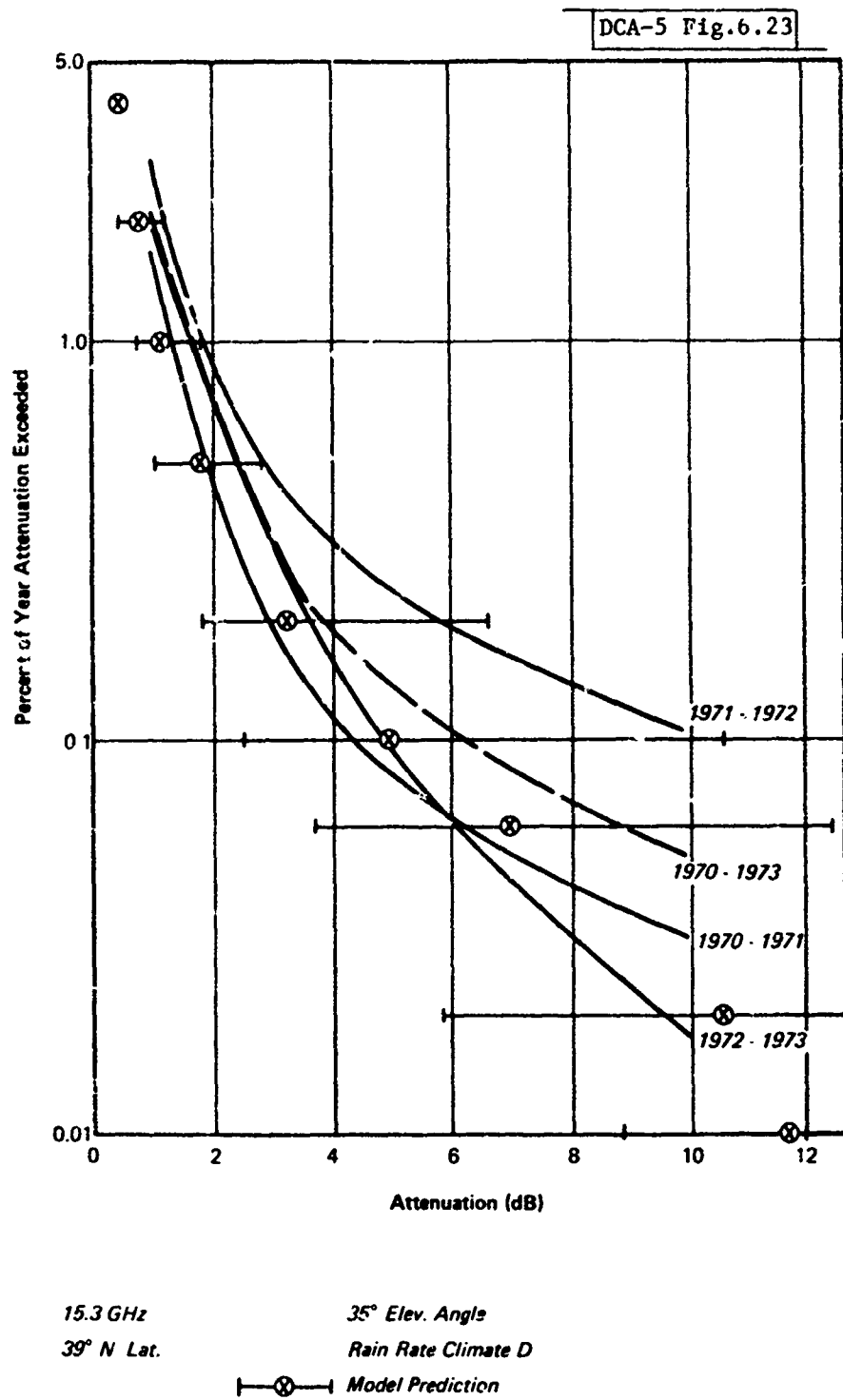


Fig. 6.23. Attenuation statistics for an Earth-space path at 15.3 GHz.

TABLE 7.4

SATELLITE OBSERVATIONS OF RAIN ATTENUATION

LOCATION	LAT	ELEV	FREQ	RR CLIMATE	0.01 Percent				0.1 Percent				1.0 Percent				Hours of Obs
					OBS	Predict			OBS	Predict			OBS	Predict			
						UB	EST	LB		UB	EST	LB		UB	EST	LB	
Greenbelt, MD USA	39°	29°	11.7	D	9.5	14.2	7.8	5.0	2.1	5.8	2.8	1.4					
Washington, D.C. USA	39°	38°	15.3	D	18	35	13.4	6	6	9.9	4.5	2.3	1.5	1.7	1.0	.6	*
Massachusetts USA	42°	36°	13	D					4	6.2	2.9	1.4	1	1.0	0.7	0.3	4112
			10						6	14.8	6.8	3.4	2	2.5	1.5	0.8	2730
Vallops Island USA	38°	42°	13	D					5	6.2	2.8	1.4	1	1.0	6		4303
			18						7.5	13.9	6.4	3.2	2	2.3	1.5		3667
Florida USA	26°	56°	13	E					6	10.0	6.8	4.3	1	1.2	0.8	0.5	3374
			18						16.5	22.6	15.4	9.8	2	2.8	1.9	1.2	1461
Paris FRANCE	49°	26°	20	C	9	25.7	15.5	10.9	4.5	8.8	4.5	3.3	2	2.1	1.4	0.8	1108
Suffolk UK	52°	23°	20	C	8	25.3	15.3	10.8	5	8.8	4.4	3.3	5	2.1	1.5	0.8	1024
			30		>30	57.0	35.2	25.2	11	20.5	10.6	7.0	5	5.1	3.6	2.0	1141
Rosman, N.C. USA	37°	45°	20	D					9.5	18.2	8.2	3.9	1.7	2.4	1.8	1.1	10.5
			30						21.7	42.3	19.5	9.4	3.4	5.8	4.5	2.8	
Birmingham UK	51°	21°	30	C					13	23.0	12.1	9.1	6	5.9	4.2	2.3	861
Slough UK	51°	22°	30	C	13-22	60.7	37.7	27.1	9	22.1	11.6	8.7	3	5.6	4.0	2.2	1742
																	9258*
Eindhoven NETHERLANDS	51°	25°	30	C	13	56.0	34.4	24.5	11	19.9	10.2	7.6	7.5	4.9	3.4	1.9	>50
Leeheim W. GERMANY	50°	27°	30	C					10	19.5	9.9	7.4	2.5	4.7	3.3	1.8	1212

* Satellite Measurements Supplemented by Radiometer Observations

* Satellite Observations Supplemented by Extrapolation Using Rain Gauge Data

E. Summary

The proposed attenuation model provides a technique for global estimates of rain attenuation. The salient features of this model are

1. New climate region definitions more accurately estimate the rainfall rates particularly in the tropical regions.
2. Attenuation prediction model (path average factor) fits measured data more accurately.

The large bounds on the attenuation estimates are inherent in the spatial and temporal averaging of the rain rate statistics. Where accurate rain rate statistics are available for specific areas, these statistics may be used with the attenuation prediction model to provide more definitive estimates. The following section uses the proposed climate region model to determine global estimates of the rain attenuation.

6.5 Global Rain Attenuation Estimates

This section presents global estimates of rain attenuation as a function of climate region, elevation angle, frequency and path availability. The rain rate probability of occurrence has been translated into path availability, i.e., percentage time when the computed attenuation values are less than the value presented. Thus the data shows the estimated uplink or downlink margin requirements which must be provided to realize a specified percentage path availability. A few comments regarding the data being presented:

1. The attenuation estimates include oxygen and water vapor absorption (Table 6.1) in addition to rain attenuation.
2. For those cases (tropical regions and 10° elevation angle) where the surface projection of the propagation path (D) exceeded 22.5 Km, the occurrence probabilities were not adjusted according to the model. In the worst case the reduction in occurrence probability is 20% (e.g., from 99.9% to 99.88% availability).

3. No estimates of the bounds on the attenuation values are presented; the proposed method of estimating these bounds has been discussed and examples given.

Table 6.5 presents a summary of the total path attenuation (atmospheric plus rain) for the eight rain climate regions for selected elevation angles, frequencies and availabilities. Appendix A presents, for each climate region, graphs of: attenuation versus path availability with frequency as a parameter for elevation angles of 10°, 20° and 90° (Figs. A1-A24); attenuation versus elevation angle with path availability as a parameter for frequencies of 20, 30, 40, and 45 GHz (Figs. A25-A56); attenuation versus frequency with path availability as a parameter for elevation angles of 10°, 20° and 90° (Figs. A57-A80).

The data of path availability versus margin requirement provide a basis for frequency selection and general system characterization but should not be considered as a definitive basis for system design. Related issues such as system availability, site diversity and response time must be addressed and are discussed in the next section.

6.6 Availability Considerations

A. System Availability

The preceding section presented the margins required to overcome rain and atmospheric attenuation for a given path availability. However, the system availability as seen by the end-to-end user is

$$A_S = A(T_T) \cdot A(L_U) \cdot A(S) \cdot A(L_D) \cdot A(T_R) \quad (6.4)$$

where A_S = system availability

$A(T_T)$, $A(T_R)$ = availabilities of the transmitting and receiving terminals, respectively

$A(S)$ = satellite availability

$A(L_U)$, $A(L_D)$ = availabilities of the uplink and downlink paths, respectively

TABLE 6.5
ESTIMATES OF ATMOSPHERIC PLUS RAIN ATTENUATION

CLIMATE REGION	AVAILABILITY (PERCENT)	ELEVATION ANGLE (DEG)																		
		10									20									
		7	20	30	40	45	50	7	20	30	40	45	50	7	20	30	40	45	50	
A	90.0%	0	1	1	2	3	10	0	1	1	1	2	5	0	0	0	0	1	2	
A	97.0%	0	2	3	5	7	15	0	1	1	1	2	3	7	0	0	0	1	1	2
A	98.0%	0	2	3	6	9	16	0	1	1	1	3	4	8	0	0	0	1	1	2
A	99.0%	0	3	4	7	11	19	0	1	2	3	5	9	9	0	0	1	1	1	3
A	99.5%	0	3	6	10	13	22	0	2	3	4	6	10	10	0	0	1	1	2	3
A	99.7%	0	4	7	12	16	24	0	2	3	5	7	12	12	0	1	1	1	2	3
A	99.8%	0	4	8	13	18	27	0	2	4	6	8	13	13	0	1	1	2	2	4
A	99.9%	1	6	11	19	24	34	0	3	6	9	12	16	16	0	1	2	3	3	5
B	90.0%	0	1	1	2	3	19	0	1	1	1	2	5	5	0	0	0	0	1	2
B	97.0%	0	3	5	8	11	20	0	1	2	3	5	9	9	0	0	0	1	1	2
B	98.0%	0	3	6	10	14	23	0	2	3	4	6	11	11	0	0	1	1	1	3
B	99.0%	0	4	8	14	19	29	0	2	4	6	8	13	13	0	0	1	1	2	3
B	99.5%	1	6	12	20	25	36	0	3	5	9	12	17	17	0	1	1	2	3	4
B	99.7%	1	7	14	24	30	41	0	3	7	11	15	20	20	0	1	2	3	4	5
B	99.8%	1	8	16	27	34	45	0	4	8	13	17	22	22	0	1	2	3	4	6
B	99.9%	1	9	20	34	42	54	0	5	10	17	21	28	28	0	1	3	5	6	8
C	90.0%	0	1	1	2	3	10	0	1	1	1	2	5	5	0	0	0	0	1	2
C	97.0%	0	3	6	11	15	24	0	1	3	4	6	11	11	0	0	0	1	1	3
C	98.0%	0	4	7	13	18	27	0	2	3	6	8	12	12	0	0	1	1	2	3
C	99.0%	1	5	11	19	25	36	0	3	5	9	11	17	17	0	1	1	2	2	4
C	99.5%	1	7	14	24	31	42	0	3	7	11	15	20	20	0	1	1	3	3	5
C	99.7%	1	8	18	30	37	50	0	4	9	15	19	25	25	0	1	2	3	4	6
C	99.8%	1	9	20	34	42	55	0	5	10	17	21	28	28	0	1	2	4	5	7
C	99.9%	1	12	28	44	54	67	0	6	14	23	29	36	36	0	2	4	6	8	10

TABLE 6.5 (Cont'd)

CLIMATE REGION	AVAILABILITY (PERCENT)	ELEVATION ANGLE (DEG)																		
		10						20						90						
		7	20	30	40	45	50	7	20	30	40	45	50	7	20	30	40	45	50	
D	90 0%	0	1	1	2	3	10	0	1	1	1	1	2	5	0	0	0	0	1	2
D	97 0%	1	5	10	18	24	35	0	2	5	8	11	16	0	1	1	1	1	2	4
D	98 0%	1	6	13	23	30	41	0	3	6	10	14	19	0	1	1	1	2	3	4
D	99 0%	1	8	18	31	39	52	0	4	9	15	19	25	0	1	2	3	4	6	6
D	99 5%	1	11	25	42	53	67	0	6	13	22	28	35	0	2	3	5	7	9	9
D	99 7%	1	14	32	52	64	79	1	8	18	29	35	43	0	2	5	8	10	12	12
D	99 8%	1	17	37	61	74	90	1	9	21	35	42	51	0	3	6	10	12	15	15
D	99 9%	1	22	50	80	96	113	1	13	30	48	58	68	0	4	10	16	19	22	22
E	90 0%	0	1	1	2	3	10	0	1	1	1	1	2	5	0	0	0	0	1	2
E	97 0%	1	7	16	28	36	49	0	3	7	12	16	22	0	1	1	2	3	4	4
E	98 0%	1	9	21	36	46	60	0	4	10	17	22	29	0	1	2	3	4	6	6
E	99 0%	1	14	31	52	64	81	0	7	16	27	34	42	0	2	4	6	8	10	10
E	99 5%	1	21	47	77	94	113	1	12	27	45	54	65	0	3	8	13	16	19	19
E	99 7%	2	29	65	105	126	146	1	18	41	65	78	90	0	6	14	23	27	32	32
E	99 8%	2	35	79	125	149	170	1	23	52	82	98	111	1	9	20	32	38	43	43
E	99 9%	3	48	106	165	194	216	2	33	75	116	137	151	1	16	36	54	64	70	70
F	90 0%	0	1	1	2	3	10	0	1	1	1	1	2	5	0	0	0	0	1	2
F	97 0%	1	6	12	21	27	39	0	2	5	9	11	17	0	1	1	1	2	3	3
F	98 0%	1	7	15	26	34	47	0	3	6	11	15	21	0	1	1	2	2	4	4
F	99 0%	1	8	19	32	42	55	0	4	9	15	19	26	0	1	2	3	4	5	5
F	99 5%	1	10	23	39	49	64	0	5	11	19	24	31	0	1	2	4	5	7	7
F	99 7%	1	12	27	45	57	72	0	6	13	23	29	36	0	1	3	5	6	8	8
F	99 8%	1	13	29	49	62	77	0	7	15	26	32	40	0	2	3	6	7	9	9
F	99 9%	1	16	36	60	74	91	1	9	20	33	40	49	0	2	5	8	10	13	13

TABLE 6.5 (Cont'd)

CLIMATE REGION	AVAILABILITY (PERCENT)	ELEVATION ANGLE (DEG)																	
		10						20						30					
		7	20	30	40	45	50	7	20	30	40	45	50	7	20	30	40	45	50
G	90 0x	0	1	1	2	3	10	0	1	1	1	2	5	0	0	0	0	1	2
G	97 0x	1	6	14	24	32	45	0	3	6	10	14	20	0	1	1	2	2	4
G	98 0x	1	8	19	33	42	56	0	4	9	15	19	26	0	1	2	3	3	5
G	99 0x	1	14	31	53	66	92	1	7	16	27	34	43	0	2	4	6	8	10
G	99 5x	1	19	43	71	87	105	1	11	24	40	49	59	0	3	7	11	13	16
G	99 7x	1	24	54	88	107	126	1	14	32	52	63	74	0	4	10	16	20	23
G	99 8x	2	28	64	103	124	144	1	17	39	63	76	88	0	6	14	22	26	30
G	99 9x	2	37	83	131	156	178	1	24	55	86	102	115	1	10	22	34	41	46
H	90 0x	0	1	1	2	3	10	0	1	1	1	2	5	0	0	0	0	1	2
H	97 0x	1	9	19	34	43	57	0	4	9	16	20	27	0	1	2	3	4	5
H	98 0x	1	11	26	44	55	71	0	6	13	22	27	35	0	1	3	4	6	8
H	99 0x	1	18	41	68	83	101	1	10	23	38	46	56	0	3	6	10	12	15
H	99 5x	2	27	61	99	119	139	1	16	37	60	73	84	0	5	13	20	24	28
H	99 7x	2	37	83	131	156	178	1	24	55	85	102	115	1	10	22	34	41	46
H	99 8x	3	45	101	158	186	209	2	31	70	109	128	142	1	14	31	49	58	64
H	99 9x	3	61	135	206	241	264	2	45	100	152	177	193	1	24	53	82	95	102

For the satellite it will be assumed that the use of highly reliable components, redundant subsystems and an on-orbit spare assure its operation, i.e., $A(S) = 1$.

The terminal availability may be expressed as

$$A_{(T)} = \frac{MTBF}{MTBF + MTTR} \quad (6.5)$$

where $MTBF$ = mean-time-between-failure
 $MTTR$ = mean-time-to-repair

The MTBF of the terminal components is of course a tradeoff between cost and reliability. The MTTR is dependent on the supply of replacement parts and the accessibility of the equipment, and varies significantly with the type of terminal. For this discussion it is assumed that the terminal availability is identical for transmitting and receiving, i.e., duplex communications is required (even if the terminal requires only report-back capability, downlink reception may be required for satellite acquisition and frequency and timing corrections).

As regards the path availability, the uplink EIRP and concomitant path availability may be driven by considerations of jamming threats and may be higher than the downlink path availability. Alternatively, the downlink path availability requirement may be more stringent than the uplink if loss of the downlink signal would incur unacceptable delays due to reacquisition of a pseudonoise code sequence. The assessment of these factors on the path availability requirements is beyond the scope of this report. For the purpose of discussion, the uplink and downlink path availabilities are assumed to be equal. Under these assumptions, the system availability can be expressed as

$$A_S = A^2(T) \cdot A^2(L) \quad (6.6)$$

where $A(T) = A(T_T) = A(T_R)$

$A(L) = A(L_U) = A(L_D)$ and it is assumed that $A(S) = 1$.

Eq. 6.6 is plotted in Fig. 6.24. If it is assumed that $A(T) = A(L)$, the rapid increase in their required availability with increasing system availability is evident, e.g., for $A(S) = 90\%$, $A(T) = A(L) = 97.4\%$. Note also that increasing $A(T)$ or $A(L)$ beyond this balanced condition incurs an extreme increase in the availability requirement of $A(T)$ or $A(L)$ for a modest increase in system availability. In the limit, if $A(T)$ or $A(L)$ is assumed to be unity, the system percentage outage is reduced by a factor of two from the balanced case. The point being made is that to a first order the terminal availability determines the system availability, if the corresponding path availability margin is achievable. Increases in system availability beyond this point must be weighed against the cost of increasing $P(T)$ or $P(L)$. As regards the latter, increasing the downlink path availability for mobile terminals would require increasing the terminal antenna size with concomitant increases in the required tracking accuracy, radome, weight and cost (decreasing receiver noise temperature would be less effective due to the noise contribution of the rain). Increasing the uplink path availability for mobile terminals will require increasing the antenna size and/or the transmitter power (increasing the prime power requirement and decreasing the reliability of the transmitter). For the fixed terminals, site diversity may be a viable alternative and is addressed later.

Table 6.6 presents required path availability as a function of system availability with terminal availability as a parameter. System availabilities of 95%, 99%, and 99.9% are assumed to be the nominal requirements for the Navy, GMF and wideband (WB) trunking communities, respectively. Note that, in order to achieve high system availability, both the terminal availability and the path availability must be high. Table 6.7 presents the required path margin as a function of path availability with frequency and climate region as parameters for an assumed elevation angle of 20° . Note the rapid increase in required path margin for path availabilities $> 99\%$. For the fixed terminals, such path

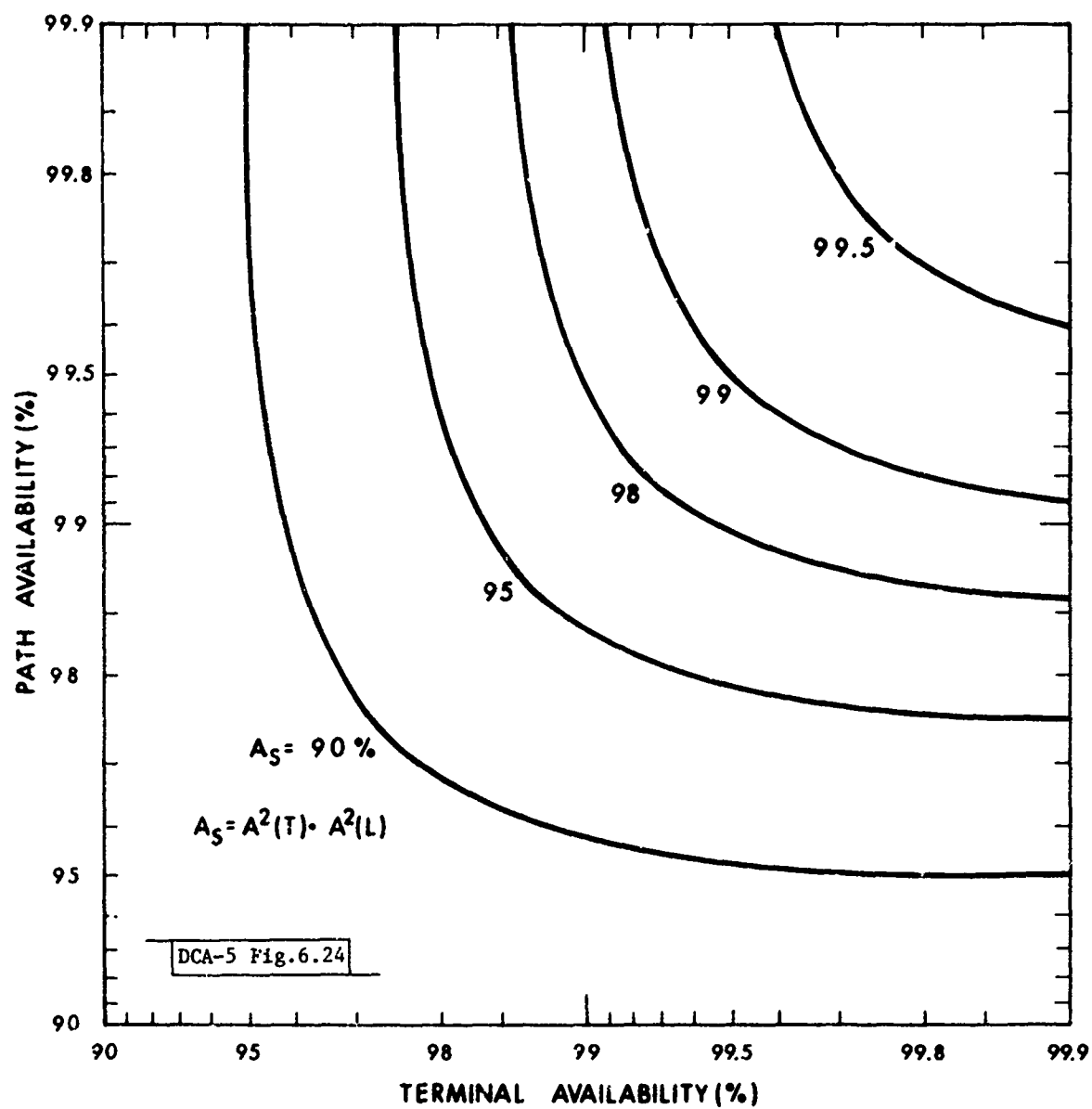


Fig. 6.24. Required path versus terminal availability with system availability as a parameter.

TABLE 6.6
REQUIRED PATH AVAILABILITY VERSUS TERMINAL AVAILABILITY

SYSTEM AVAILABILITY (%)	REQUIRED PATH AVAILABILITY (%)				
	TERMINAL AVAILABILITY (%)				
	95	98	99	99.9	99.99
90	99.9	96.8	95.8	95.0	94.9
95 (NAVY)		99.5	98.4	97.6	97.5
97			99.5	98.6	98.5
99 (GMF)	SEE (1)				99.5
99.9 (WB)					99.96 (2)

(1) Increased Terminal Availability Required, i.e., $A(L) > 1$

(2) Site Diversity Required

TABLE 6.7
REQUIRED PATH MARGINS DUE TO ATMOSPHERIC AND
RAIN ATTENUATION (20° ELEVATION ANGLE)

REQUIRED PATH AVAILABILITY (%)	REQUIRED PATH MARGIN (dB)												
	CLIMATE REGION D (1)						CLIMATE REGION H (2)						
	FREQUENCY (GHz)						FREQUENCY (GHz)						
	20	40	30	45	50		20	40	30	45	50		
97	2	8	5	11	16		4	16	9	20	27		
98	3	10	6	14	19		6	22	13	27	35		
99	4	15	9	19	25		10	38	23	46	56		
99.5	6	22	13	28	35		16	60	37	73	84		
99.7	8	29	18	35	43		24	86	55	102	115		
99.8	9	35	21	42	51		31	109	70	128	142		
99.9	13	48	30	58	68		45	152	100	177	193		

(1) Climate Region D: Moderate Rain Rate (Large Areas of Europe and Eastern Conus)

(2) Climate Region H: Highest Rain Rate (Tropics)

availabilities may be achieved by utilizing site diversity; for the mobile community, the duration of these high attenuation, low-probability-of-occurrence outages and their impact on communications must be considered. These factors are addressed in the following sections.

B. Site Diversity

It was shown in the previous section that the path margins required for a system availability of 99.9% may be impractical to implement in a single fixed terminal. Site diversity, the use of two or more geographically separated ground terminals, may provide a technique to substantially reduce these margin requirements. A dual diversity* system which employs two transmitting terminals and two receiving terminals, with each pair of terminals ideally separated so that the rain rate statistics at the individual terminal sites are uncorrelated, has a system availability which can be expressed as

$$A_S^D = A(T_T) \cdot A(L_U) \cdot A(T_R) \cdot A(L_D) \cdot [2 - A(T_R) A(L_D)] \cdot [2 - A(T_T) A(L_U)] \quad (6.7)$$

If it is assumed that the availabilities of the terminals for transmitting and receiving are equal and that the path availabilities for the uplink and downlink are also equal, Eq. 6.7 may be expressed as

$$A_S^D = A^2(T) \cdot A^2(L) \cdot [2 - A(T) A(L)]^2 \quad (6.8)$$

Table 6.8 lists the required individual path availabilities for this type of diversity system. The reduction in the required path and terminal availabilities is obvious, in particular, a system availability requirement of 99.9% may be satisfied with path and terminal availabilities of 99%. This analysis is of course idealistic and the implementation of such a system may be unrealistic in terms of cost and complexity. For the wideband trunking between CONUS and Europe, the traffic is not symmetrical and a detailed system study

*Dual diversity may be required to reduce the terminal outages as well as path outages.

TABLE 6.8
REQUIRED PATH AVAILABILITY FOR DUAL DIVERSITY SYSTEM

SYSTEM AVAILABILITY (%)	REQUIRED PATH AVAILABILITY (%)			
	TERMINAL AVAILABILITY (%)			
	95	98	99	99.9
99	97.8	94.8	93.9	93.0
99.5		96.9	96.0	95.1
99.9		99.8	98.8	97.9
99.95	SEE (1)			98.5
99.99				99.4

(1) Increased Terminal Availability Required, i.e., $A(L) \geq 1$

is required to assess the need for diversity on a link-by-link basis. Preliminary study of the downlink traffic to CONUS indicates that the use of dual diversity may be required on this link. The uplink data rate from CONUS to Europe may be two orders of magnitude less than the downlink. The uplink margins may afford adequate availability without diversity (some delays in transmission may have to be tolerated). If uplink diversity from CONUS is required, the operational considerations such as switchover, buffering, inter-site linking, etc., should be studied. For the terminals located in Europe, a link-by-link analysis of the data rates, rain rate and attenuation statistics and tolerance to delays must be conducted. For the purpose of discussion, it is assumed that dual diversity reception will be required on the East Coast and is discussed next.

The design of a path diversity system is primarily determined by the spatial characteristics of the rain cells. For given meteorological conditions, the performance of a diversity system will depend on the separation between the ground terminals, the orientation of the baseline between them and the azimuth and elevation angles of the propagation path. The level of diversity improvement achieved depends upon the size and spacing of the rain cells. Heavy rain is associated with small convective cells having diameters of the order of 3 Km and typical spacings of 7 to 10 Km. Propagation paths spaced on the order of 10 to 20 Km apart generally show some diversity improvement, as it is rare for the two closest cells to simultaneously intercept the two propagation paths. These intense cells contribute to the attenuation values to be expected 0.01 percent of the year or less. For the nearly statistically horizontally homogeneous rainfall that occurs in the 0.1 to 0.5 percent range, less improvement is possible from diversity, as only the random fluctuations in the widespread regions of rain contribute to the diversity action. For widespread rain, diversity improvement may still be achieved by using terminal separations of many tens of kilometers but the attractiveness of site diversity is substantially reduced.

Earth-space path diversity studies have been performed at 16 GHz using radiometers^(46, 47, 48) and more recently at 20 and 30 GHz using the ALS-6 satellite^(49, 50). Using the data obtained at 16 GHz in New Jersey for an elevation angle of 30°, diversity improvements of a factor of 2.5 in attenuation were obtained at 0.1 percent of the year for separations in excess of 11 Km. Substantial reductions in the total time a given level of attenuation was exceeded were observed, e.g., at 10 dB attenuation, reductions of a factor of 50 to 100 were observed at 0.1 percent. However, the experimenters caution that relatively few events comprise the tails of the attenuation distribution and more data are needed to substantiate the level of improvements. The data obtained at 30 GHz in Texas for an elevation angle of 55° shows a reduction in probability of exceedance from 0.1 percent to 0.01 percent at 15 dB attenuation with a diversity separation of 11 Km. Due to the dependence of the diversity improvement on local climatology, it is not possible to accurately extrapolate from other observations to another region. However, radar measurements have permitted mapping of rain cells, which coupled with local rain rate statistics, allow for the calculation of expected single-path attenuation and diversity improvement. Hence for areas where climatological and meteorological data are available, the diversity improvement can be estimated as a function of separation distance, baseline orientation, elevation angle and frequency.

C. Response Time

The application of site diversity, while a viable technique for achieving higher availability for fixed terminals, is not relevant for mobile terminals. There are, however, other factors which must be considered in determining the system availability for the mobile community. For terminals which communicate infrequently (duty factor < 1), the assumption that the statistics of the path availability and the need to communicate are uncorrelated results in a reduction in the average link outage time proportional to the duty factor. The "effective" system availability is proportionately increased. Of more significance for these terminals is the impact of short delays in their ability to communicate due to infrequent (less than 1% of the time) heavy rainfall, and is discussed next.

It is beyond the scope of this report to assess the magnitude of the delays and blockages that the military community is experiencing with current MILSATCOM systems. Fig. 6.25⁽⁵¹⁾ presents a sample of data for traffic via the TACSAT satellite from various locations; mostly from the U. S. mainland to a ship in the Pacific. The cumulative delay times shown represent the interval between the assignment of a date/time group at the sender's communications center and the arrival of the message at the communications center on board ship; the delays do not include message handling times outside the communications centers. The curves are for an average day during several months of operation. Note that the median delay for flash traffic, the highest precedence, is on the order of 20 minutes (for routine or priority traffic the median delay is in excess of 3 hours). It appears reasonable to assume that delays of a few minutes due to rain attenuation would be tolerable in such systems. One may speculate that operation at EHF with a significant increase in the number of available circuits and/or improvements in system operation* may reduce the delay time, even when delays due to rain attenuation are included. It remains to determine the duration of the periods of heavy rain.

Previous discussions of path availability have not addressed the distribution of the outages throughout the year; Table 6.9 presents average outages versus path availability. The distribution of the outage will have different impacts on the system, e.g., for a path availability of 99.9%, the theoretical extreme could consist of either a consecutive 9-hour outage per year or a 4-second outage every hour of the year. High path availabilities ($> 99\%$) in fact correspond to heavy rainfalls having extents of a few kilometers and durations of a few minutes. Fig. 6.26 presents histograms of fades greater than 5 and 10 dB at 19 and 37 GHz⁽⁵²⁾. Note that fades of 5 dB at 19 GHz and 10 dB at 37 GHz have durations in excess of 30 minutes. Minimum rain margins of this order must be provided to prevent such delays. Fig. 6.27 presents fade duration histograms at 30 GHz from ATS-6 observations⁽⁵³⁾. Note the wide fade duration distribution for fades ≥ 5 dB which are characteristic of widespread

*For example, it is reported⁽⁵¹⁾ that the time to correct uplink power imbalances ranges from a few minutes to several hours; the use of on-board satellite processing would eliminate these delays.

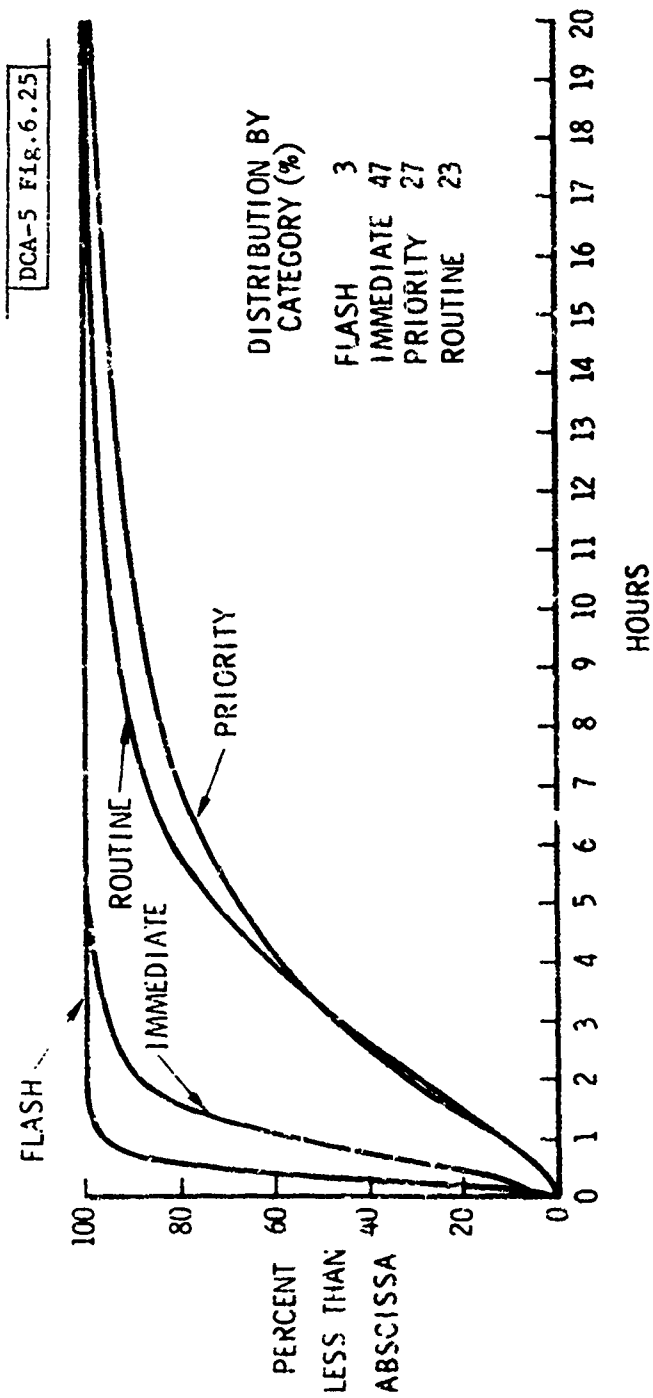


Fig. 6.25. Automatic satellite message transfer time (from Ref. 51).

TABLE 6.9

AVERAGE OUTAGES VERSUS PATH AVAILABILITY

PATH AVAILABILITY (%)	AVERAGE OUTAGE PER			
	YEAR	MONTH	WEEK	DAY
99.99	1 hr	4 min	1 min	9 sec
99.9	9 hrs	44 min	10 min	86 sec
99.5	44 hrs	4 hrs	50 min	7 min
99	88 hrs	7 hrs	100 min	14 min
95	438 hrs	36 hrs	8 hrs	72 min

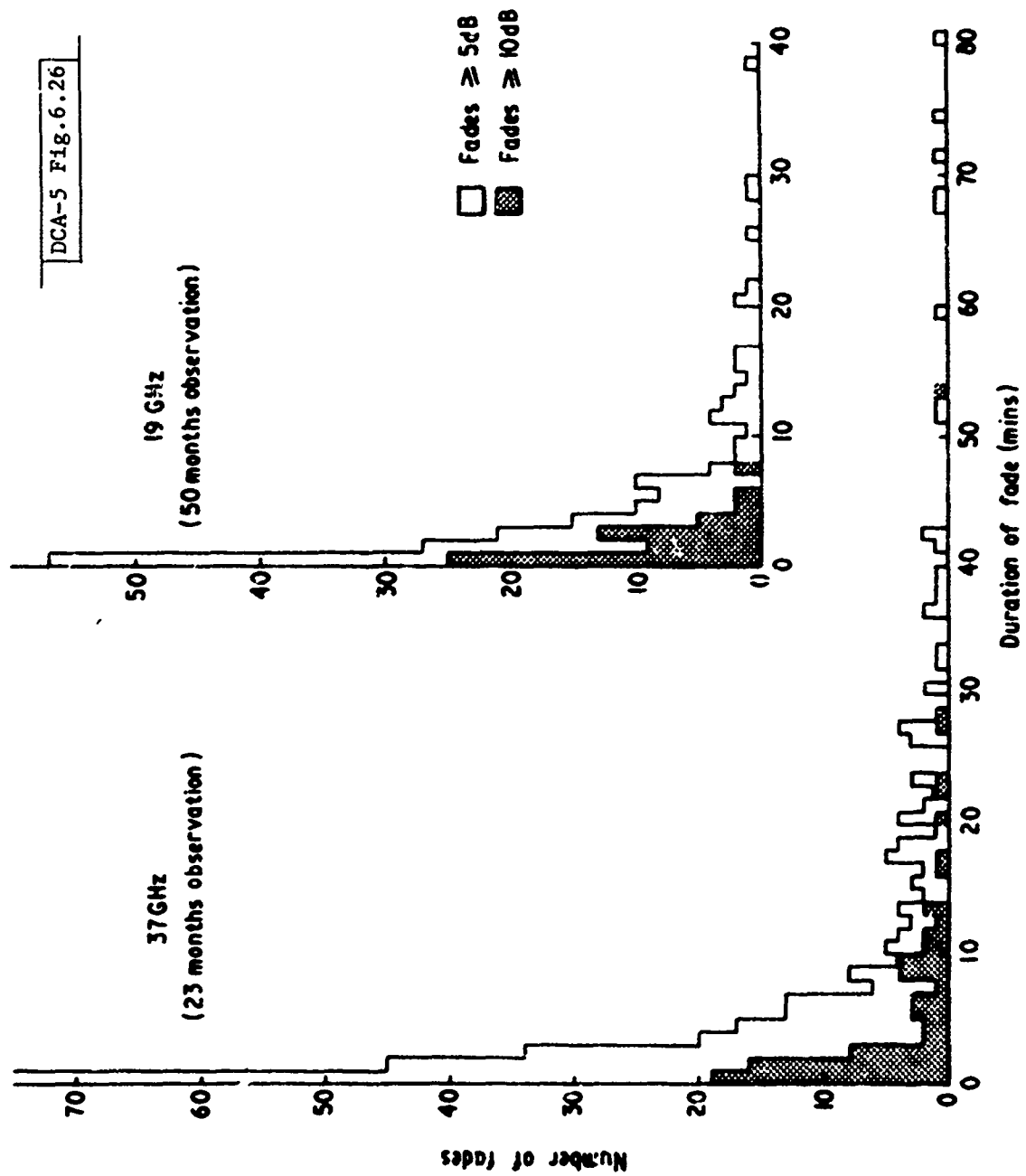


Fig. 6.26. Fade duration histograms at 19 and 37 GHz (from Ref. 52).

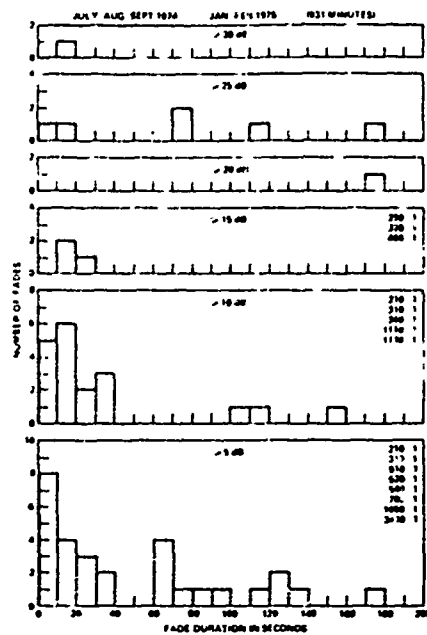


Fig. 6.27. Fade duration histogram at 30 GHz (from Ref. 53).

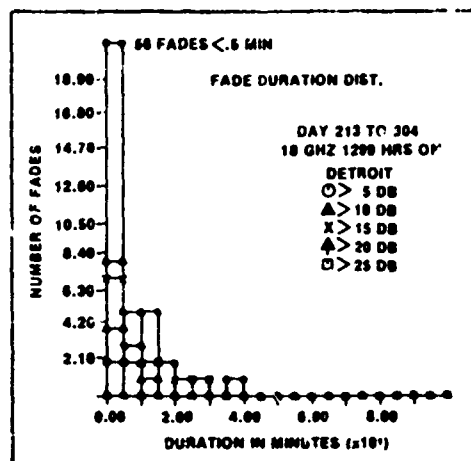


Fig. 6.28. Fade duration histogram at 18 GHz (from Ref. 54).

rain. Note the drastic decrease in the fade duration characteristics for fades ≥ 15 dB which are characteristic of periods of high intensity rainfall. At the 15 dB level, one 8-minute fade was observed; for levels ≥ 20 dB no fades exceeded 3 minutes. Fig. 6.28 presents fade duration histograms from ATS-6 observations⁽⁵⁴⁾ at 18 GHz. Note that in these results, no fades of greater than 4 minutes duration were observed during the 1299 hours of observation. Note also that fades > 20 had durations less than 2 minutes.

In summary, the data presented indicates that the duration of large fades at EHF (≥ 20 dB) due to rain attenuation may be only a few minutes. However, the observations are for fairly limited time periods and for only two geographic locations. A model is required which relates rain rate to the extent and velocity of the rain cells. From such a model, fade duration distributions may be generated for the frequencies of interest. It would then remain for the potential user communities to assess the impact of such communication delays on their system requirements. It is evident that tolerance of some delay in response time will afford a substantial increase in "effective" availability. The alternative of improving system availability by substantially increasing the required link margins will strongly influence the system cost and complexity.

6.7 Summary

A. Rain Attenuation Estimates

The rain climate model and attenuation prediction model presented in Section 6.4 are representative of the current state-of-the-art in global rain attenuation estimates. It is recommended that the rain attenuation estimates derived from these models be utilized as a basis for frequency selection, assessment of system availability, and the determination of general system parameters.

The large uncertainty bounds on the attenuation estimates are inherent in the statistical averaging processes, in particular, the temporal and spatial averaging of the rain rate statistics over large geographic regions. For

specific areas where long term (> 10 years) rain rate statistics are available, refined estimates of rain attenuation may be obtained by applying these statistics to the attenuation prediction model. The definition of smaller rain rate climate regions (R. K. Crane is presently subdividing the current climate regions) will reduce the bounds on the attenuation estimates within these subregions; such improvements should be incorporated in the model.

Improved attenuation estimation models should be based on further observations of rain rate distributions along the propagation path, not on observations of rain attenuation. As regards the latter, such models are typically derived from a limited data base, may not provide representative estimates for the region of observation, and will not be applicable to attenuation predictions for other frequencies and regions.

In regard to future rain attenuation observations at EHF, a voluminous amount of data will be required before it will provide a basis for refined rain attenuation estimates. In the near term, as observed rain rate and attenuation statistics become available (e.g., Japanese experience with CS), the measured data should be compared with the current predictive model to see if it falls within the estimated bounds. Only in the far term, as the data base expands and attenuation statistics become stationary, may the validity of the current or future rain attenuation estimation models be assessed.

B. Availability Considerations

The factors affecting end-user to end-user availability of a MILSATCOM system include, in addition to equipment and path availabilities, the type of transmission, acceptable bit error rates, use of error-correcting codes, type of satellite processing, non-propagation margins and tolerance to delays. In regard to the latter, such factors as saturation, switching time, processing, handling, decision making, and power, frequency and timing corrections are among the contributors to delays. The impact of future improvements, in particular on-board satellite processing on mitigating these delays is an important consideration. The determination of system availability requires analysis of

each of the above parameters, is beyond the scope of this report, and requires further study. A detailed study should be undertaken which is directed toward the collection and analysis of data on outages and delays which, coupled with EHF architectural considerations, will provide the tradeoffs between system availability and system cost and complexity. Based on the constrained system availability analysis presented in this section, path availability studies are required to support such systems analysis and specific recommendations are presented next.

For the wideband trunking community some path diversity will be required to achieve a system availability of 99.9%. The number of terminals within the network requiring diversity and the possible requirement for uplink as well as downlink diversity must be determined from a link-by-link analysis. Space-earth path diversity studies have shown its potential for substantially decreasing the margin requirements for a given probability of occurrence (or decreasing the outage time for a given margin); the diversity improvement realized is dependent on site specific factors. Where climatological and meteorological data is available, the design and evaluation of a dual diversity system can be performed before committing any expenditure for its implementation; such a study should be undertaken. Although site diversity is normally considered to be a receive technique, there is no fundamental reason which precludes transmit diversity. If uplink diversity is required, operational considerations such as buffering, switchover, intersite linking and delays and interruptions should be studied. The following is a summary of recommendations for further study in regard to system availability considerations for the wideband trunking community:

1. Link-by-link analysis of the data rates, rain rate and attenuation statistics and tolerance to delays; parametric study of the trade-offs between terminal design, satellite design (e.g., on-board processing or TDMA) and path diversity requirements for each link to achieve the required system availability.

2. Analysis and evaluation of a dual diversity system for the down link to CONUS based on available climatological and meteorological data; design and cost analysis of candidate system.
3. Design and cost analysis of providing uplink diversity including buffering, switchover, intersite linking and the impact of delays.

For the mobile community, link margin requirements must be determined from global estimates of rain attenuation with their inherently large uncertainty bounds. Achieving high path availability via more robust terminal designs will strongly impact the system cost and complexity. The unresolved factors which impact path availability requirements are concerned with response time; i.e., the tolerance of some delay in response time will afford a substantial increase in "effective" availability. The specific factors to be assessed include the magnitude of the delays experienced in current MILSATCOM systems, the duration and distribution of anticipated delays at EHF due to intense rain, and the potential reduction in delays with system improvements. More data are required on the factors affecting delays in day-to-day operations between MILSATCOM terminals to place the delays due to high rain fades at EHF in proper perspective. A model is required which estimates the fade duration distributions for the frequencies of interest. Finally, the system design issues which impact potential improvements must be addressed, e.g., the use of on-board satellite processing would eliminate delays due to uplink power balancing. These recommendations for further study in regard to system availability considerations for the mobile community are summarized below.

1. For each potential user community, assessment of the factors affecting end-user-to-end-user delays and their magnitude, including blockages, saturation, switching time, processing, handling, decision making, etc.
2. Development of a model, relating rain rate to the extent and velocity of rain cells, from which fade duration distributions may be estimated for the frequencies and path availabilities of interest.

3. Design studies which assess potential improvements in system operation to provide reduced outage time, e.g., on-board satellite processing and TDMA.

VII. TECHNOLOGY DEVELOPMENT/STUDY RECOMMENDATIONS

7.1 Overview

The orderly transition of potential MILSATCOM users to EHF will obviously require the timely availability of the necessary technology. Although a technology base exists at EHF, commercially available equipment is essentially nonexistent. However, among the technologies potentially applicable to EHF are opportunities for providing further improvements in performance, smaller simpler mobile terminals, and more cost-effective terminals. Consequently, a vigorous R&D program will be required with extensive long-term planning, coordination and integration within the DoD community. The following is a summary of those factors relevant to the implementation of the required R&D programs and ultimate realization of the necessary technology:

1. A technology base exists from which the technology necessary to support future EHF MILSATCOMs can evolve. However, there is not currently available an adequate commercial or product support base at EHF to provide the necessary support. R&D programs in all the major component and subsystem areas are required.
2. In the author's opinion, commercial interest, adequate to support R&D in the EHF bands, will not materialize in the next decade. Rather, increasing commercial capacity requirements for COMSAT systems will be satisfied in the 14/11 GHz bands via extensive frequency reuse. Consequently, the DoD must be the primary source of funding* for EHF technology development above this band.
3. The planned evolution of MILSATCOMs to EHF over the next decade affords opportunities for the development of improved system designs and efficient, reliable, cost-effective technology. The implementation of on-board signal processing, and multiple-beam, adaptive-nulling and time-hopped-beam antennas offers the potential for reducing terminal size,

*Current studies by NSA, particularly the 30/20 GHz Program at LRC, may lead to EHF band development contracts. Should such events occur, close coordination between DoD, NSA and other Government agencies is obviously indicated.

complexity and cost. In the component area, solid state devices may provide higher-reliability, lower-cost replacements for current thermionic devices.

4. The need for a concerted, long range EHF technology development program within the DoD is evident. Such a program plan should include among its objectives the delineation, coordination and continuation of the necessary technology development efforts to insure the timely availability of the technology necessary to support future EHF MILSATCOM systems.

There are two major issues which impact the definition of long term technology development programs and which must be addressed with urgency. The major issue is, of course, the essential system studies addressing the orbital considerations, multiple-access and modulation techniques, on-board processors and antenna nulling. These factors obviously impact the space and ground segment complexity and hence the concomitant technology requirements. On-going DCA/MSO efforts are directed toward such studies. A secondary issue is the role of rain attenuation on EHF system design as it impacts orbital considerations and terminal design. The technology recommendations which follow, although primarily directed toward hardware developments, include proposed studies regarding the impact of rain attenuation and are a necessary adjunct to the current system studies.

As regards the recommendations for hardware development, there are few if any technological limits imposed on the strawman subsystem requirements at EHF. However, there are technology boundaries whereby achieving a given performance level requires a more complex and costly technology. A cost versus performance study is required in these areas.

The technology recommendations are divided into near term (3-5 years) and far term (6-10 years). The near-term recommendations are primarily directed toward supporting a 30/20 GHz capability for the wideband data relay and GMF users, initiating development of 44/40 GHz technology, and incorporating relevant studies into the system design efforts. The far-term recommendations

are directed toward improved 30/20 GHz subsystems, the realization of 44/40 GHz subsystems, and the implementation of advanced system techniques.

Nine specific areas are delineated as necessary technology development and/or study efforts in support of EHF MILSATCOM systems:

1. Low-noise receivers
2. TWT power amplifiers
3. Solid-state power amplifiers
4. Antenna surface accuracy
5. Antenna tracking accuracy
6. Radomes
7. Ground-segment antennas
8. Space-segment antennas
9. Rain attenuation factors

7.2 Low-Noise Receivers

Low-noise receiver requirements may be readily satisfied by currently available devices, i.e., mixer/IF amplifiers for the space segment and thermoelectrically-cooled ($T_{OP} = -40^{\circ}\text{C}$) or thermoelectrically-stabilized ($T_{OP} = 40^{\circ}\text{C}$) paramps for the fixed and mobile terminals, respectively. However, the development of low-noise FET amplifiers is indicated as a more reliable, cost-effective alternative and, in addition, will provide lower noise receivers for the space segment. For the near term, devices of particular interest include:

- a. Low-noise FET amplifier ($0.5\ \mu\text{m}$) with a 1 GHz bandwidth and a 3 dB noise figure operating at 20 GHz for the ground segment.
- b. Space-qualified, low-noise FET amplifier ($0.5\ \mu\text{m}$) with a 1 GHz bandwidth and a 5 dB noise figure operating at 30 GHz.
- c. Low-noise FET amplifier ($0.25\ \mu\text{m}$) with a 1 GHz bandwidth and a 6 dB noise figure operating at 40 GHz for the ground segment.

- d. Should a requirement for extremely low-noise receivers (i.e., $\leq 100^\circ\text{K}$) arise for the fixed terminals, cryogenically-cooled FET amplifiers should be investigated as an alternative to paramps.

In the far term, continued development of low-noise FETs (0.25 μm) should result in amplifier noise figures which are better than current TE-cooled paramps at 30/20 GHz and significantly improved at 44/40 GHz. Far term goals include:

- a. Low-noise FET amplifiers with 1 GHz bandwidth, and 2 dB noise figure at 20 GHz and 3.5 dB noise figure at 40 GHz.
- b. Space-qualified, low-noise FET amplifiers with 2.5 dB noise figure at 30 GHz and 4 dB noise figure at 44 GHz.

7.3 TWT Power Amplifiers

TWTA technology is relatively mature and the theory of operation well understood. However, TWTA requirements at EHF represent the most significant area of hardware development, particularly for the space segment.

A. Ground Segment

For the near term, the TWTA technology base appears adequate to support the initial implementation and demonstration of EHF MILSATCOM capabilities. For the mobile terminals, the projected capabilities of liquid-cooled, PPM-focused TWTA's appear adequate; the development of the required tubes remains to be undertaken. For vehicular terminals restricted to air-cooled TWTA's, the projected output power is approximately one-half that of liquid-cooled tubes; further studies of terminal parameters will be required if these power levels prove to be restrictive. For the large fixed terminals, near-term capabilities are of the order of a few kW. Potential TWTA capabilities for the near term include:

- a. Air-cooled, PPM-focused TWTA capabilities:
(limit of current technology)
- 500 W at 30 GHz (1 GHz bandwidth)
- 250 W at 44 GHz (2 GHz bandwidth)

- b. Liquid-cooled, PPM-focused TWTA capabilities:
(limit of current technology)
1 kW at 30 GHz
500 W at 44 GHz
- c. Liquid-cooled, solenoid-focused TWTA capabilities:
(requires substantial development)
2 kW at 30 GHz
1 kW at 44 GHz

For the far term the potential TWTA requirements are assumed to be for higher CW power levels for the fixed terminals and for average-power-limited tubes for TDMA operation. For the large, fixed terminals, projected capabilities for CW output power range from 10 to 100 kW. However, the cost and development effort associated with the required technology must be assessed vis à vis alternative methods of providing increased capacity (narrow, time-hopped beams), increased path availability (site diversity) or increased AJ protection (antenna nulling). Projected far term TWTA capabilities and required technology include:

- a. 10 kW solenoid-focused TWTA operating at 30 GHz (requires significant development).
- b. 100 kW gyrotron operating at 30 GHz with 40% efficiency (potential average-power-limited tube).
- c. Average-power-limited TWTAs for the mobile users for TDMA operation, e.g., 5-kW peak power output (10% duty cycle).

B. Space Segment

TWTAs have played a dominant role in space communications and, for high power requirements at EHF, will continue to maintain a significant role. To insure the availability of improved performance, highly reliable (7-10 year life) TWTAs at EHF, development efforts should now be underway. Specific tube capabilities warranting development* in the near term include:

*The recommendations are typically one-half the maximum predicted output power levels.

- a. 20-watt helix TWTA with 1 GHz bandwidth and efficiency $\geq 25\%$ operating at 20 GHz.
- b. 5 to 10-watt helix TWTA with 1 GHz bandwidth operating at 40 GHz.

For the far term, improvements in helix TWT technology should provide at least a factor-of-two increase in output power. For higher output power requirements, coupled-cavity TWTA's offer a factor-of-four further increase in power but will require more extensive development and space qualification. Specific TWTA capabilities warranting development include:

- a. Helix TWTA's with 1 GHz bandwidth and 30% efficiency providing 40 watts at 20 GHz and 20 watts at 40 GHz.
- b. Coupled-cavity TWTA's with 1 GHz bandwidth and 40% efficiency providing 200 watts at 20 GHz and 100 watts at 40 GHz.

c. TWT Technology Developments

The further development of TWT technology must be considered as important a task as developing specific tube capabilities. Basic developments and improvements in TWT technology provide broad support to all MILSATCOM systems as well as other DoD programs. Improvements in TWT efficiency, power output and reliability are obvious goals.

Recommended areas of development for TWTs for the space segment include:

- a. Multistage depressed collectors for increased efficiency.
- b. Dispenser-type cathodes for increased current-density capability.
- c. Materials for the helix, helix support and internal attenuator to reduce loss and increase thermal capacity.
- d. Velocity tapering of the helix both for higher interaction efficiency (pitch reduction) and lower AM/PM conversion (pitch increase).
- e. Improvements in production processes, circuit testing and reliability assurance.

f. Improvements in life testing including:

1. Develop accelerated and space-simulated life tests.
2. Begin life-testing phase early in development program.
3. Develop high-voltage power supply reliability and life tests.

Recommended areas of development for TWTs for the ground segment include:

- a. Incorporate the latest design technology (e.g., cavity, cathode, collector, etc.) including European developments to increase power and efficiency.
- b. Extend tube lifetime with improved thermal designs.
- c. Reduce costs with new circuit designs to simplify manufacturing processes.

7.4 Solid-State Power Amplifiers

Solid-state devices offer the potential for orders-of-magnitude increase in reliability and reduction in voltage requirements over TWTAs while TWTAs will continue to surpass solid-state devices in output power and efficiency. The potential availability of both technologies at EHF affords the opportunity to employ the optimum device for the specific application. While there are medium-power (10-20 watts) requirements where solid-state and TWT amplifiers will be competitive on a one-for-one replacement basis, there are also unique applications for each. Requirements for high power (100 watts) in a single envelope (e.g., wideband data relay users) would best be served by TWTAs, while requirements for individual power amplifiers (1 watt) on each feed or array element of a time-hopped-beam antenna (e.g., for mobile users) would best be served by solid-state devices. Consequently, parallel development efforts are recommended in both technologies.

Within solid-state technology, there are two potential devices: IMPATT diodes which will provide useful added power capability over the entire EHF band in the near term, in fact a factor-of-four higher power than will be

available from FETs; and Ga As FETs which will provide linear amplification, higher efficiency and ease of combining advantages over IMPATTs. Both devices warrant development for EMF applications and will also provide a technology base for applications at higher (e.g., IMPATTs at 60 GHz) and lower (e.g., FETs at 8 GHz) frequency bands.

To extend the power limitations of individual solid-state devices, power-combining techniques are required and recommendations in this area are included. It should be noted that many of the recommended development efforts are contained in current or planned SAMSO/AFAL programs and these efforts should be provided expanded support and long-term continuity. Specific near-term recommendations for developments in device and combiner technology include:

- a. Space-qualified (Ga As DD Read) IMPATT diodes providing 4 watts of added power with 25% efficiency at 20 GHz and 1 watt of added power with 15% efficiency at 40 GHz.
- b. Design and development of (rectangular) cavity combiners to accommodate 8-12 IMPATT diodes at 20 or 40 GHz and provide graceful degradation with device failure.
- c. Space-qualified, IMPATT amplifiers with 1 GHz bandwidth providing 40 watts at 20 GHz and 10 watts at 40 GHz.
- d. Space-qualified, 1-watt Ga As FETs with 30% efficiency operating at 20 GHz.
- e. Design and development of (radial) combiner techniques to accommodate 10 to 20 FETs with high (80 to 90%) combining efficiency.
- f. Develop accelerated and space-simulated life tests for IMPATT and FET devices to insure that high reliability is not compromised for higher added-power capability.
- g. Develop complete amplifier tests including failure mode and communication performance (e.g., AM/FM conversion and BER) testing.

Far term projections for power-added capability predict a factor of 2 to 4 increase for both IMPATTs and FETs. The particular areas of interest for development, both for near-term and far-term improvements include: improvements in thermal design (e.g., diamond heat sinks), in device profiles for improved efficiency, and in impedance matching (e.g., integrated matching circuits) for IMPATTs; improvements in high-frequency FET fabrication and implementation techniques to achieve uniform device illumination, reduced parasitic effects and improved circuit matching of large gate-width devices. Potential device capabilities include:

- a. Space-qualified IMPATT diodes providing added-power capabilities of 12 watts at 20 GHz and 3 watts at 40 GHz.
- b. Space-qualified FETs providing added-power capabilities of 3 watts at 20 GHz and 0.5 to 1 watt at 40 GHz.
- c. Development of circuits capable of efficiently combining 20 to 40 devices at EHF.

7.5 Antenna Surface Accuracy

The antenna surface accuracy required at EHF (.010 to .015 in.) is beyond the capabilities of current commercial technology. The realization of the requisite surface accuracy will entail:

- a. For small mobile terminals ($D \leq 4$ ft.), more refined manufacturing techniques for one-piece reflectors will have to be employed (e.g., precision spinning or molding); the most cost-effective process remains to be determined.
- b. For medium transportable terminals ($8 \text{ ft.} \leq D \leq 20 \text{ ft.}$), refinements in panel manufacturing (machined cast or molded panels), backup structure fabrication and antenna assembly will be required; the most cost-effective process remains to be determined.
- c. For large fixed terminals ($D \approx 40$ ft.), new fabrication techniques must be developed; the cost/performance tradeoffs may be studied, but the use of radomes is recommended.

7.6 Antenna Tracking Accuracy

For mobile terminals, current antenna tracking technology will support operation of proposed antennas at EHF. However, there are technology boundaries between the various tracking systems which represent increased cost and complexity. The following factors should be addressed in system studies as potential limits on mobile terminal antenna size:

- a. Establish achievable tracking accuracy for the various tracking systems (e.g., step track, pseudomonopulse, monopulse) based on operational experience.
- b. Determine the cost, weight, reliability, flexibility, etc. of the various tracking systems and impact on the particular platform.
- c. Integrate these potential antenna gain limitations into system design studies, in particular, the tradeoff between satellite and ground terminal complexity.

Note that the large uplink to downlink frequency ratio at EHF imposes more stringent requirements on antenna tracking accuracy to limit the loss at the uplink frequency. This factor must be considered in the above study.

For large fixed terminals, the required tracking accuracy is at the limit of current technology. As wind loads are the dominant limiting factor, the use of radomes must be addressed.

7.7 Radomes

Radomes will be required for airborne and shipboard terminals, and will be needed for large fixed terminals to mitigate the effect of wind loads on antenna surface and tracking accuracy. The major difference in radome requirements at EHF is the larger ratio of uplink to downlink frequency and its impact on radome performance and cost. Specific areas to be addressed include:

- a. For airborne terminals, dual-band radome technology has been demonstrated (AN/ASC-28); design, fabrication and testing of radomes for the

specific frequencies, antenna diameters and operational conditions are required.

b. For shipboard terminals, new radome designs are required to accommodate widely separated frequency bands; cost/performance tradeoffs between solid-laminate (single-tuned) and sandwich (double tuned) construction are required.

c. For large fixed terminals, a radome study is required to assess the cost/performance tradeoffs between existing and new radome designs, and the cost, performance and maintenance considerations regarding rain effects.

7.8 Ground-Segment Antennas

For the ground segment, antenna requirements will be satisfied by parabolic reflector antennas. In addition to the antenna surface and tracking accuracy considerations previously delineated, the impact of the bandwidth requirements and insertion loss at EHF on antenna subsystem design, and the potential use of low-sidelobe antennas warrant further consideration.

As the uplink-to-downlink frequency separation will impact the design of high-efficiency and tracking feeds, polarizers, diplexers, etc., the following recommendations are made:

a. For 30/20 GHz operation, antenna subsystem designs can benefit from the extensive component technology at 6/4 GHz; due to the tolerance requirements at 30/20 GHz, development efforts will be required in fabrication techniques.

b. For larger band separations (e.g., 44/20 GHz), new feed and component designs will be required and development efforts should be undertaken.

For antenna sizes or installations requiring significant lengths of waveguide, the insertion loss of standard rectangular waveguide at EHF is prohibitive and the development of higher-order mode waveguide and components is required. Specific recommendations include:

- a. Develop and bring to production availability higher-order mode waveguide components (e.g., flexible waveguide, bends, transitions, rotary joints, etc.) for the bands of interest.
- b. For large fixed terminals, the use of beam-waveguide techniques should be investigated to eliminate waveguide and rotary joints.

The LPI detection range and tolerable AJ threat levels for both downlink and uplink jamming (assuming a repeat-back jammer) are directly proportional to the antenna sidelobe levels of the terminal. Consequently, reductions in antenna sidelobe levels should be investigated and should be implemented within the constraints of reasonable cost and minimum impact on the performance and operation of the terminal. Specific areas warranting further study include:

- a. Achievable reduction in sidelobe levels with special antenna feed and feed-support designs based on current technology.
- b. Sidelobe reduction via offset-fed reflectors must be assessed vis a vis the cost and operational constraints.
- c. Achievable sidelobe reduction with absorber tunnels (10 to 20 dB) must be weighed against the cost, and environmental and maintenance considerations.
- d. Adaptive sidelobe nulling techniques can provide 30 dB additional jammer suppression; the required circuit technology is extant and emphasis should be placed on the number of cancellation loops, design and implementation of the auxiliary antenna, and performance evaluation.

7.9 Space-Segment Antennas

Advances in satellite antenna technology offer significant improvements in antenna capabilities: MBAs can provide variable-beam and multiple-beam coverage; the use of narrow, time-hopped beams offers the opportunity for significantly reducing ground terminal cost and complexity, and/or increasing capacity; the implementation of adaptive-nulling antennas offers orders of magnitude

improvement in AJ protection and the potential for reducing terminal cost and complexity. The realization of high resolution antenna beams or nulls ($\leq 1^\circ$) are readily achievable at EHF, and, consequently, MILSATCOM operation at EHF affords the opportunity to implement this advanced antenna technology to full advantage. Toward that end, the following areas are recommended for further studies and development efforts.

A. Phased Arrays

To provide a single beam for an area coverage, the use of phased arrays appears to have advantages over mechanically steerable reflector antennas, particularly for power combining solid-state transmitters. Areas to be addressed include:

- a. Tradeoffs between the phased array and reflector antenna in regards to weight, volume and packaging constraints, reliability (phase shifters versus gimbals and rotary joints), and RF losses (corporate feed networks and phase shifters versus flexible waveguide and rotary joints).
- b. For spatial power combining applications, development efforts should address the effect of device degradation and failure on array antenna performance.

B. Time-Hopped Beam Antennas

A single time-hopped beam may be provided either by a phased array or by a lens fed by an array of feeds; the beam control would be provided by phase shifters or switches, respectively. The theoretical gain of these generic antenna types is essentially identical. The choice between them then depends upon the specific application, i.e., uplink, downlink with single transmitter or spatial power combining, and the beam switching rate. For applications favoring the phased array (e.g., spatial power combining), the choice between ferrite or diode phase shifters will depend upon the beam switching rate. Particular areas warranting further study and development include:

- a. Development of phased array and lens antennas to determine achievable performance and implementation constraints.
- b. Development of space-qualified, low-loss phase shifters (both ferrite and diode) and ferrite switches at the frequency bands of interest.
- c. Study of prime power tradeoffs as a function of antenna type, state-changing device, beam-switching rate and beam-switching algorithms.

D. Multiple-Beam Antennas

The capabilities of multiple-beam antennas (MBAs) are numerous, and the far-term use of MBAs in EHF MILSATCOMS is assumed. In order to realize this capability, there is a need to:

- a. Develop a broadband waveguide and/or dielectric lens MBA.
- b. Develop the variable power dividers (VPDs) required for the associated beam-forming network (BFN).

F. Adaptive-Nulling Antennas

Adaptive-nulling antennas afford the opportunity for an additional 30 dB or more suppression of jammer signals. Their potential for reducing terminal cost and complexity for a given current threat or mitigating future increased jamming threats is obvious. The salient issues to be addressed in adaptive-nulling antenna technology are achieving 1 or 2 GHz nulling bandwidths and the implementation of high resolution antennas to realize the full advantage of operation at EHF. Concomitant with these goals, it is essential to:

- a. Develop broadband adaptive-nulling circuits capable of operating over a 1 or 2 GHz bandwidth both at EHF and IF frequencies.
- b. Study and develop techniques for implementing high resolution EHF antennas, e.g., filled or thinned arrays, space-fed arrays, lens antenna, MBA.

7.10 Rain Attenuation Factors

Rain attenuation at EHF is one of the critical parameters affecting frequency selection, system availability, elevation angle restrictions and terminal costs. Further studies are required to place the role of rain attenuation in EHF MILSATCOMs in proper perspective and such efforts should be an adjunct to system design studies. Particular areas warranting study efforts are delineated below.

A. Global Rain Attenuation Estimates

For studies requiring global estimates of rain attenuation, the following recommendations are made:

- a. The rain rate distribution and attenuation prediction models presented in this report are representative of the current state-of-the-art and should be utilized.
- b. For specific areas where long term rain rate statistics are available, refined estimates of rain attenuation may be obtained by applying those statistics to the attenuation prediction model.

B. Site Diversity Considerations

For the wideband-data-relay community, some path diversity will be required to achieve a system availability of 99.9%. The number of terminals within the network requiring diversity, the implementation of downlink site diversity, and the possible requirement for uplink diversity must be addressed. Recommendations for further study include:

- a. Link-by-link analysis of the data rates, rain rate and attenuation statistics, and tolerance to delays; parametric study of the tradeoffs among terminal design, satellite design, and path diversity requirements for each link.
- b. Performance analysis of dual diversity systems for the downlink (particularly to CONUS) based on available climatological and meteorological data; design and cost analysis of candidate systems.

- c. Design and cost analysis of providing uplink diversity including buffering, switchover, intersite linking and the impact of delays.

C. Response Time Considerations

For the mobile community, the tolerance of some delay in response time will afford a substantial reduction in the required rain attenuation margins (or a substantial increase in "effective" path availability). The specific factors to be assessed include the magnitude of the delays experienced in current MILSATCOM systems, the duration and distribution of anticipated delays at EHF due to intense rain, and the potential reduction in delays with system improvements at EHF. These factors should be addressed, as the alternative of achieving high path availability via more robust terminals will strongly impact terminal cost and complexity. Recommendations for further study in this regard include:

- a. For each user community, assessment of the factors affecting end-user-to-end-user delays and their magnitude, including uplink power balancing and frequency correction, blockages, message processing and handling, etc.
- b. Development of a model, relating rain rate to the extent and velocity of rain cells, from which fade duration distributions may be estimated for the frequencies and path availabilities of interest.
- c. Design studies which assess potential improvements in system operation at EHF to provide reduced outage time, e.g., on-board signal processing.

ACKNOWLEDGMENTS

The author is pleased to acknowledge the support of numerous people who have contributed to this study. Particular thanks are due to Dr. Pravin C. Jain of the DCA/MSO and Dr. Leo J. Ricardi of Lincoln Laboratory for their guidance and assistance; to the staff at AFAL, DCEC, MSO, NAVELEX, NOSC, NRL, RADC, SAMSO and SATCOMA for many informative discussions, particularly regarding their R&D programs and operational considerations; to colleagues in the Communications Division (Division 6) at Lincoln Laboratory for numerous comments and suggestions, particularly in the areas of their on-going work and system concepts; and finally, to the staff of the numerous manufacturers for their timely and informative responses to the author's many inquiries. The author also extends a special thanks to Maureen Bartlett who typed and edited the manuscript.

REFERENCES

1. E. J. Dutton, et al., "Modeling the Effects of Clouds and Rain upon Satellite-to-Ground System Performance," COM-75-10950, Office of Telecommunications, Boulder, CO, 38 (March 1973).
2. J. Whelehan, "Low-Noise Millimeter-Wave Receivers," IEEE Trans. MTT MTT-25, 268 (1977).
3. S. Weinreb and A. R. Kerr, "Cryogenic Cooling of Mixers for Millimeter and Centimeter Wavelengths," IEEE Journal of Solid-State Circuits SC-8, 58 (1973).
4. H. C. Okean and A. J. Kelly, "Low-Noise Receiver Design Trends Using State-of-the-Art Building Blocks," IEEE Trans. MTT MTT-25, 254 (1977).
5. "Ga As FETs: Market and Technology Review," Microwave J., 22 (February 1978).
6. C. F. Krumm, et al., "30 GHz Ga As FET Amplifier," IEEE MTT Symposium Digest, 383 (1978).
7. J. V. DiLorenzo, "Ga As FET Development -- Low Noise and High Power," Microwave J., 39 (February 1978).
8. H. Fukui, "Optimal Noise Figure of Microwave Ga As MESFETs," To be published in IEEE Transactions on Electron Devices.
9. J. H. Scholtz and J. P. Vaszari, "An Air Cooled 200 Watt CW TWT at 30.5 GHz with High Interaction Efficiency," IEDM Technical Digest, 360 (1977).
10. T. Ishida, et al., "Program of Medium-Capacity Communications Satellite for Experimental Purposes," AIAA/CASI 6th Comm. Satellite Systems Conference, Paper No. 76-244 (April 1976).
11. H. Seunik, et al., "1-kW CW PPM-Focused TWT for Upper Ka-Band," Microwave System News, (June/July 1974).
12. H. Seunik, et al., "High Power CW PPM-Focused TWT for Upper Q-Band," IEDM Technical Digest, 128 (1977).
13. J. P. Vaszari, "Development of 5.0 kW, Ku-Band Traveling-Wave Tube for Communication Systems," IEDM Technical Digest, 249 (1976).
14. T. F. Godlove and V. L. Granatstein, "Gyrotron: Reborn Tube is a Millimeter Powerhouse," Microwave Systems News, 75 (November 1977).

REFERENCES (Cont'd)

15. "Gyrotron Aims for 200 kW at 28 GHz," Microwave Systems News, 21 (December 1977).
16. E. N. Sosa and P. A. Gianfortune, "A 5 W Ka-Band TWT for Space Communications," IEDM Technical Digest, 419 (1975).
17. P. E. Clark, et al., "New Developments in Ka-Band: A 10 W CW Helix Type TWT," IEDM Technical Digest, 373 (1976).
18. E. F. Miller, et al., "Performance Characteristics of the 12 GHz, 200 Watt Transmitter Experiment Package for CTS," NASA TR X-71773, Lewis Research Center, Cleveland, OH, no date.
19. W. A. Harman, et al., "Design of PPM Focused High Efficiency Space TWTs at Millimeter Wavelengths," IEDM Technical Digest, 377 (1976).
20. D. Deml, "Design Considerations, Design Limits and Interface Problems for High Frequency Satellite TWTs," Proc. of Symp. on Advanced Satellite Communications Systems, Genoa, Italy, 167 (December 1977).
21. F. J. Bayuk and J. E. Raue, "Ka-Band Solid State Power Amplifier," IEEE Microwave Symposium Digest, 29 (1977).
22. "Compact Radial Power Combiner," Microwaves, 9 (October 1977).
23. "X-Band Planar Combiner Module Using Ga As FETs," Microwave Journal, 34 (February 1978).
24. T. Schellenberg and M. Cohn, "A Wideband Radial Power Combiner for FET Amplifiers," ISSCC Technical Digest, 164 (February 1978).
25. J. Ruze, "Antenna Tolerance Theory-A Review," Proc. IEEE 54, 633 (April 1966).
26. D. J. Frediani, "Technology Assessment for Future MILSATCOM Systems: The 30/20 GHz Band," Project Report DCA-4, Lincoln Laboratory, M.I.T. (24 August 1978).
27. Defense Satellite Communications System Phase III, Critical Design Report for the Communications Subsystem, Vol. I, General Electric Space Division, Philadelphia, PA, 27 March 1973.
28. Air Force Avionics Laboratory Satellite Communications Project, AFAL/AAD Wright Patterson AFB, OH, no date.

REFERENCES (Cont'd)

29. Shipboard Satellite Communication Sets AN/WSC-2 (XN-2) (V), Naval Electronic Systems Command Contract Specification, ELEX-S-138, February 23, 1973, with Addendum 2, September 10, 1973.
30. Satellite Communication Terminal AN/MS-61, USASATCOMA Technical Requirements, SCA-2180, April 1, 1976.
31. Prime Item Specification for Communication Satellite Terminal AN/TSC-86(), USASATCOMA Technical Requirements, SM-A-775168A, March 3, 1976.
32. U.S. Army Satellite Communications Agency Brochure No. 88693, "Progress in Communications from Signal Flags to Satellites," no date.
33. O. Hachenberg, et al., "The 100-Meter Radio Telescope at Effelsberg," Proc. IEEE, 61, 1288 (1973).
34. "A 25-Meter Telescope for Millimeter Wavelengths," 25-Meter Telescope Working Group, National Radio Astronomy Observatory, 32 (July 1977).
35. A. R. Dion, "A Wideband Waveguide Lens," Technical Note 1977-8, Lincoln Laboratory, M.I.T. (2 February 1977).
36. R. K. Crane, "Global Model for Rain Attenuation Prediction," EASTCON '78 Record, 391 (1978).
37. R. K. Crane, "Propagation Phenomena Affecting Satellite Communications Systems Operating in the Centimeter and Millimeter Wavelength Bands," Proc. IEEE 59, 173 (1971).
38. J. W. Ryde and D. Ryde, "Attenuation of Centimeter and Millimeter Waves by Rain, Hail, Fog and Clouds," Res. Labs. of the General Electric Company, Wembley, England Rep. 8670 (1945).
39. J. B. Snider, "A Proposed Program for the Study of Atmospheric Attenuation of Satellite Signals," ESSA Technical Report RL 62-WPL 1 (January 1968).
40. R. L. Olsen, et al., "The aR^b Relation in the Calculation of Rain Attenuation," IEEE Trans. Ant. Prop. AP-26, 318 (1978).
41. J. Goldhirsh, "Prediction Methods for Rain Attenuation Statistics at Variable Path Angles and Carrier Frequencies between 13 and 100 GHz," IEEE Trans. Ant. Prop. AP-23, 786 (1975).

REFERENCES (Cont'd)

42. J. Goldhirsh, "Prediction of Slant Path Rain Attenuation Statistics at Various Locations," Radio Science, 12, 741 (1977).
43. S. H. Lin, "Nationwide Long Term Rain Rate Statistics and Empirical Calculations of 11 GHz Microwave Rain Attenuation," Bell System Tech. J., 56, 1581 (1977).
44. S. H. Lin, "Empirical Calculation of Microwave Rain Attenuation Distributions on Earth-Satellite Paths," EASTCON '78 Record, 379 (1978).
45. CCIR Report 563-1, "Propagation in Non-Ionized Media," (Study Group 5), International Radio Consultative Committee (CCIR), International Telecommunications Union, Geneva (1975).
46. R. W. Wilson, "A Three-Radiometer Path-Diversity Experiment," Bell System Tech. J., 49, 1239 (1970).
47. R. W. Wilson and W. L. Mammei, "Results from a Three-Radiometer Path-Diversity Experiment," in Propagation of Radio Waves at Frequencies above 10 GHz, IEEE Conference Publication No. 98, 23 (1973).
48. D. A. Gray, "Farth Space Path Diversity: Dependence on Base Line Orientation," G-AP International Symposium, Boulder, CO (1972).
49. D. B. Hodge, et al., "ATS-6 Millimeter Wavelength Propagation Experiment," Rep. 3863-6, Electroscience Laboratory, Ohio State University, Columbus, OH (1976).
50. W. J. Vogel, et al., "Attenuation Diversity Measurements at 20 and 30 GHz," Radio Science, 11, 167 (1976).
51. N. E. Feldman and S. J. Dudzinsky, Jr., "A New Approach to Millimeter-Wave Communications," R-1936-RC, The Rand Corporation (April 1977).
52. P. G. Davies, "Slant Path Attenuation at Frequencies above 10 GHz," in Propagation of Radio Waves at Frequencies above 10 GHz, IEEE Conference Publication No. 98, 10 (1973).
53. L. J. Ippolito, "Millimeter Wave Propagation and Communications Experiments at 20 and 30 GHz," IEEE Trans. Aero. Elect. Sys. AES-11, 1067 (1975).
54. G. Hyde, "Preliminary Results from the 13/18 GHz COMSAT Propagation Experiment," IEEE Trans. Aero. Elect. Sys. AES-11, 1084 (1975).

APPENDIX A

ESTIMATES OF RAIN ATTENUATION

This appendix presents global estimates of rain attenuation based on the proposed rain attenuation prediction model described in Section VI. The attenuation estimates include oxygen and water vapor absorption (Fig. 6.1) in addition to rain attenuation. The data are presented, for each climate region, as graphs of

Figs. A1-A24: attenuation versus path availability with frequency as a parameter for elevation angles of 10° , 20° and 90° .

Figs. A25-A56: attenuation versus elevation angle with path availability as a parameter for frequencies of 20, 30 40 and 45 GHz.

Figs. A57-A80: attenuation versus frequency with path availability as a parameter for elevation angles of 10° , 20° and 90° .

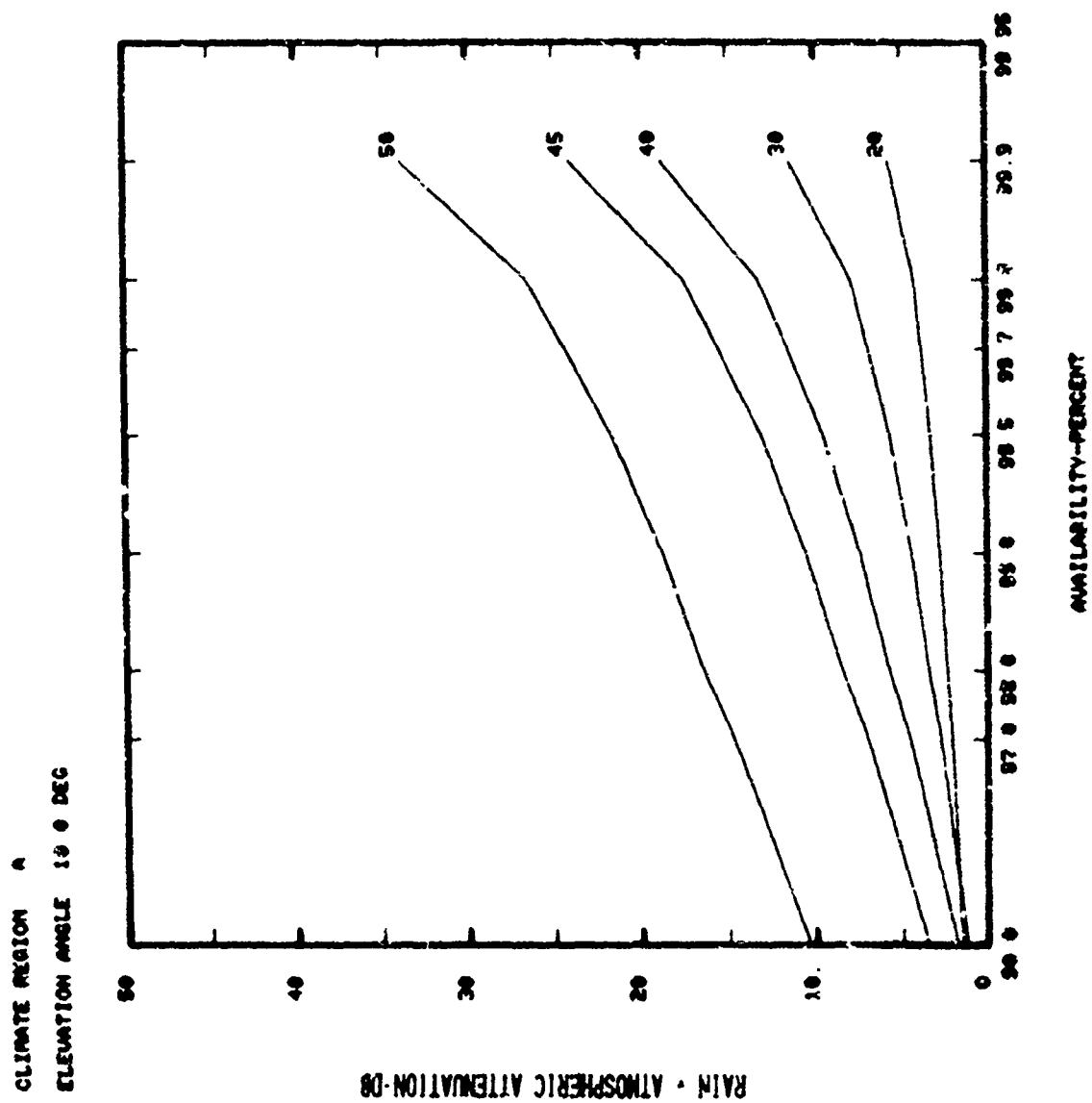


Fig. A-1

CLIMATE REGION A
ELEVATION ANGLE 20.0 DEG

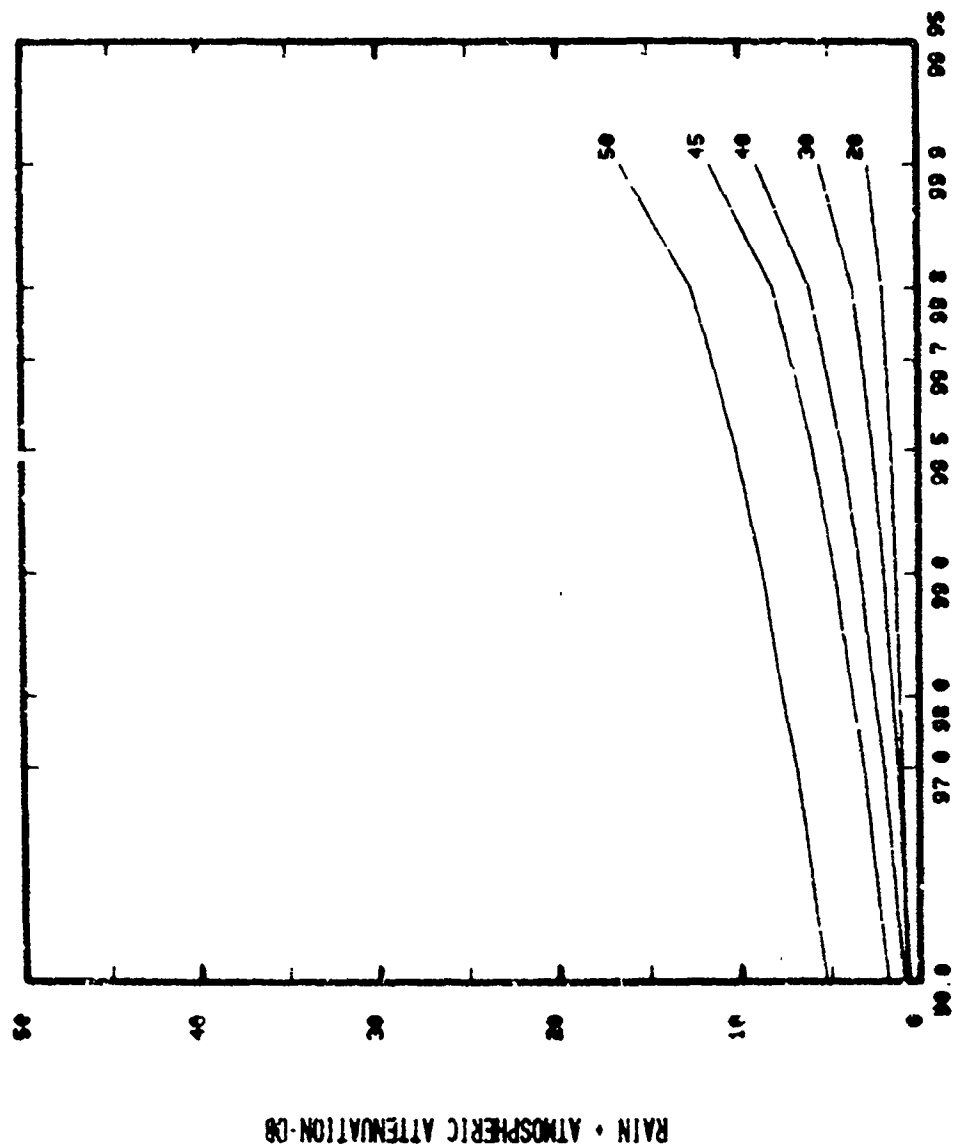


Fig. A-2

CLIMATE REGION H
ELEVATION ANGLE 90 ° DEG

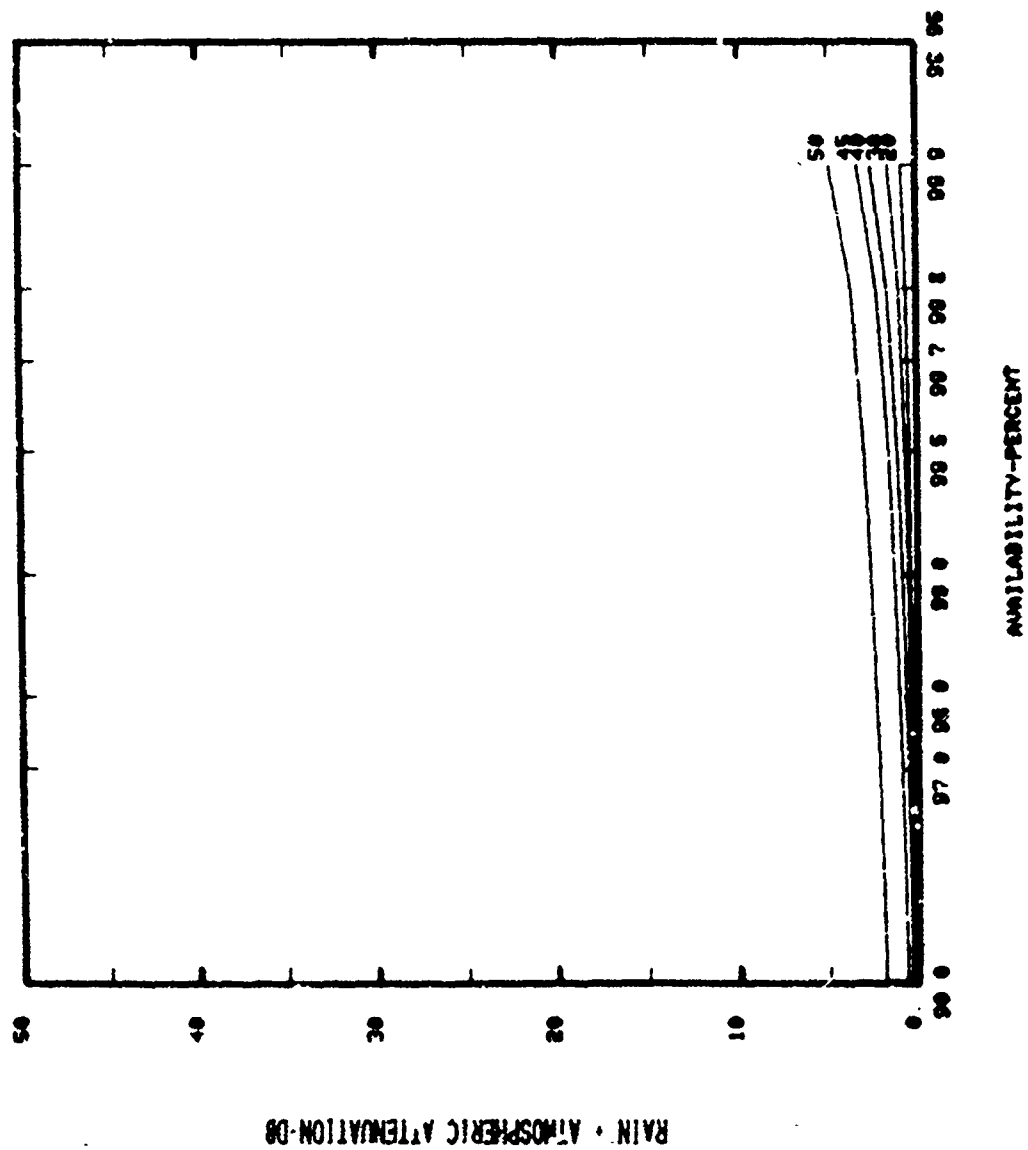


Fig. A-3

CLIMATE REGION 3
ELEVATION ANGLE 10.0 DEG.

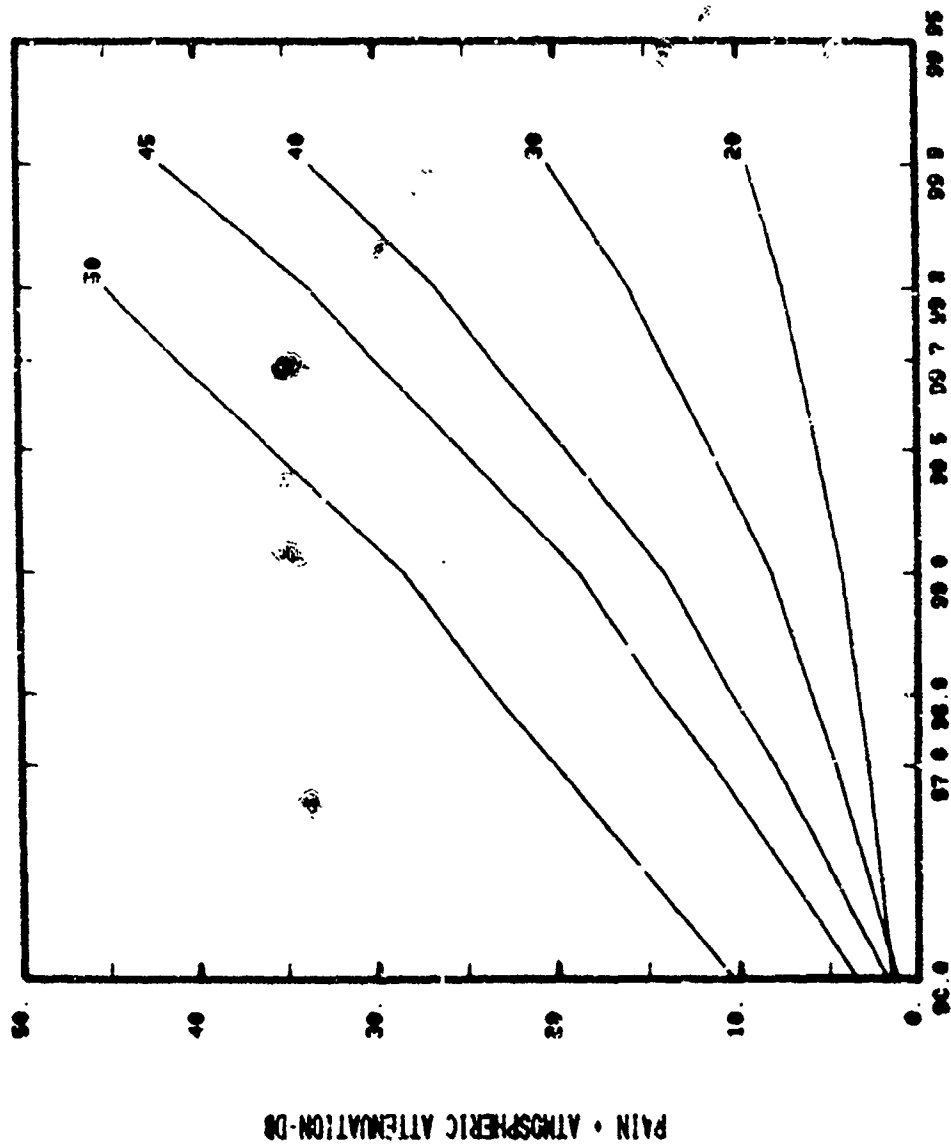


Fig. A-4

CLIMATE REGION B
ELEVATION ANGLE 20.0 DEG

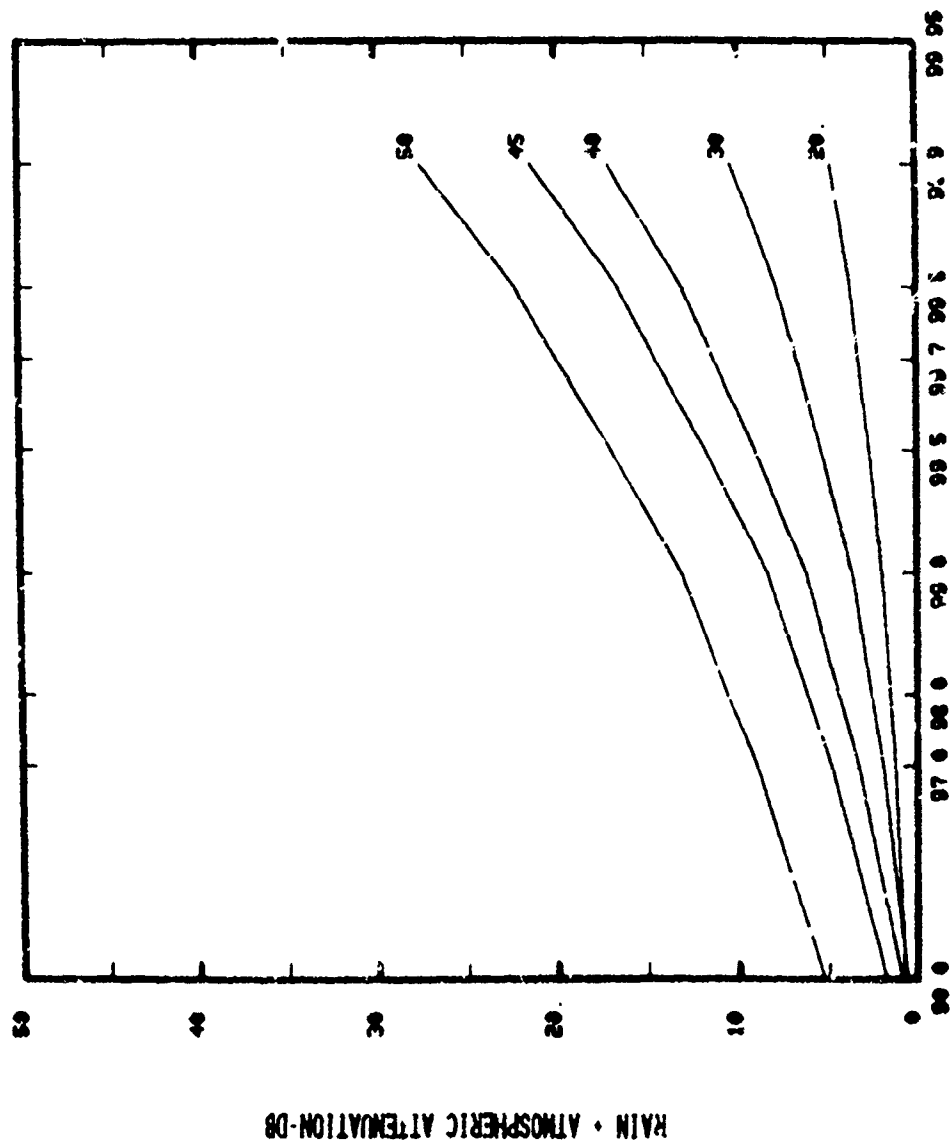
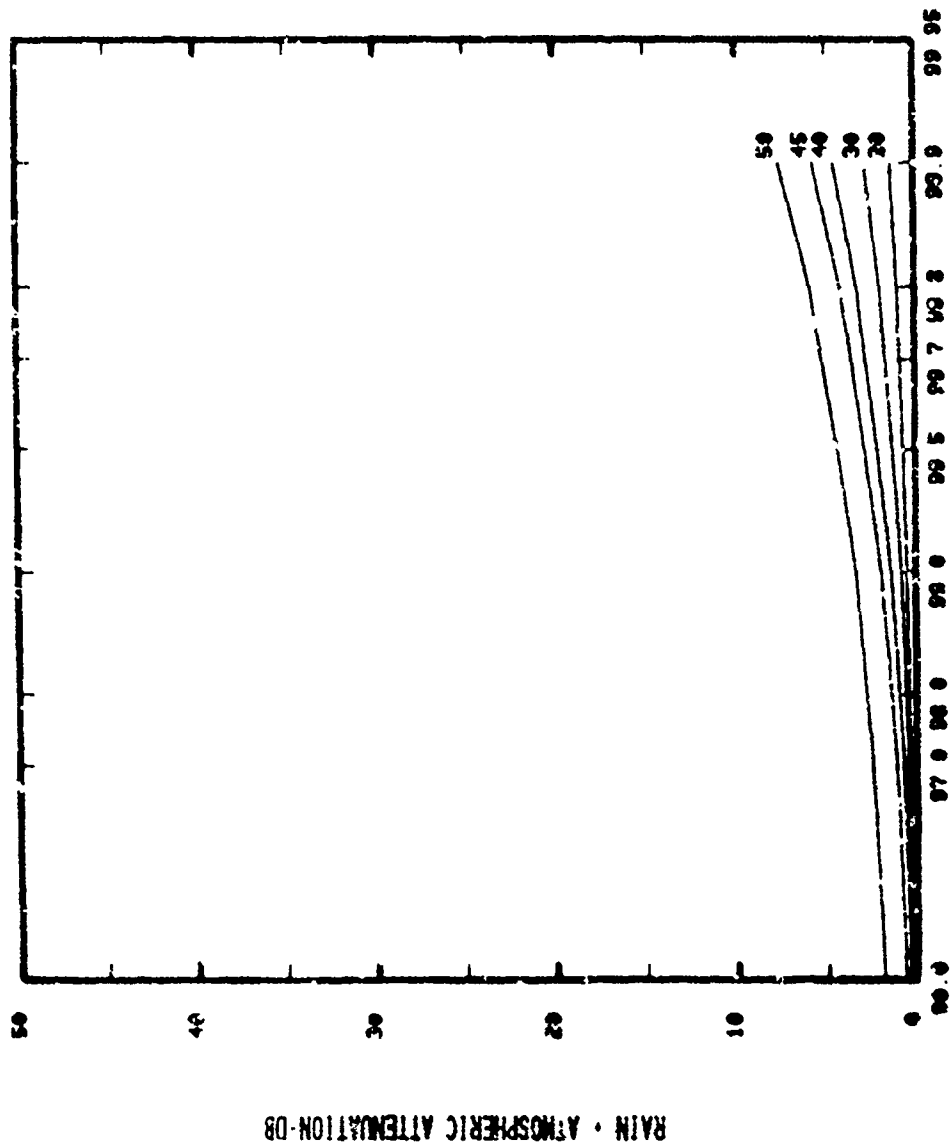


Fig. A-5

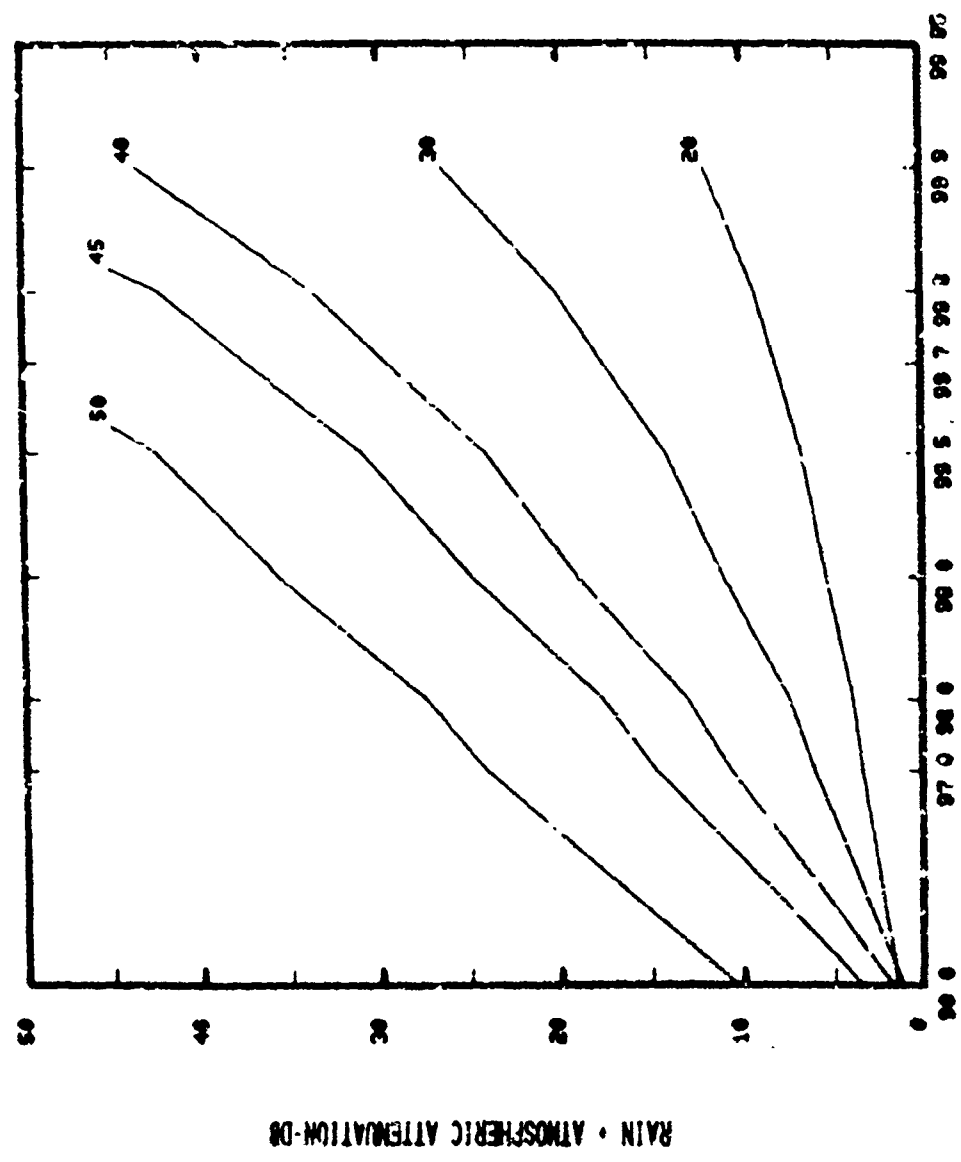
CLIMATE REGION B
ELEVATION ANGLE 90 DEG



AVAILABILITY-PERCENT

Fig. A-5.

CLIMATE REGION C
ELEVATION (FOOT) 10.0 DEG



AVAILABILITY-PERCENT

Fig. A-7

CLIMATE REGION C
ELEVATION ANGLE 20 ° DEG.

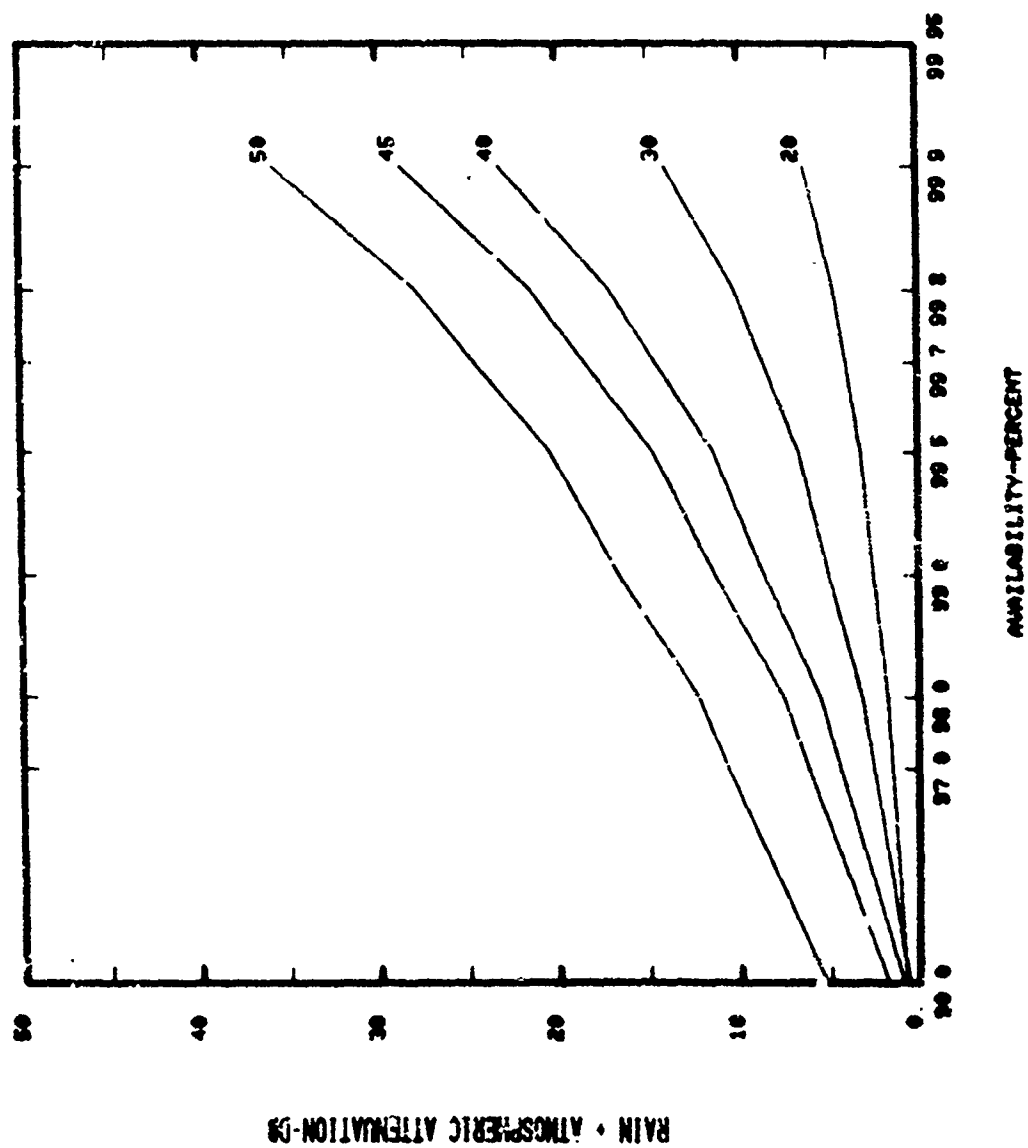


Fig. A-8

CLIMATE REGION C
ELEVATION ANGLE 90.0 DEG

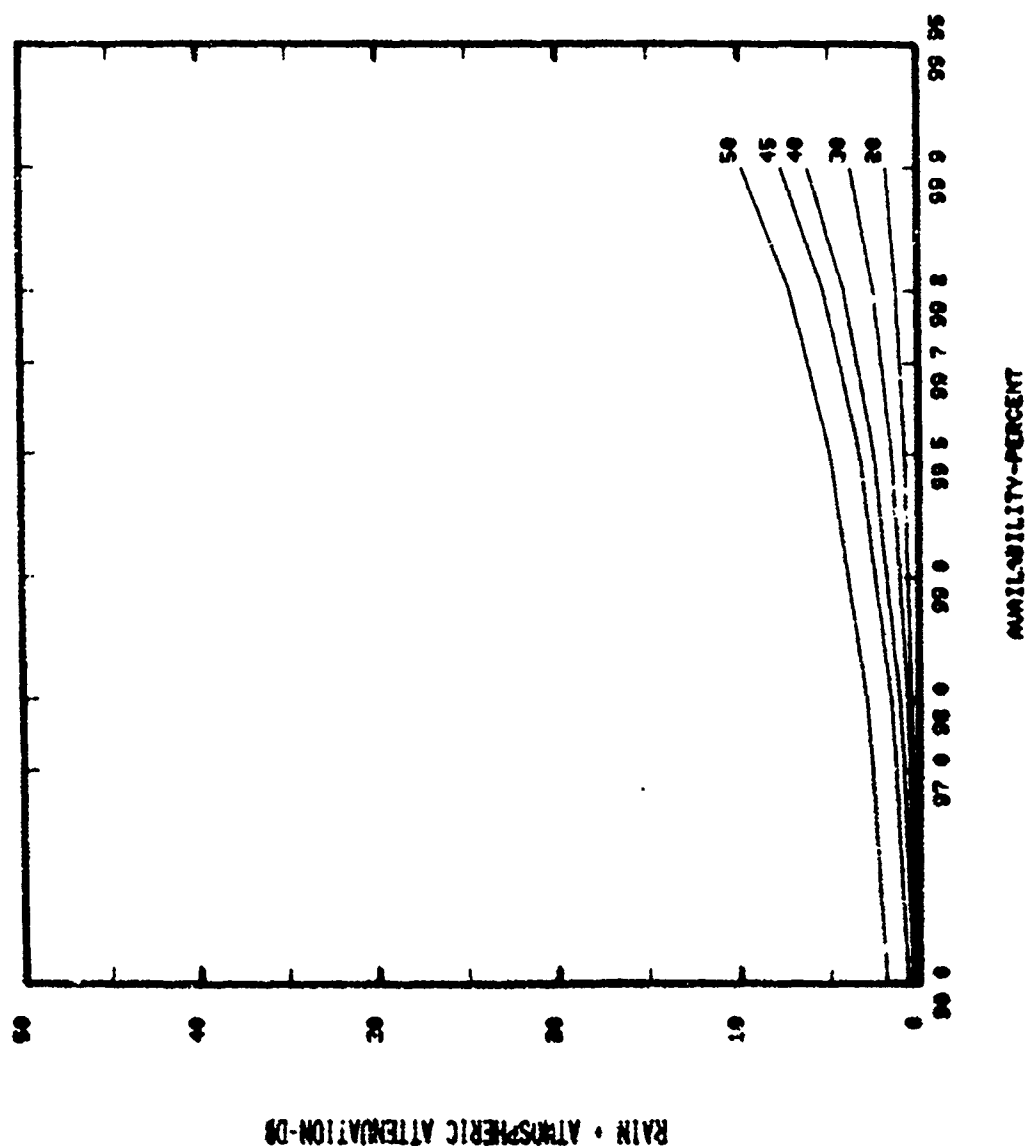


Fig. A-9

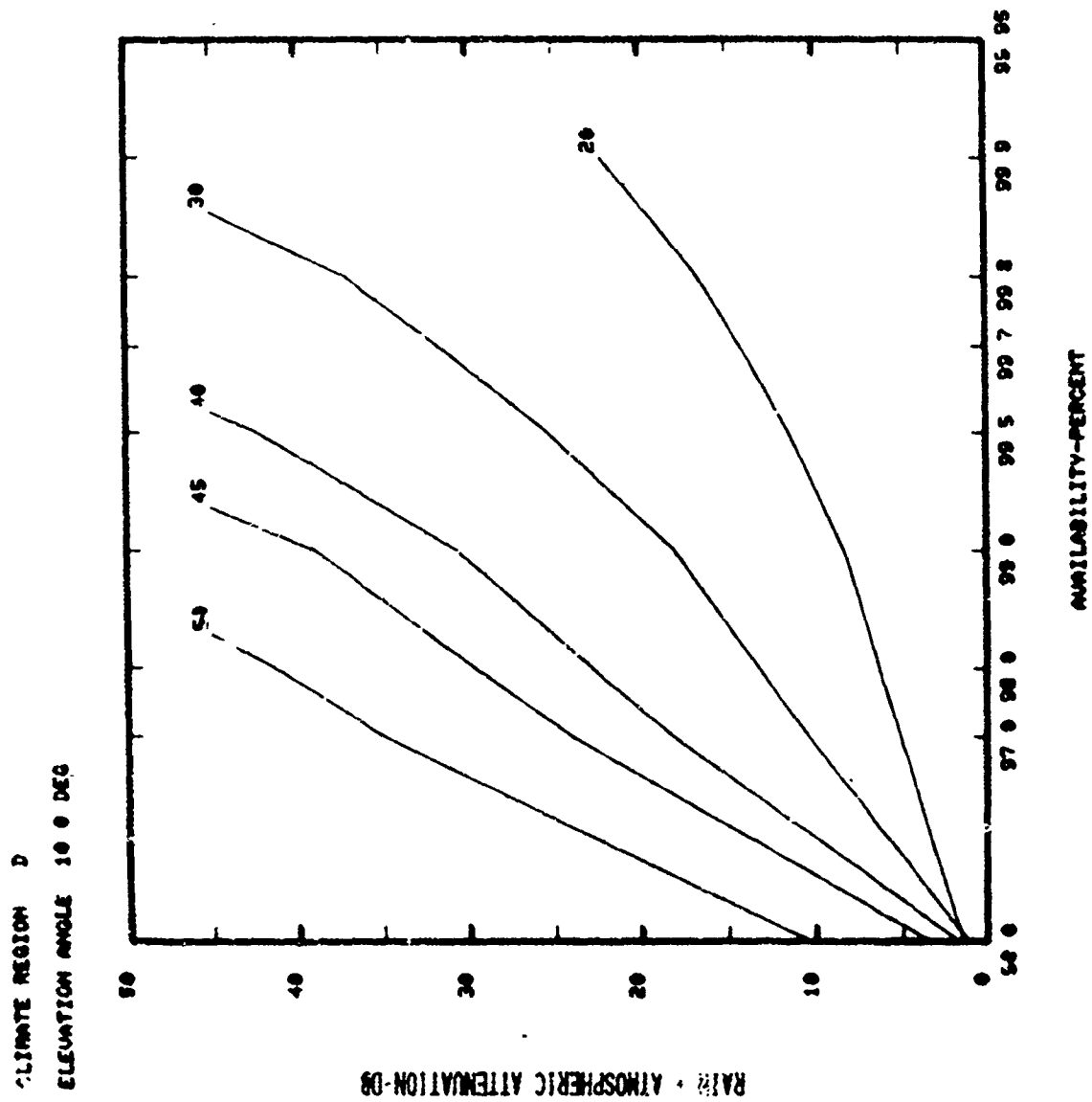


Fig. A-10

CLIMATE REGION D
ELEVATION ANGLE 30 ° DEG

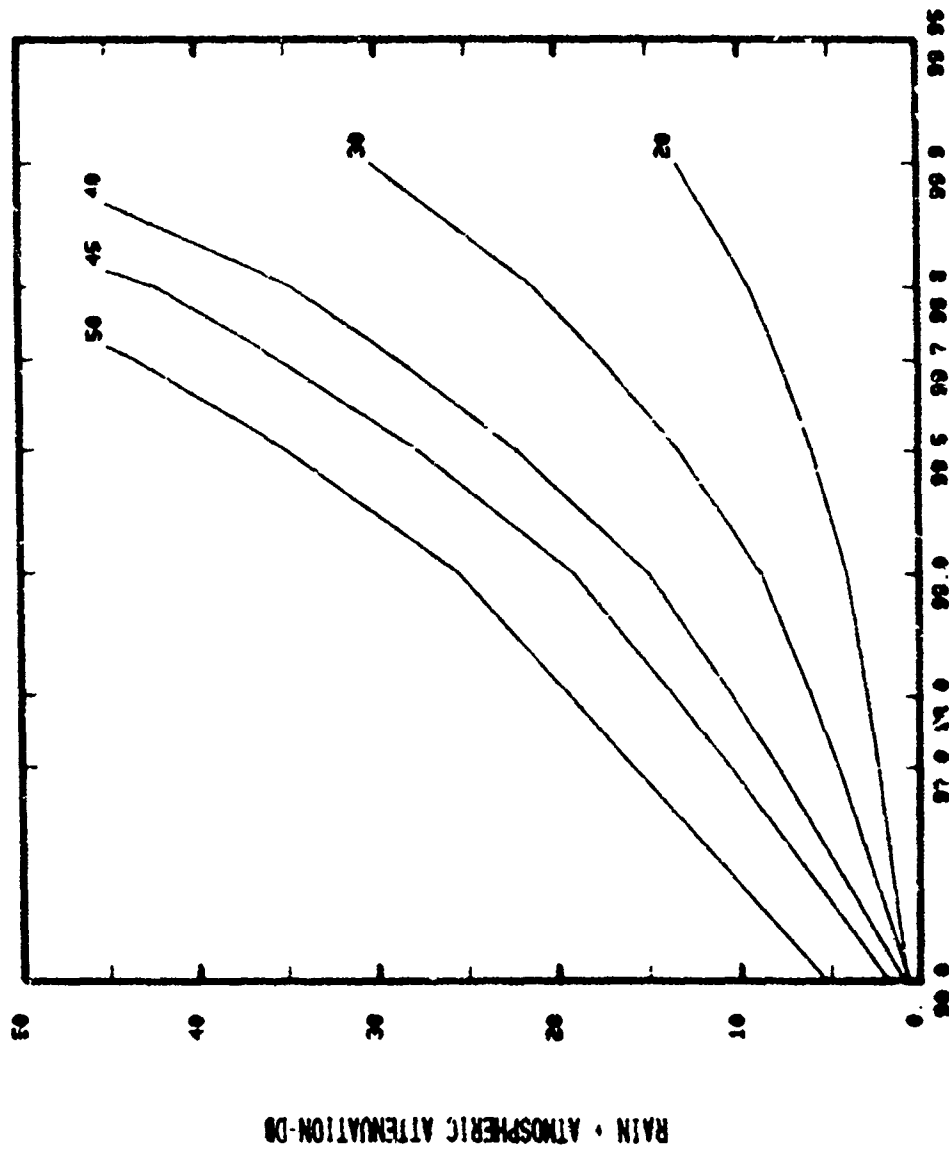


Fig. A-11

CLIMATE REGION D
ELEVATION ANGLE 50.0 DEG

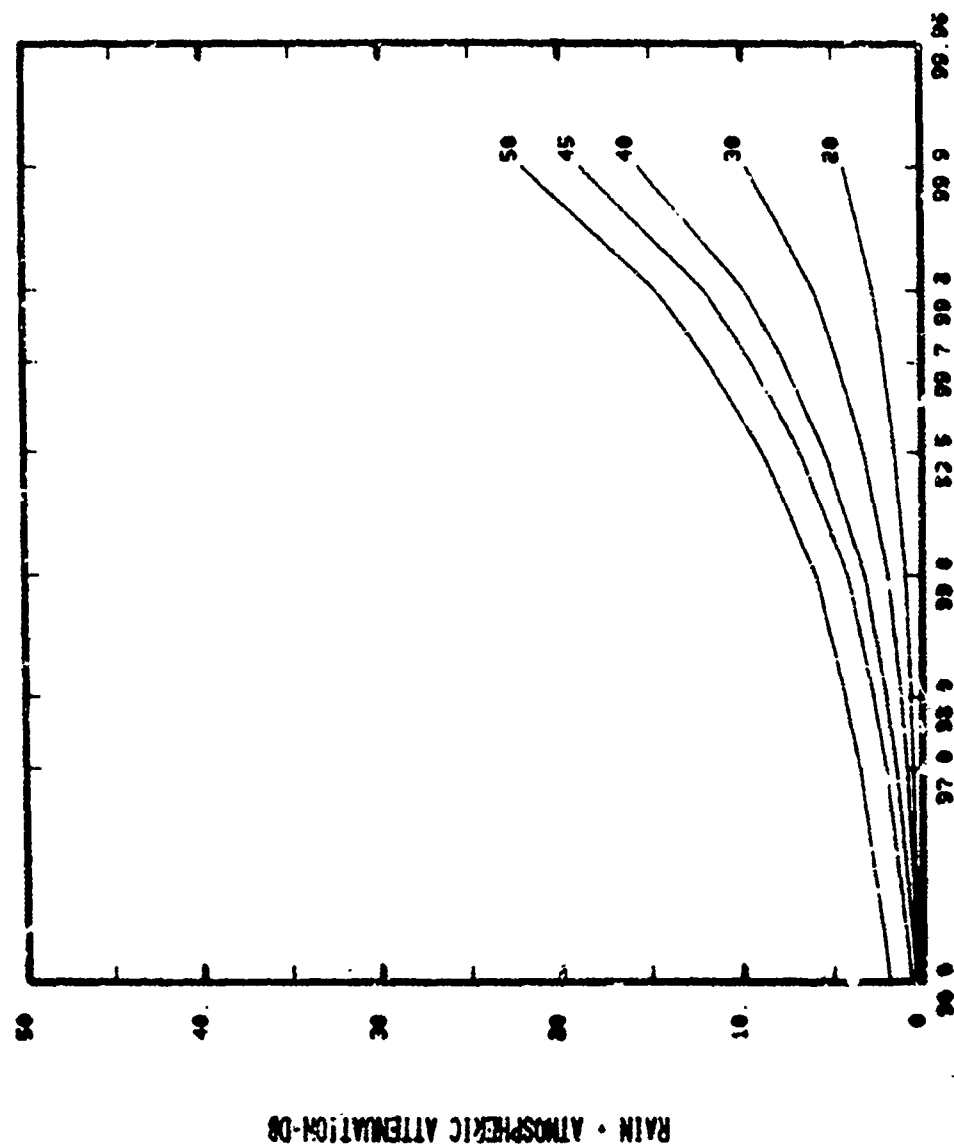
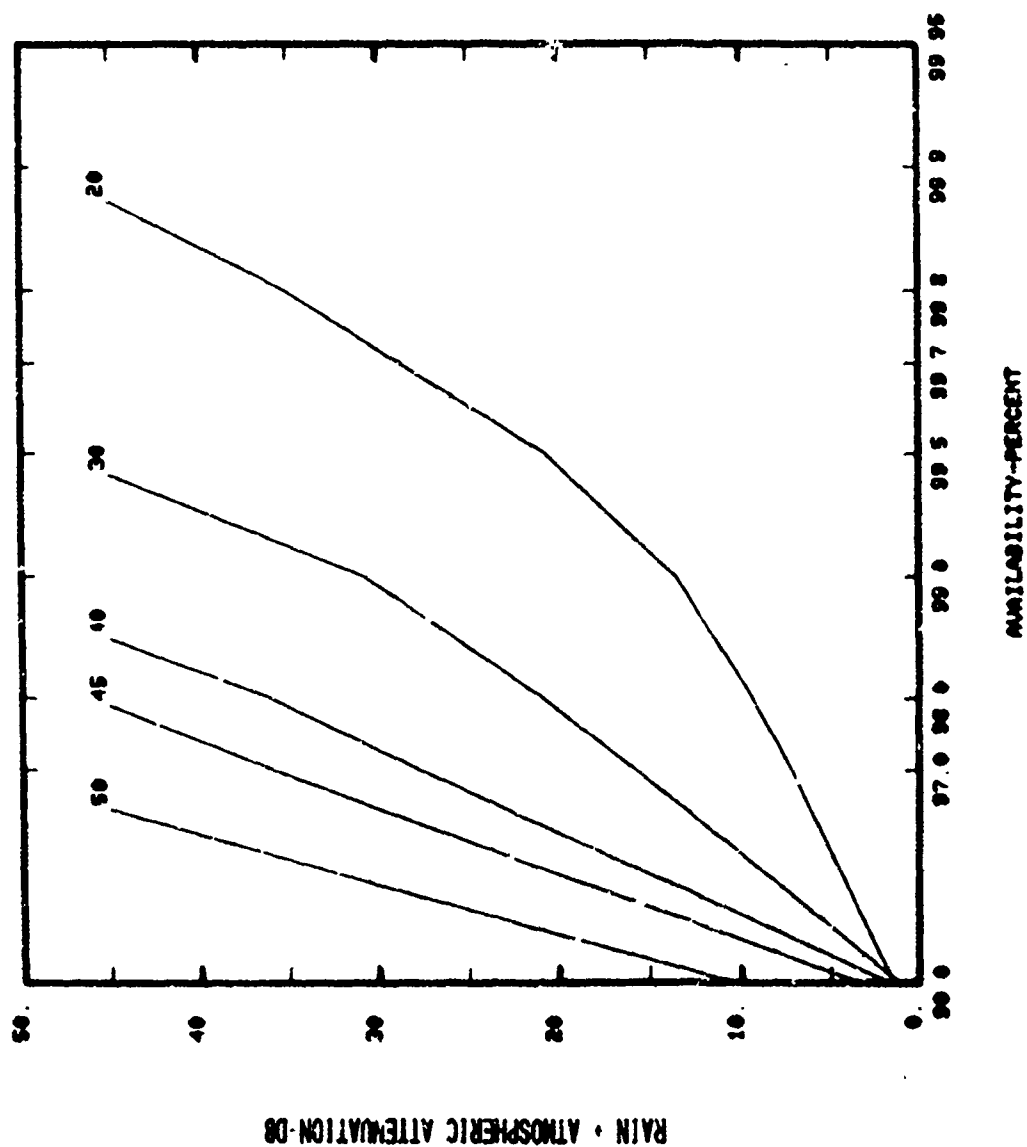
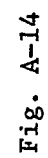


Fig. A-12

CLIMATE REGION E
ELEVATION ANGLE 10.0 DEG





CLIMATE REGION E
ELEVATION ANGLE 90.0 DEG

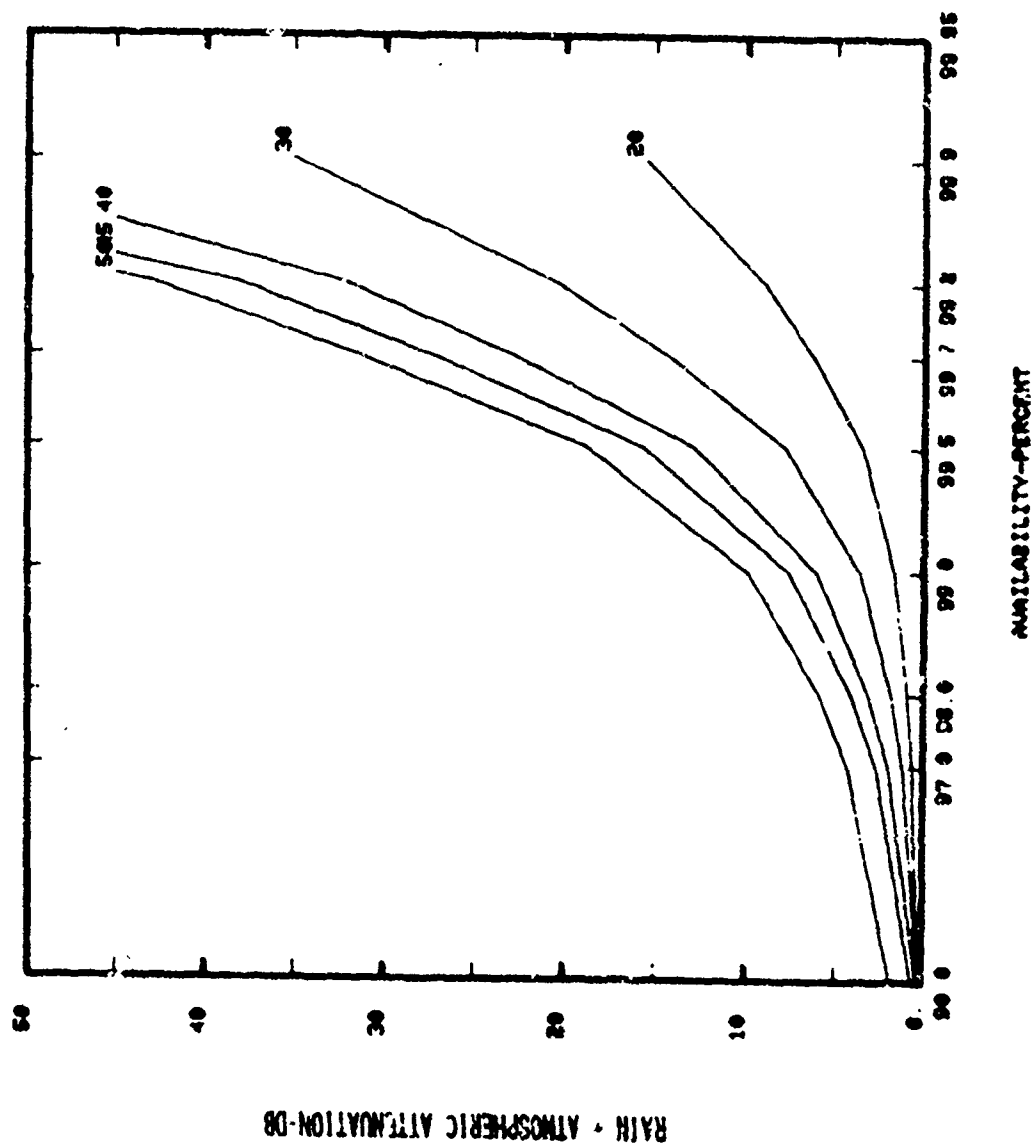


Fig. A-15

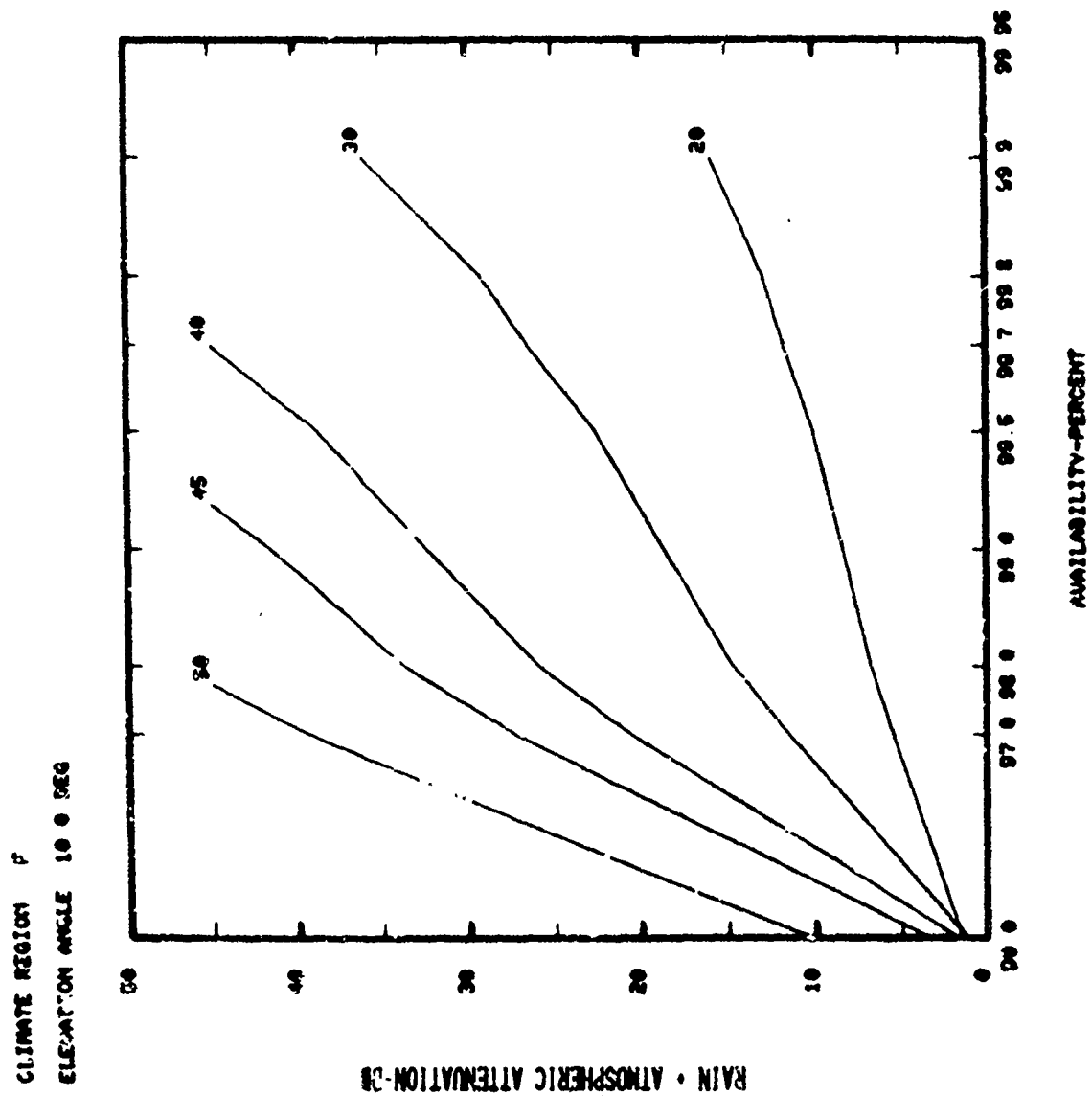


Fig. A-16

CLIMATE REGION F
ELEVATION ANGLE 20.0 DEG

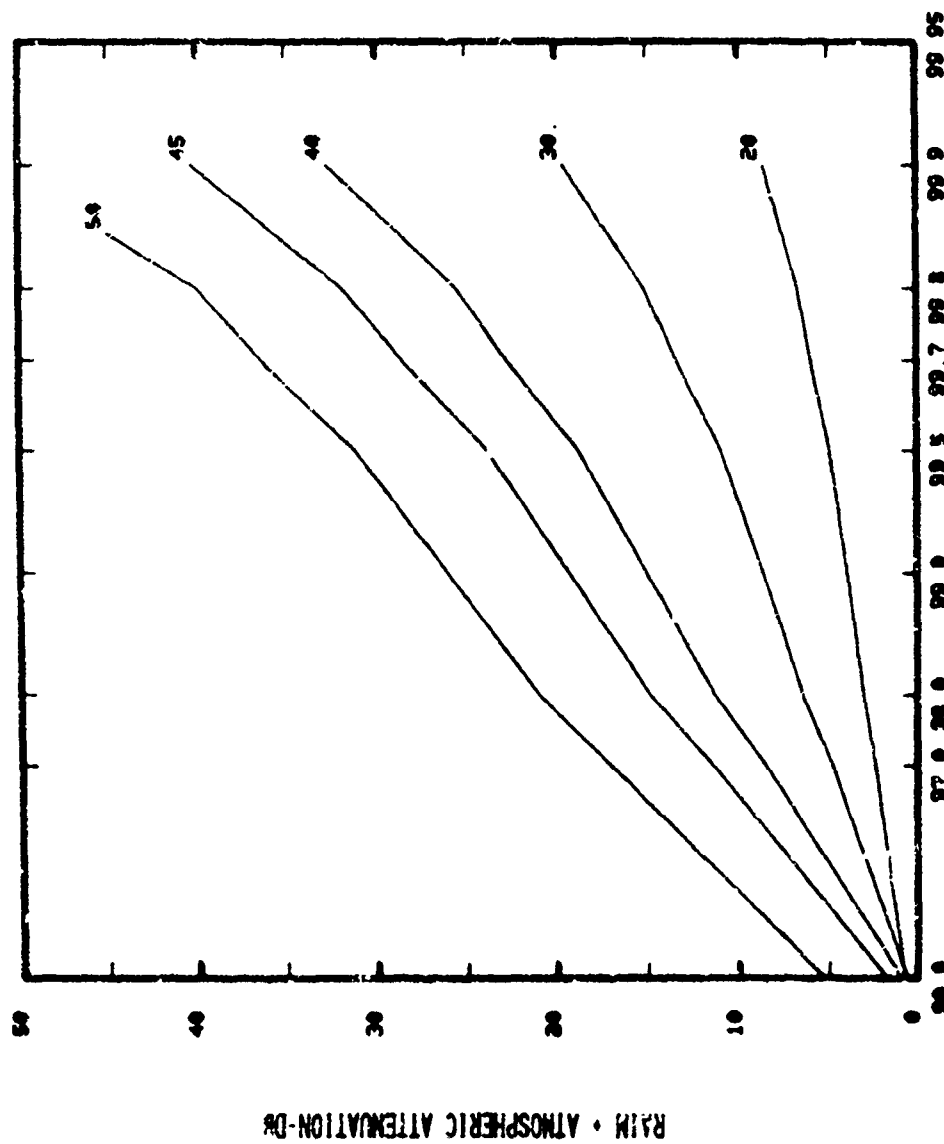


Fig. A-17

CLIMATE REGION F
ELEVATION ANGLE 90 0 DEG

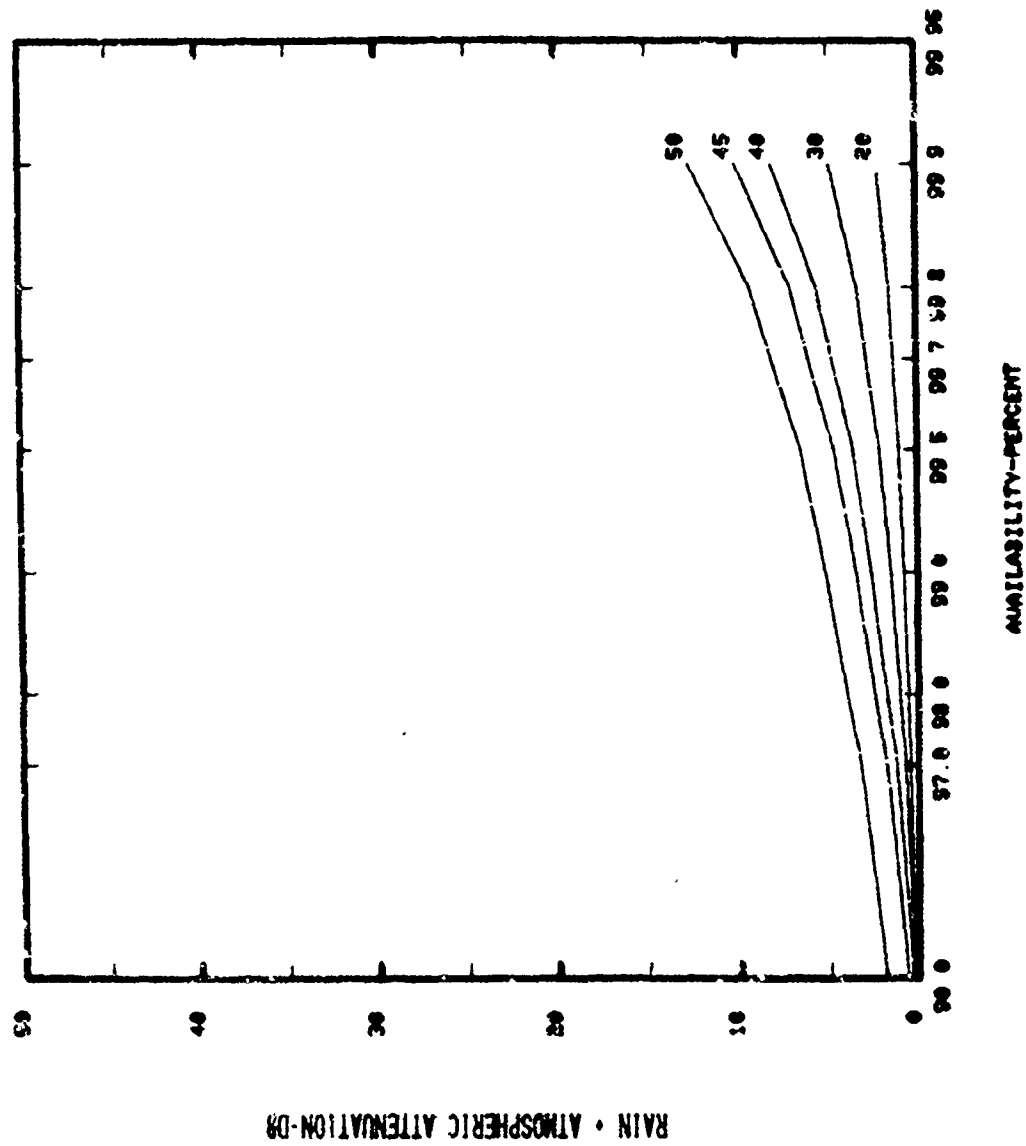


Fig. A-18

CLIMATE REGION 2
ELEVATION ANGLE 1.3 DEG

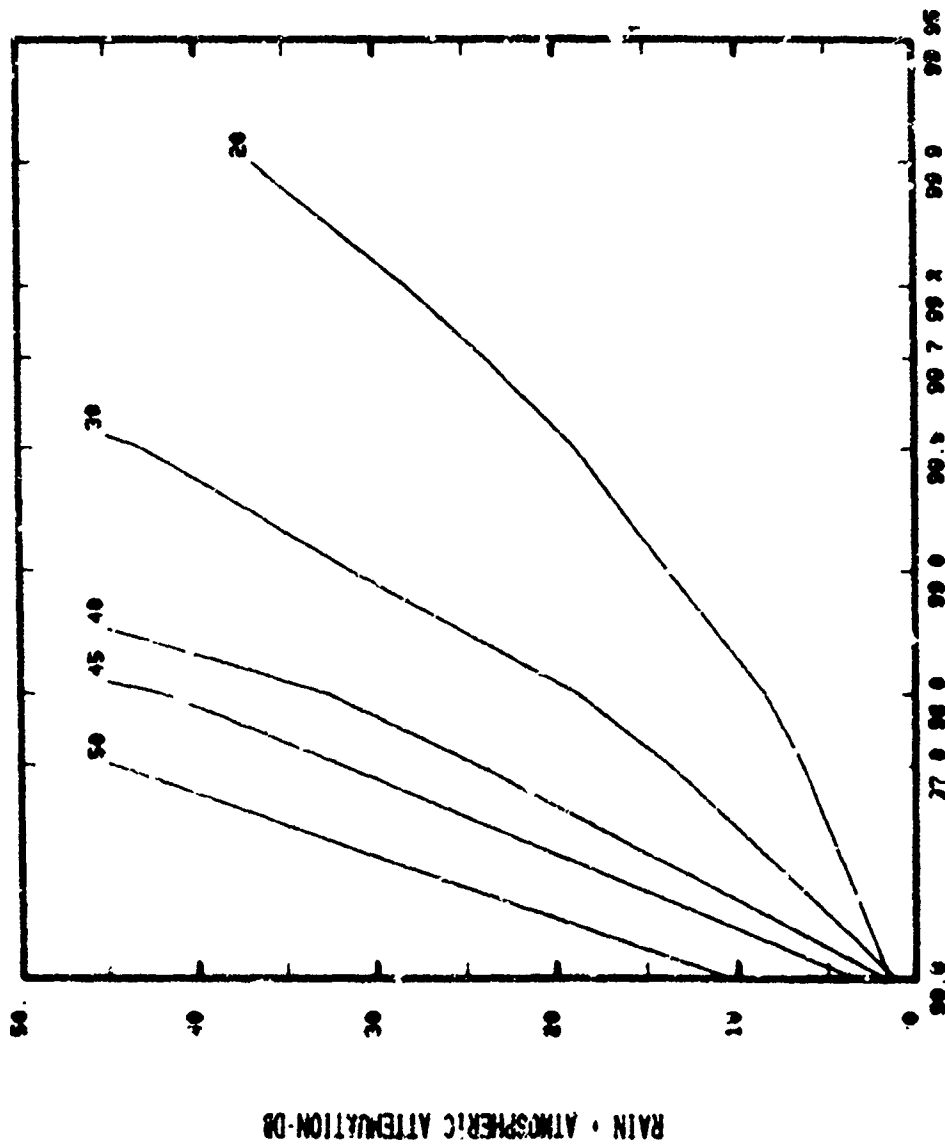


Fig. A-19

CLIMATE REGION: 0
ELEVATION ANGLE: 20.0 DEG

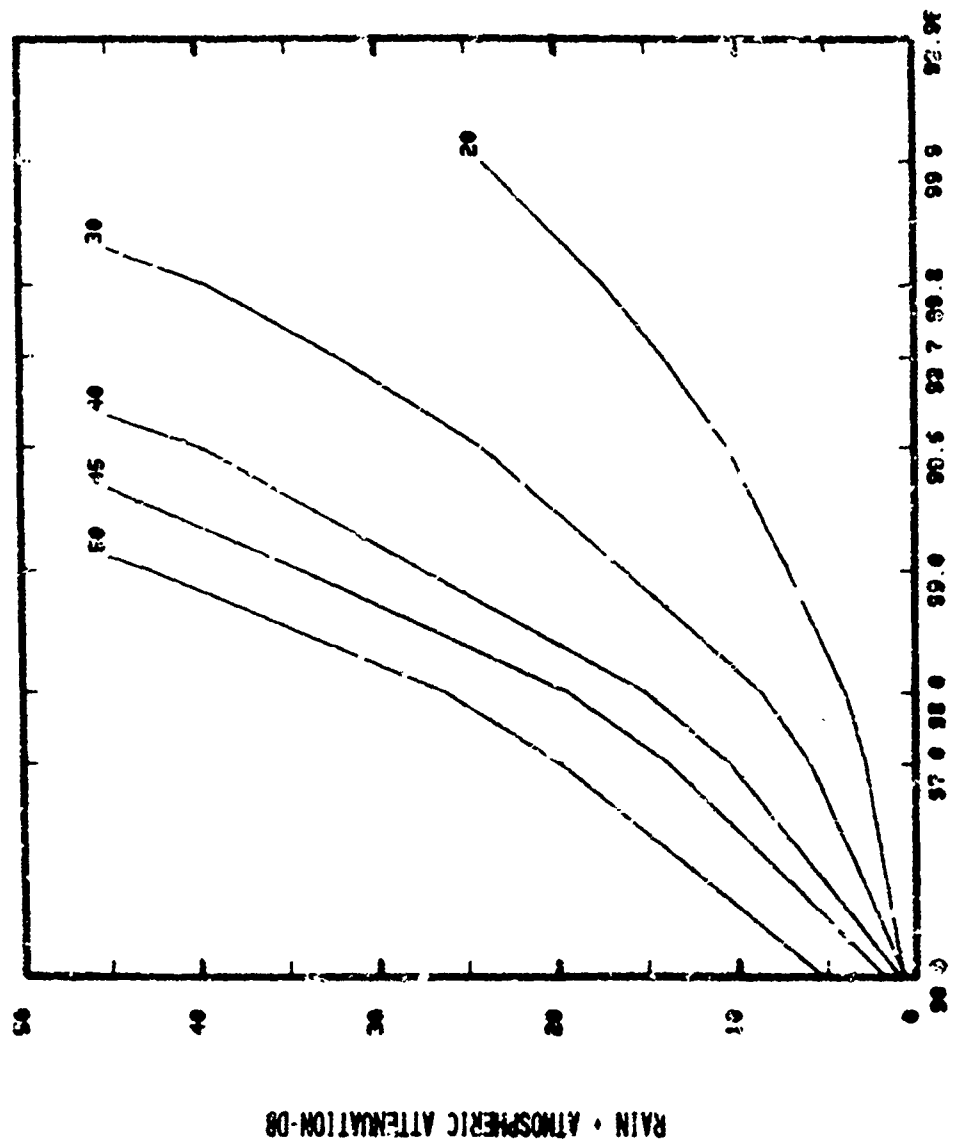
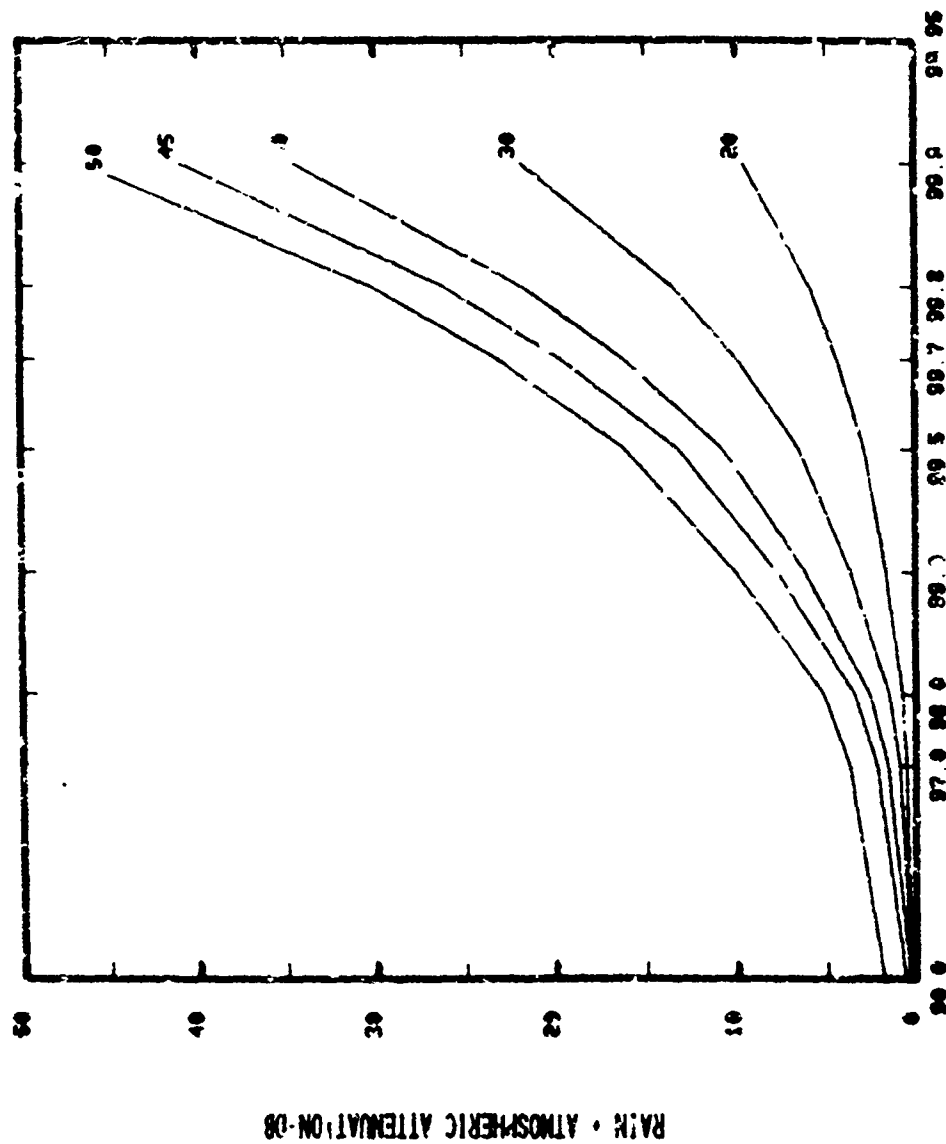


Fig. A-20

CLIMATE REGION 0
ELEVATION ANGLE 90.0 DEG.



AVAILABILITY-PERCENT

Fig. A-21

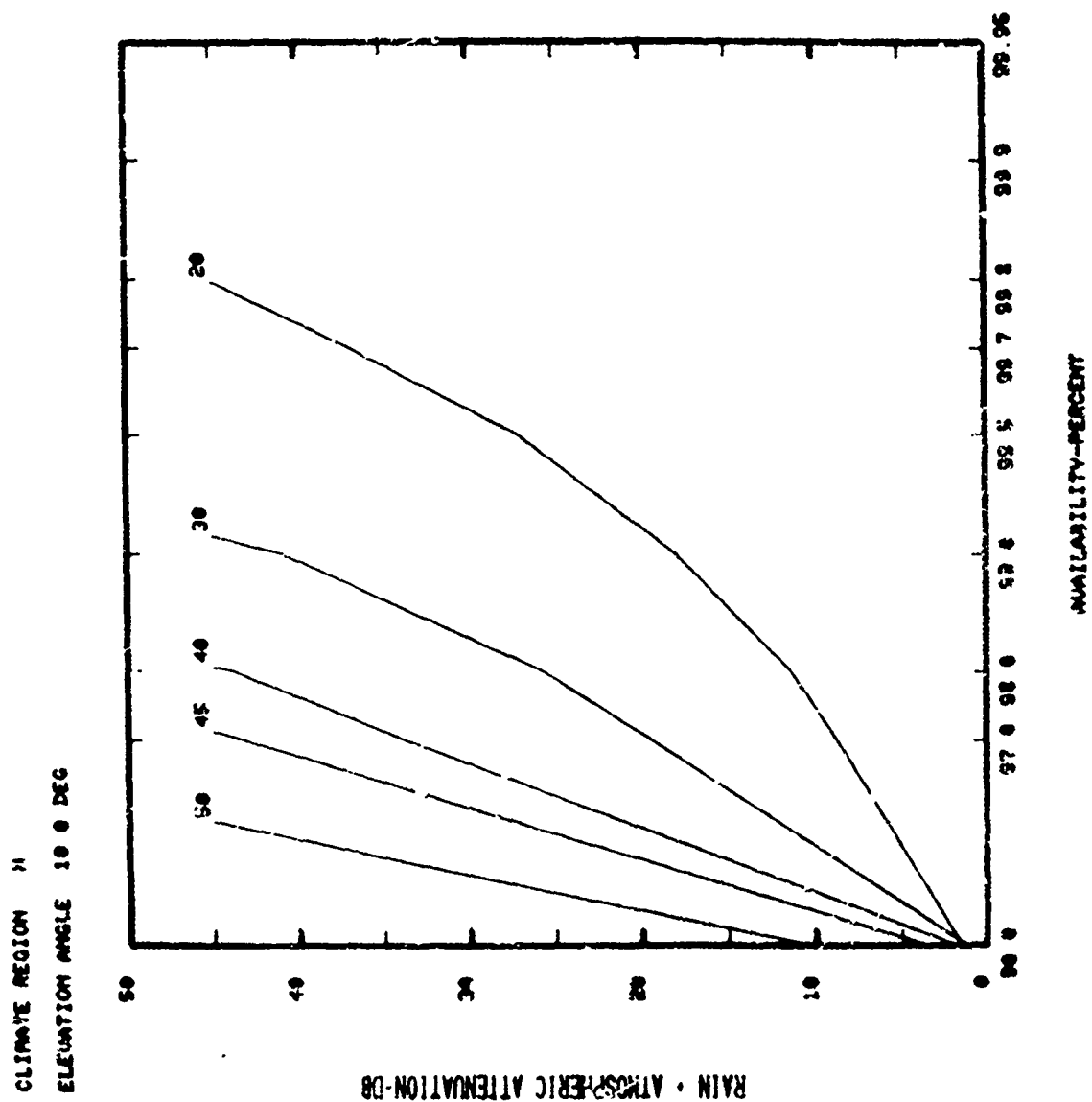
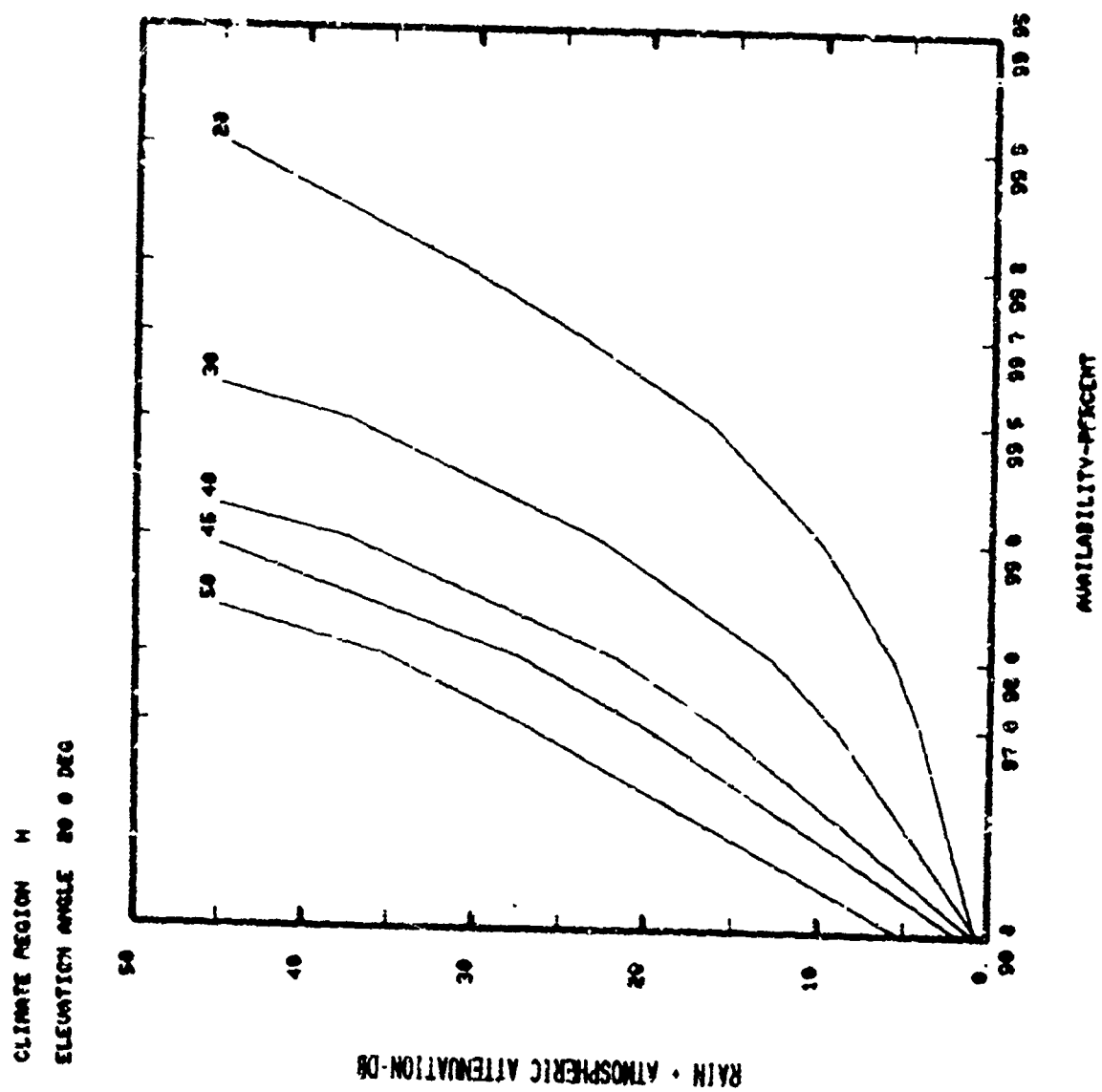


Fig. A-22



CLIMATE REGION H
ELEVATION ANGLE 90.0 DEG

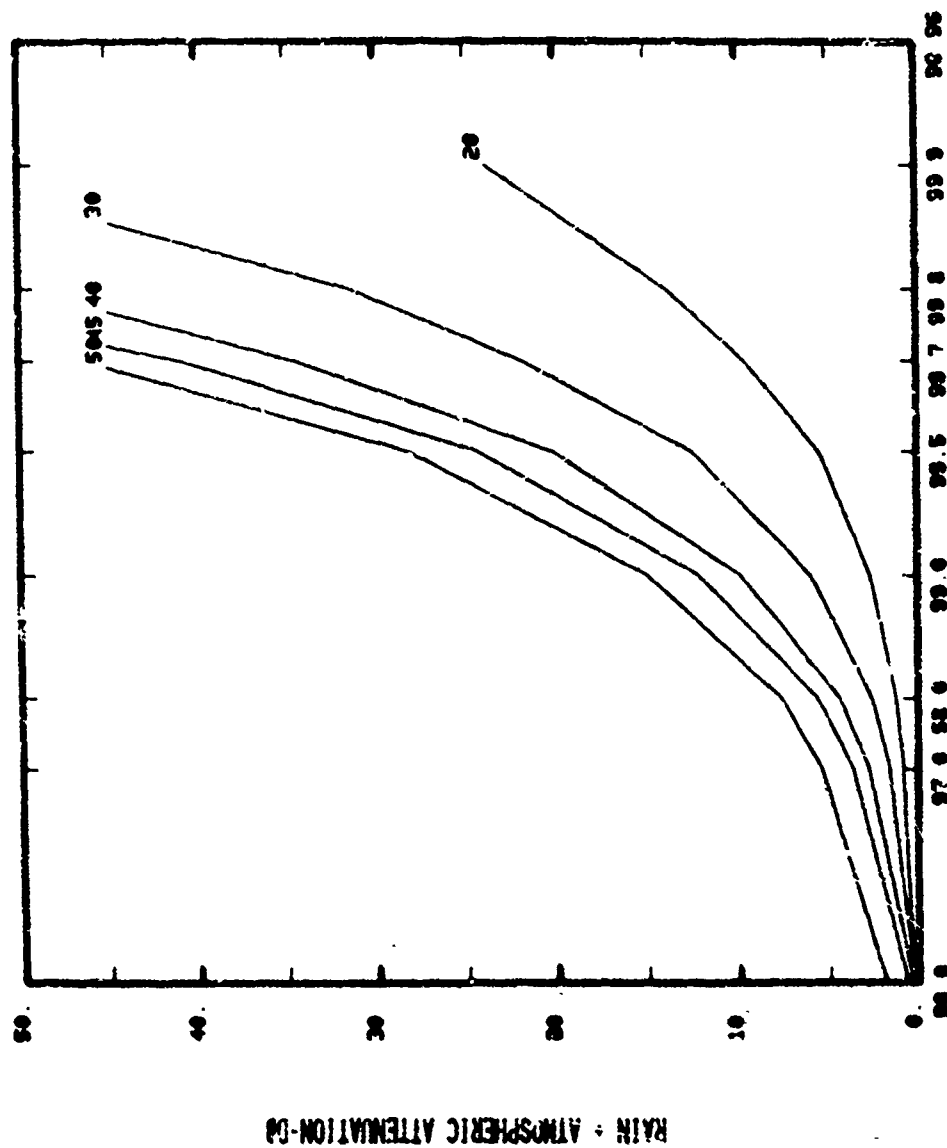


Fig. A-24

CLIMATE REGION A
 FREQUENCY 30.0 GHz

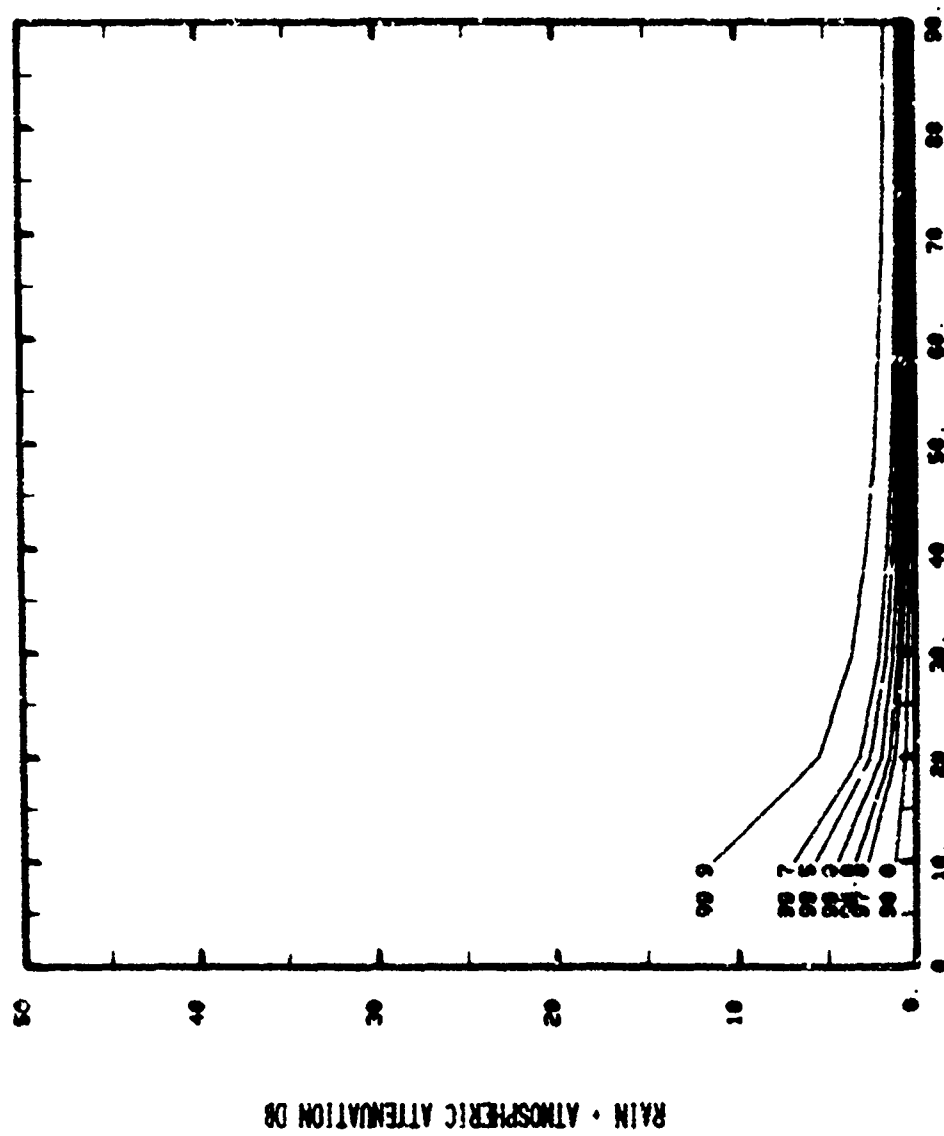
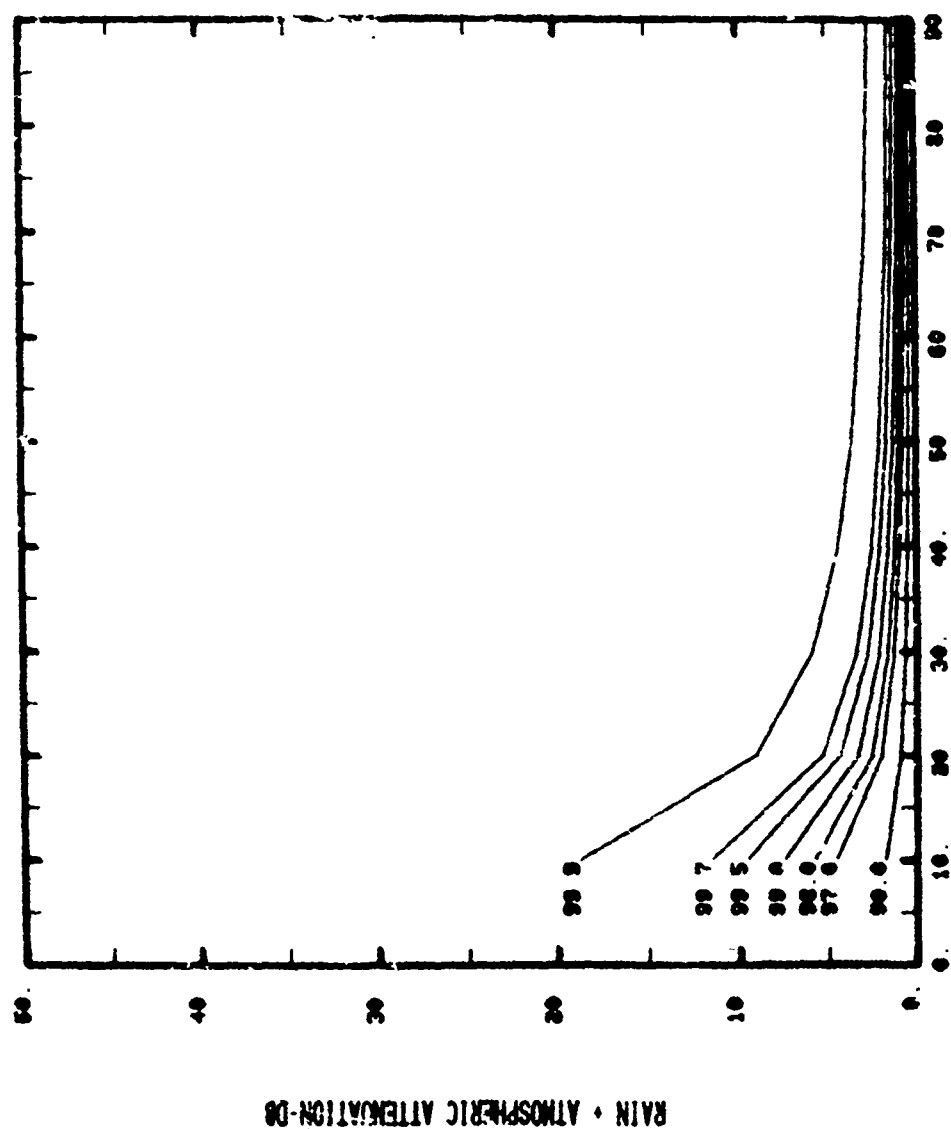


Fig. A-26

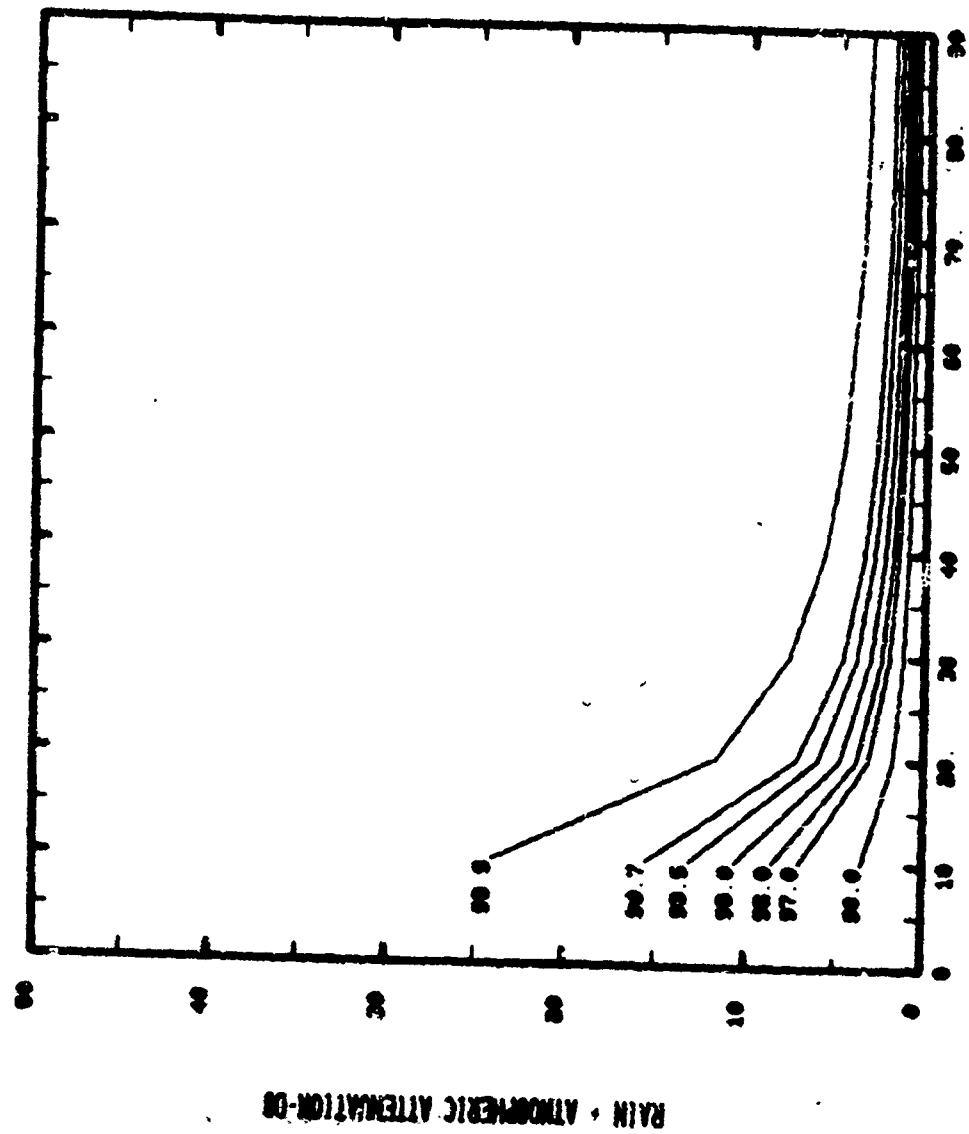
CLIMATE REGION A
FREQUENCY 40.0 GHz



ELEVATION ANGLE-DEG

Fig. A-27

CLIMATE REGION A
FREQUENCY 45.0 GIG



ELEVATION ANGLE DEGREES

Fig. A-28

CLIMATE REGION 3
 FREQUENCY 30.0 MHz

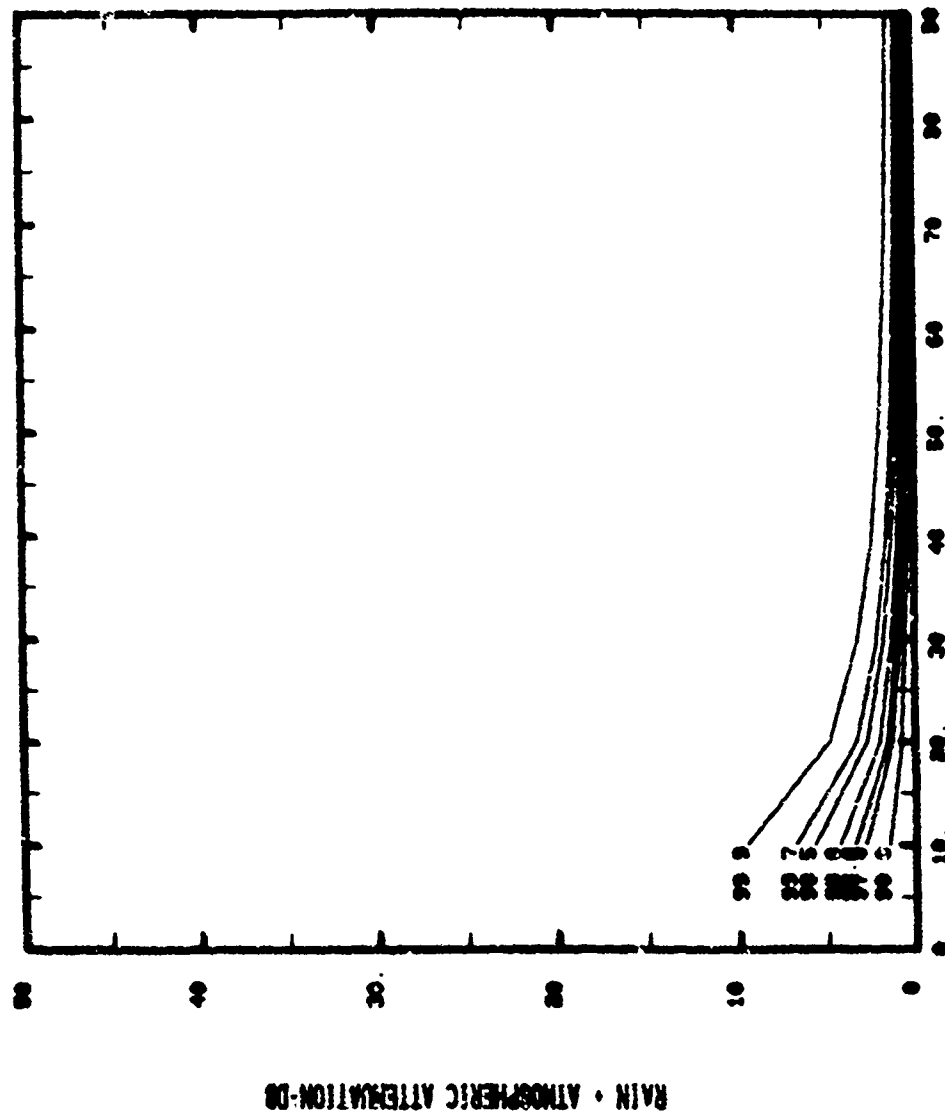
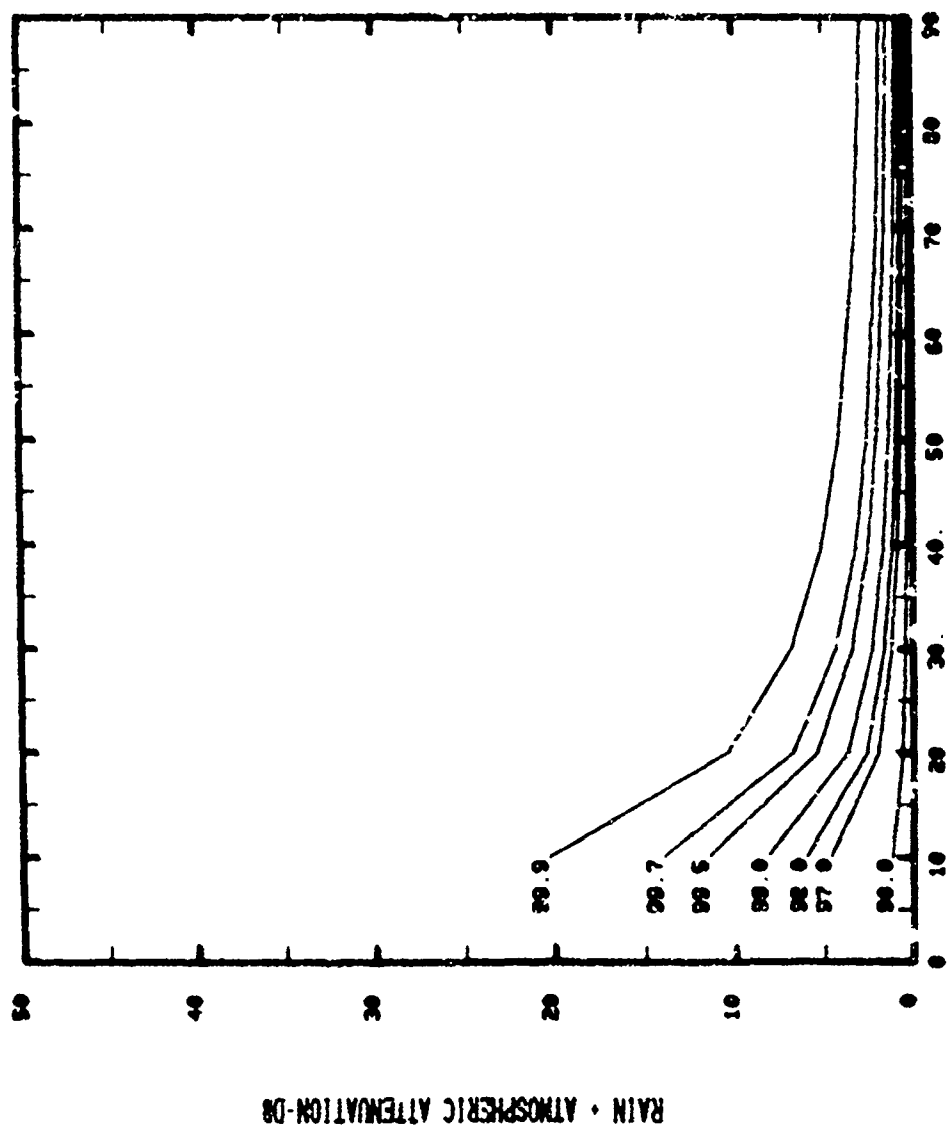


Fig. A-29

CLIMATE REGION 3
 FREQUENCY 30.0 GHz



ELEVATION ANGLE-DEG

Fig. A-30

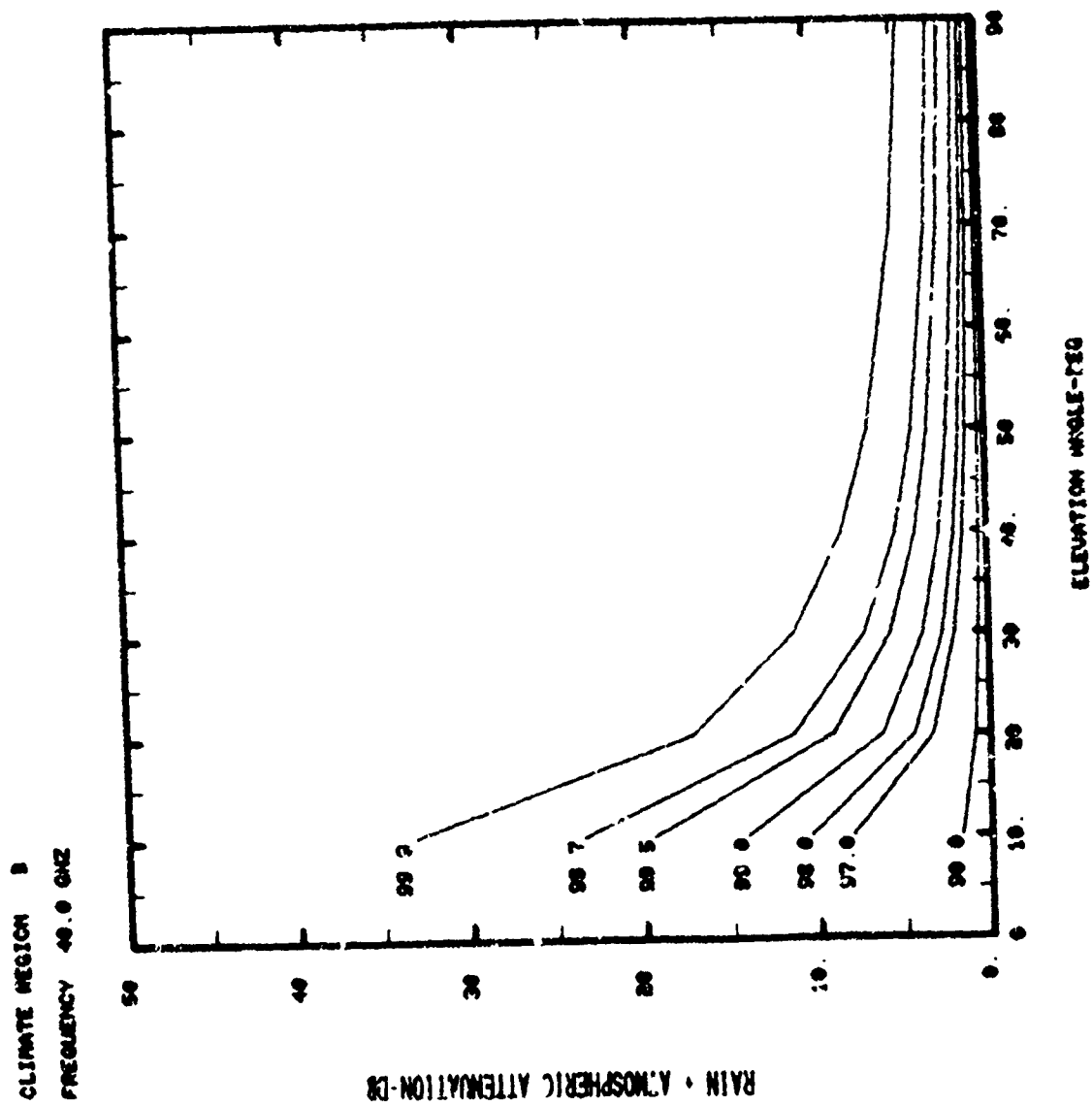


Fig. A-31

CLIMATE REGION 3
 FREQUENCY 45.0 GHz

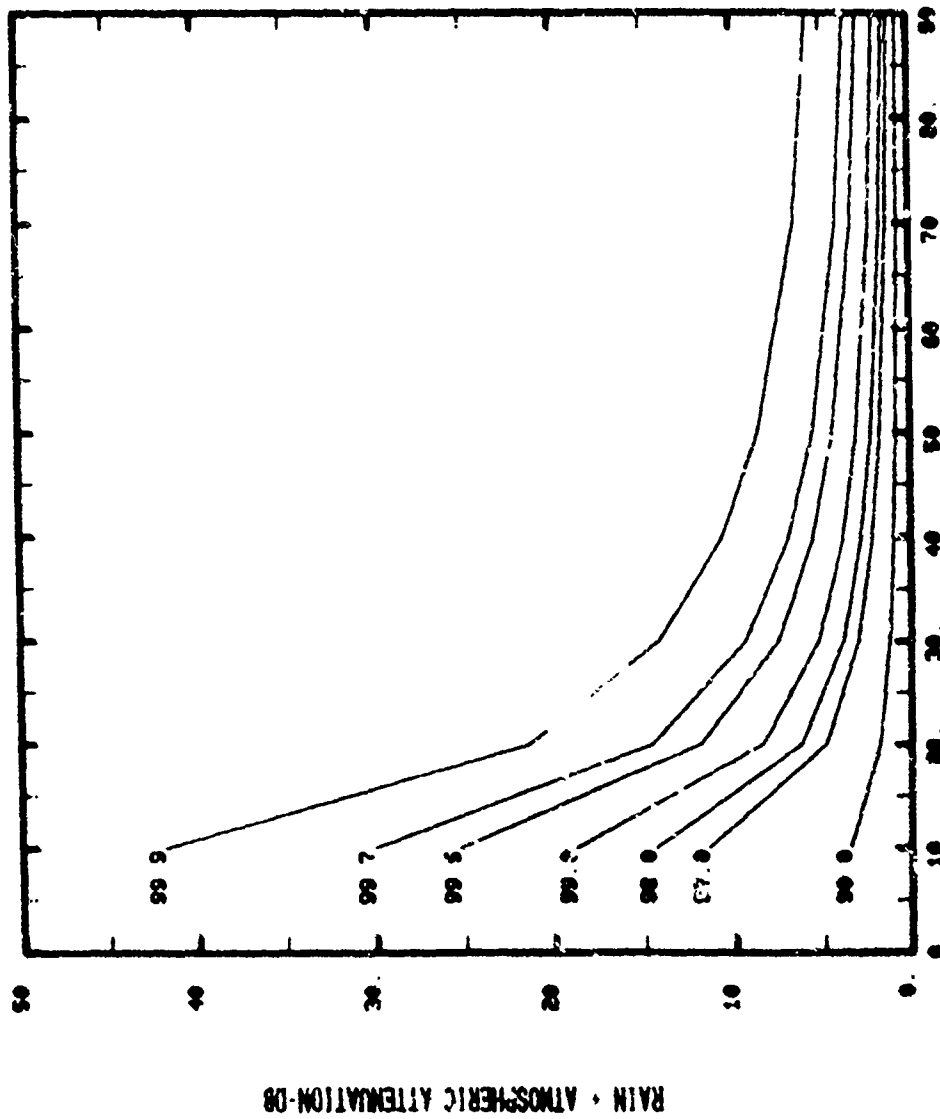


Fig. A-32

CLIMATE REGION C
FREQUENCY 30.0 GHz

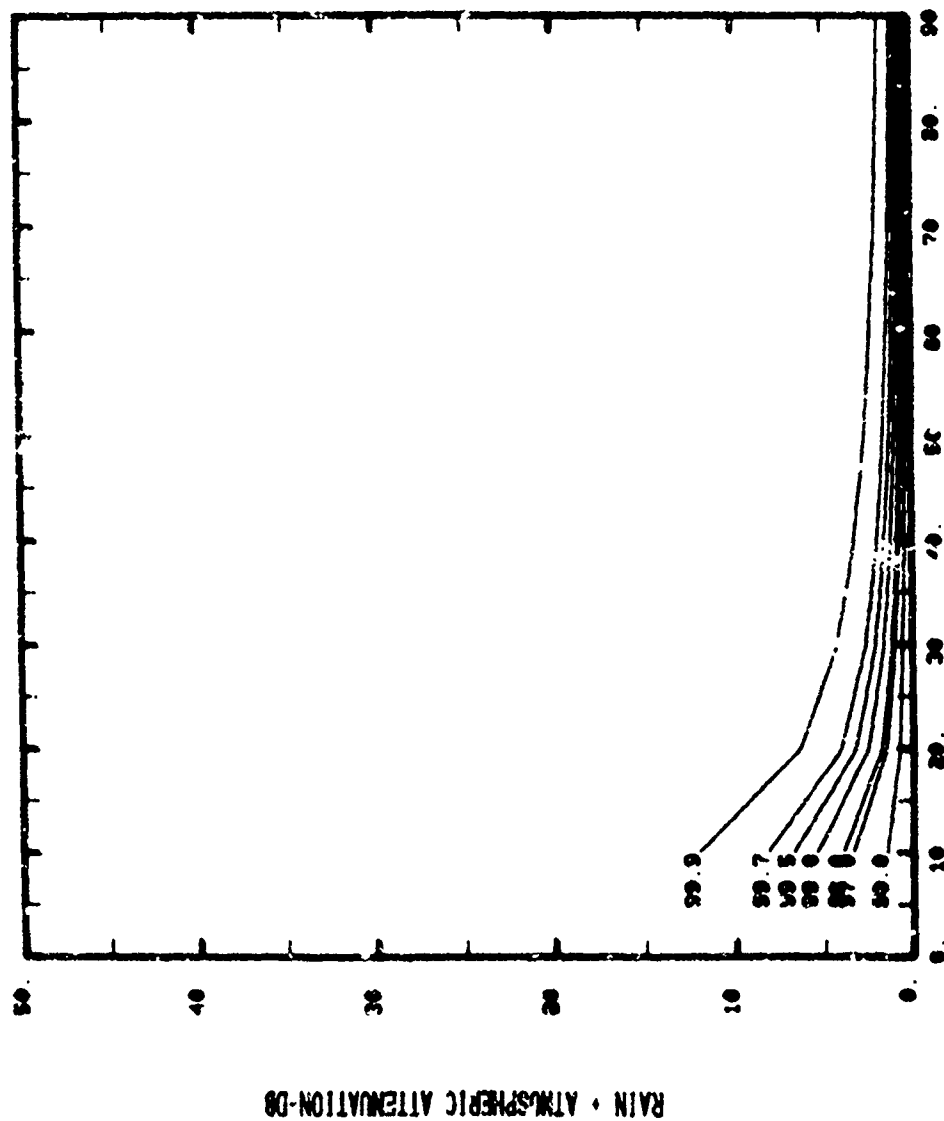


Fig. A-33

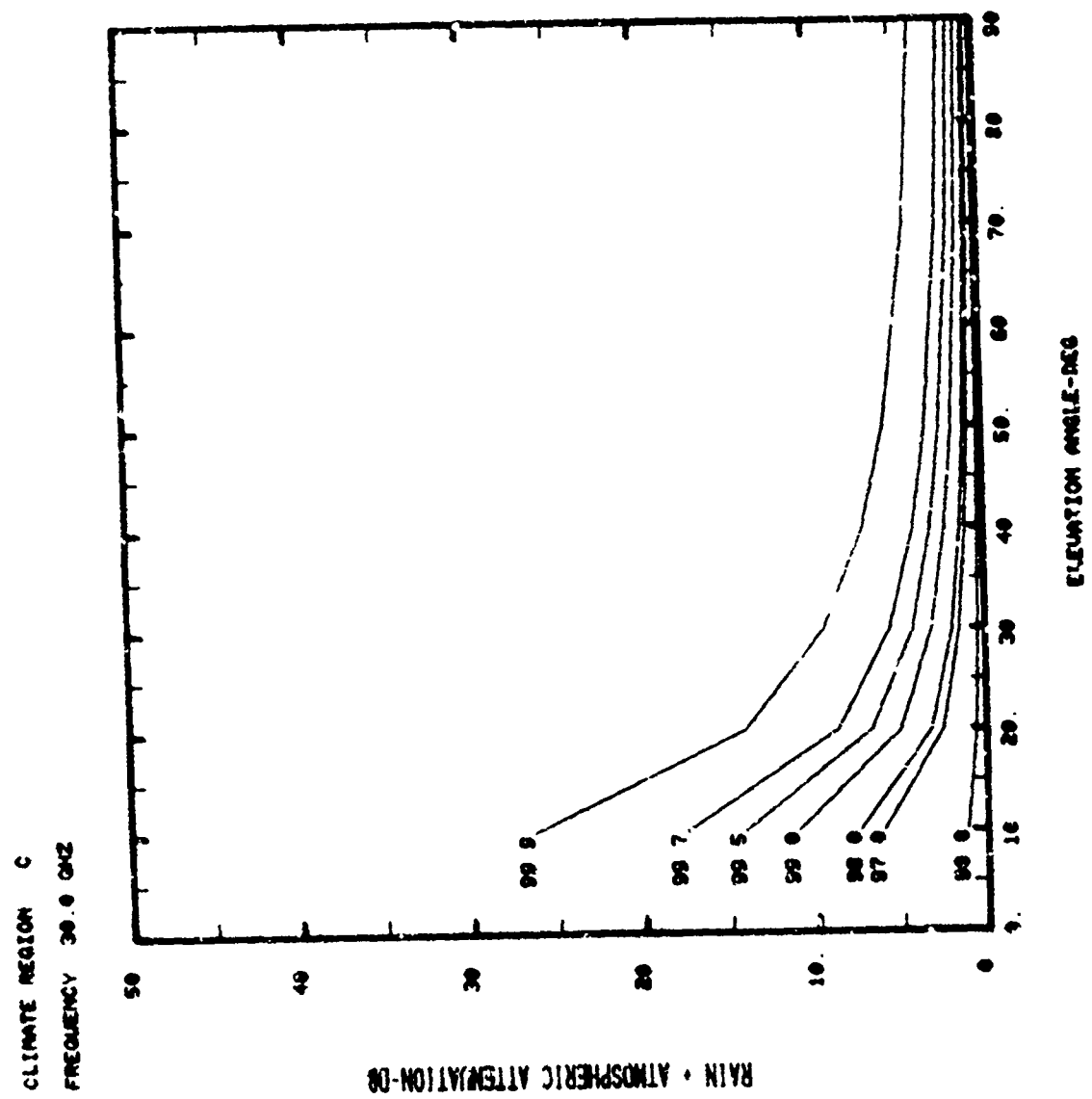


Fig. A-34

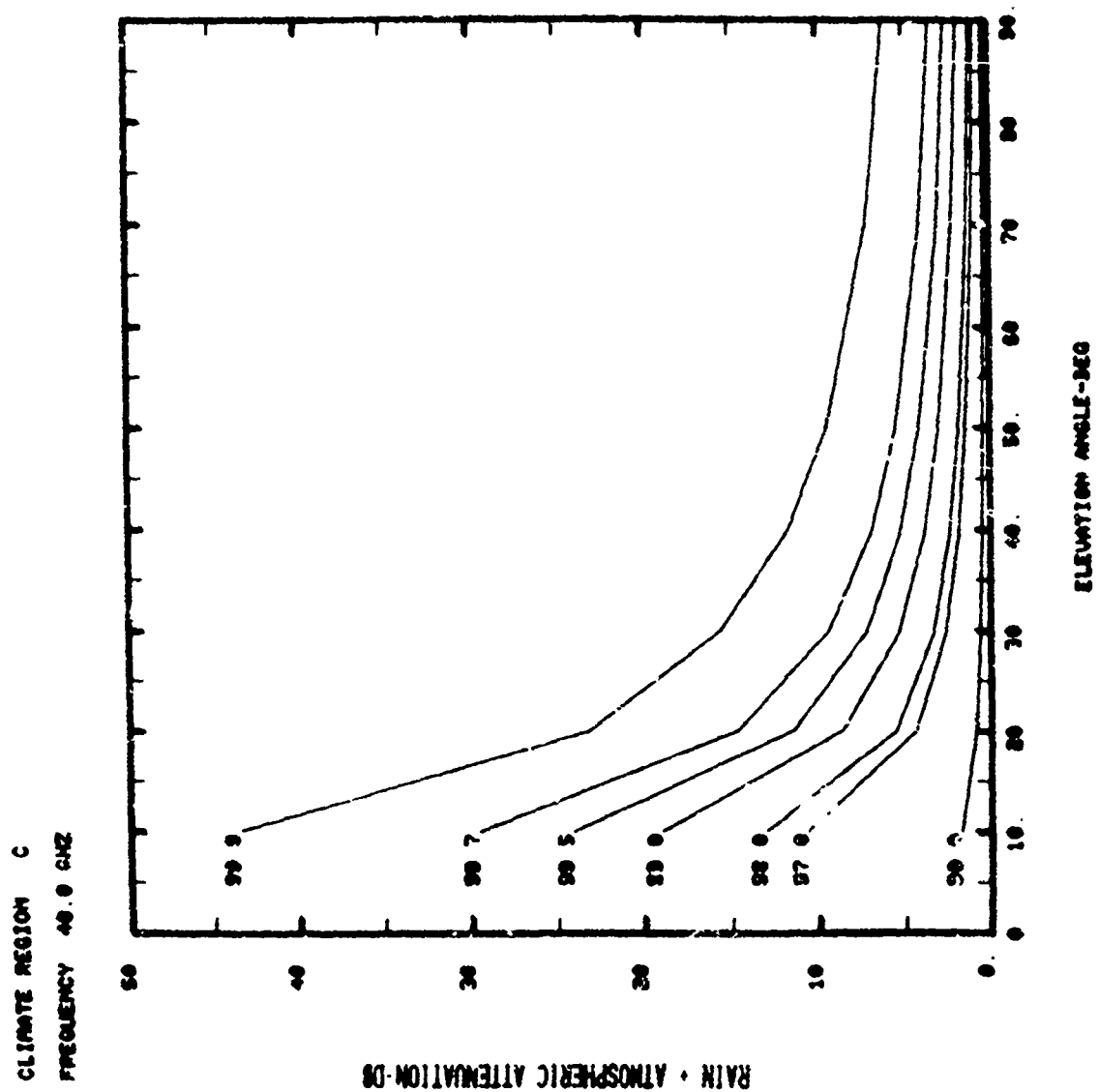


Fig. A-35

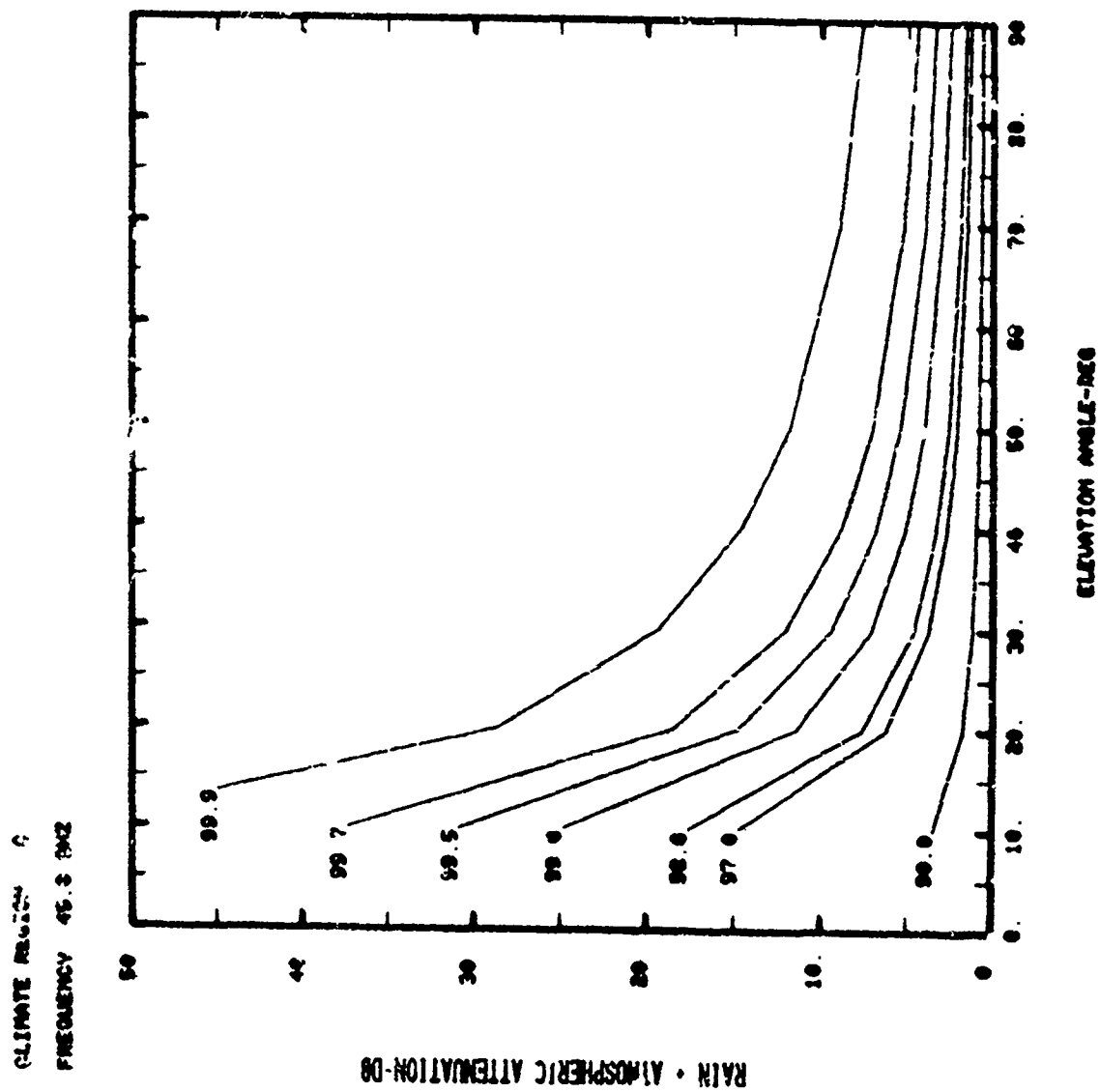


Fig. A-36

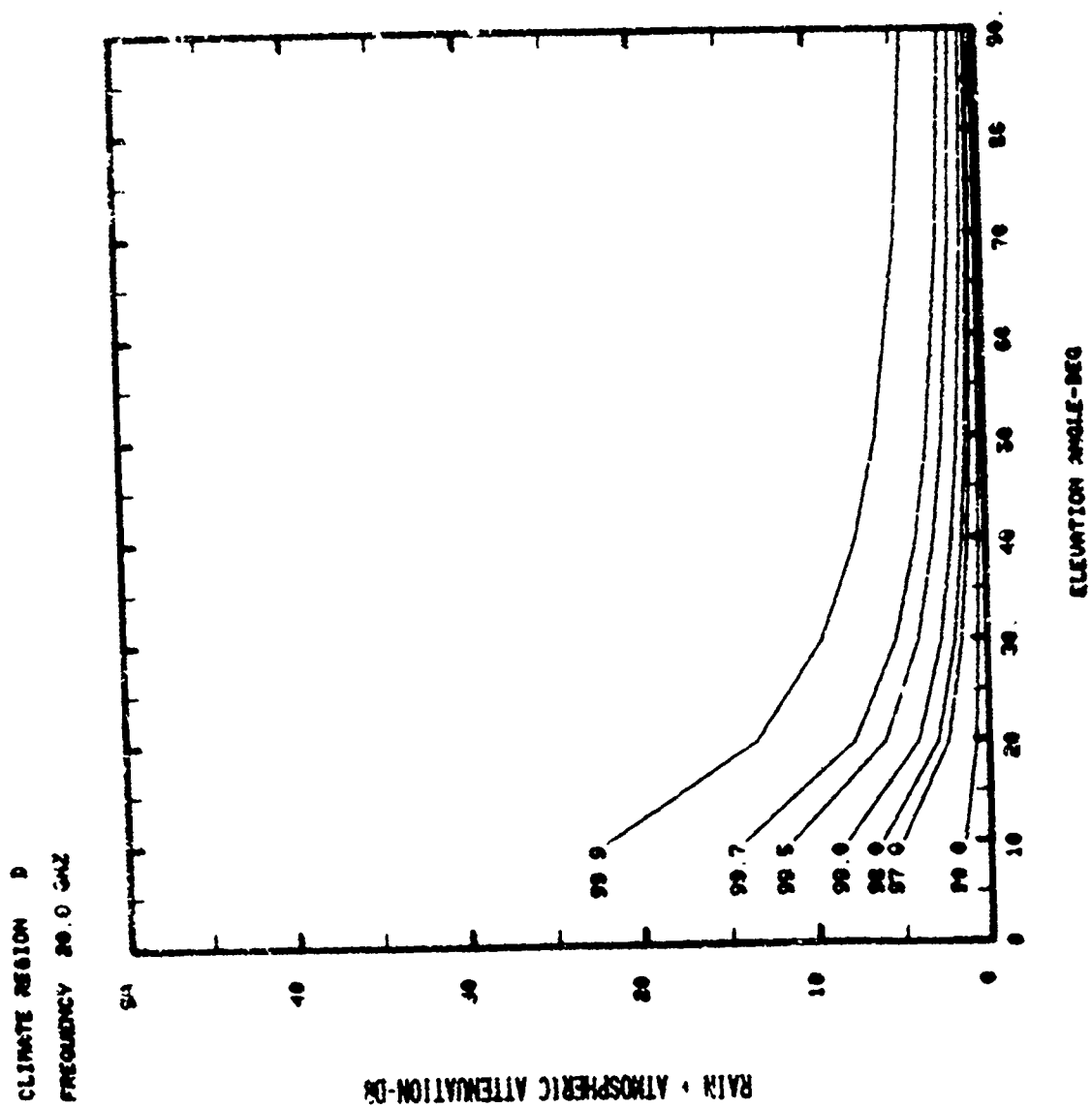
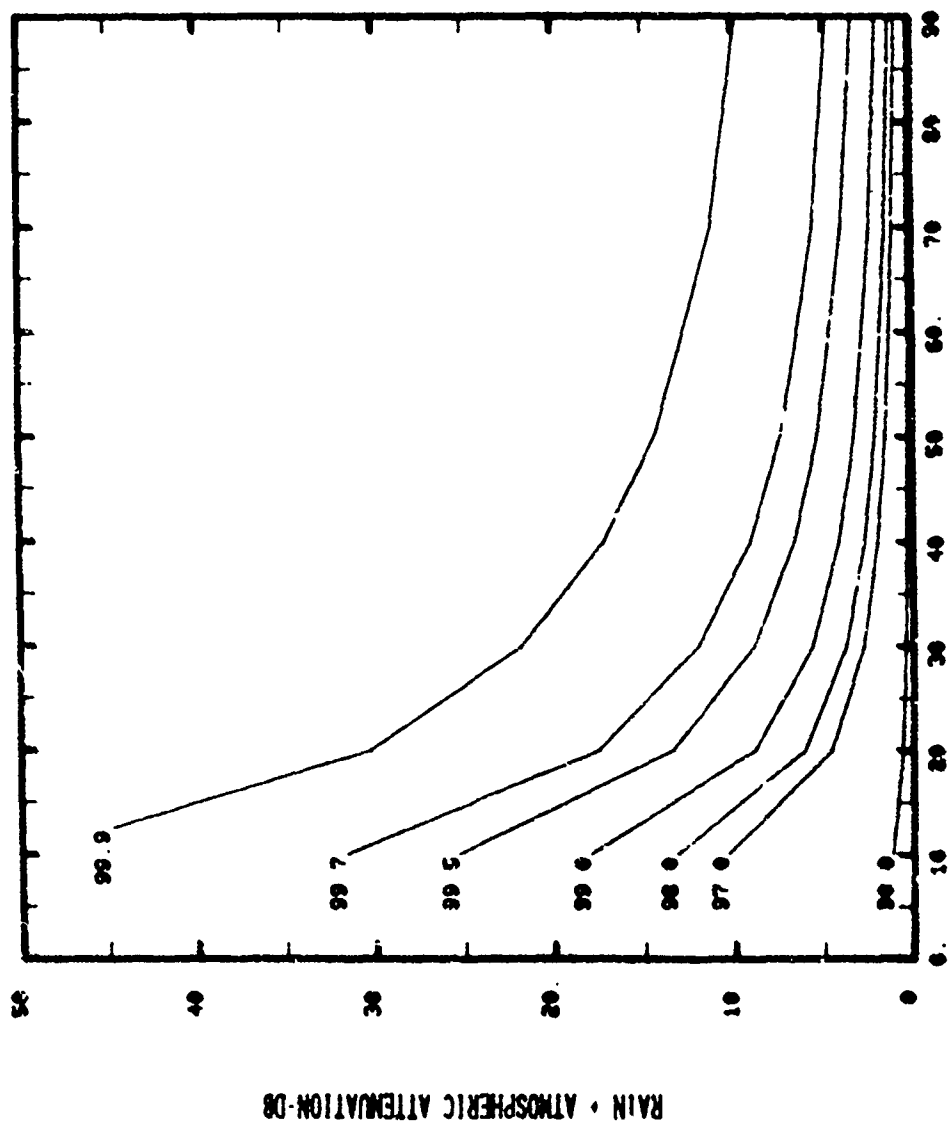


Fig. A-37

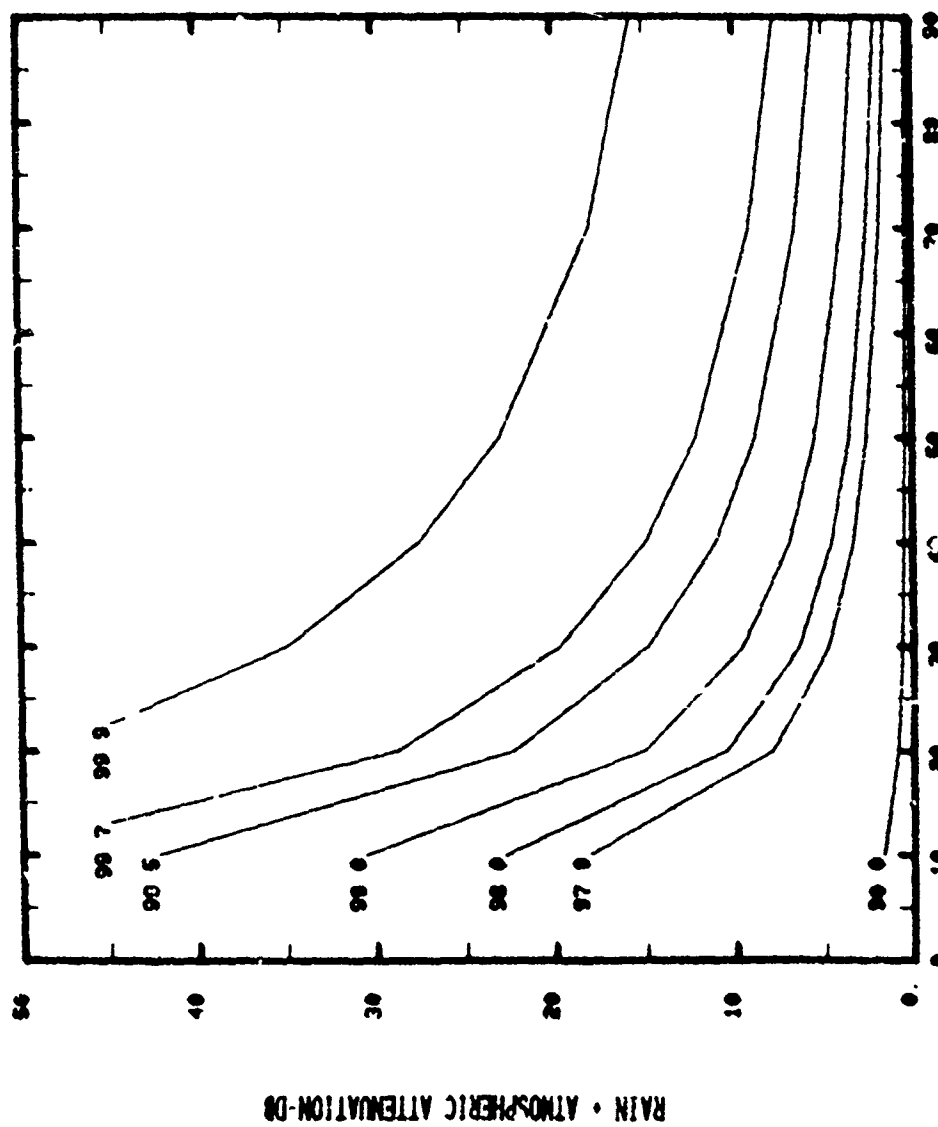
CLIMATE REGION D
FREQUENCY 30.0 GHz



ELEVATION ANGLE-DEG

Fig. A-38

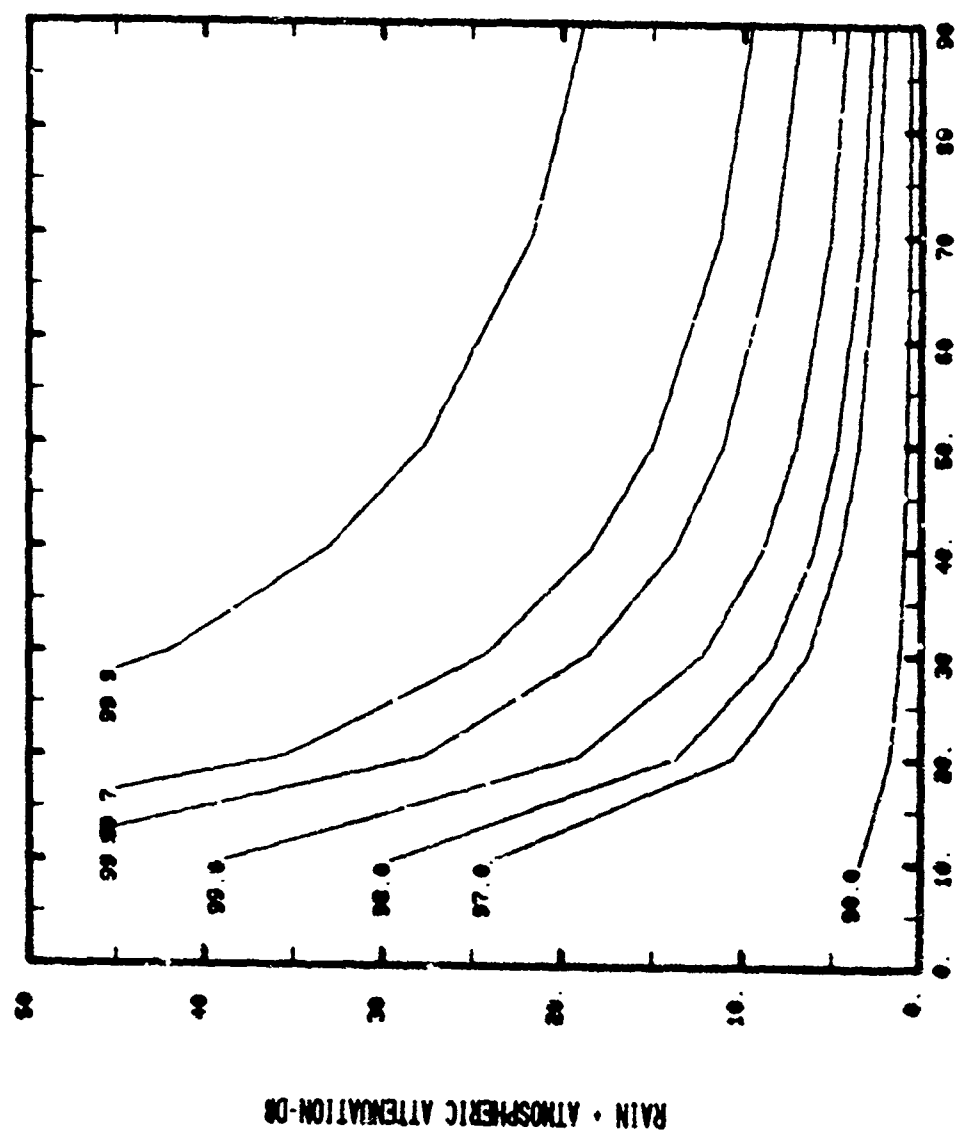
CLIMATE REGION D
FREQUENCY 40.0 GHz



ELEVATION ANGLE-DEG

Fig. A-39

CLIMATE REGION 2
 FREQUENCY 45.0 GHz



ELEVATION ANGLE-DEG

Fig. A-40

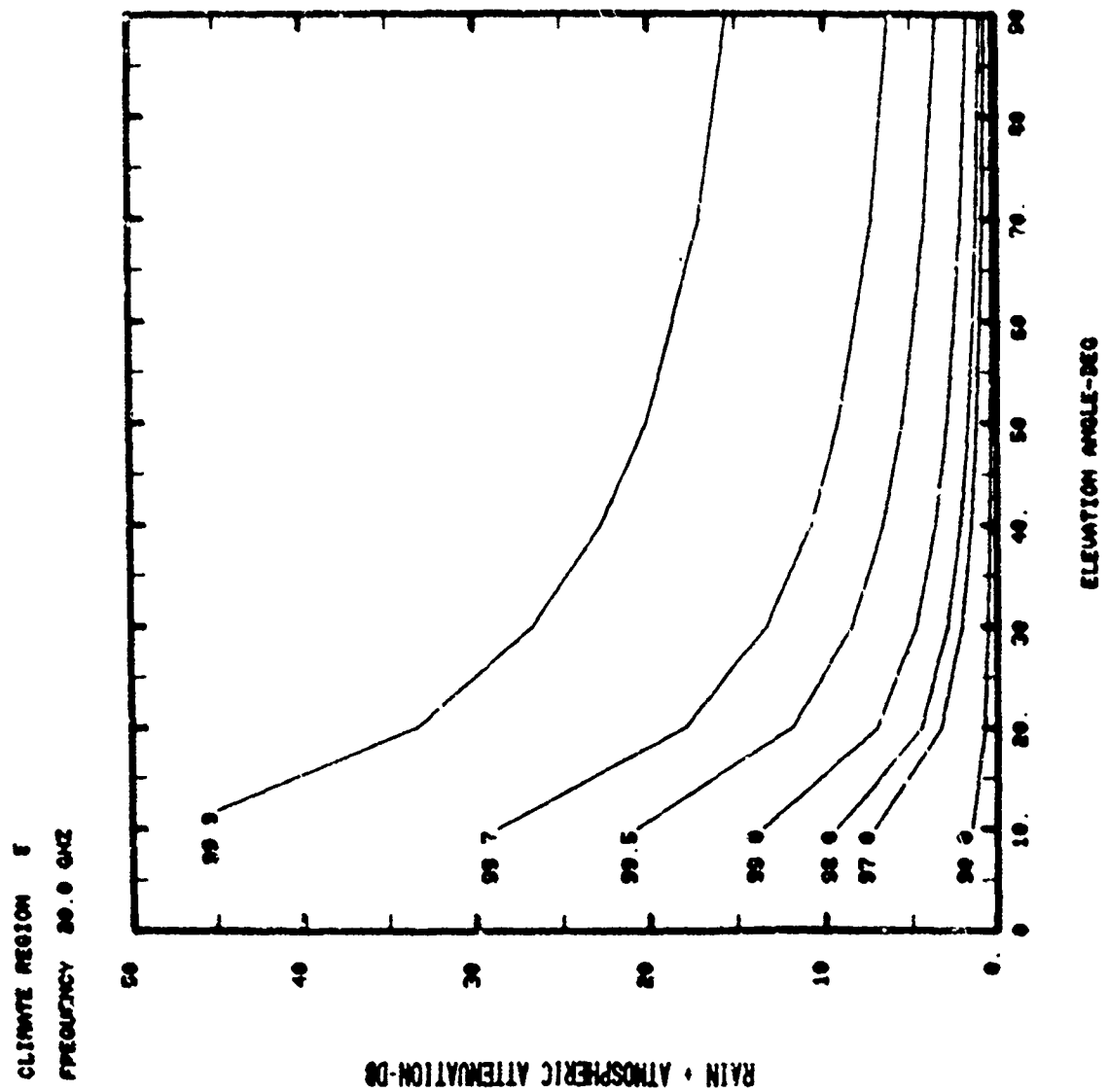
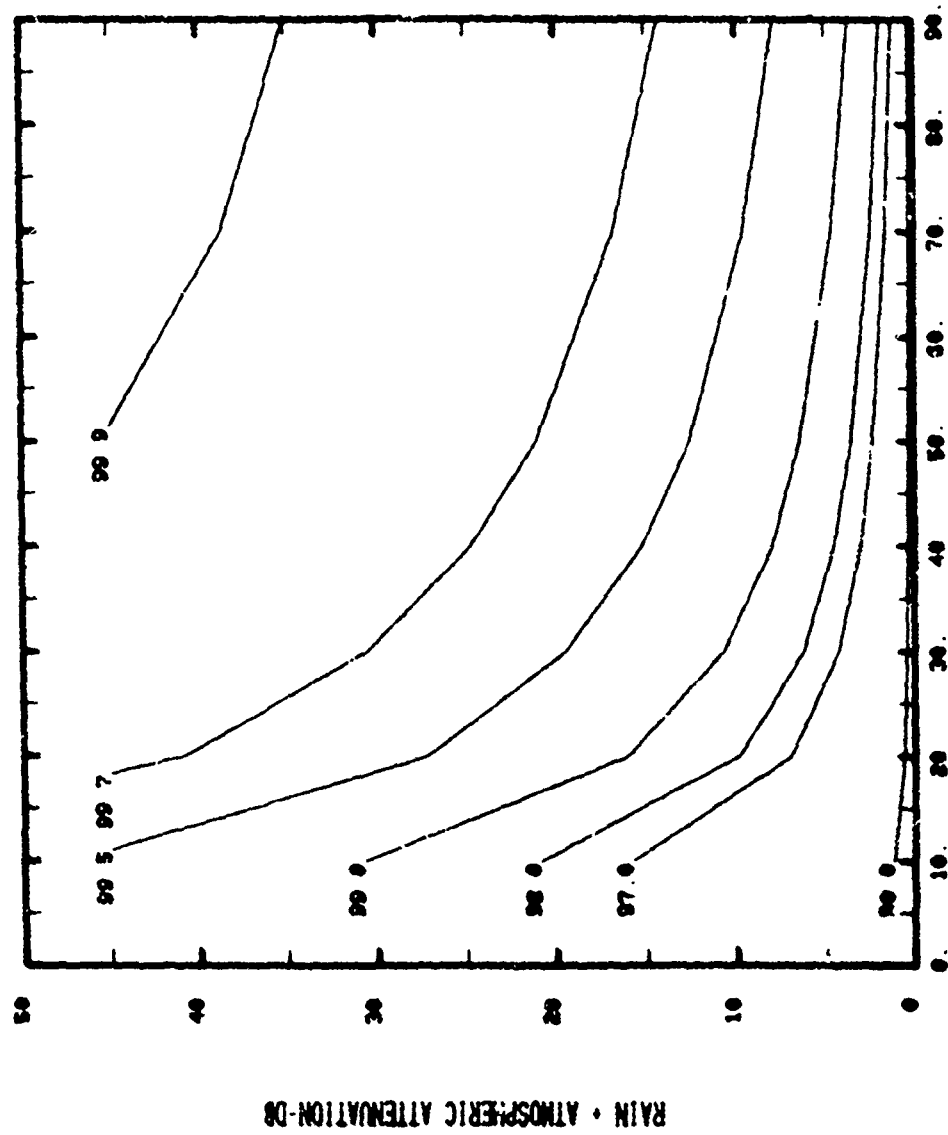


Fig. A-41

CLIMATE REGION C
FREQUENCY 30.0 MHz



ELEVATION ANGLE-DEG

Fig. A-42

CLIMATE REGION I
FREQUENCY 40.0 MHz

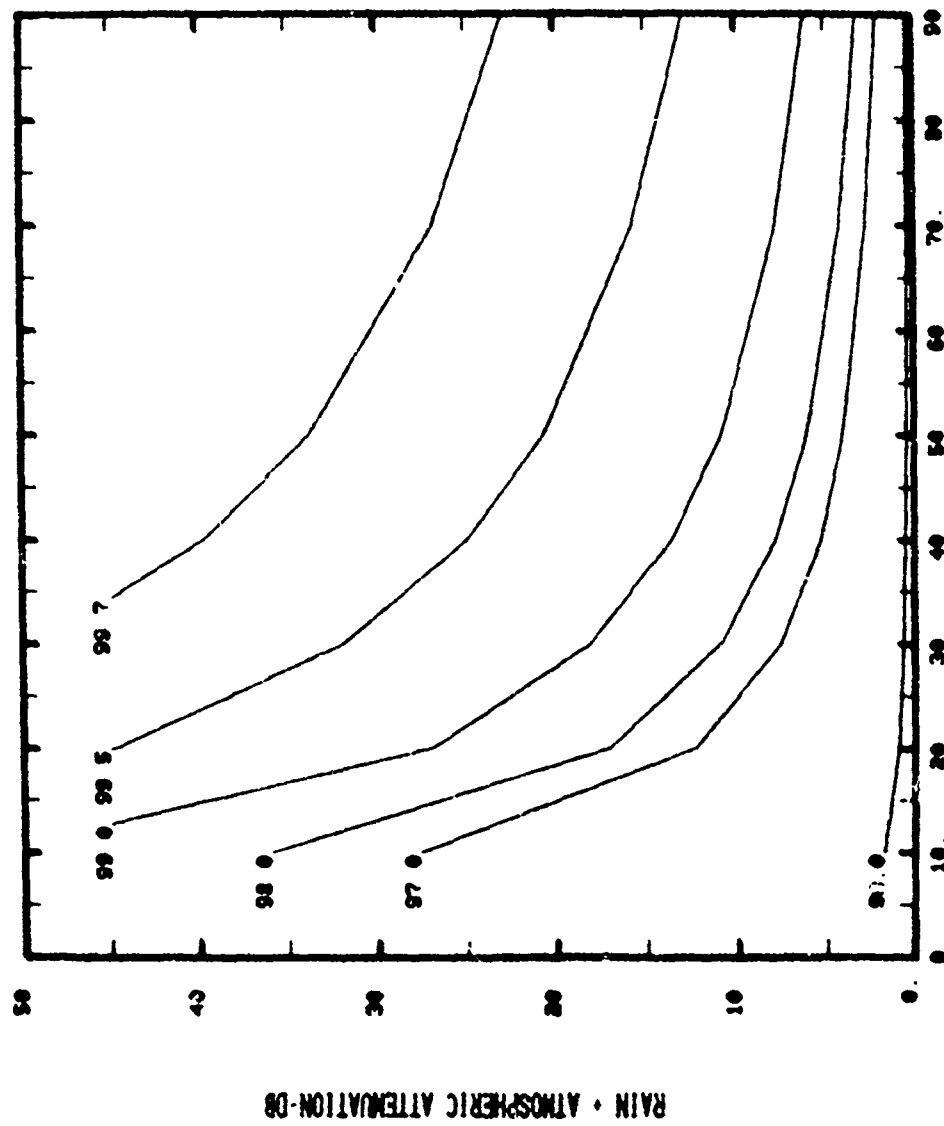


Fig. A-43

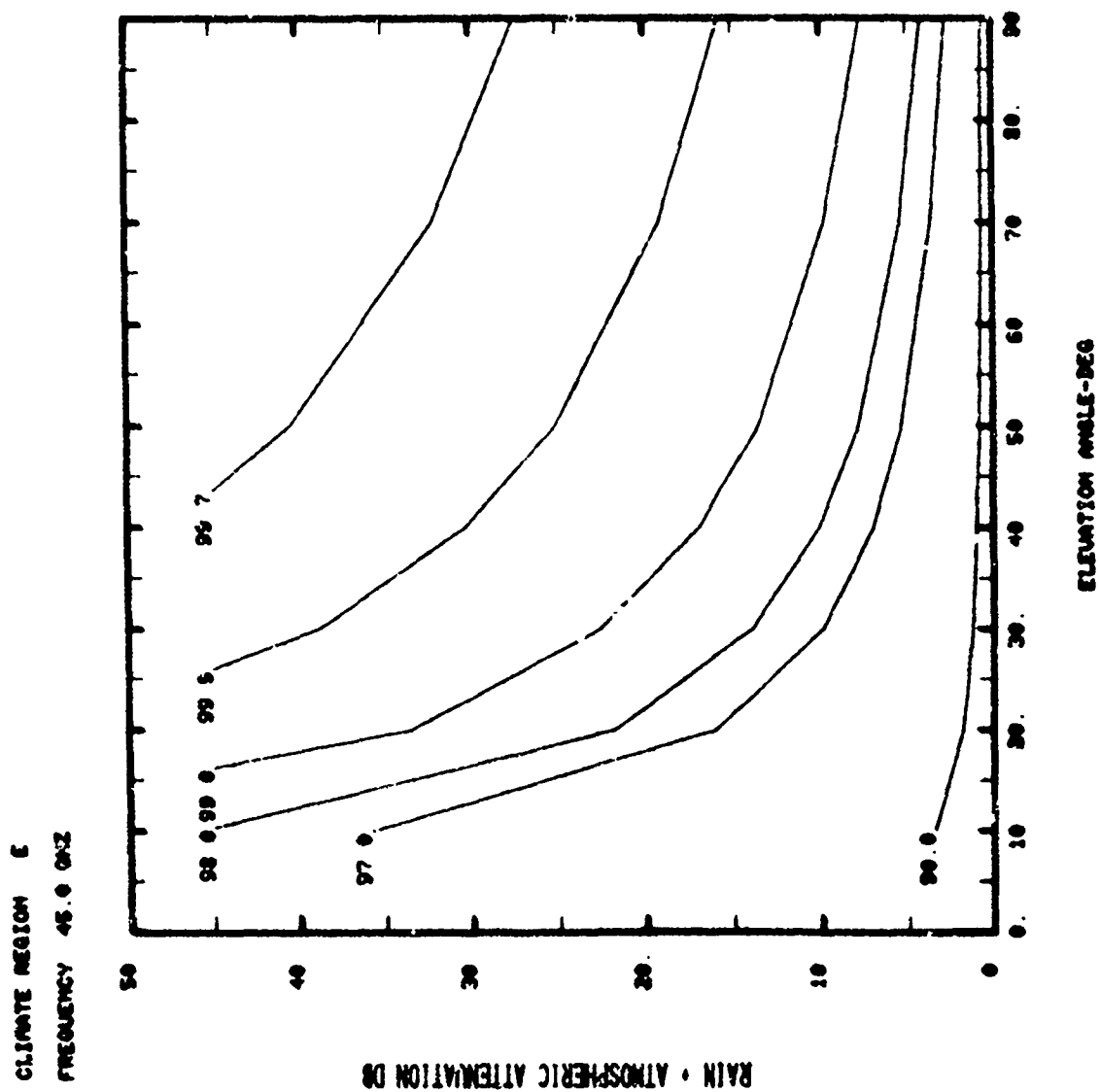


Fig. A-44

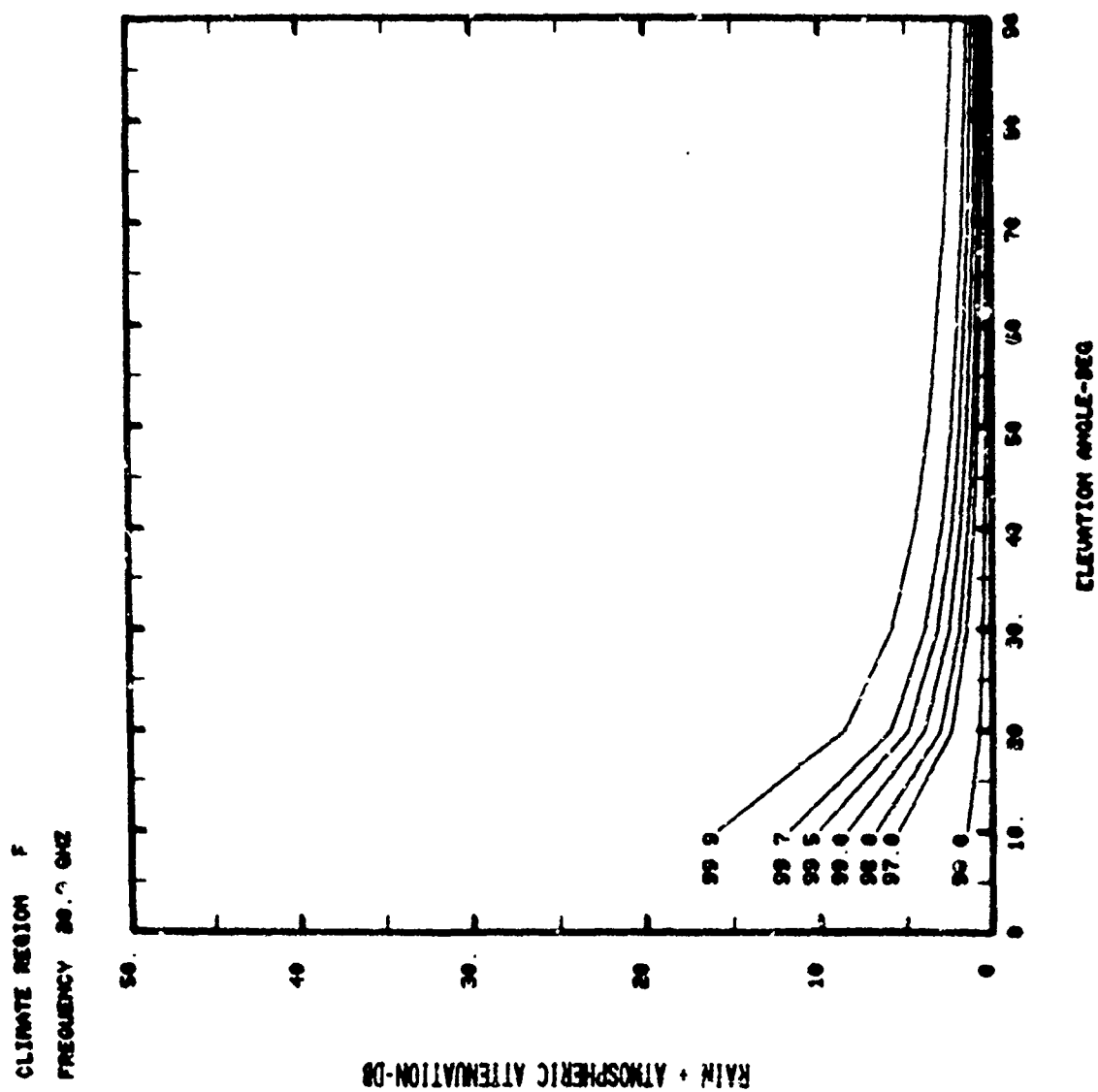


Fig. A-45

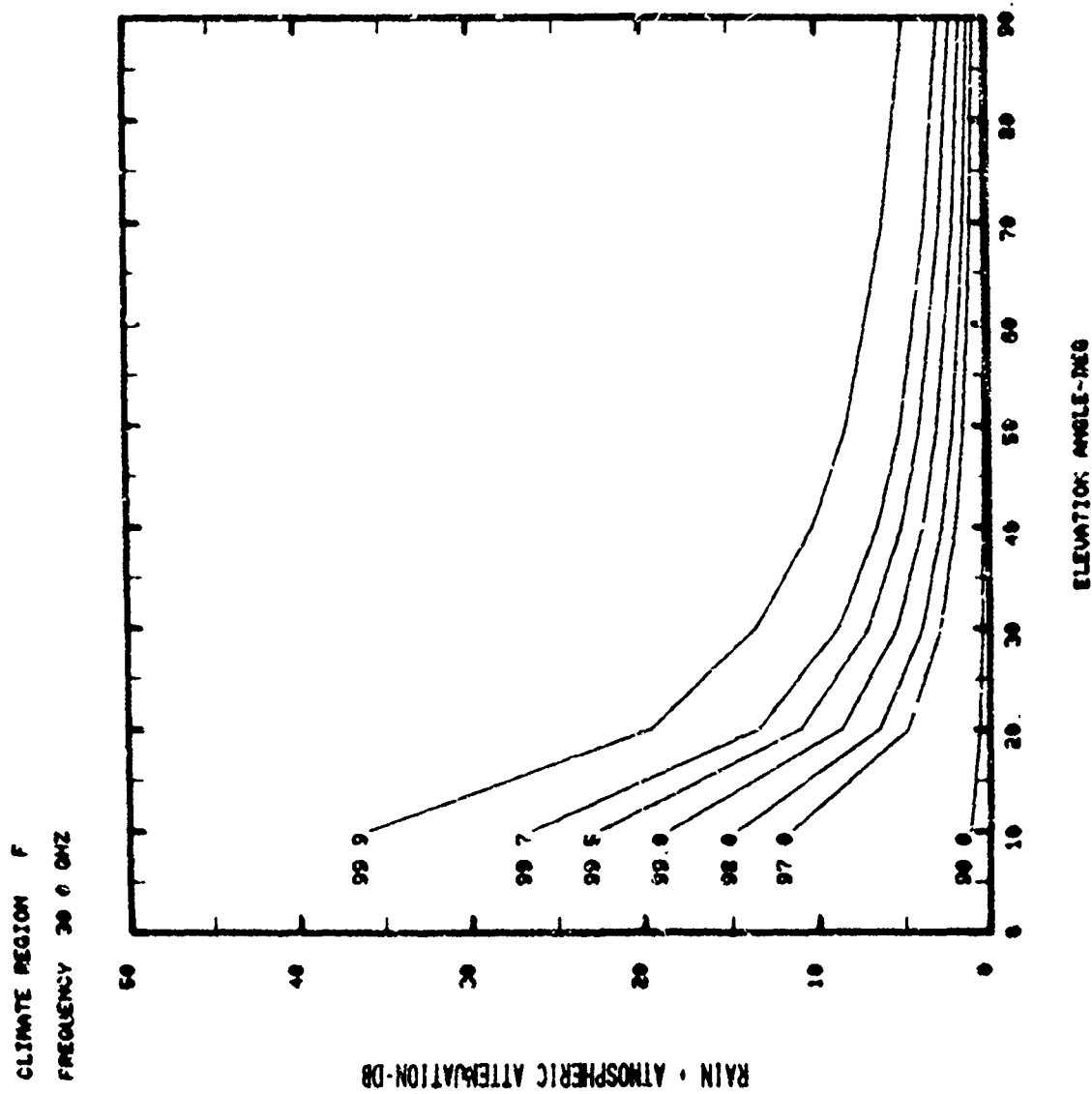


Fig. A-46

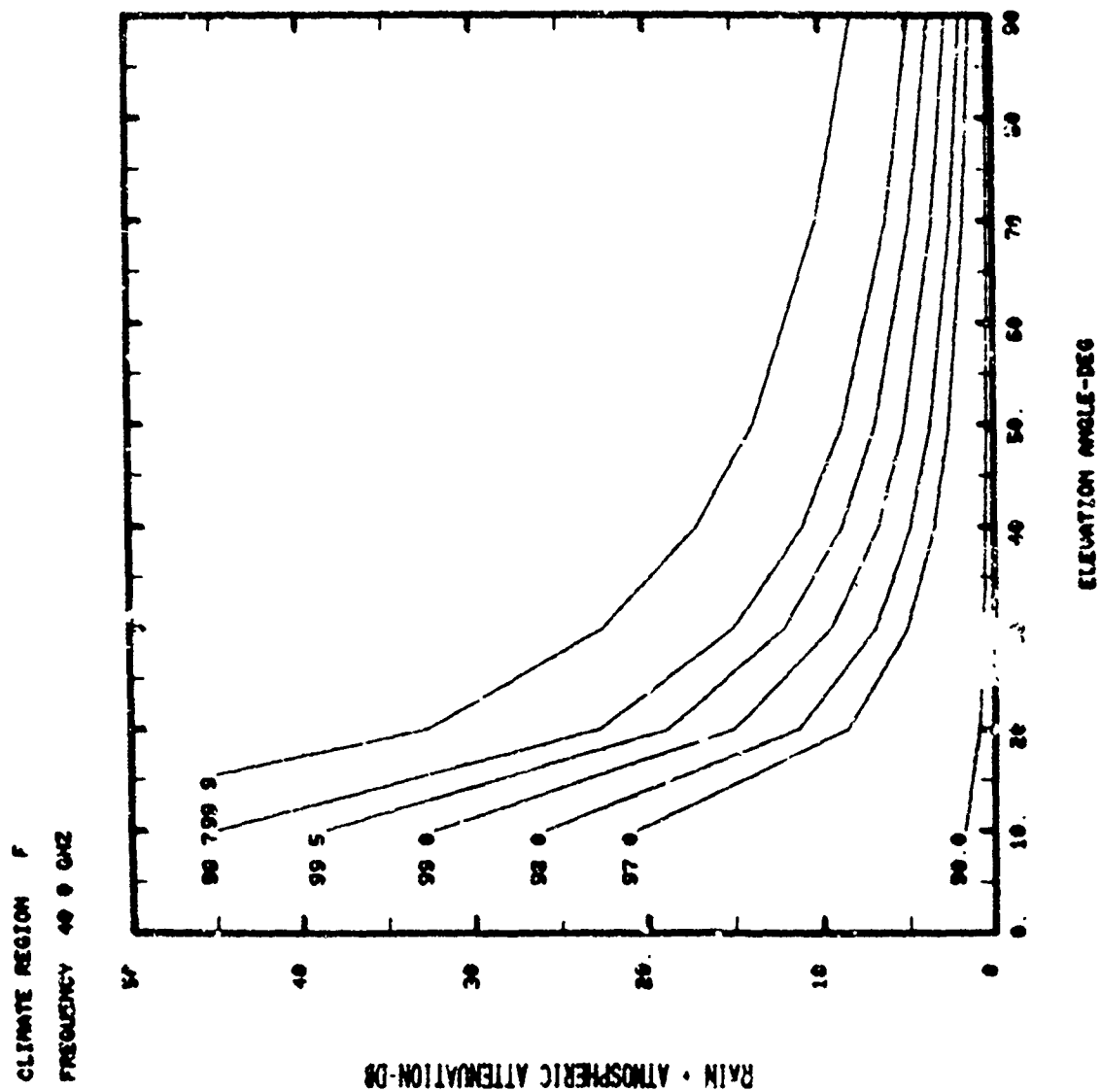


Fig. A-47

CLIMATE REGION F
FREQUENCY 48.0 CMZ

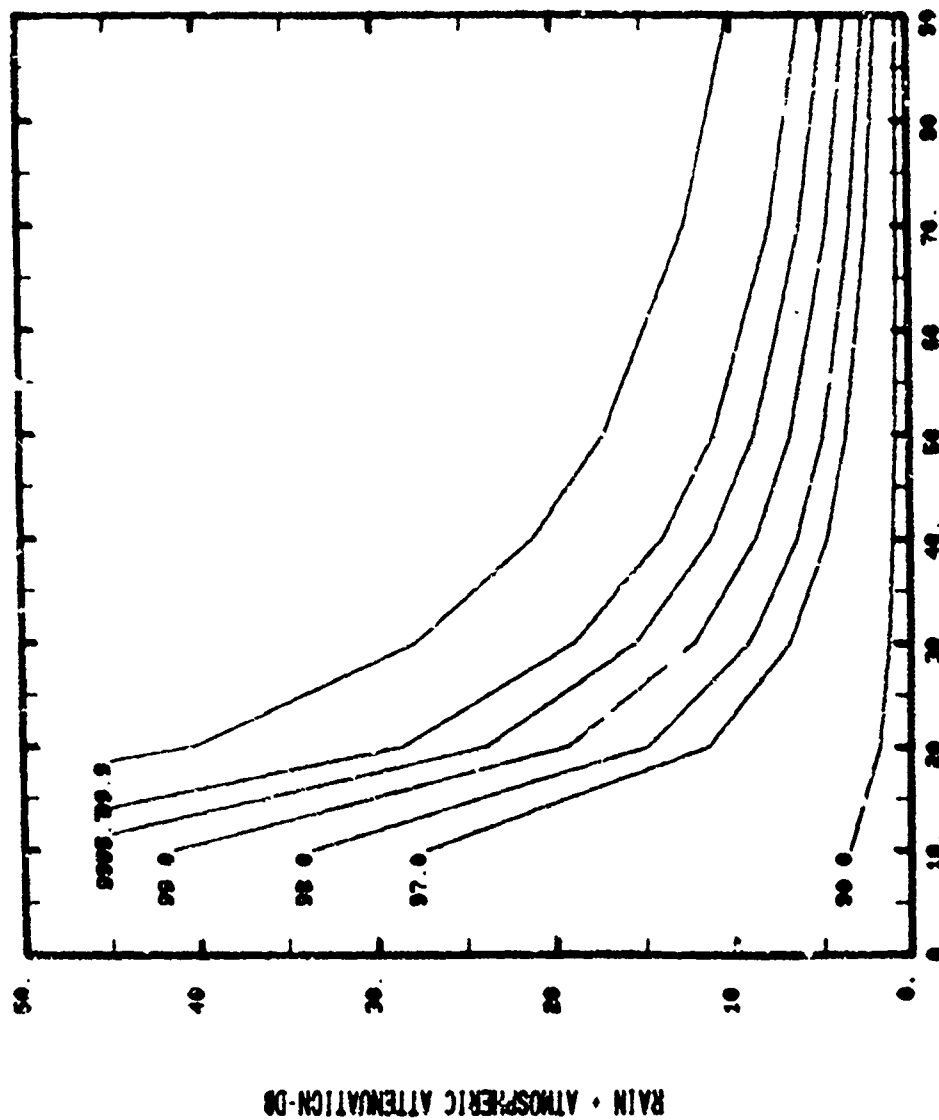


Fig. A-48

CLIMATE REGION 6
 FREQUENCY 20.0 GHz

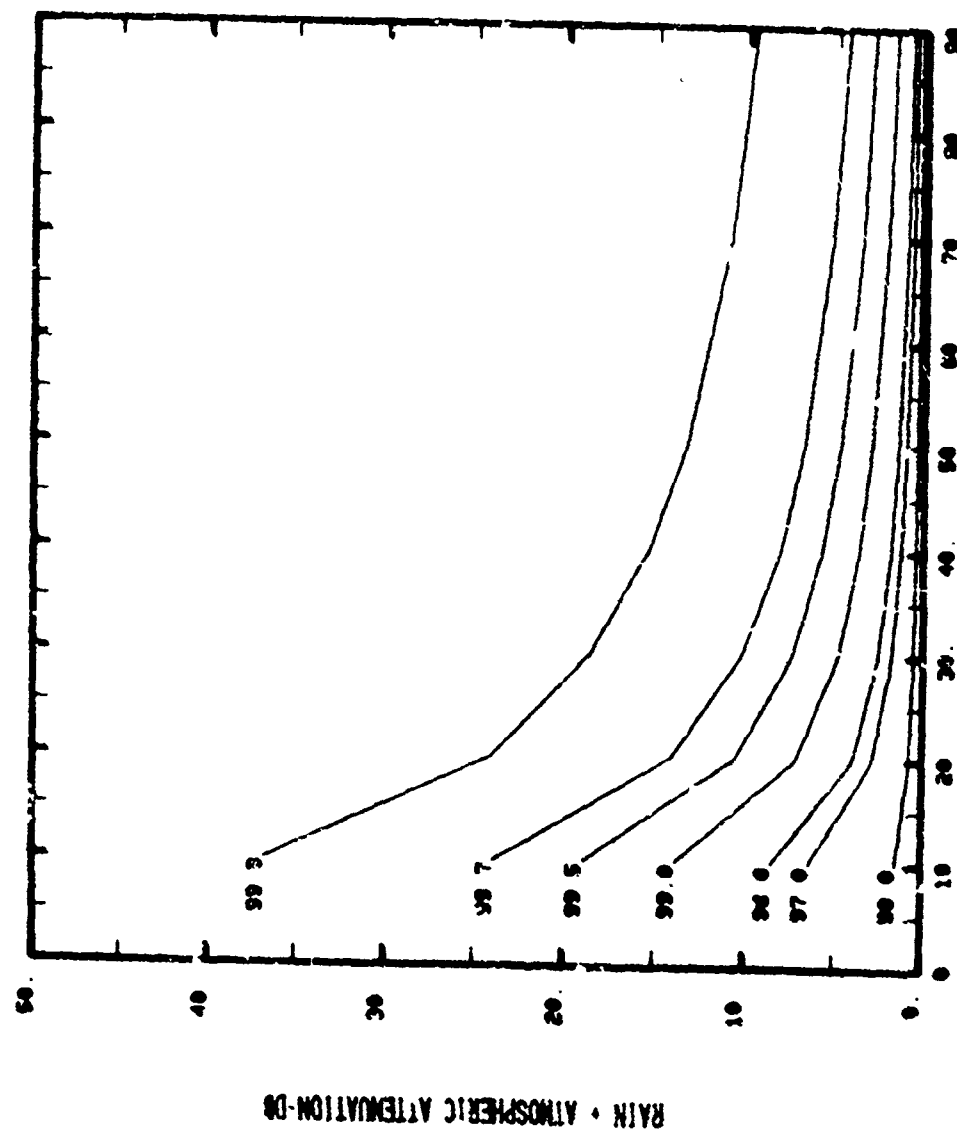


Fig. A-49

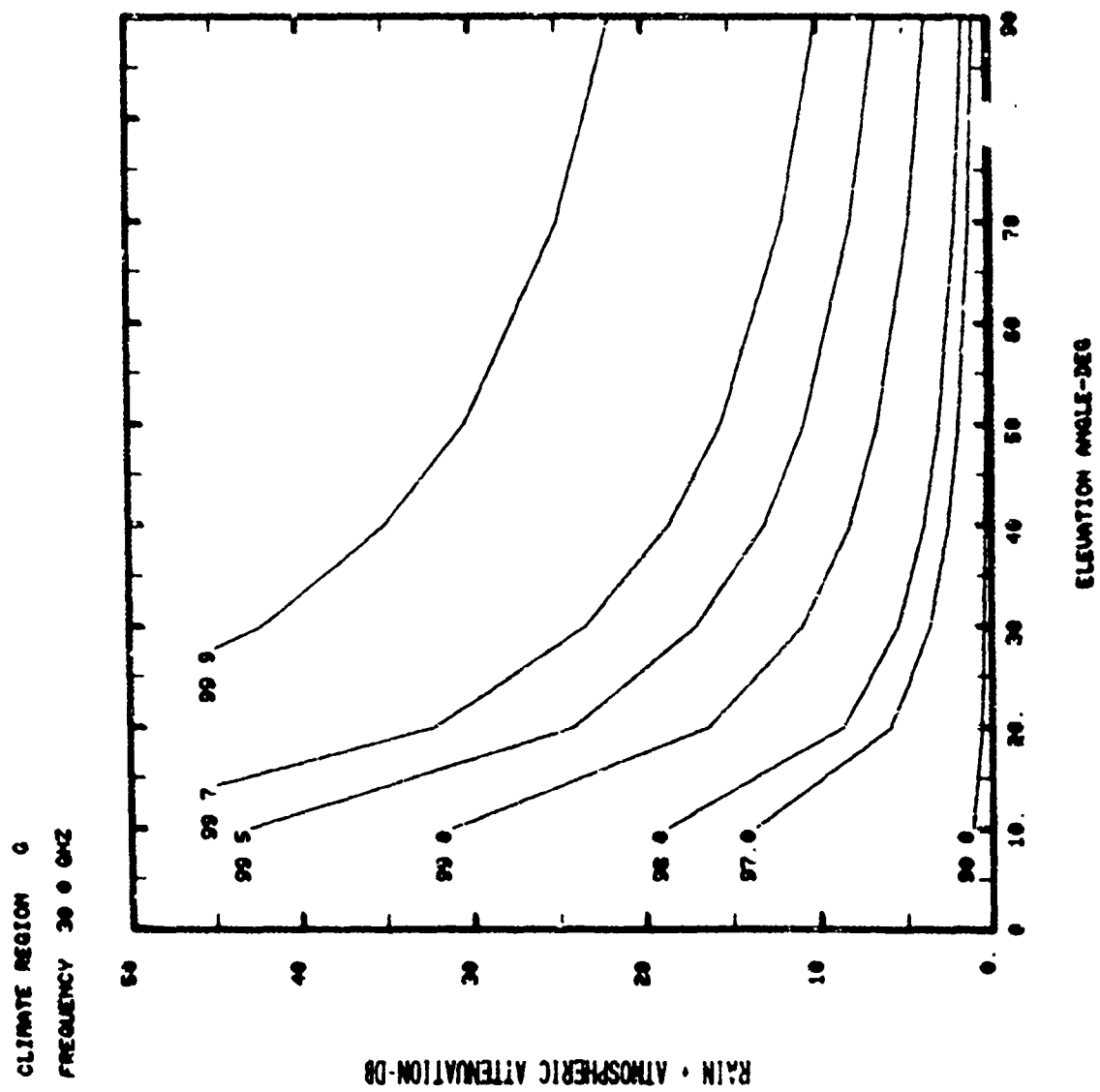


Fig. A-50

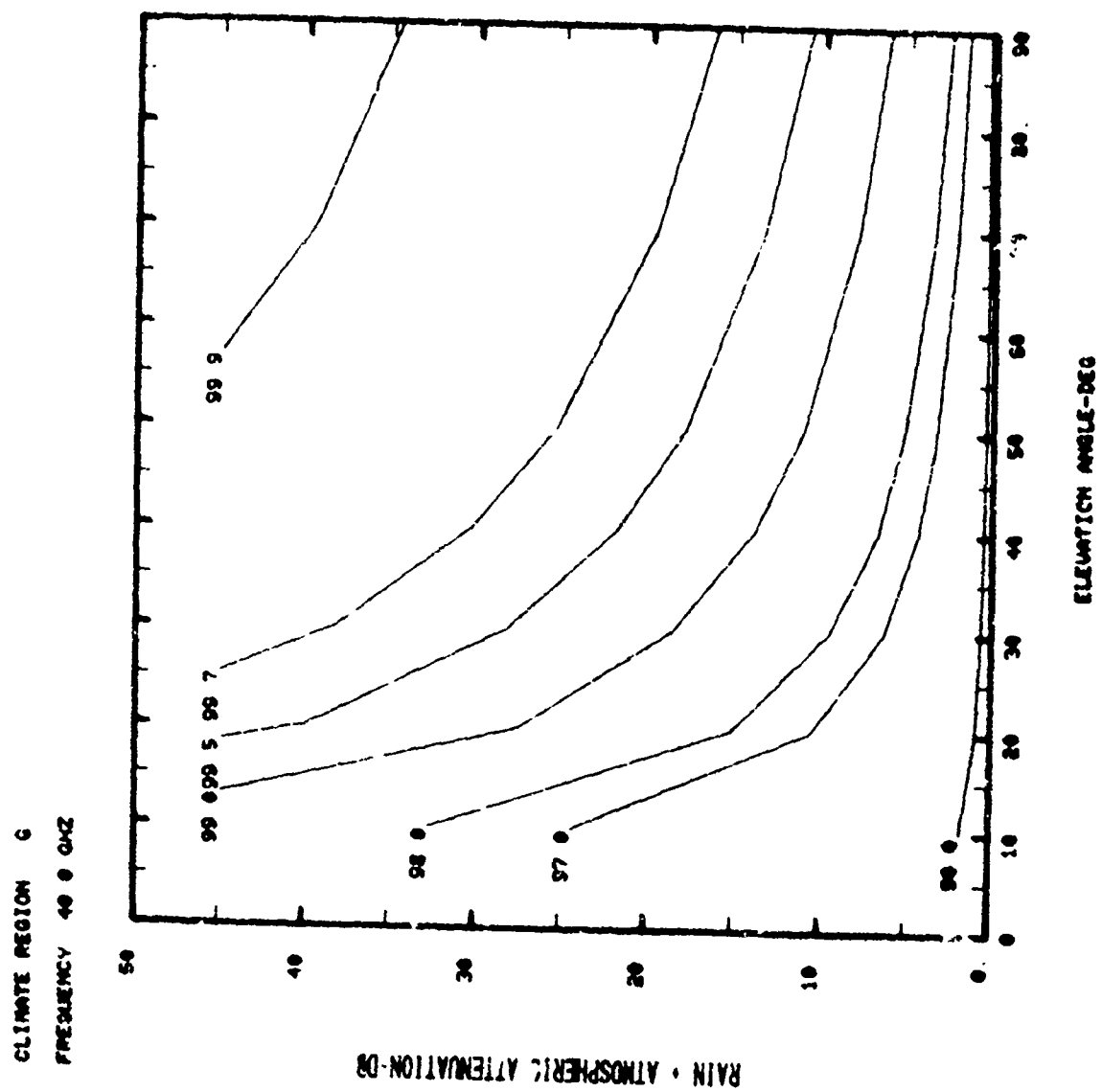


Fig. A-51

CLIMATE REGION 0
 FREQUENCY 45 0 0432

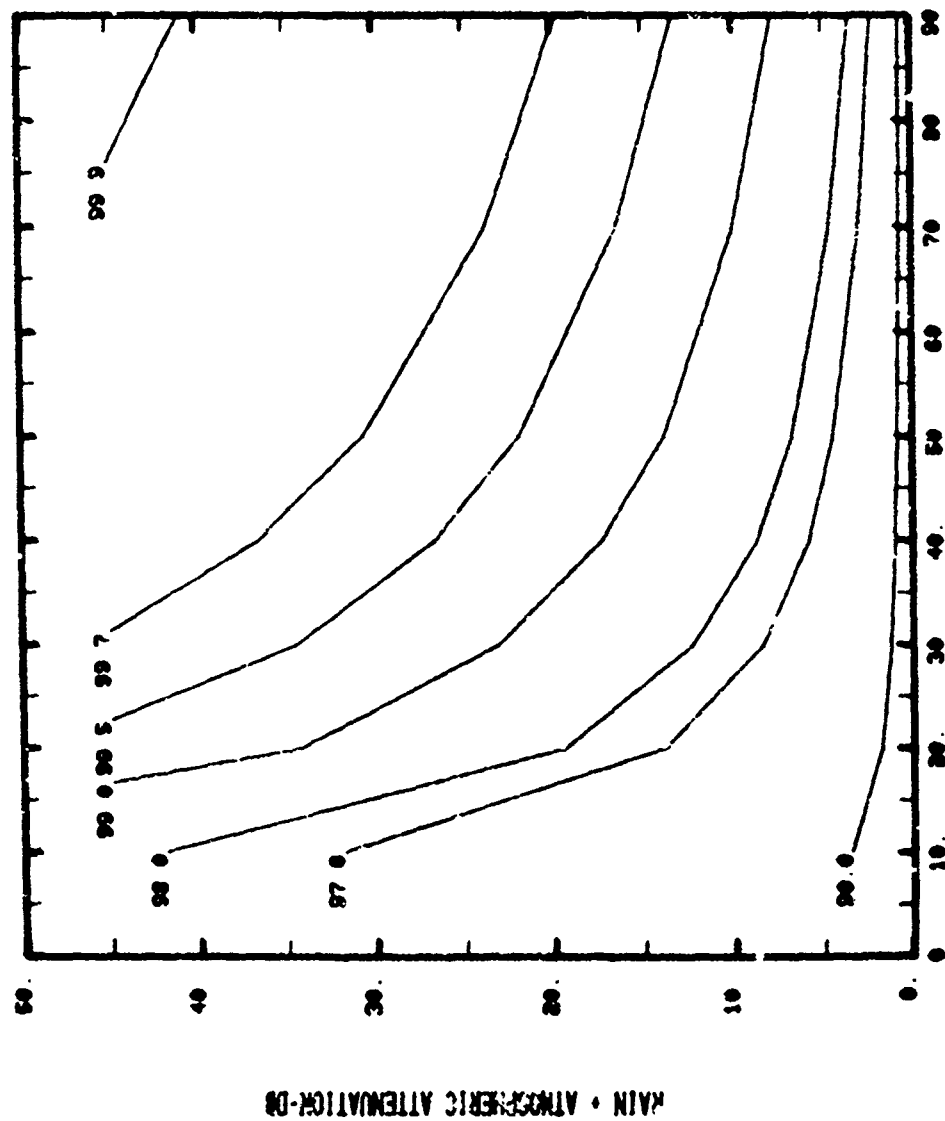


Fig. A-52

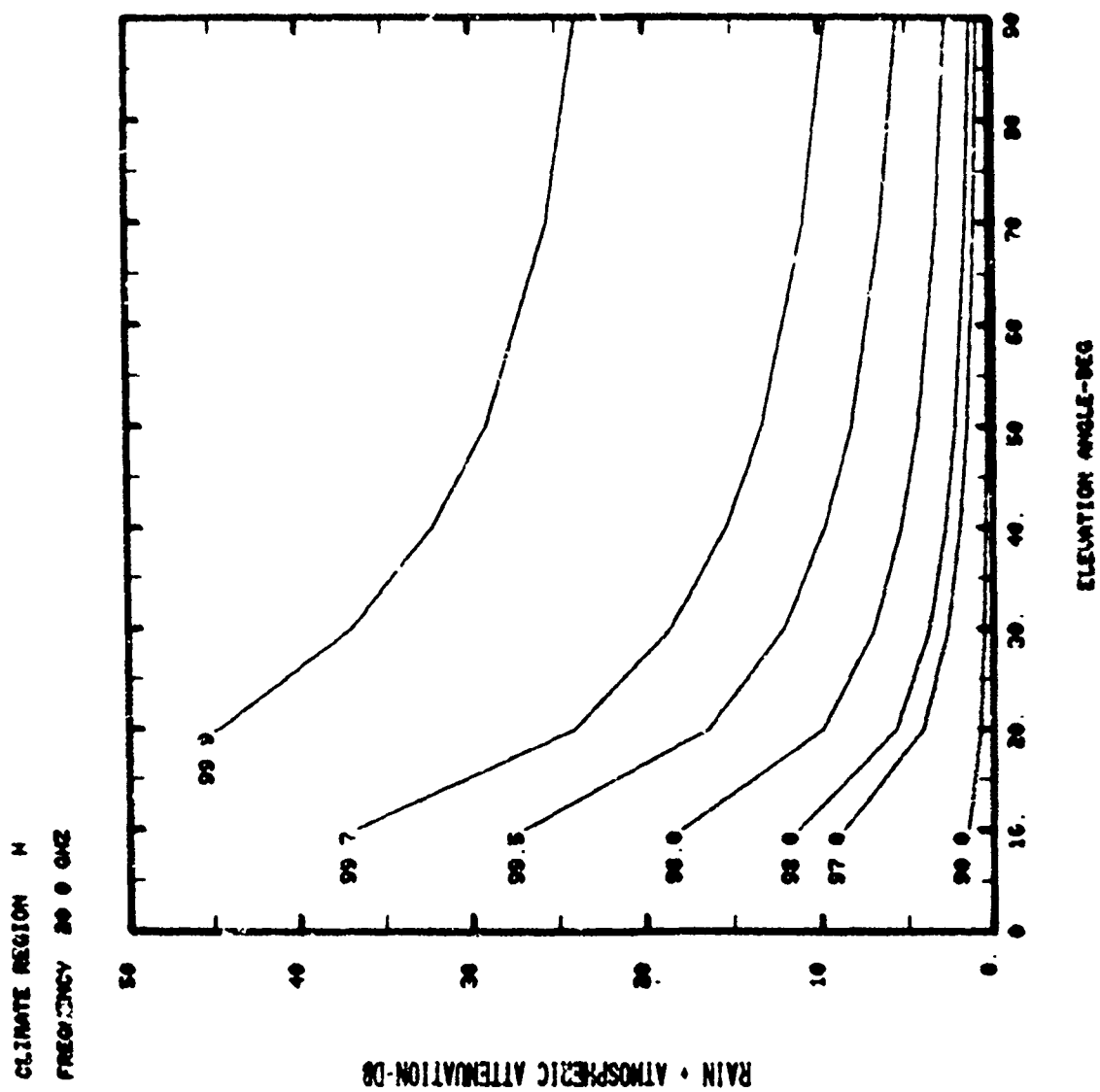


Fig. A-53

CLIMATE REGION M
FREQUENCY 30.0 GHz

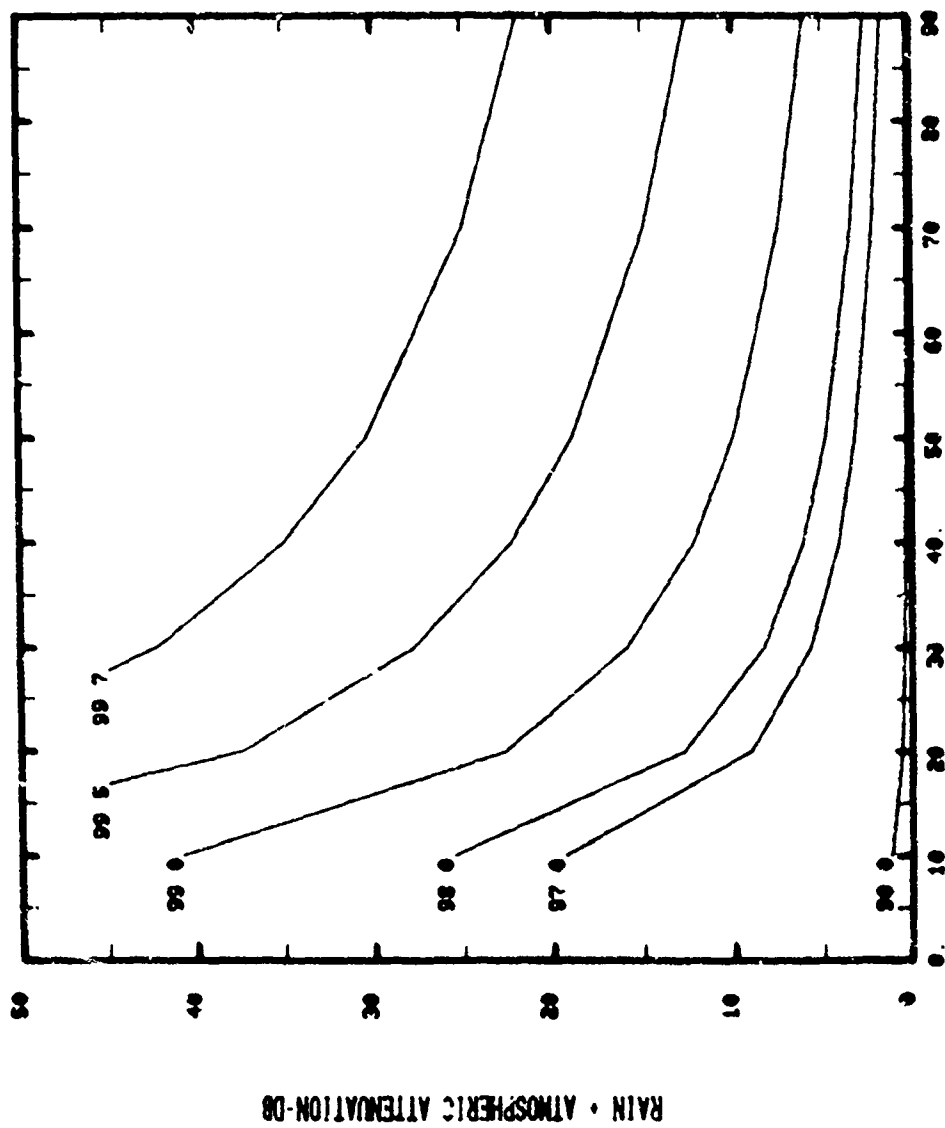
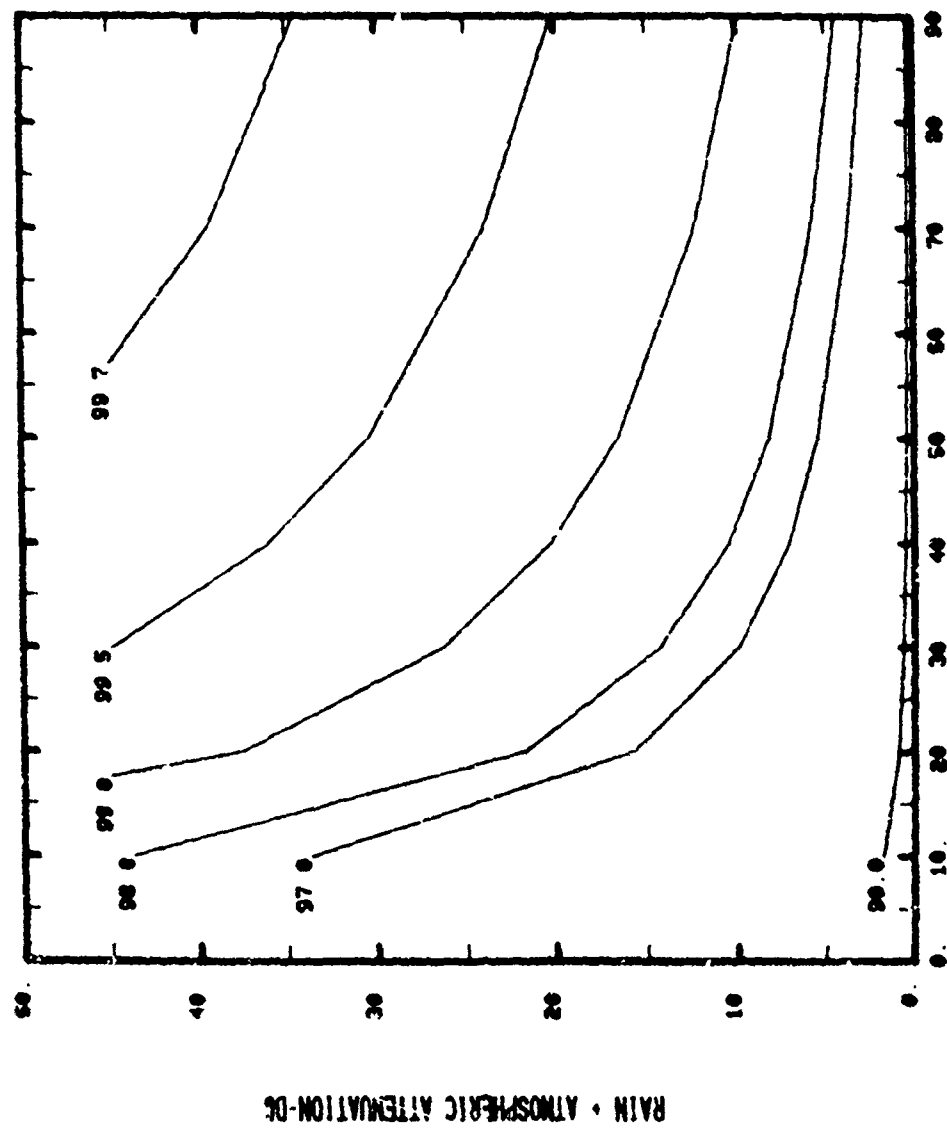


Fig. A-54

CLIMATE REGION II
 FREQUENCY 40.0 GHz



ELEVATION ANGLE-DEG

Fig. A-55

CLIMATE REGION H
 FREQUENCY 46.0 GHz

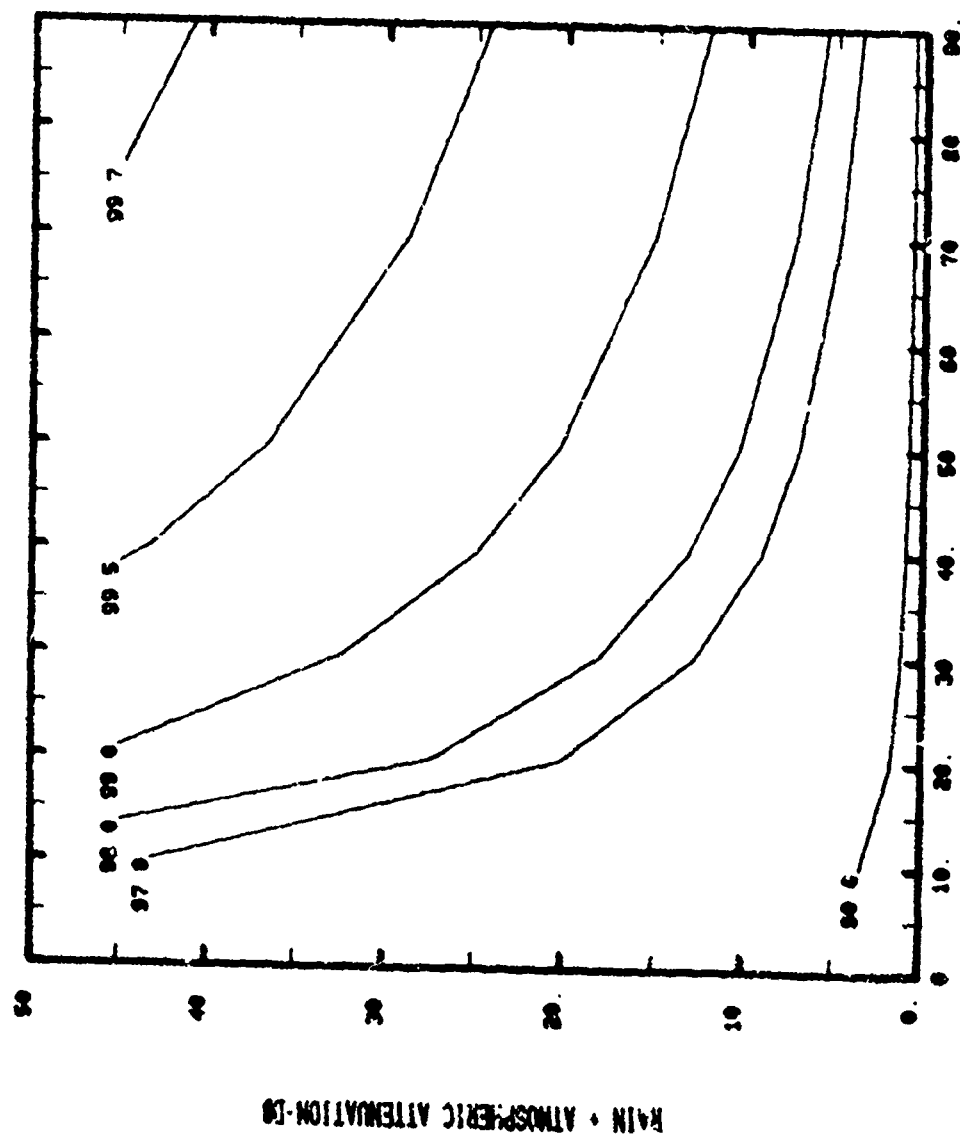


Fig. A-56

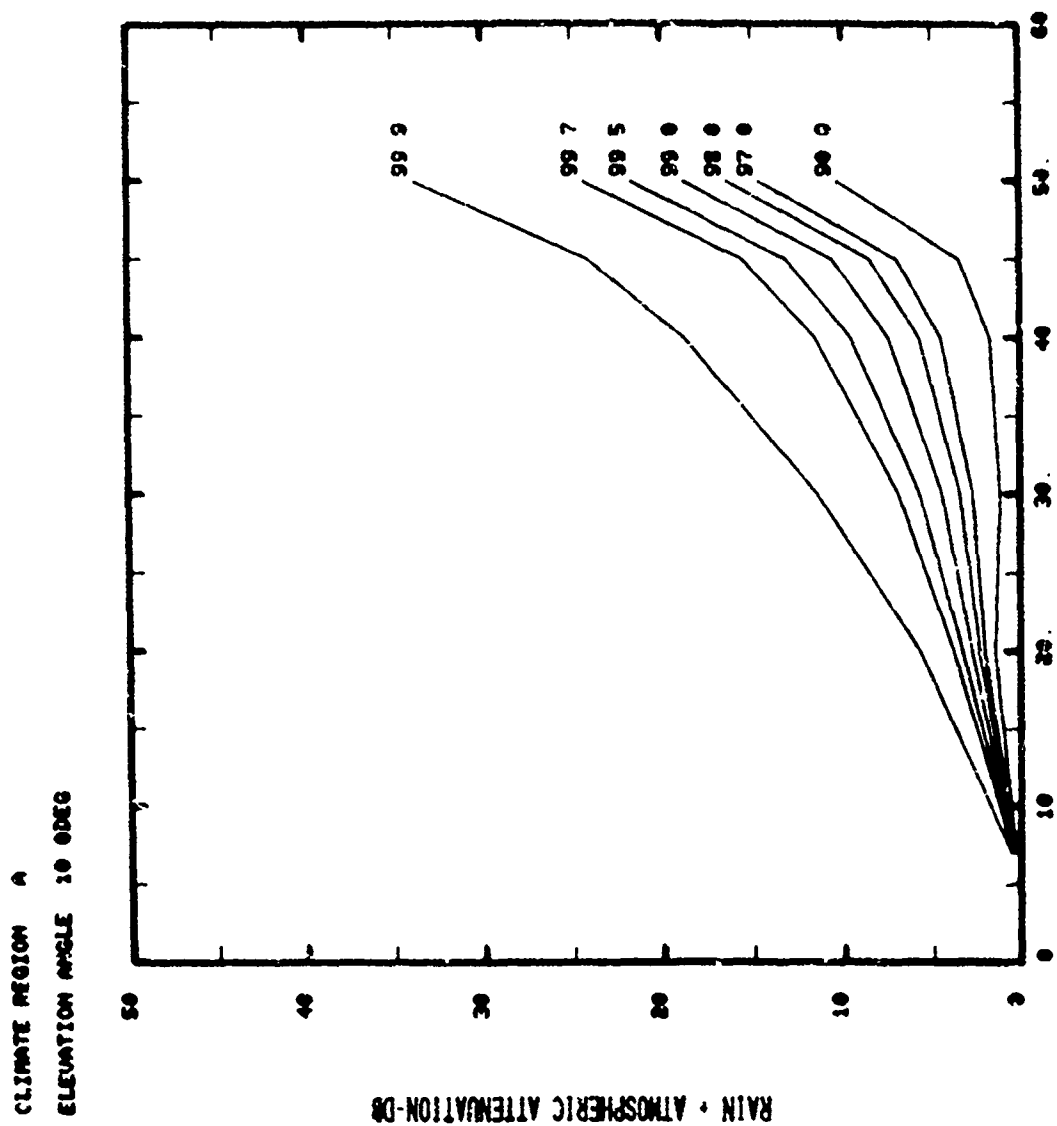


Fig. A-57

CLIMATE REGION A
ELEVATION ANGLE 20 DEG

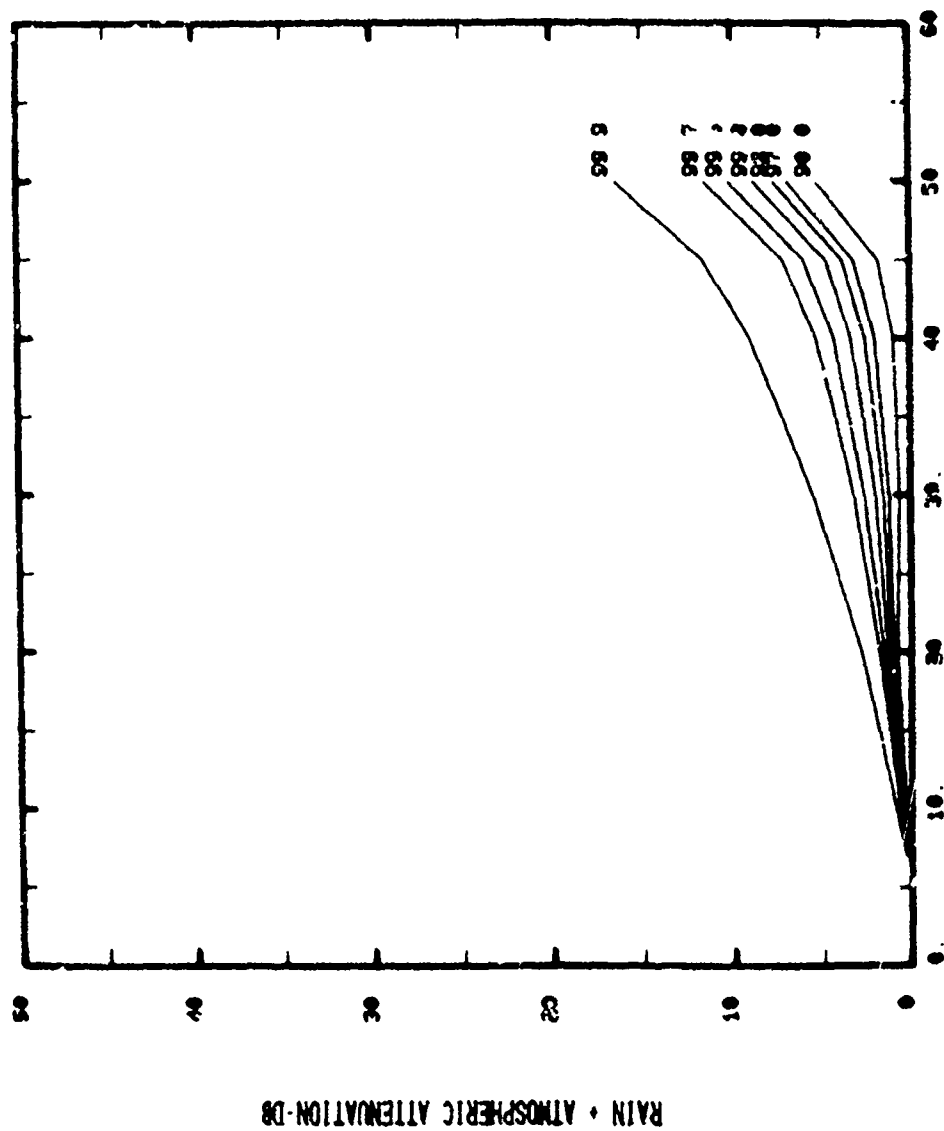


Fig. A-58

CLIMATE REGION A
ELEVATION ANGLE 90.0 DEG

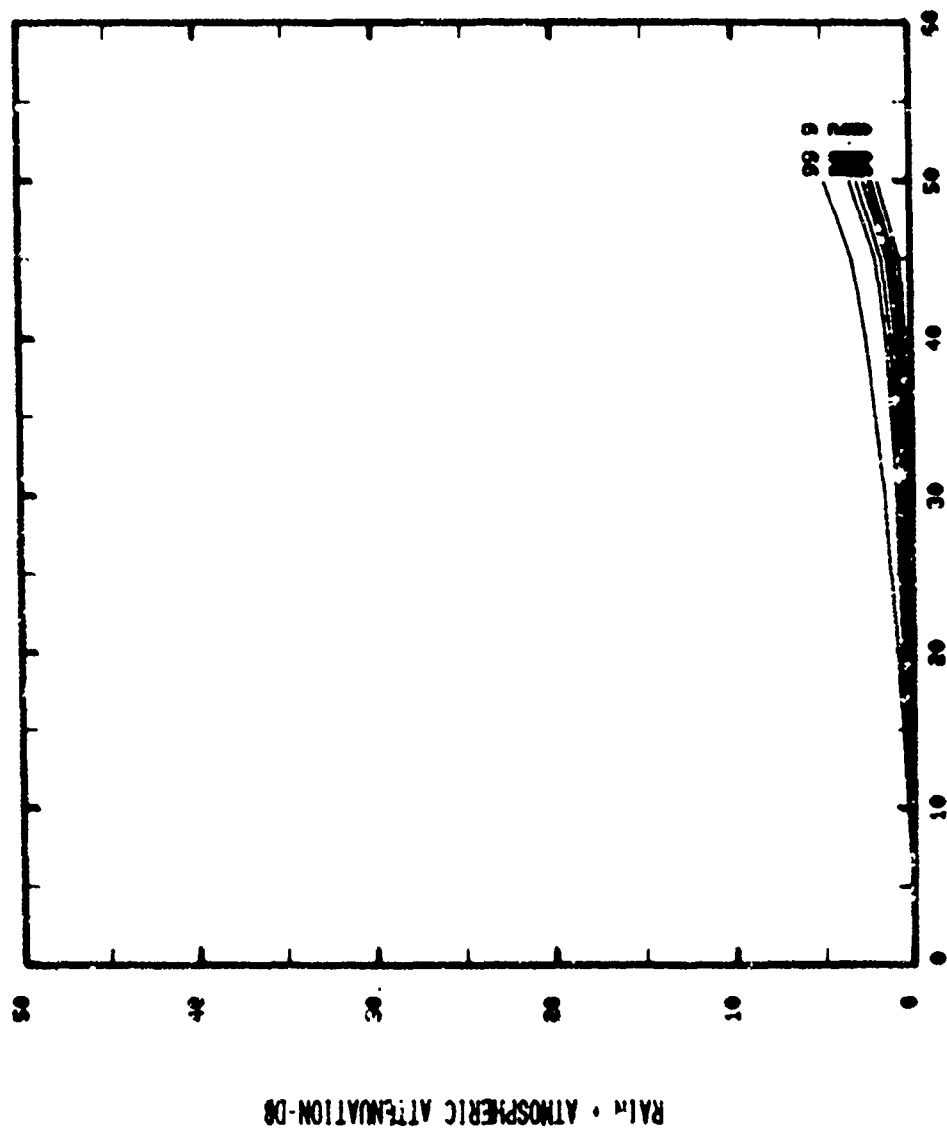
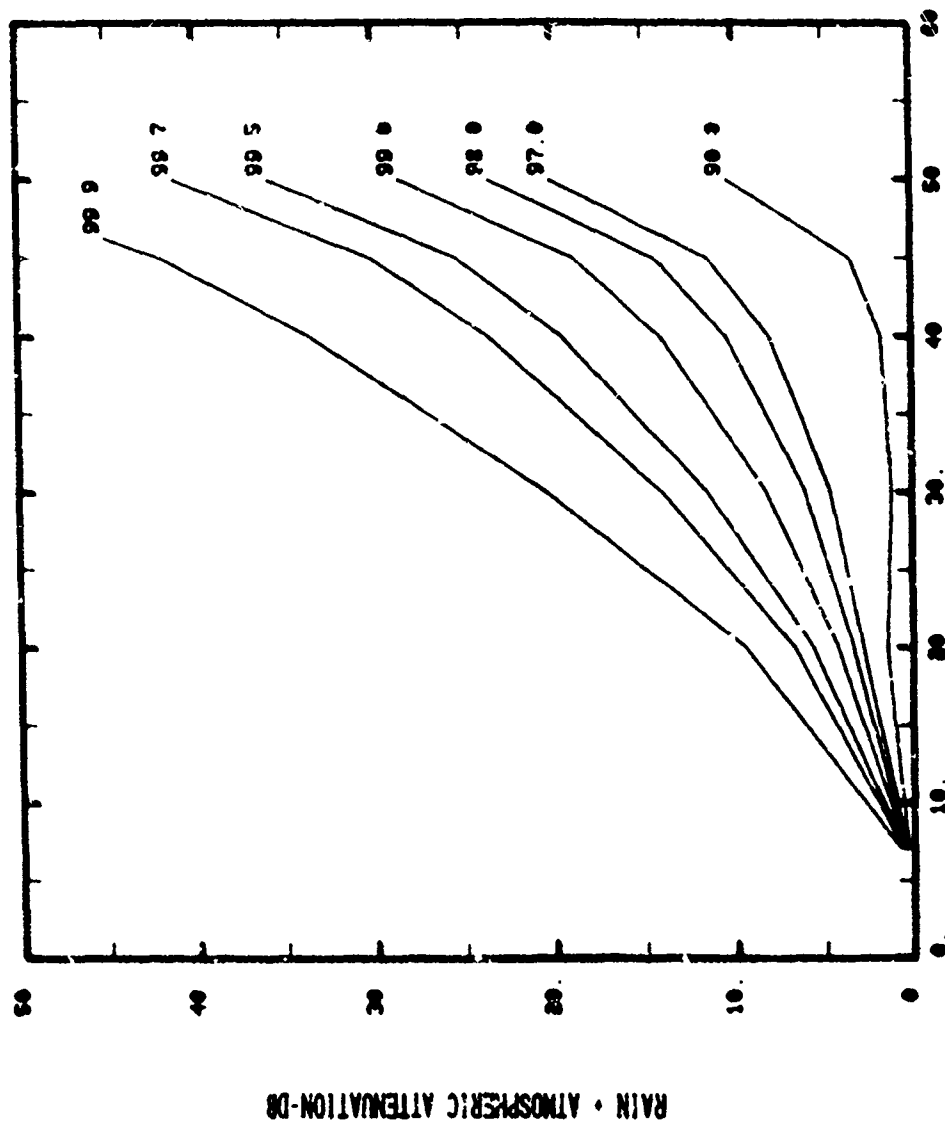


Fig. A-59

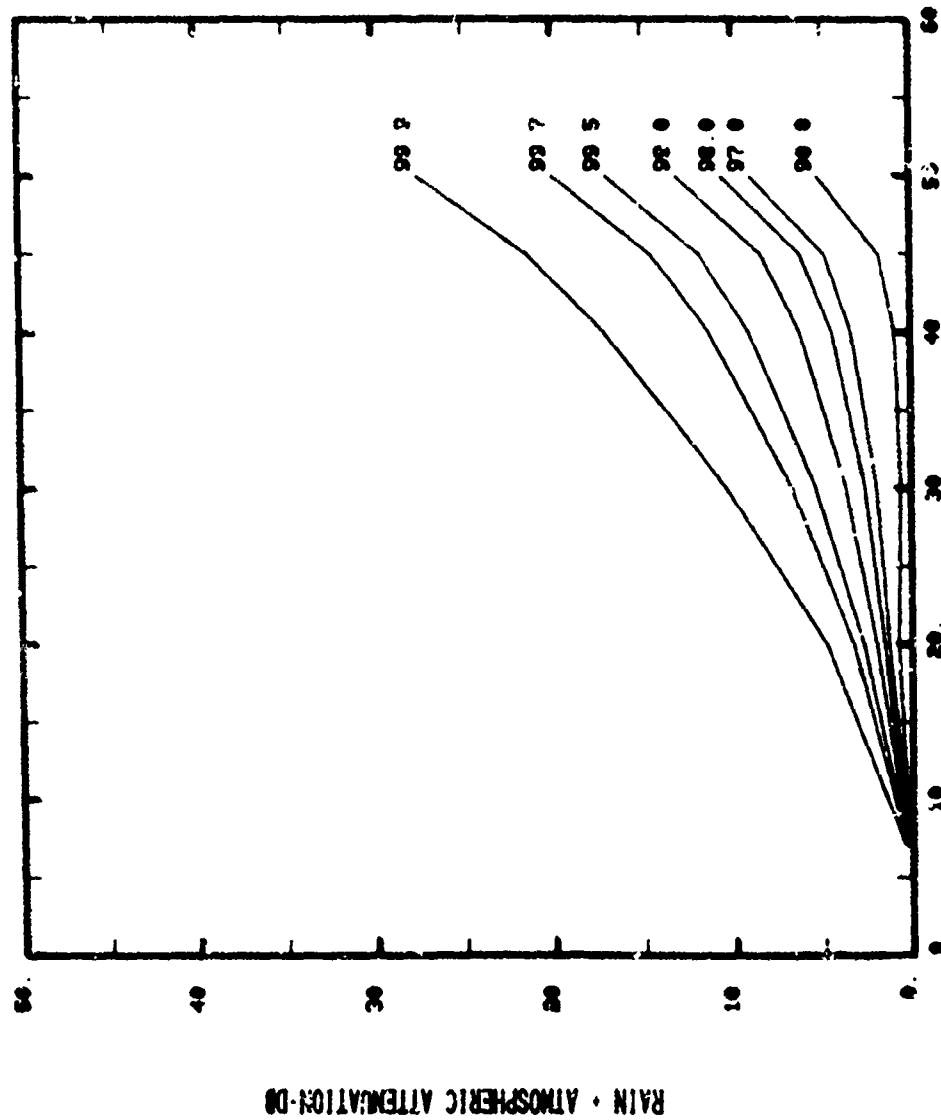
CLIMATE REGION B
ELEVATION ANGLE 10 DEG



FREQUENCY-GHZ

Fig. A-60

CLIMATE REGION B
ELEVATION ANGLE 30 DEG



FREQUENCY-MHZ

Fig. A-61

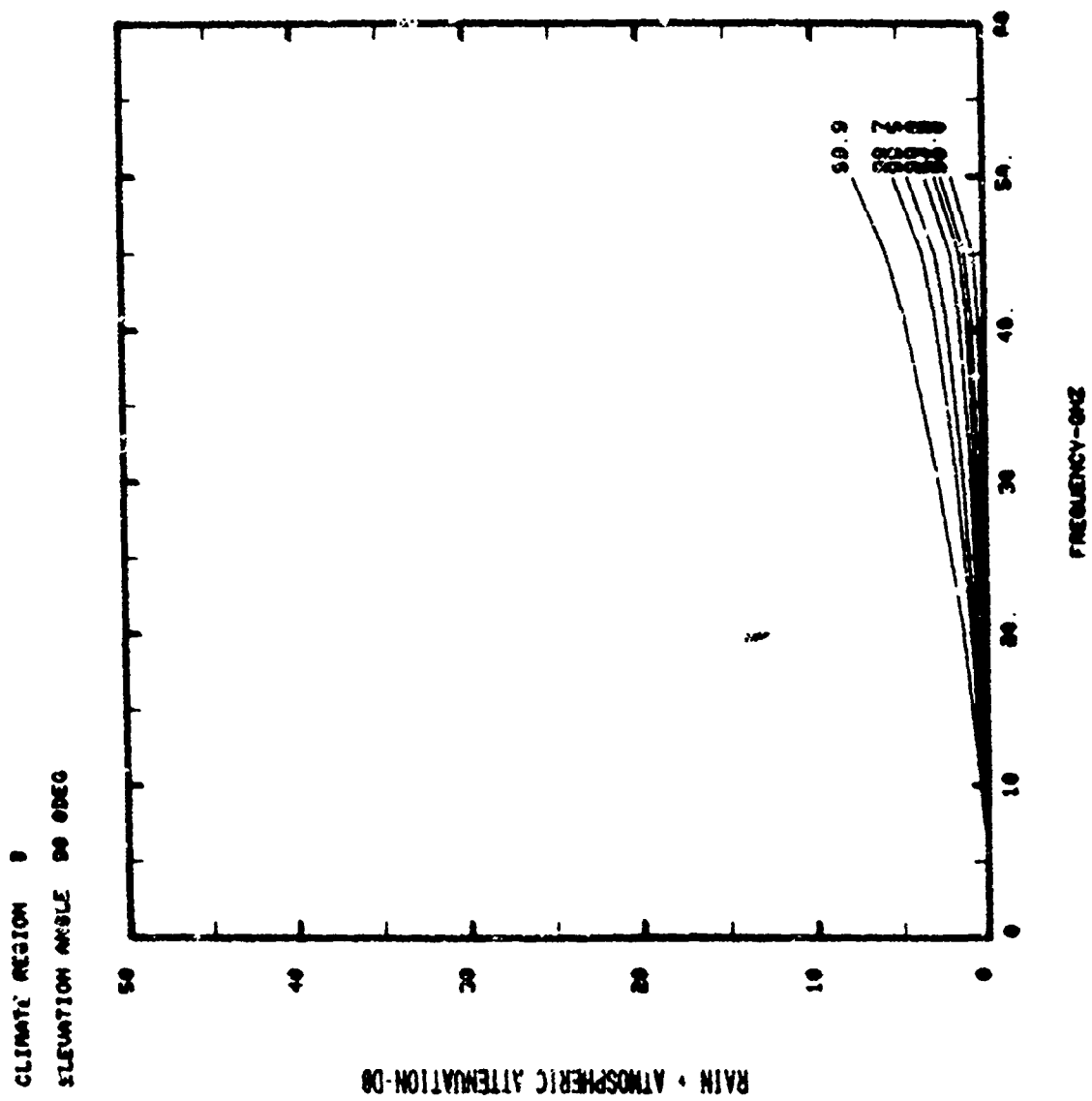


Fig. A-62

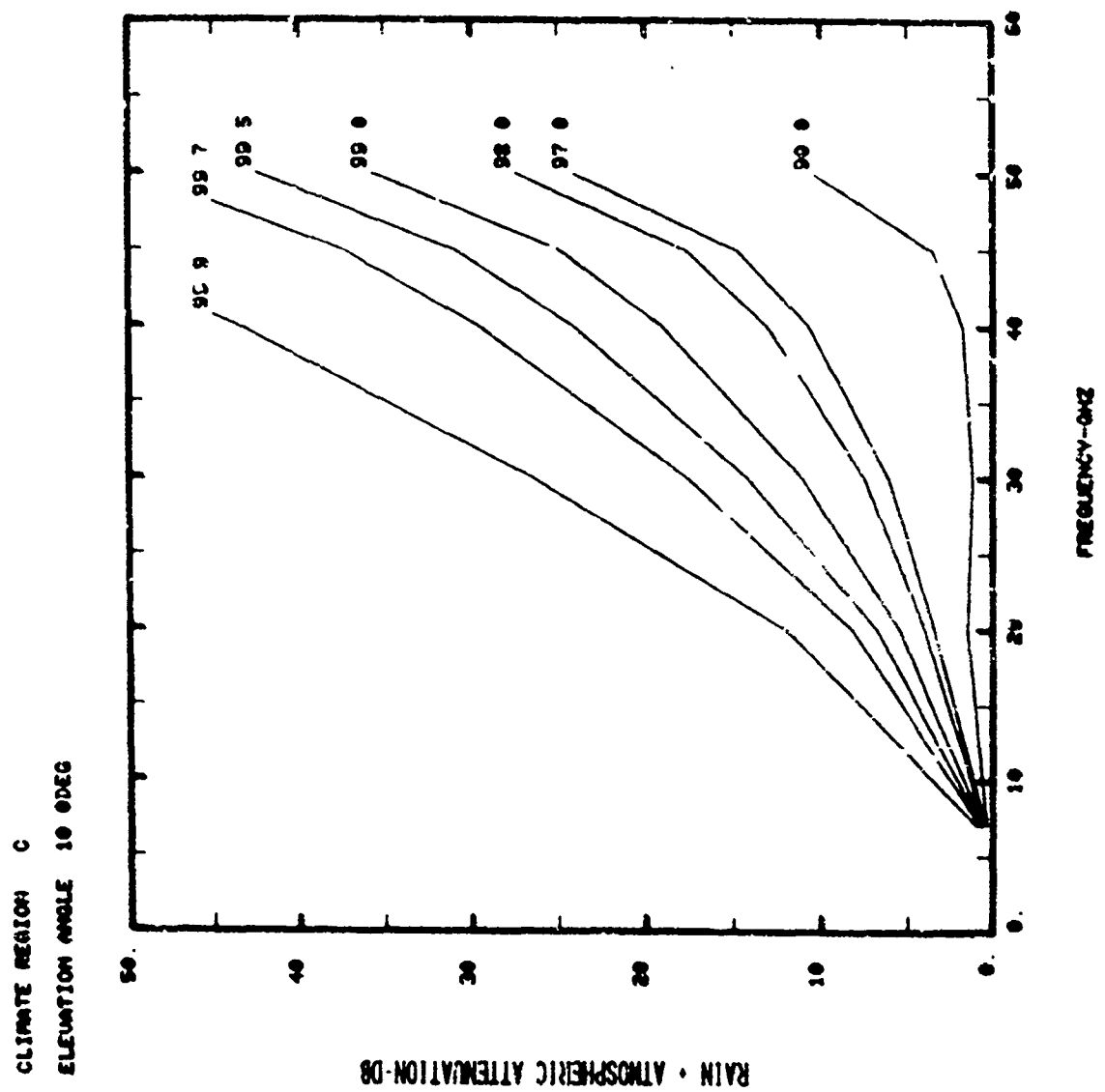


Fig. A-63

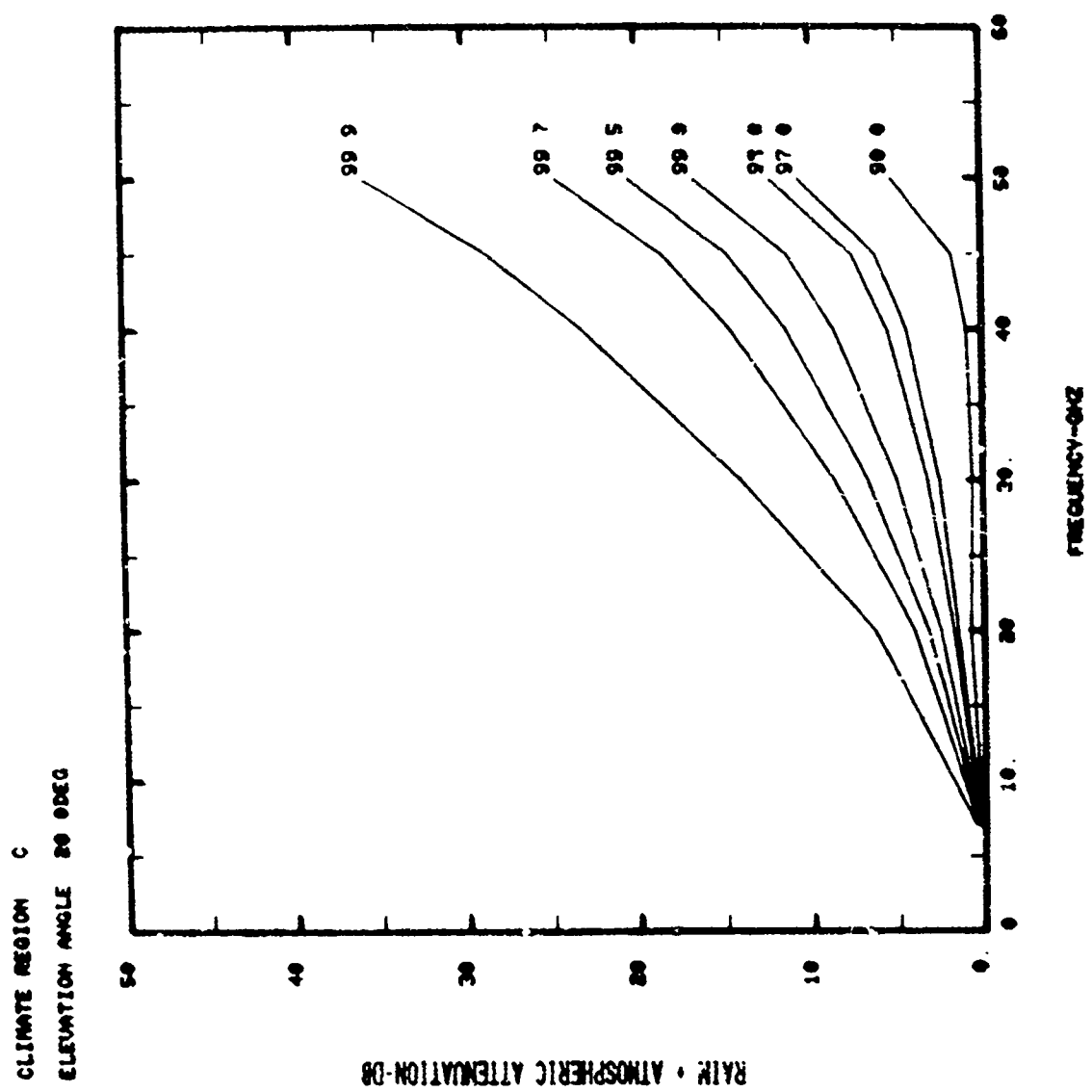


Fig. A-64

CLIMATE REGION C
ELEVATION ANGLE 90.0°

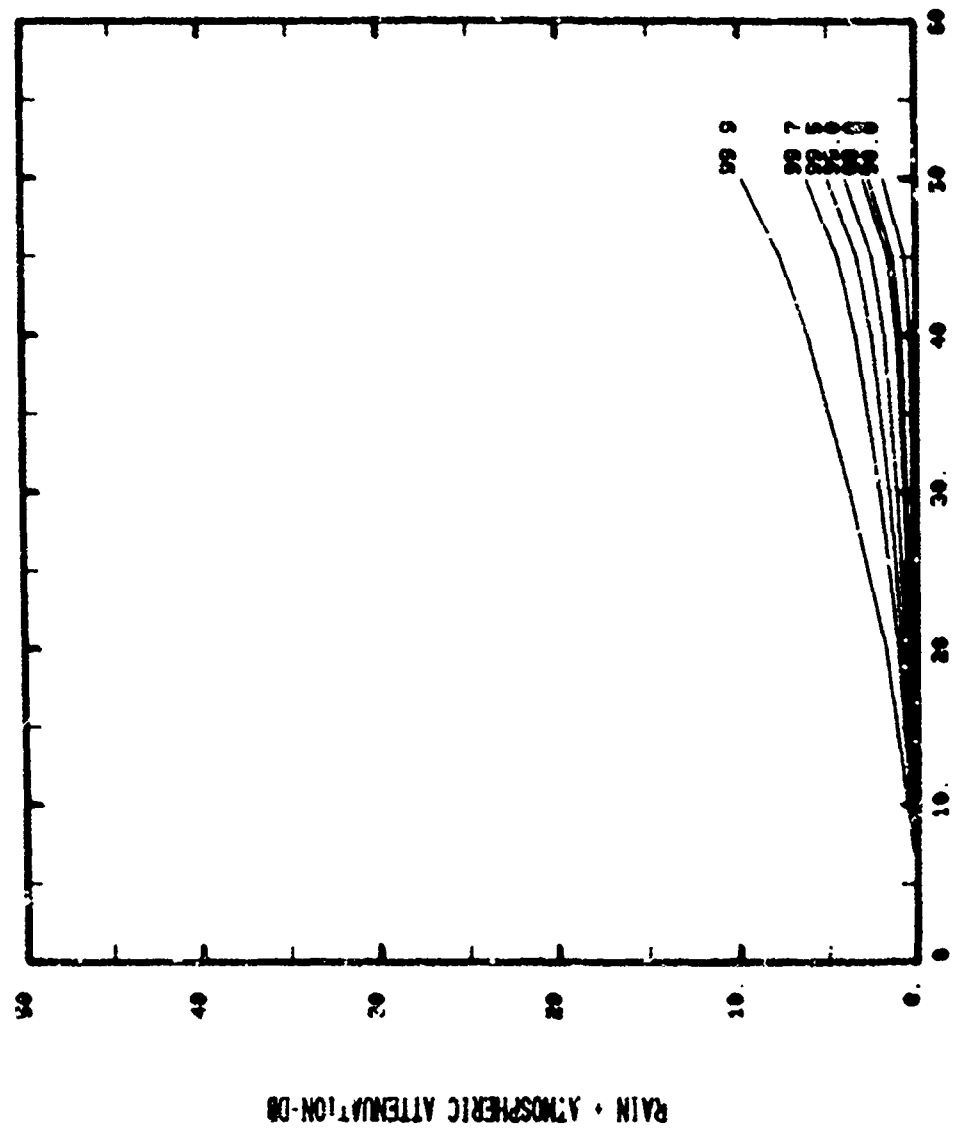


Fig. A-65

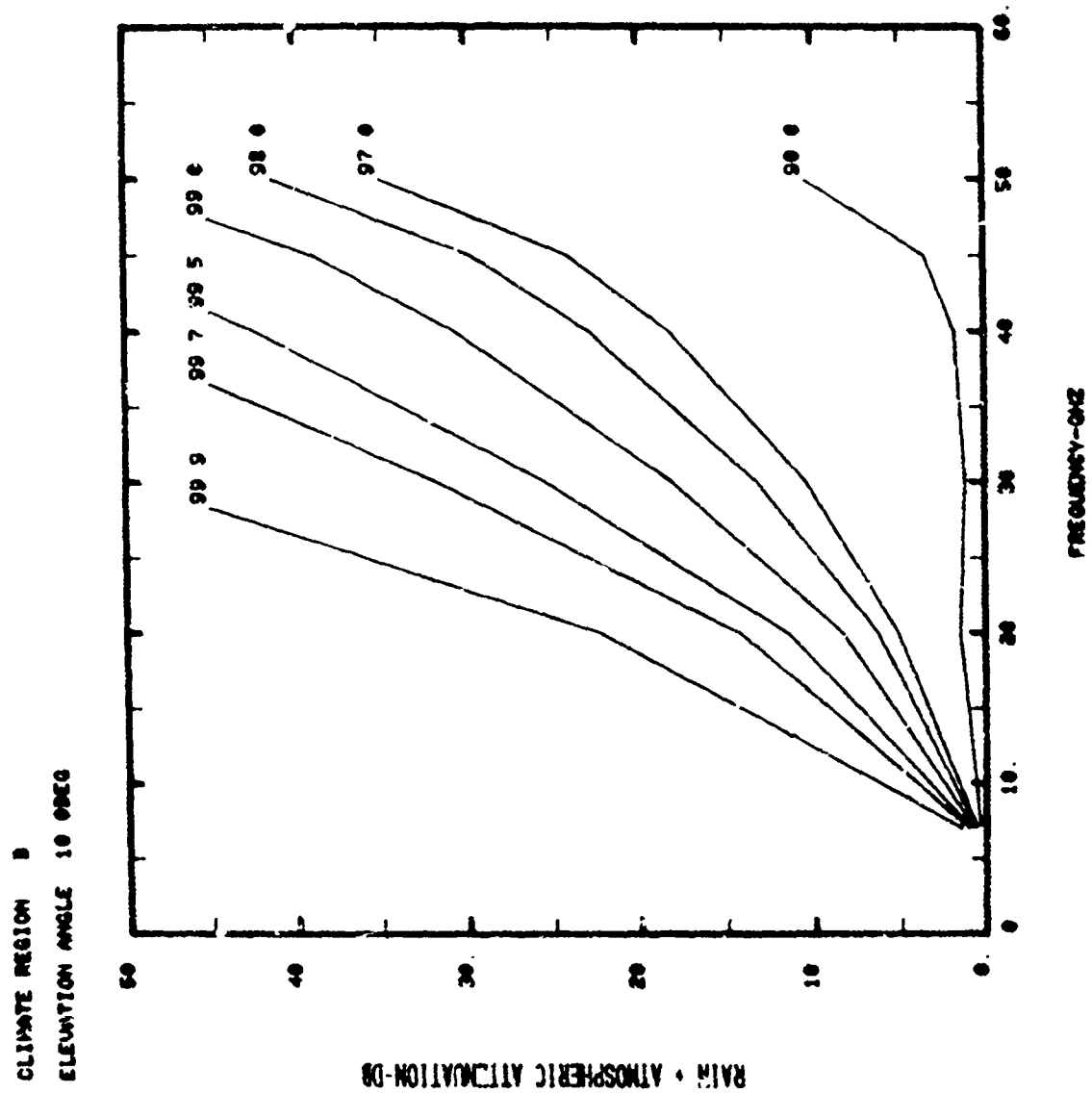


Fig. A-66

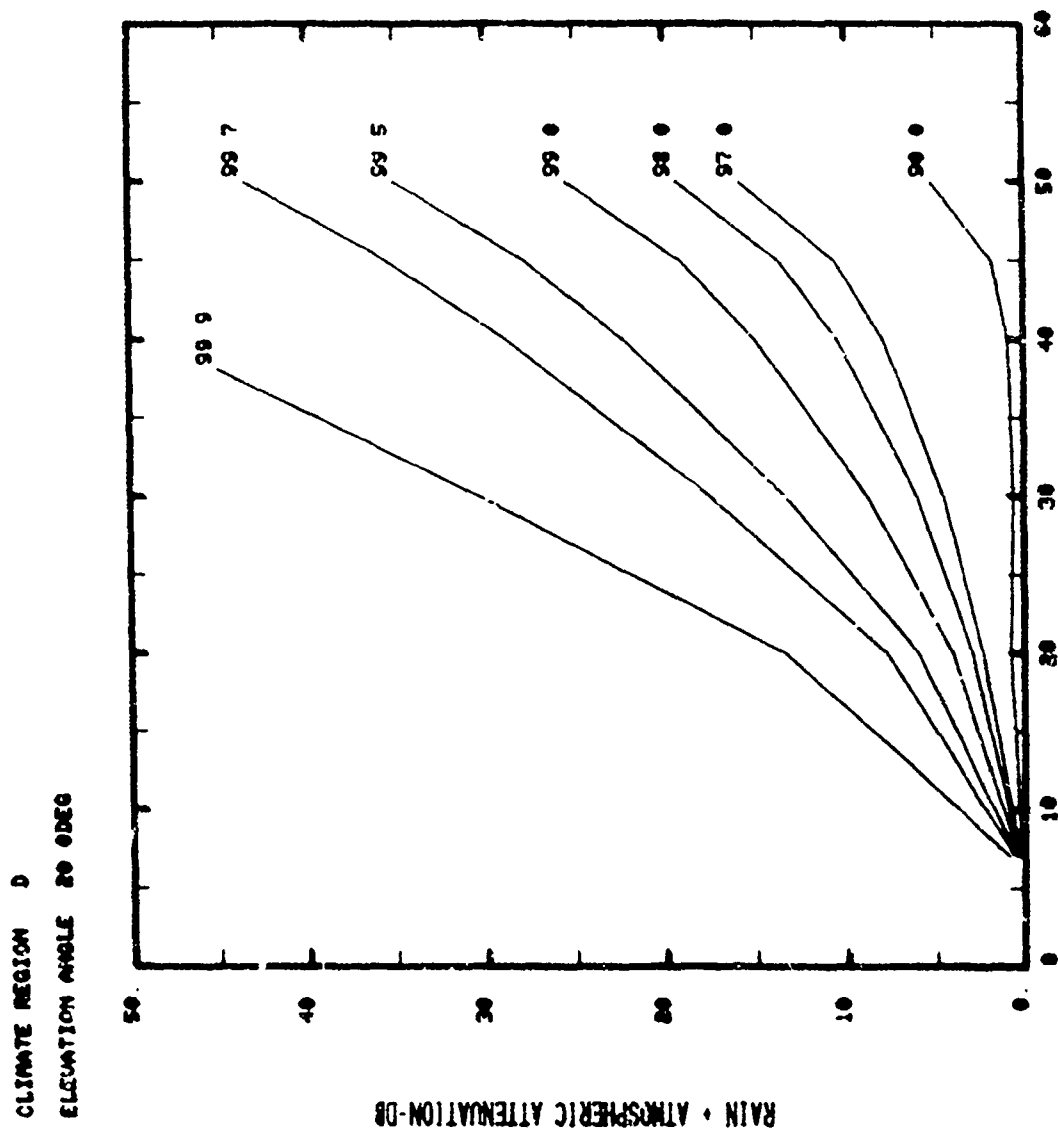


Fig. A-67

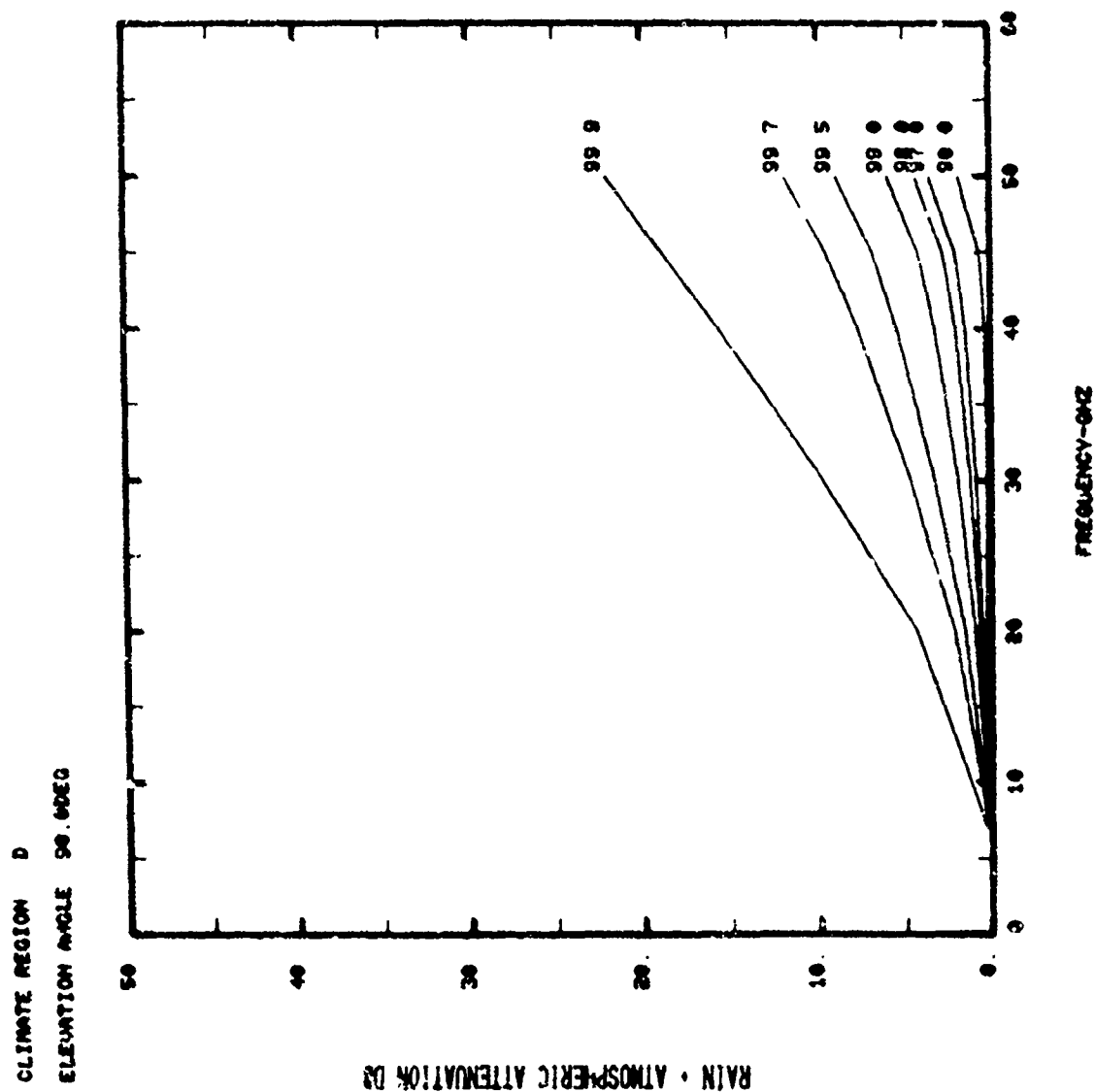


Fig. A-68

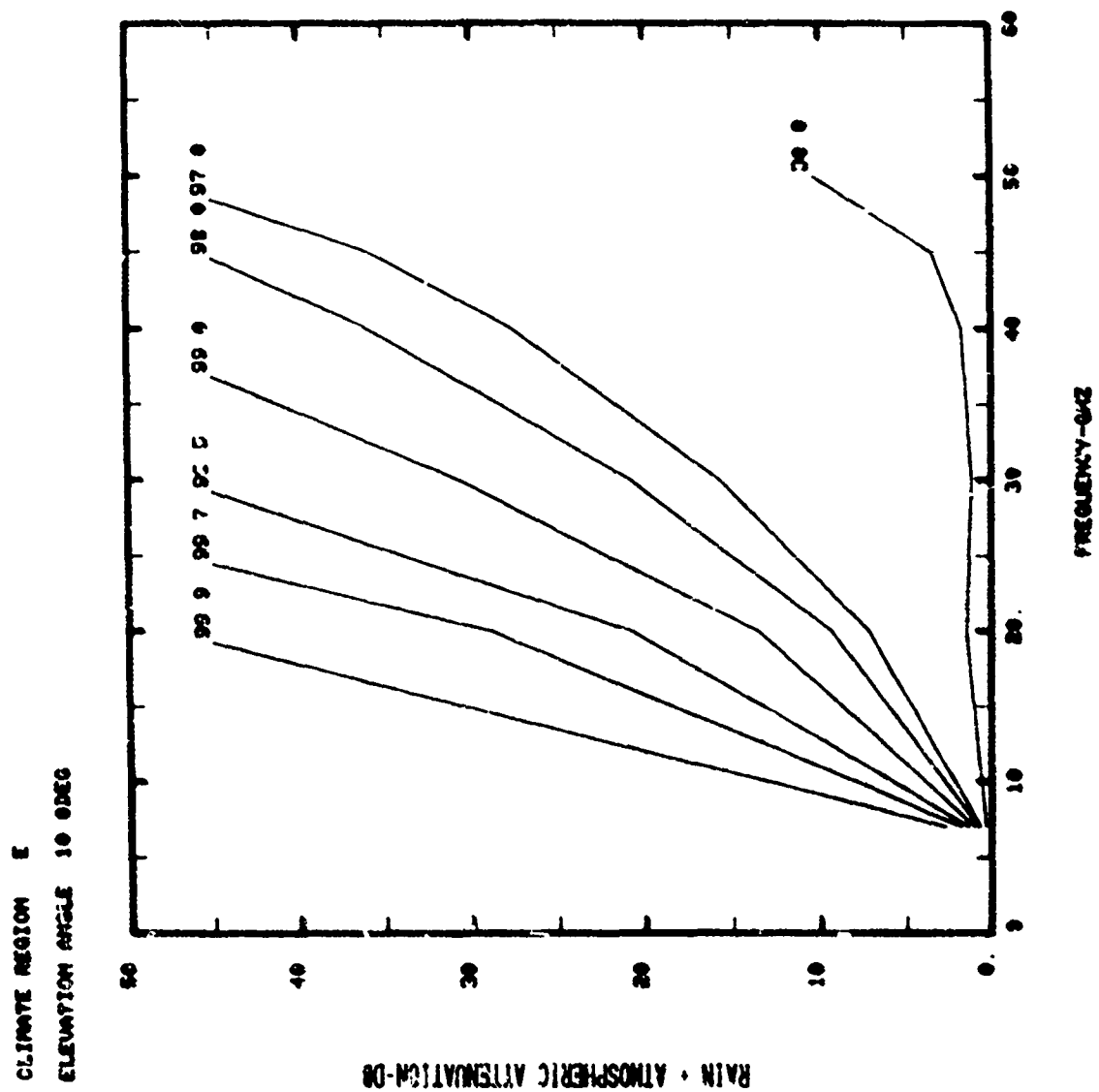


Fig. A-69

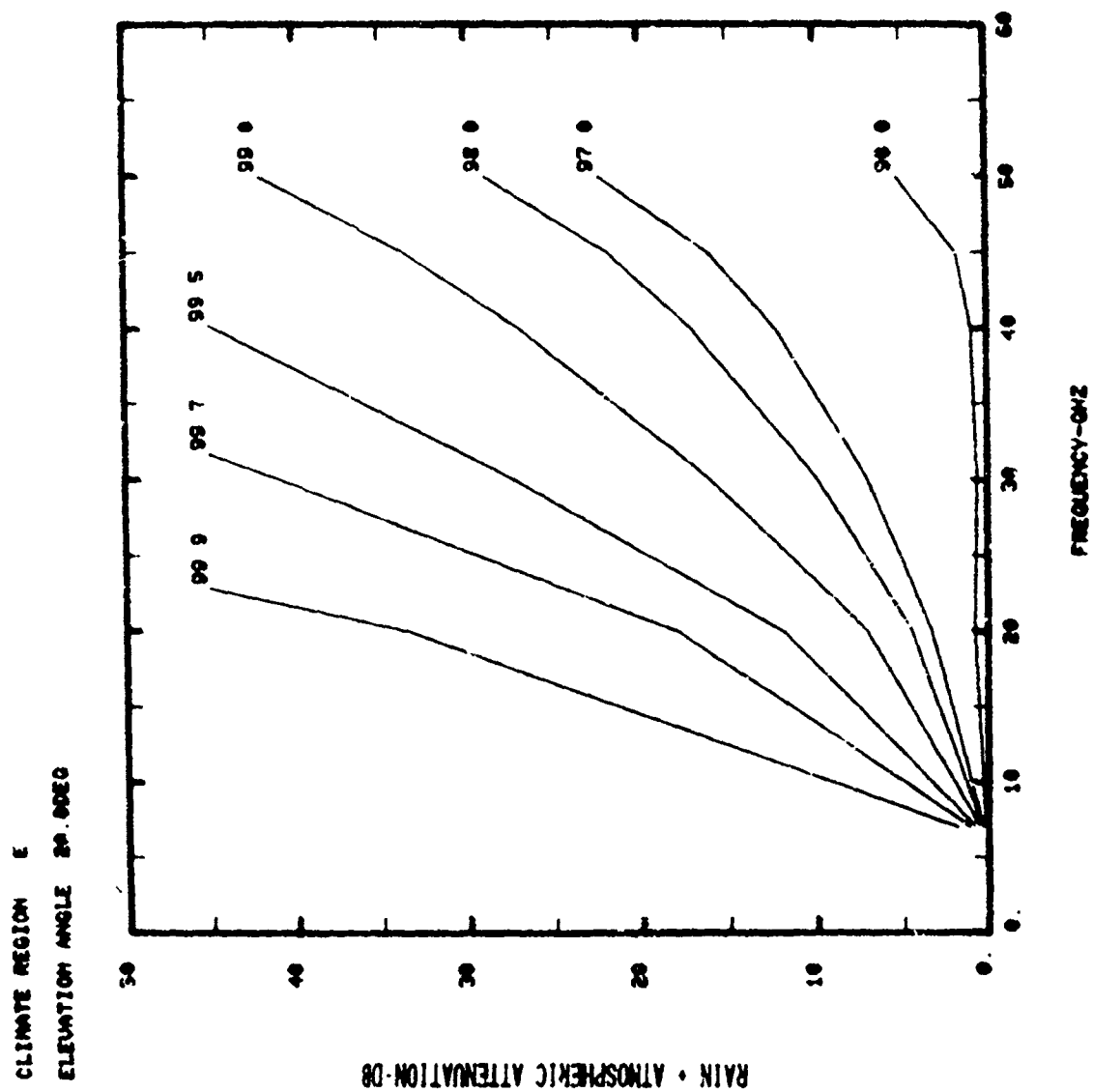


Fig. A-70

CLIMATE REGION E
ELEVATION ANGLE 90 DEG

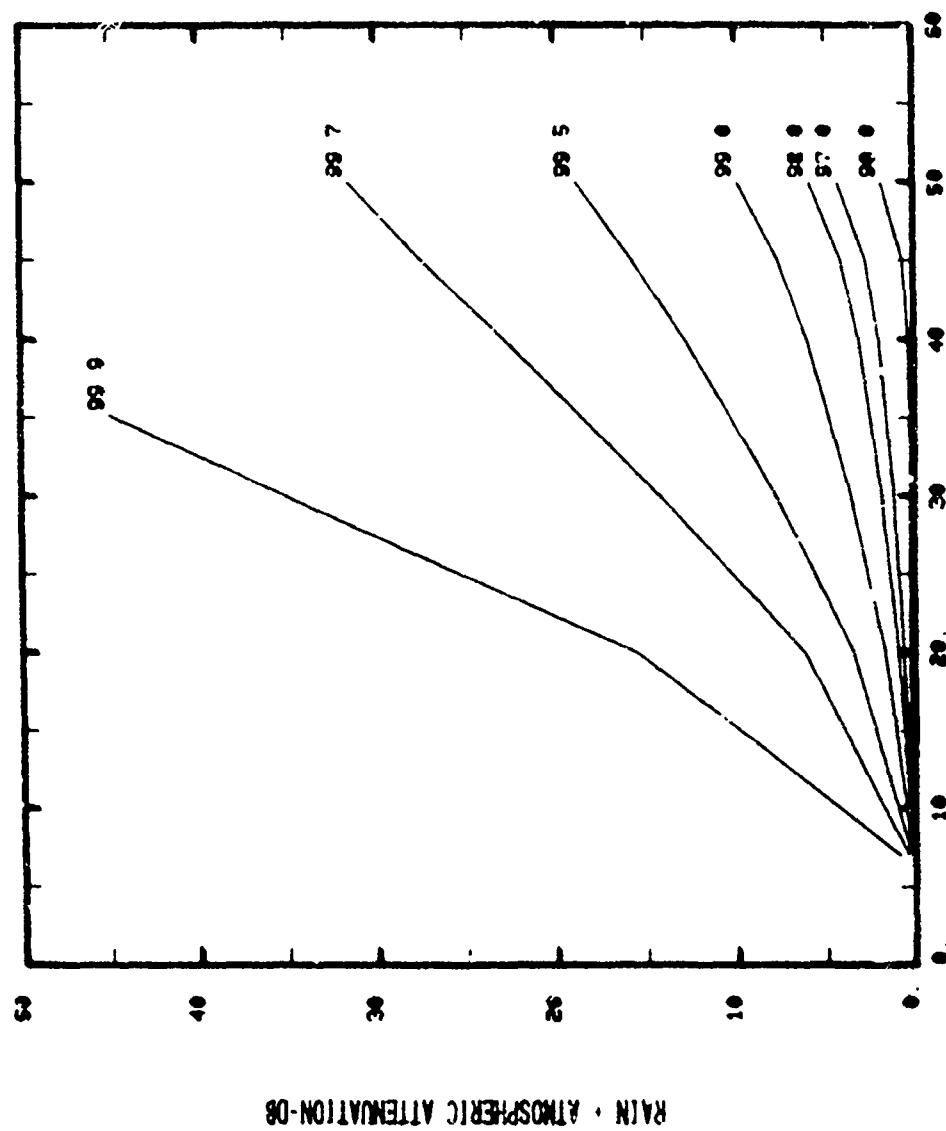


Fig. A-71

CLIMATE REGION F
ELEVATION ANGLE 10.0 DEG

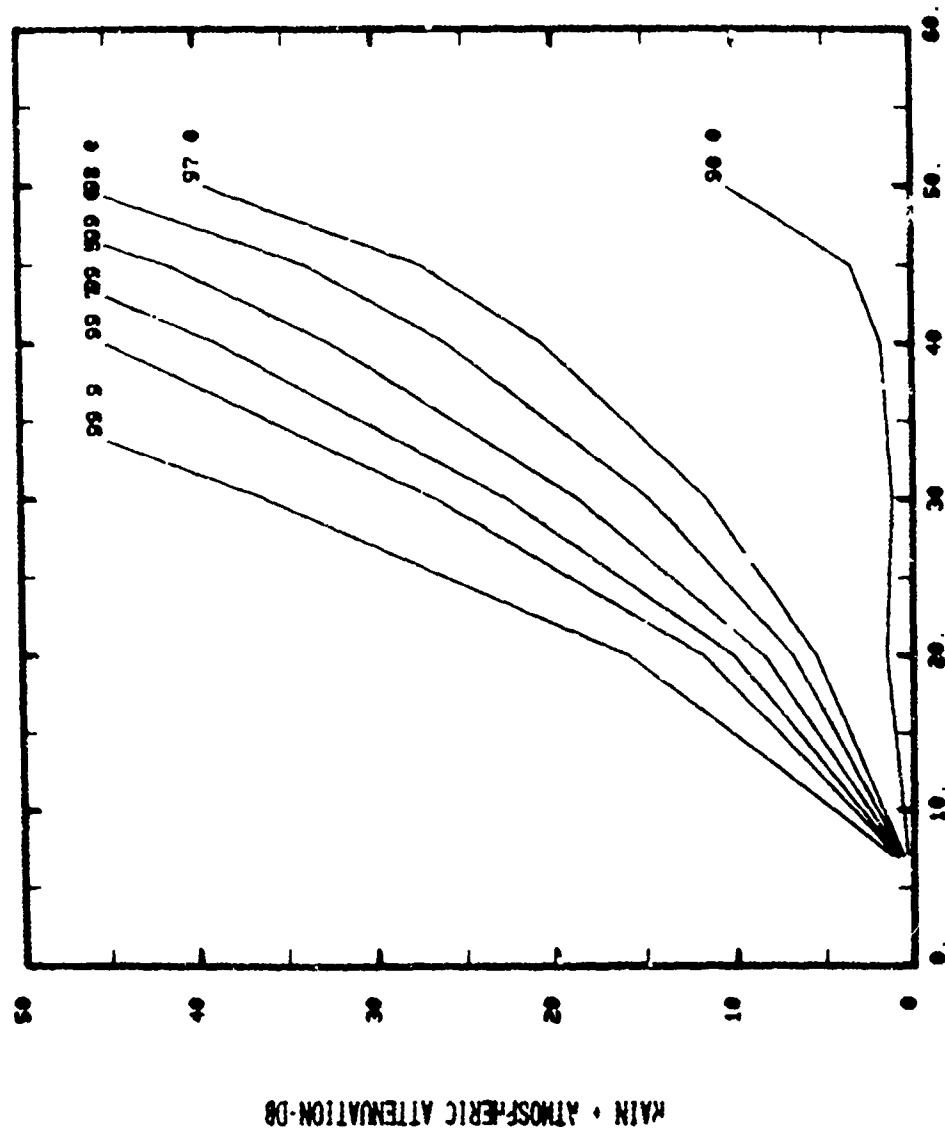


Fig. A-72

CLIMATE REGION F
ELEVATION ANGLE 80.0DEG

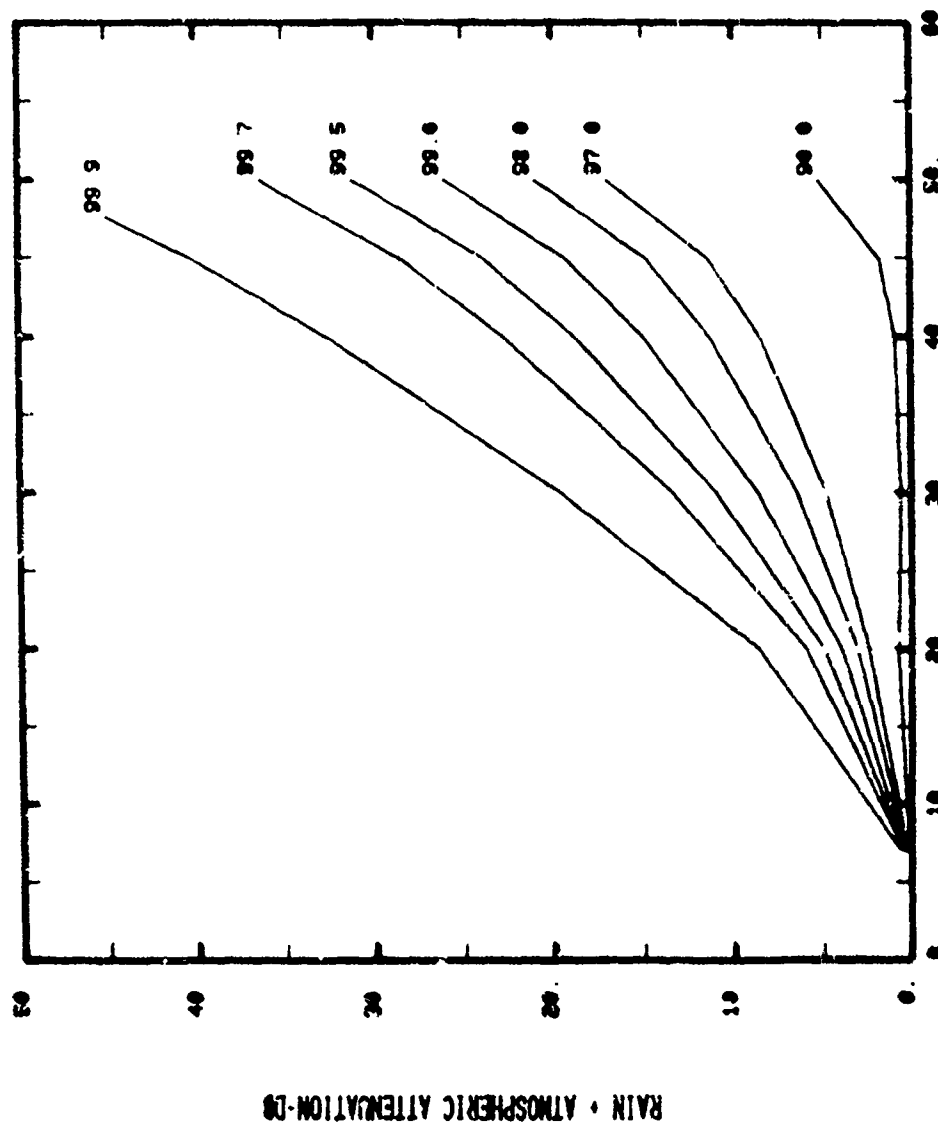


Fig. A-73

CLIMATE REGION F
ELEVATION ANGLE 90 DEEG

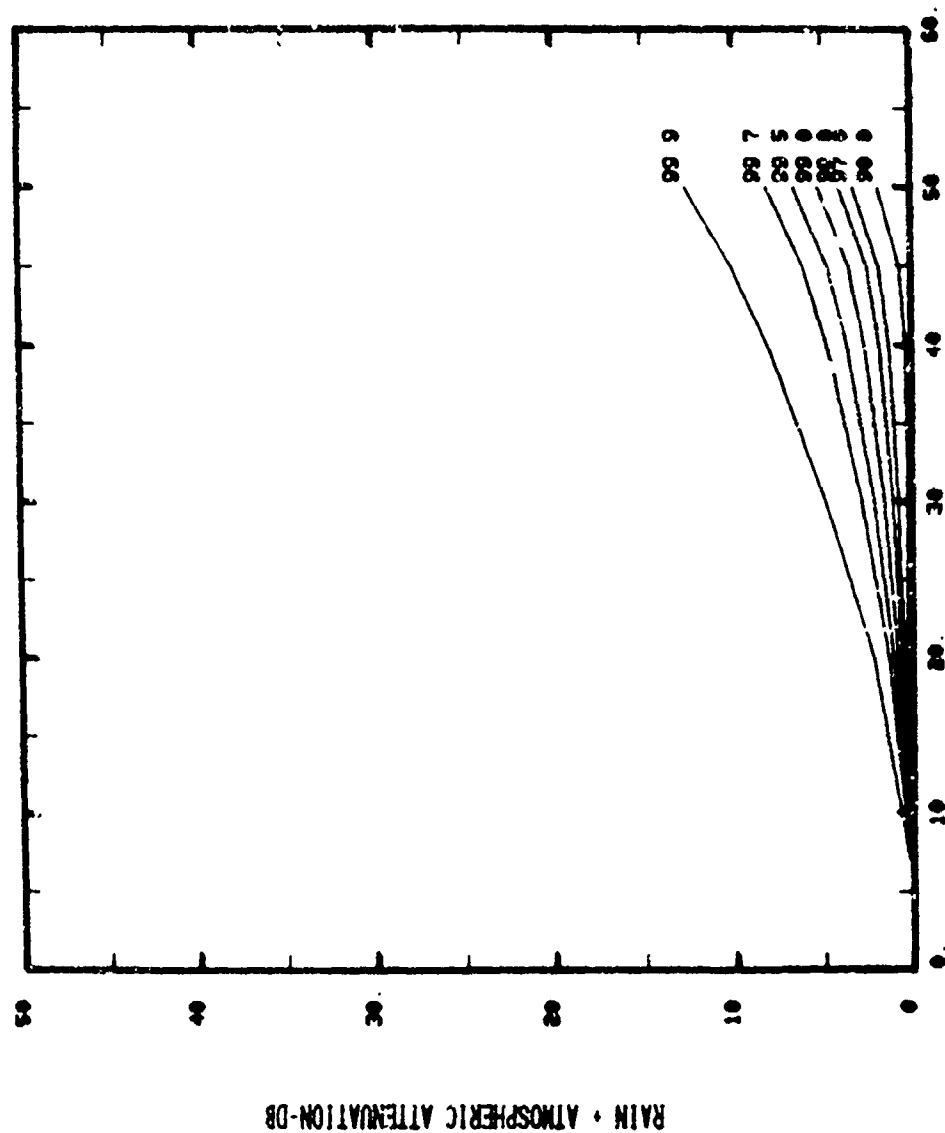


Fig. A-74

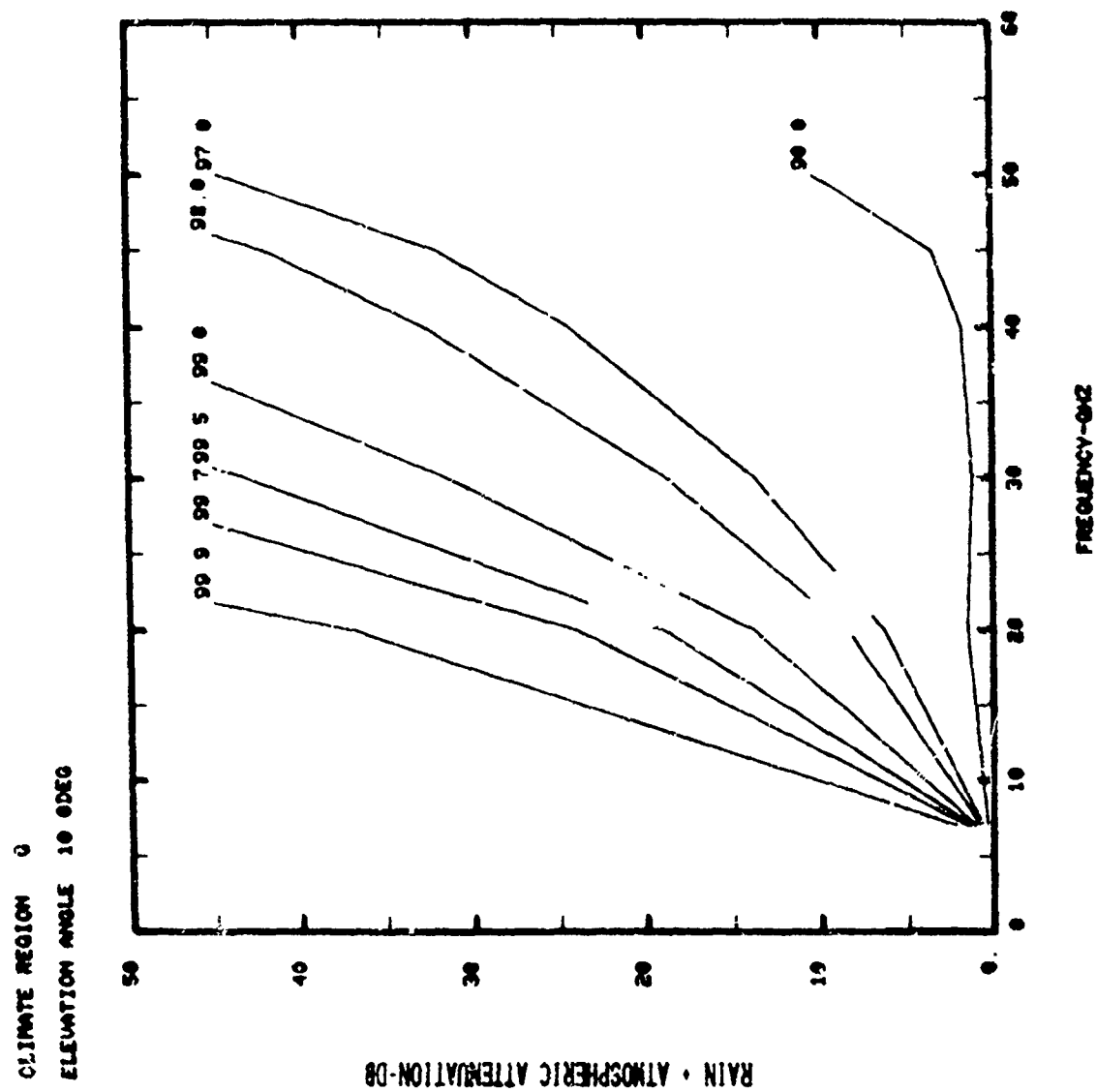


Fig. A-75

CLIMATE REGION C
ELEVATION ANGLE 20.00EG

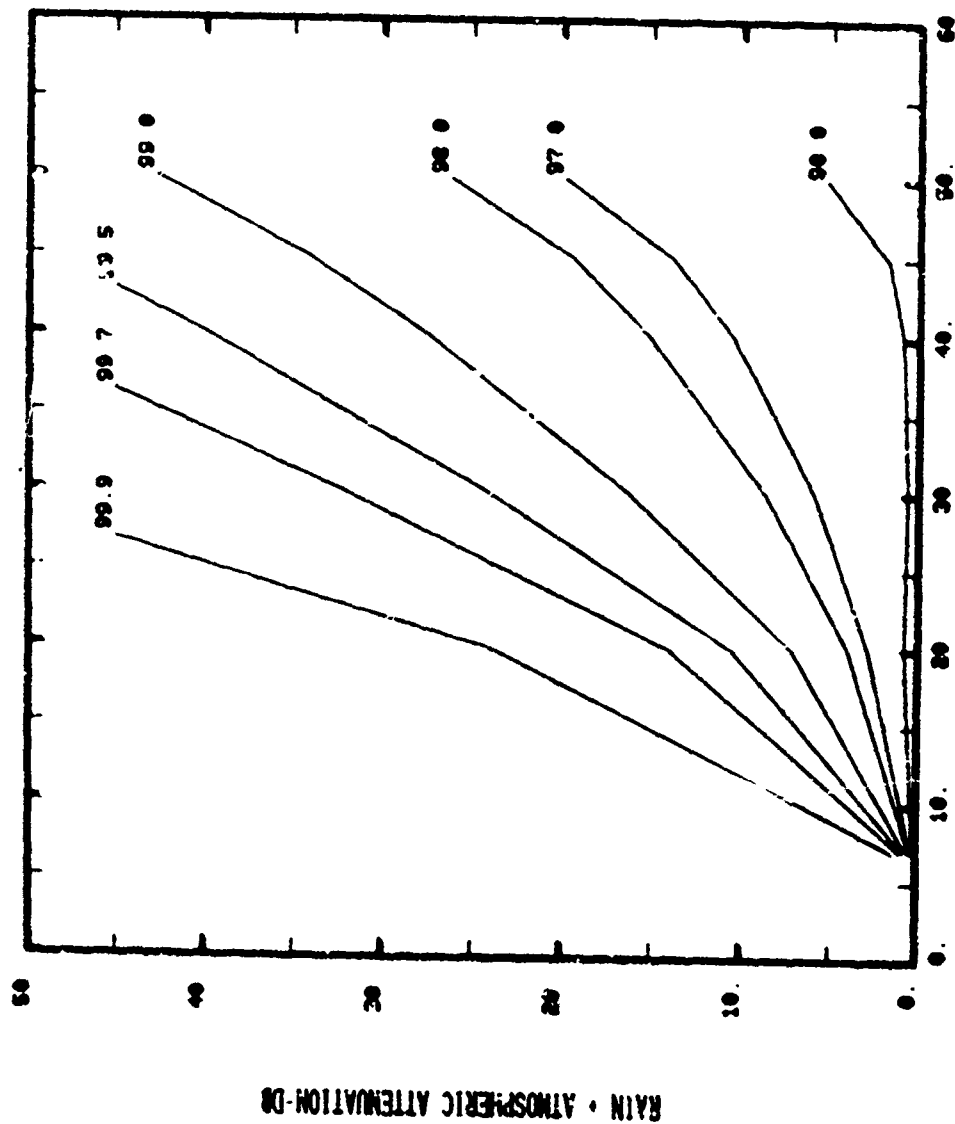
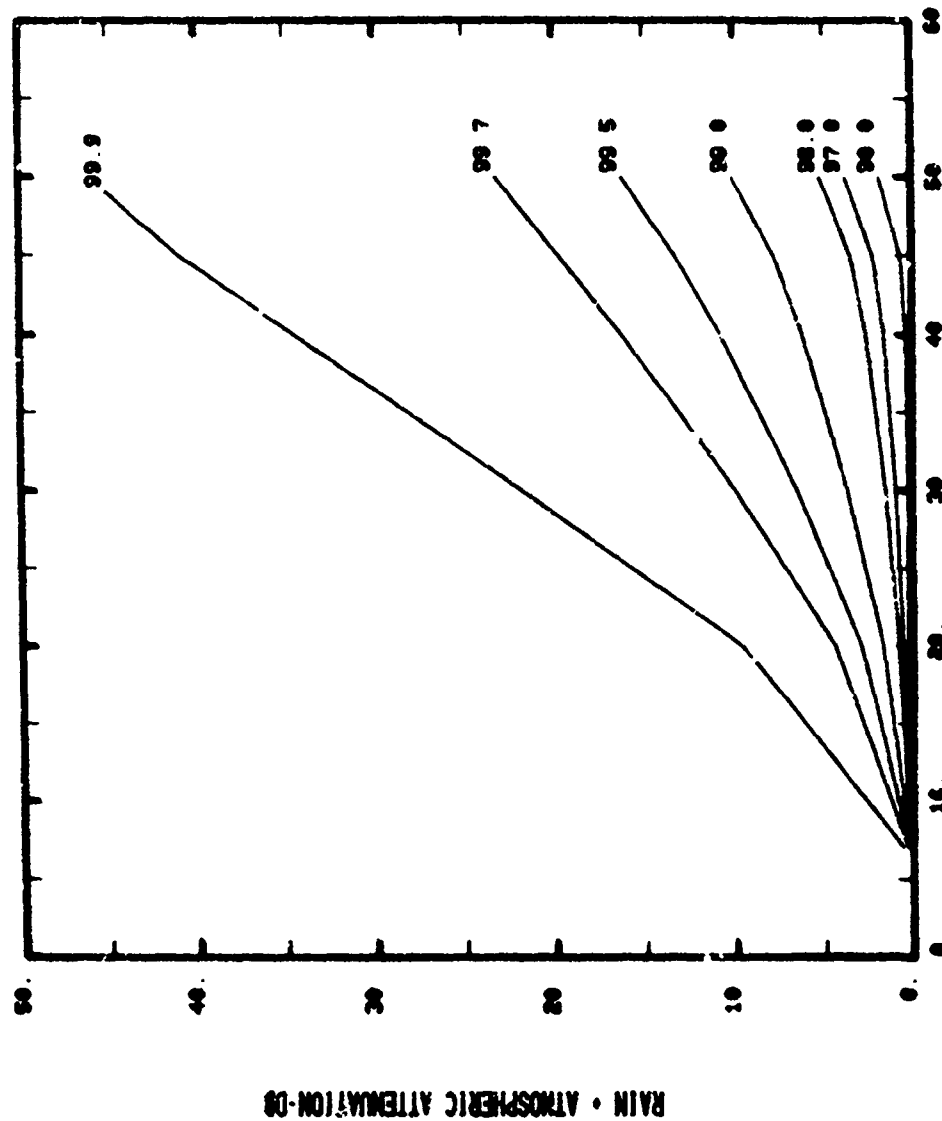


Fig. A-76

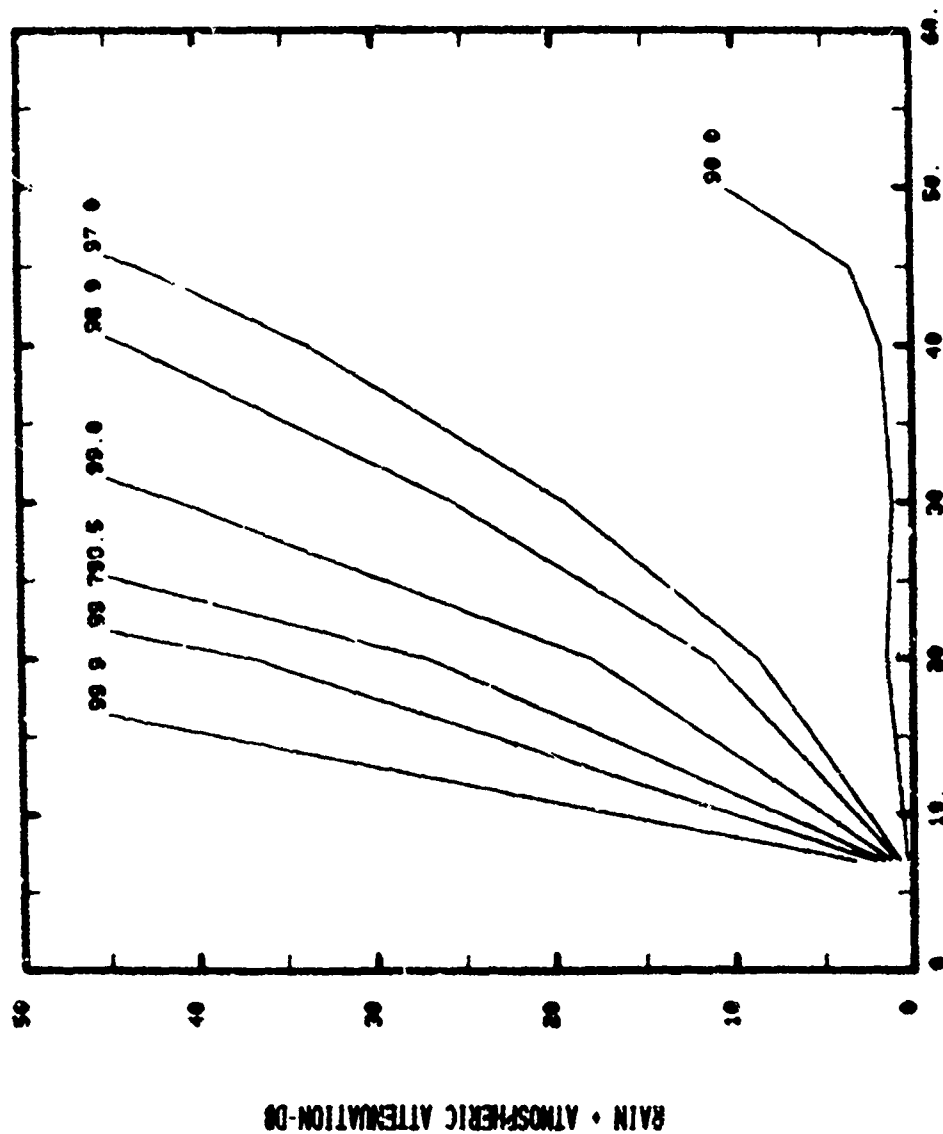
CLIMATE REGION 0
ELEVATION ANGLE 90.0DEG



FREQUENCY-GHZ

Fig. A-77

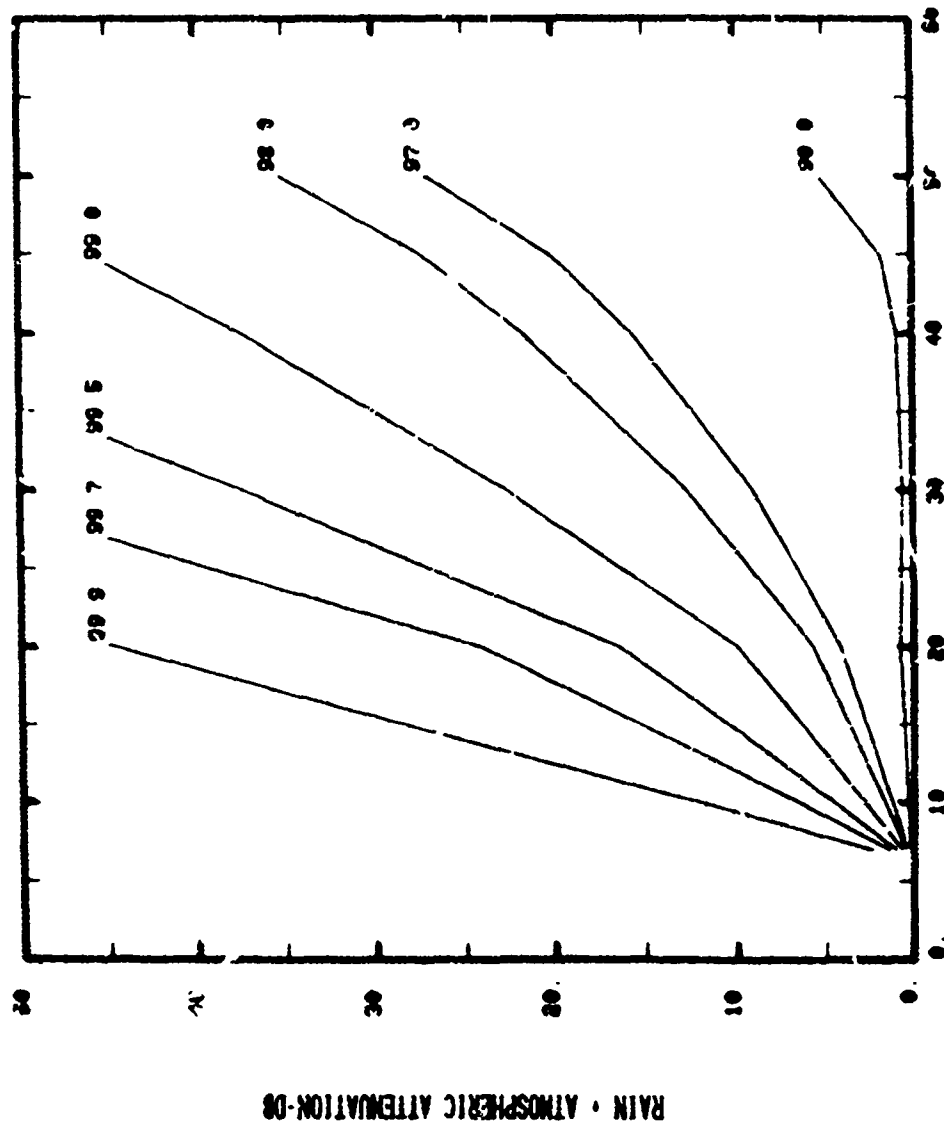
CLIMATE REGION H
ELEVATION ANGLE 10.0009



FREQUENCY-MHz

Fig. A-78

CLIMATE REGION H
ELEVATION ANGLE 20 DEG



FREQUENCY-GHZ

Fig. A-79

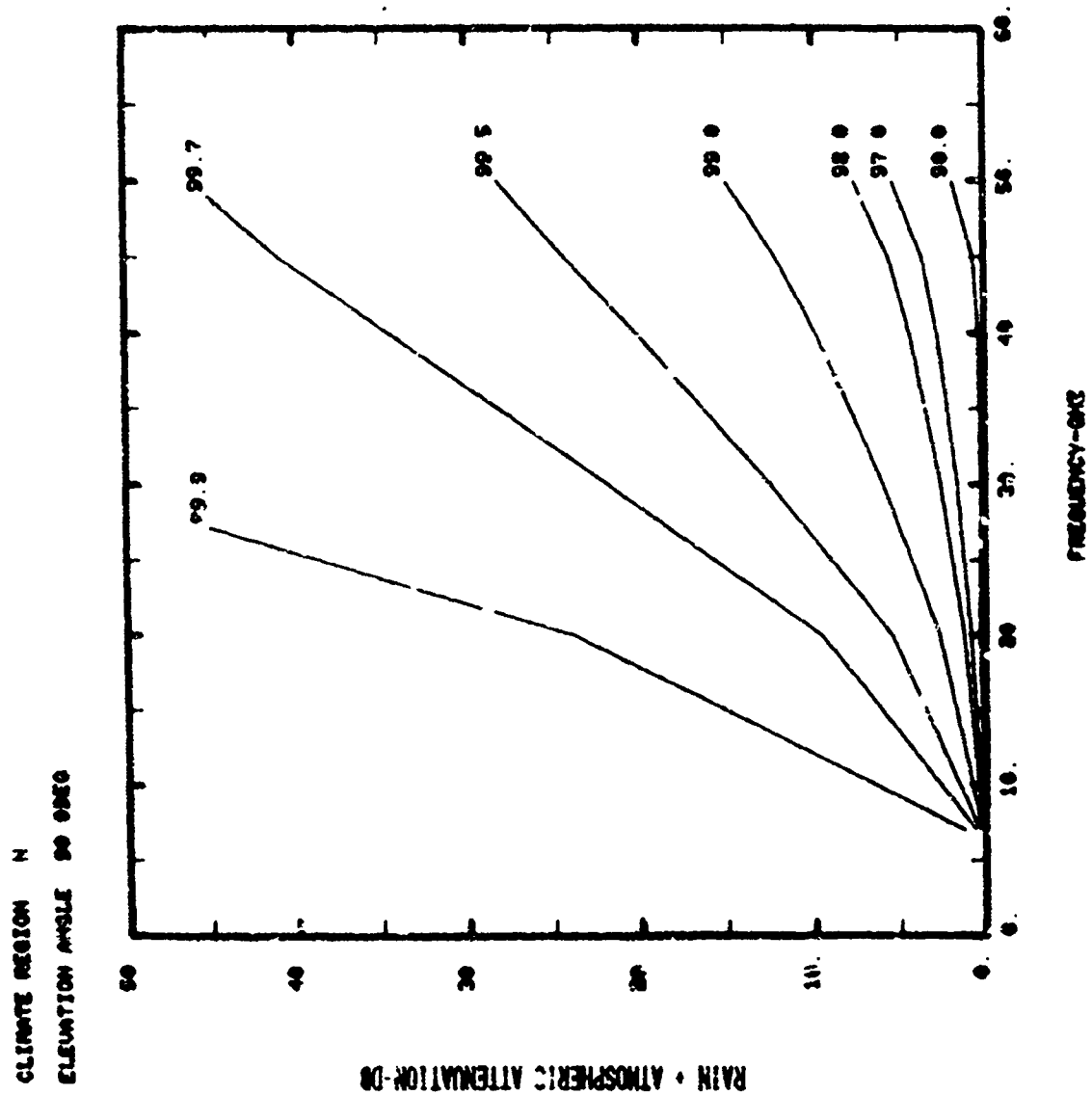


Fig. A-80

UNCLASSIFIED

SECURITY CLASSIFICATION OF THIS PAGE (When Data Entered)

19 REPORT DOCUMENTATION PAGE		READ INSTRUCTIONS BEFORE COMPLETING FORM
1. REPORT NUMBER (13) ESD-TR-79-43	2. GOVT ACCESSION NO.	3. RECIPIENT'S CATALOG NUMBER
4. TITLE (and Subtitle) Technology Assessment for Future MILSATCOM Systems: The EHF Bands	5. TYPE OF REPORT & PERIOD COVERED Project Report	
7. AUTHOR(s) David J. Frediani	6. PERFORMING ORG. REPORT NUMBER Project Report DCA-5	
9. PERFORMING ORGANIZATION NAME AND ADDRESS Lincoln Laboratory, M. I. T. P.O. Box 73 Lexington, MA 02173	8. CONTRACT OR GRANT NUMBER(s) F19628-78-C-0002	
11. CONTROLLING OFFICE NAME AND ADDRESS Defense Communications Agency 8th Street & So. Courthouse Road Arlington, VA 22204	10. PROGRAM ELEMENT, PROJECT, TASK AREA & WORK UNIT NUMBERS Program Element No. 35126K	
14. MONITORING AGENCY NAME & ADDRESS (if different from Controlling Office) Electronic Systems Division Hanscom AFB Bedford, MA 01731	12. REPORT DATE 12 Apr 1979	
	13. NUMBER OF PAGES 294	
	15. SECURITY CLASS. (of this report) Unclassified	
16. DISTRIBUTION STATEMENT (of this Report) Approved for public release; distribution unlimited.		
17. DISTRIBUTION STATEMENT (of the abstract entered in Block 20, if different from Report)		
18. SUPPLEMENTARY NOTES None		
19. KEY WORDS (Continue on reverse side if necessary and identify by block number) EHF technology low-noise receivers power amplifiers antennas antenna gain limitations rain attenuation		
20. ABSTRACT (Continue on reverse side if necessary and identify by block number) This report assesses the technology necessary to support future MILSATCOM systems operating at frequencies between 20 and 50 GHz (EHF). The specific MILSATCOM subsystems assessed include low-noise receivers, RF power amplifiers and antennas for the space and ground segments. The antenna gain limitations imposed by antenna surface accuracy and tracking accuracy are also addressed. Also provided are a global rain attenuation model and consideration of the related issue of system availability. Finally, recommendations are presented for technology development efforts and further studies necessary to support future EHF MILSATCOM deployment.		

207 657

57B